Activated unsaturated sand filter as an alternative technology to remove copper, manganese, zinc and nickel from waters.

Djembarmanah, Rachmawati Sugihhartati

Swansea University
Prifysgol Abertawe

ACTIVATED UNSATURATED SAND FILTER AS AN ALTERNATIVE TECHNOLOGY TO REMOVE COPPER, MANGANESE, ZINC AND NICKEL FROM WATERS

RACHMAWATI SUGIHHARTATI DJEMBARMANAH

Env. Eng (Bandung Institute of Technology, Indonesia)

MEnv. Stud (The University of New South Wales, Australia)

Submitted to Swansea University in fulfilment of the requirements for the Degree of Doctor of Philosophy

SWANSEA UNIVERSITY

2012

DEDICATION

I dedicate this thesis to:

My late mum and dad

May blessings and peace be upon you

My lovely princess (Putri Emas)

and son (Muhammad Rizki)

For support, patience, and unconditional love

SUMMARY

An activated unsaturated sand filter (AUSF) is one of only a few of the filtration technologies utilized to treat waters and wastewaters that use unsaturated filter media. AUSF employs sand coated with potassium permanganate and operates with an open chamber allowing free air flow into the column of sand. The AUSF also benefits from operation without the need for a sedimentation unit. Previous studies have demonstrated the efficient removal of iron and manganese using an AUSF, however, to date there are still very limited studies available that use AUSF technology for the removal of metals from waters and wastewaters. Thus, there is an urgent need and opportunity to exploit this technology further. This research was conducted in order to develop and study the characteristics and subsequent operational performance of a novel AUSF media. The study focuses on the removal of copper, manganese, zinc and nickel from a synthetic wastewater and extends current knowledge to a passive aeration process rather than the active aeration used in the previous study by Lee et. al. (2004). The characterisation involved the use of sieving, Brunauer-Emmett-Teller (BET) analysis, water evaporation studies and scanning electron microscopy (SEM) for structural analysis such as particle size, surface area, porosity and topography. Energy dispersive X-ray analysis (EDX), acid/alkali resistance, isoelectric point determination and acid digestion analysis were used to determine the chemical constituency, chemical stability, electrical charge properties and the binding efficiency of the media. Finally, tracer studies were employed to determine the flow characteristics through the particle media.

The manganese coated sand was proven effective for the removal of copper in both agitated tank batch studies and continuous column studies. The batch studies showed that the equilibrium sorption of copper followed a Langmuir isotherm and the sorption rate was best modelled using the pseudo-second-order kinetic model. This suggests that adsorption is taking place as a single homogeneous layer on the surface of the sand particle via the chemisorption method. The Weber-Morris and Bangham models were used to determine the rate-controlling mechanism and this was found to be predominantly intra-particle diffusion. This was confirmed for column studies using the Bohart-Adams model that demonstrated that liquid-film mass transfer was not significant. Several mechanisms of metal removal are proposed and these include precipitation, electrostatic attraction, adsorption, ion exchange and complex ion formation.

The column studies demonstrated that dispersion was low under the operating conditions and plug flow performance could be inferred, thus justifying the use of the AUSF model employed. Copper was best removed when operating as an unsaturated particle bed and the removal capacity was increased by approximately 100% when compared to a saturated particle bed. Moreover, the pH increase that occurs on exposure of the process water to the unsaturated column further improves removal capacity. Thus, there is no requirement for an expensive pH adjustment as a pre-treatment process prior to this unit operation. In addition, the removal capacity of the AUSF was demonstrated to increase with lower metal concentrations, lower water flow rates, smaller sand particles, an increase in manganese to sand ratio and an increase in particle bed height. The AUSF performance in removing metals followed the order Cu > Mn > Zn > Ni for individual and mixed component solutions and Cu > Ni > Zn > Mn for a synthetic wastewater typical of the electroplating industries.

In conclusion, the novel manganese coated AUSF developed is effective in the removal of metals from solution and offers the potential of a sustainable low cost treatment method for the purification of waters and wastewaters.

DECLARATION

This work has not previously been accepted in substance for any degree and is not being concurrently submitted in candidature for any degree.

Signed .. .. (candidate)

Date 20/07/2012 .....

STATEMENT 1
This thesis is the result of my own investigations, except where otherwise stated. Where correction services have been used, the extent and nature of the correction is clearly marked in a footnote(s).
Other sources are acknowledged by footnotes giving explicit references. A bibliography is appended.

Signed ... . (candidate)

Date 20/07/2012 .....

STATEMENT 2
I hereby give consent for my thesis, if accepted, to be available for photocopying and for inter-library loan, and for the title and summary to be made available to outside organisations

Signed .... (candidate)

Date 20/07/2012 .....

CONTENTS

ACKNOWLEDGEMENTS

I am very grateful to my supervisor Dr. Chedly Tizaoui for his excellent comments, ideas, support and help throughout my research. He had been always motivating me to work hard, be perfect and helped me to reach the enjoyment of being "a true scientist".

I am also grateful to my other supervisor Professor Nidal Hilal for his help and motivation throughout my study. His warmth comments and support helped me to stay in UK, study for PhD while at the same time look after my kids.

I would like to thank Dave Mee for setting up my AUSF column and Chris Sommerfield for first teaching me how to use the AAS at The University of Nottingham, UK. Thanks also go to Gary Tuckett and Dr. Paul Williams from Swansea University for helping me doing my experiments. I would also like to thank Mabrouk Zanain for helping me doing BET analysis and Afshin Tarat and Alex M. Lord for helping me doing SEM/EDX analysis. Special thanks go to Alex M. Lord for his patience and hard work in finding all my studied elements in SEM/EDX analysis, his help in checking my writing, and his support and motivation.

To all my colleagues and friends, thank you for the friendships you had been given me throughout my study. Special thanks go to Shamma Al-Malek for the endless sisterhood, support and motivation.

I would like also to thank Indonesian Government for funding my study and National Institute of Technology (ITENAS), Bandung, Indonesia for their support.

Finally, I would like to thank all my family for their endless support and love, particularly to my lovely princess, Putri Emas who had been looking after her brother and me throughout my study.

NOMENCLATURE

a	lower limit of integration
a_c	absorptivity constant (L/mg/cm)
a_{qs}	saturation capacity of the adsorbent per unit volume of the packed bed (mg/g)
A	absorbance
b	upper limit of integration
c	velocity of light (m/s)
c_L	Langmuir empirical constants related to the binding energy of the sorption system (L/mg)
C	effluent element concentration (mg/L) measured at a time t (min)
C_a	concentration of the absorbing species (mg/L)
^oC	degree Celcius
C_e	equilibrium adsorbate concentration (mg/L)
C_{in}	input or initial element or adsorbate concentration (mg/L or mg/cm^3)
C/C_{incalc}	calculated C/C_{in}
C/C_{inexp}	C/C_{in} obtained from the experiment
$C(t)$ or C_i	tracer concentration at time t or ith observation (mg/L)
C_{WM}	a constant in Weber-Morris' model that gives idea about the thickness of the boundary layer (mg/g)
d	diameter of the column (mm)
d_n	dispersion number (unit-less)
dm_r/dt	rate of accumulation of mass in the sand column within a period of time (mg/s)
D	coefficient of axial dispersion (m^2/s)
D_L	axial dispersion coefficient (cm^2/sec)
E	removal efficiency (%)
ΔE	the energy difference between two excited states (J)
E_e	energy to knock electron out from its shell (keV)
$f(x)$	integrand
h	initial sorption rate (mg/(g. min))

h_P	Planck constant = 6.63 x 10^{-34} Js
H	height of sand (mm)
$K_{\alpha 1}$ $K_{\alpha 2}$ $L_{\alpha 1}$ $L_{\alpha 2}$ $M_{\alpha 1}$ $M_{\alpha 2}$	$\alpha 1$, $\alpha 2$ line series of K, L and M shell electron
$K_{\beta 1}$ $K_{\beta 2}$	$\beta 1$, $\beta 2$ line series of K shell electron
K_1	pseudo-first-order (adsorption) rate constant (1/min)
K_2	pseudo-second-order rate constant (g/(mg.min))
K_f	Freundlich capacity factor (mg adsorbate/g adsorbent)*(L water/mg adsorbate)$^{1/ra}$
K_{id}	intra-particle diffusion rate constant (mg/g.min$^{1/2}$)
K_o	constant in Bangham's model (L/gL)
K_{so}	equilibrium constant
${}^{c}K_{so}$	concentration or conventional product constant
${}^{c*}K_{so}$	solubility equilibrium constant for metal hydroxides
K_w	equilibrium constant for ionization of water, H_2O = 1.0 x 10^{-14} at 25^0C
L	length or column length (m or mm)
L_b	path length through the flame (cm)
m	mass (g) or mass of adsorbent per liter of solution (g/L)
m_r	mass of element retained in the sand column (mg)
m_{salt} or $m_{T,out}$	total mass of salt measured at the reactor effluent (mg)
m_{sand}	mass of sand (g)
$m_{T,in}$	actual mass of tracer added (mg)
M_v	gram molecule volume (= 22410 mL)
n	total number of data points selected or total sample
N	Avogrado number (= 6.023 x 10^{23} molecules/g molecule)
$1/r_a$	Freundlich intensity parameter
P	pressure at which adsorption occurs
q or q_t	removal capacity (mg/g or mmol/g) or amount of metal sorbed at any time, t (mg/g)
q_e	equilibrium adsorption uptake (mg of adsorbate/ g of adsorbent)
q_m	maximum sorption capacity (mg/g)

q_{Mmax}	maximum metal adsorbed onto the sand (mg/g)
q_{Mmax}/q_{Mn}	ratio of maximum metal adsorbed to the amounts of manganese (mg/mg)
q_{Mn}	amounts of manganese on the sand (mg/g)
q_s	saturation capacity of the adsorbent (mg/g)
Q	volumetric flow rate (mL/min)
r	shaker speed (rpm)
r_a	rate of adsorption
r_{BA}	Bohart-Adams rate constant (cm^3/mg.sec)
r_c	radius of coloumn (mm)
R	removal rate of element (%) or correlation factor
R_L	separation factor or equilibrium parameter
s	standard deviation of a sample
s^2	sample variance
S	column surface area (mm^2)
S_w	specific surface area (m^2g^{-1})
t or t_i	time at ith observation or travel time or contact time (min)
$\bar{t}_c$	theoretical mean detention or residence time (min) obtained from C curve
t_{calc}	calculated time (min)
$\bar{t}_{\Delta c}$	mean residence time based on discrete time step observations (min)
t_e	equilibrium time (min)
t_1	time of water initially discharging from the spray (min)
Δt_i	constant sampling interval selected
t_{95}	time at which the metal removal is 95%
t_2	time of water initially discharging from the filter (sand) (min)
T_x	residence time (the time for x percent of the tracer mass to come to the effluent for a pulse input tracer test (min))
u	velocity of fluid (m/s) or superficial velocity (cm/sec)
V	volume of gas adsorbed or solution volume (mL)
V_m	monolayer capacity (mL)
V_s	volume of sand column (mL)

$V_{solution}$	solution volume (mL)
V_t	total volume of substance
V_v	volume of void space
w	adsorbent mass (g)
$\bar{x}$	sample mean
z	column axial coordinate (cm)
Z	atomic number

Greek letters

α	constant (<1) in Bangham's equation
ε or $\emptyset$	total voidage in the column or column void fraction or porosity
ε_G	fraction of volume occupied by the gas to the total column volume
ε_L	fraction of volume occupied by liquid to the total column volume
$\bar{\theta}$	normalised mean detention time (unitless)
λ	X-ray wavelength (A^0 or m)
μ	population mean
v	interstitial velocity (cm/sec)
σ	area occupied by one adsorbate molecule (=16.2 x 10^{-20} m^2 for nitrogen)
σ_c^2	variance obtained from C curve (s^2)
$\sigma_{\Delta c}^2$	variance based on discrete time observation (min^2)
σ_θ^2	variance of normalised tracer response C curve (s^2)
τ	hydraulic or theoretical detention time (min)

Abbreviations

AAS	atomic absorption spectrometry
AES	atomic emission spectrometry
AUSF	activated unsaturated sand filter
BET	Brunauer, Emmet, Teller
cip	common intersection point
CRT	cathode ray tube
CSTR	continuous flow stirred tank reactor
DAF	dissolved air flotation
DBPs	disinfection by products
DETA	diethylenetriamine
DNA	deoxyribonucleic acid
DO	dissolved oxygen
EAAS	electrothermal atomic absorption spectrometry
EBCT	empty-bed contact time (min)
EC	electrical conductivity
ED	electrodialysis
EDS	energy-dispersive spectrometer
EDX	energy dispersive X-rays
EPA	Environmental Protection Agency
EPMA	electron probe microanalyser
FAAS	flame atomic absorption spectrometry
FBR	fluidized-bed reactor
GAC	granular activated carbon
HPLC	high-performance liquid chromatography
ICP	Inductively coupled plasma
IE	ion exchange
IEP	iso-electric point
$KMnO_4$	potassium permanganate
LBOD	luminescent biochemical oxygen demand
MAlC	micro-alloyed aluminium composite
MCA	multichannel analyser

MDC	minimum detection limit
MS	mass spectrometry
PFR	plug flow reactor
PVC	polyvinyl chloride
pzc	point of zero charge
RDI	recommended daily intake
RNA	ribonucleic acid
SEM	scanning electron microscopy
SRB	sulphate reducing bacteria
STEM	scanning transmission electron microscopy
TEM	transmission electron microscopy
UCBR	ultra-compact biofilm reactor
UF	ultra-filtration
UNICEF	United Nations Children's Fund
USATSDR	United States Agency for Toxic Substances and Disease Registry
UV	ultra violet
Varian AA240FS AAS	Varian AA240FS Fast Sequential Atomic Absorption Spectrometry
WDS	wavelength dispersive analysis
WHO	World Health Organisation
XPP	*x*-coordinates of image corrected by pixel projection

CHAPTER 1

INTRODUCTION

1.1 Background

Access to safe drinking water is a key factor for public health. However, in 2010, 13% of the global population (or about 0.88 billion people), most of them particularly live in developing regions, were short of access to sufficient water supply, and thus prone to chemically contaminated water (WHO and UNICEF, 2010).

High concentrations of metals were found globally in ground waters, for example, manganese: up to 1.93 mg/L (Paramarta et al., 1988; Teng et al., 2001b; Vaaramaa and Lehto, 2003; Choo et al., 2005; Pacini et al., 2005; Halim et al., 2009), and zinc: up to 3.09 mg/L (Halim et al., 2009). Other elements with high concentrations, such as iron: up to 17.06 mg/L, arsenic: up to 3.7 mg/L, calcium: up to 188.79 mg/L, magnesium: up to 116.6 mg/L, sodium: 1027 mg/L and potassium: 35.1 mg/L were also found worldwide in ground waters (Paramarta et al., 1988; Vaaramaa and Lehto, 2003; Magalhaes, 2002; Halim et al., 2009).

Water obtained from surface water may also be polluted (with metals) as human and/or industries discharge their waste water to the nearby water body. For example, rivers impacted by rural, urban, industrial and agricultural activities may contain iron, manganese, chromium, lead, aluminium, and calcium (Neal and Robson, 2000); rivers receiving effluent from electro plating industries may contain copper, zinc, nickel, chromium (VI) and manganese (Chen et al., 2007b; Wang et al., 2007b); from textile industries may contain chromium (Indorama, 2003) and from coal mining operations may contain iron and aluminium (Laus et al., 2007).

The availability of safe drinking water in developing countries is still scarce due to their public water supplies often fail to provide the water. Thus, in many cases, the provision of the water has become the individual household responsibility.

Some of the technologies proposed to treat water at household level are not practical (Ahammed and Meera, 2010). Therefore, there is a need to find a low cost, simple and practical technology to treat water so as to ensure safety and to meet the World Health Organisation (WHO) drinking water quality standard for consumption.

Precipitation followed by filtration tends to be the most commonly used technique for metal removal from water due to the simplicity of the precipitation-filtration processes. Precipitation involves changing the dissolved metal ions into insoluble solid state species by a chemical reaction with a precipitant such as alkali or sulphide. Precipitation of metal hydroxides is by far the most commonly used technique. Filtration of the water is then used to remove the formed precipitate (Chen et al., 2009). Many filtration technologies used to treat waters are those of wet filters or filter media are fully saturated in the water being treated (Rutledge and Gagnon, 2002; Huisman, 2004; Cho, 2005; American Planning Association, 2006; Devi et al., 2008). Few used dry filters or un-saturated filter media (Shimojima and Sharma, 1995; Jin et al., 2000; Kuechler and Noack, 2007).

While filtration commonly involves fully submerged filter media in water, integration of the two steps (i.e. precipitation and filtration) in one step is beneficial. To this end, filtration on reactive media is an option to achieve integration of both processes. Such technique is termed as activated unsaturated sand filter (AUSF), which was first studied by Paramarta et al. (1988). Basically AUSF is an activated granular media (e.g. sand) filter which operates under unsaturated conditions (i.e. water does not occupy all the media pores). The activation of the media can be done by creating active sites on the media surface using potassium permanganate ($KMnO_4$) solutions. Previous studies have shown that manganese coated sand was effective for heavy metal (manganese, copper and lead) removal (Hu et al., 2004; Lee et al., 2004; Han et al., 2006a). Moreover, the presence of water-free pores in the filter ensures aeration of the water which also promotes the chemical reactions in solution (Paramarta et al., 1988). Solid metal species formed as a result of the precipitation reaction precipitate and are removed by the filter media. Since this treatment technique combines both precipitation and filtration processes in a single unit, this technique offers the advantage of not requiring a separate sedimentation unit.

AUSF was found to be a low cost, simple, easy and safe to use in a household scale. The AUSF could treat iron and manganese from water and was able to achieve iron and manganese concentrations that met the Indonesian water standards for example (iron: 0.3 mg/L, manganese: 0.1 mg/L) or even below. Besides, AUSF costs were significantly low as compared to those reported by the Indonesian water utility (Paramarta et al., 1988; Rachmawati et al., 2006a). A mechanism of iron and manganese removal with $KMnO_4$ activated sand filter was proposed in Paramarta et al. (1988).

Despite the fact that AUSF technique was efficient to remove iron and manganese, currently there are only a very limited number of research studies on AUSF. Therefore this research was done in order to find out the characteristics and performances of AUSF in removing heavy metals.

The characteristics studied are those of sand particles and sand bed characteristics. The properties (kinetics and equilibrium) of manganese coated sand in removing the studied metals from synthetic solutions were first investigated in batch system. A detailed investigation on copper removal was made in this study and the effect of initial concentration, mass of sand, pH, dissolved oxygen (DO) content, and manganese to sand ratio on the sorption of copper by manganese coated sand were observed. Five different linear types of the Langmuir model and the linear form of the Freundlich model were used to model the equilibrium data. The behaviour of copper adsorption process by manganese coated sand was analysed using the pseudo-first-order Lagergren equation, the six types of pseudo-second-order, the intraparticle diffusion of Weber and Morris, and the Bangham models.

Copper was chosen not only because copper was found in the groundwater (Vaaramaa and Lehto, 2003), surface water (Neal and Robson, 2000) and industrial waste water (Chen et al., 2007b), but also due to the fact that the trivalent copper is rarely formed naturally (Eisler, 2007). Therefore, the oxidation of Cu^{2+} to Cu^{3+} is not a possible route of copper removal, hence the reactions occurred in the AUSF are expected to be somewhat different from that of the reactions for iron and manganese removal. The performances of the AUSF in removing metal (i.e. copper) at various operating conditions were then investigated.

The various operating conditions are those of different saturated conditions, heights of sand bed, flow rates, diameters of sand particles, input concentrations of copper, ratio of manganese to sand, and reusing times of sand bed material. The results obtained from the column studies (AUSF) were then compared to those from the batch studies.

From the study (e.g. investigating the performances of the AUSF in removing copper at different operating conditions), optimal operating conditions were obtained. Therefore, the study was extended to find out the performances of the AUSF in removing copper and other metals individually, including manganese, zinc and nickel; and in removing these mixed metals under those optimal operating conditions. Manganese, zinc and nickel were selected because they were found globally in ground and surface water as well as in industrial waste water (Neal and Robson, 2000; Vaaramaa and Lehto, 2003; Wang et al., 2007b; Halim et al., 2009). Zinc and nickel may also experience different reactions in AUSF from iron and manganese removal as they are divalent in solution (Eisler, 2007), thus the oxidation of Zn^{2+} and Ni^{2+} is not likely their route of removal.

Furthermore, to understand the capability of the AUSF in removing "real" wastewater, the AUSF was then examined to remove those metals from artificial electroplating waste water. The artificial waste water was used in this study to mimic the actual raw electroplating waste water examined in the study done by Wang et al. (2007b). This raw waste water was chosen due to it containing all the metals studied in this research.

Finally, the ability of a moderately simple fixed-bed model, known as the Bohart-Adams equation (Bohart and Adams, 1920), to describe the behaviour of the metals removal in the AUSF was studied. This model was employed as the model is simple and practical, yet the model can predict quantitatively the effects of major system variables on the column dynamics (Chu and Hashim, 2007).

1.2 Aim and Objectives

The aim of this research was to study the AUSF in order to treat waters contaminated by heavy metals up to the required standards (e.g. WHO guidelines), so as the community worldwide, particularly those living in the developing regions, could be benefited and used the waters safely for the daily life of the community.

The objectives of this research are thus:

1. To study the characteristics of AUSF i.e. the sand particles and sand bed characteristics.
2. To examine the sorption properties (equilibrium and kinetics) of manganese coated sand in removing copper through batch studies.
3. To investigate the performances of the AUSF in removing copper at different operating conditions.
4. To find out the performances of the AUSF in removing copper and other metals individually, such as manganese, zinc and nickel, under optimal operating conditions.
5. To develop possible mechanisms governing the removal of copper, manganese, zinc and nickel in the AUSF.
6. To study the performances of the AUSF in removing mixed metals (i.e. copper, manganese, zinc and nickel) under optimal operating conditions.
7. To investigate the performances of the AUSF in removing metals (i.e. copper, manganese, zinc and nickel) from an artificial electroplating waste water under optimal operating conditions.
8. To model the removal of copper, manganese, zinc and nickel in the AUSF using the Bohart-Adams equation.

1.3 **Scope and Limitations**

The scope of this study was:

- The characteristics of sand particles were those of the sand particles size (mm), surface area (m^2/g-sand), surface area morphology, surface bearing elements, resistance towards acid and alkali, point of zero charge (pH_{pzc}), effect on pH, porosity, and the amounts of manganese on the coated sand.
- The characteristics of sand bed were those of the flow hydrodynamic characteristics of the sand bed, i.e. the theoretical mean detention time ($\bar{t}_c$), the spread of the distribution (σ^2_c), the total mass of salt measured at the reactor effluent (m_{salt}), the degree of dispersion (d), the total voidage in the column (ε), the fraction of volume occupied by liquid to the total column volume (ε_L), and the fraction of volume occupied by the gas to the total column volume (ε_G).
- The sorption properties (equilibrium and kinetics) of manganese coated sand in removing copper in batch studies were observed by studying the effect of initial concentration, mass of sand, pH, DO content and manganese to sand ratio on the sorption of copper by manganese coated sand.
- Different DO contents, manganese to sand ratios, pH values, mass of sand, and initial copper concentrations investigated in batch studies were those of 0.29, 2.4, 8.95 and 17.08 mg/L, 0 and 0.0709 mgMn/gsand, 3 to 9, 5, 7.5, 10, 30, 50, and 100 g, and 6.87, 13.90, 17.98 and 23.32 mg/L respectively.
- The performances of the AUSF in removing metals were those of the percentage of metal removal (R), the time (t_{95}) at which the copper removal was 95%, the mass of copper retained in the sand column, the removal capacity (q), and the ratio of maximum metal adsorbed to the amounts of manganese (q_{Mmax}/q_{Mn}). The batch studies performances were R, t_{95}, m_r, q, and removal efficiency, E.
- The different operating conditions were those of various flow rates (81.91, 74.40, 55.01, and 37.78 mL/min); heights of sand bed (450, 350, 250 and 150mm); diameters of sand particles (0.850, 0.710, 0.500 and 0.400mm); input concentrations of copper (20, 15, 10, 5, 4, and 3 mg/L); ratio of manganese to sand (0.00, 0.0709, 0.1261 and 0.1341 mg-Mn/g-sand); and reusing times of sand bed material (0, 1, 2 times).

Whereas the limitations of this study were:

- The study was done under room (laboratory) temperature.
- The dissolved oxygen was only measured in batch studies.
- The Brunauer, Emmet, Teller (BET) method was only used for analysing 0.710mm uncoated, coated and copper bearing coated sand.
- The scanning electron microscopy (SEM)/energy dispersive X-rays (EDX) analysis was merely done for 0.710mm sand coated with 0.0709 mg Mn/g sand.
- The metal studied under different operating conditions was merely copper.
- The optimal operating conditions only covered optimal flow rate, height of sand bed, diameter of sand particle, and reusing times of sand bed material.
- The metals studied under optimal conditions were only copper, manganese, zinc and nickel.
- Artificial electroplating waste water was made to mimic the actual raw electroplating waste water investigated in the study done by Wang et al (2007b).

1.4 **Chapter Overview**

This thesis consists of eight chapters and the general overview of each chapter is depicted as follows. Chapter 1 is an introduction that describes the background as well as the aim and objectives of conducting this research. The scope of the research along with the limitations of the research is also defined. The overview of every chapter is also given to explain the content of the chapter, and to make this report well structured hence easier to be read and understood.

Chapter 2 reviews all the related literature for this research. The AUSF is explained first along with the characteristics of water worldwide, the elements and their levels to be treated by the AUSF in this research. The characteristics of each of these elements together with the removal technology of the element are then discussed.

The WHO guide line values for drinking water quality standard are displayed afterwards.

Then the AUSF and other technologies available to remove the studied metals are compared; and the conclusion as to why AUSF was considered as a potential technique to treat those studied elements is defined. Sand particles, sand bed characterisations and the methods available to analyse those characteristics are illustrated. Next, the analysis of the AUSF performance parameters is depicted. Then, the mechanisms that may involve in the removal of metals are identified followed by speciation. Fixed-bed modelling is described next together with the Bohart-Adams model. Finally, statistics as the method for analysing data is illustrated.

Chapter 3 describes the materials and methodology used in this research. First, experimental set up is illustrated in terms of sand preparation, batch studies and column built up. Following this, analytical methods are clarified. Finally, data analysis and modelling used in this research are identified.

Chapter 4 to 7 illustrate the data and results obtained within this study along with the analysis. Chapter 4 shows the data, results and analysis for sand particles and sand bed characterisation. Chapter 5 illustrates the removal of copper in batch and column studies and their comparison. The reactions that may be involved within the copper removal are assumed along with the copper speciation in water. Chapter 6 explains the removal of metals (copper, manganese, zinc and nickel), both individually and mixed, under optimal conditions. The removals of individual and mixed metals are also compared. The reactions that may be involved in the removal of those metals are then proposed along with the metal speciation in water. The removal of metals (copper, manganese, zinc and nickel) from artificial waste water is also described in this chapter. The comparison of metals removal between mixed metals under optimal conditions and in artificial waste water is also shown.

Chapter 7 shows the use of Bohart Adams equation (Bohart and Adams, 1920) to model the removal of copper at various conditions as well as individual metal under optimal conditions.

Finally, Chapter 8 provides the conclusions and recommendations made in this work.

CHAPTER 2

LITERATURE REVIEW

This chapter reviews all the related literature for this research. The activated unsaturated sand filtration (AUSF) and the reactions occurred within the AUSF, the characteristics of water worldwide, the elements and their levels to be treated by the AUSF, the characteristics of each of these elements, the comparison of AUSF and other technologies available to remove the studied metals, and the conclusion as to why AUSF was considered to treat those studied elements are described. In addition, sand particles and sand bed characterisations are explained along with the methods available to analyse them. The analytical methods used in this study, the AUSF performance parameters and their analyses are also defined. Furthermore, the reactions that may be involved in the removal of metals, fixed-bed modelling and Bohart-Adams model are explained. Finally, the statistics of one of the methods to analyse the results are illustrated.

The activated unsaturated sand filtration (AUSF) along with the reactions occurred within it the AUSF are first described below.

2.1 Activated un-saturated sand filter (AUSF)

The activated un-saturated sand filter (AUSF) studied first by Paramarta et al (1988) is a filter which utilized granular media, and run in a certain way, so as to assure that this media is not inundated in the water being filtered. This single unit system, which united the aeration and filtration process on the sand filter media, was utilized to remove iron and manganese without a sedimentation process. They used the term of *dry sand filter* as in this system, the inter particle's void of the sand media was always filled with air, as water that passed through the filter was regulated, so as the capacity of the water was smaller than this void could contain.

This condition could then assure the aeration process to occurr, and produce iron and manganese precipitates which could then be filtered. In this work, the term of *un-saturated sand filter* is preferably used than *dry sand filter*. Paramarta et al (1988) also used the term of *activated sand* filter as the filter used sand media that was soaked in $KMnO_4$ solution to activate the filter media. By combining those terms together, this filter is then called an *activated un-saturated sand filter (AUSF).*

Paramarta et al (1988) only used one sand size (uniform), but three different studies carried out afterwards used different sand sizes, both uniform and stratified and even mixed with zeolite (Rachmawati et al., 2004; Rachmawati et al., 2006a; Rachmawati et al., 2006b).

All of those studies used quartz sand and different input artificial raw water concentrations ranging from 3 to 10 mg/L iron and manganese. However, Paramarta et al (1988) did not mention their flow capacity as Rachmawati et al (2004; 2006a; 2006b) did i.e. 0.185 L/sec, 0.389 L/sec. In addition, they all used the Indonesian Department of Health water standard quality. They all tested iron and manganese level in the water. More over, they all used PVC as their laboratory model filters. The sizes were 4 and 6 inch diameter filled with sand of 600 and 1000 mm height. The height of the filter was 1500 mm.

In their findings, they all agreed that the reduction of iron and manganese decreased as their input concentrations increased, the filter depth required to remove iron and manganese increased as the input concentrations increased, the reduction of iron and manganese increased as the filter depth increased. The filter was also economic as the filter cost only about 60% of the government region (Bandung, West Java, Indonesia) water supply company cost (Rachmawati et al., 2006a). Furthermore, iron and manganese were found to be reduced as to meet the water quality standard and further reduced to almost 0 mg/L by the filter.

2.2 Mechanism of the processes occurring within the AUSF

2.2.1 Iron

Paramarta et al (1988) stated that there were two reactions occuring in the AUSF for removing iron. First was oxidation. Soluble ferrous ion (Fe^{2+}) was oxidized to insoluble ferric ion (Fe^{3+}) as follows (Kirby and Brady, 1998):

$$Fe^{2+}_{(aq)} + ¼\ O_{2\,(g)} + H^{+}_{(aq)} \rightleftarrows Fe^{3+}_{(aq)} + ½\ H_2O_{(l)} \quad \text{....(Equation 2.1)}$$

The rates of this oxidation (by air) increased with pH and at pH 7, 90% ferrous iron was converted to ferric iron (Tekerlekopoulou et al., 2006). Oxygen was derived naturally in AUSF by designing the filter accordingly so as natural air could pass through the filter easily.

Second was precipitation. The ferric ion was then precipitated to become ferric hydroxide as follows (Kirby and Brady, 1998):

$$Fe^{3+}_{(aq)} + 3\ H_2O_{(l)} \rightleftarrows Fe\ (OH)_{3\,(s)} + 3\ H^{+}_{(aq)} \quad \text{....(Equation 2.2)}$$

This reaction was depended on pH, and at pH = 7 - 8 iron precipitates (Tekerlekopoulou et al., 2006). The ferric hydroxide was then filtered by the filter media (sand) so as the filtrate (effluent water) was free of iron. By using $KMnO_4$ (pH > 7), the reaction followed was very fast (5 min) (Kawamura, 2000; Guan et al., 2009)):

$$3\ Fe^{2+}_{(aq)} + [MnO_4]^{-}_{(aq)} + 7\ H_2\,0_{(l)} \rightleftarrows 3\ Fe(OH)_{3\,(s)} + MnO_{2\,(s)} + 5\ H^{+}_{(aq)} \quad \text{..(Equation 2.3)}$$

2.2.2 Manganese

The reactions that occurred in the AUSF for removing Mn were similar to those for Fe (Paramarta et al., 1988). First was oxidation.

Soluble manganous ion (Mn^{2+}) was oxidized to insoluble manganic manganese (Mn^{4+}) as follows:

$$Mn^{2+}_{(aq)} + 1/2\ O_{2\,(g)} + 2\ H^{+}_{(aq)} \rightleftarrows Mn^{4+}_{(aq)} + H_2O_{(l)} \quad \text{.....(Equation 2.4)}$$

Second was precipitation; the manganese (IV) was next precipitated to become manganese dioxide as follows:

$$Mn^{4+}_{(aq)} + 2\ H_2O_{(l)} \rightleftarrows MnO_{2\,(s)} + 4\ H^{+}_{(aq)} \quad \text{.....(Equation 2.5)}$$

The reaction was dependent on pH (pH >9) (Katsoyiannis and Zouboulis, 2004). The filtrate was free of manganese as the manganese dioxide was then filtered by the sand. By using $KMnO_4$ (pH > 7), the following reaction was very fast (5 min) (Van Benschoten et al., 1992):

$$3\ Mn^{2+}_{(aq)} + 2\ [MnO_4]^{-}_{(aq)} + 2\ H_20_{(l)} \rightleftarrows 5\ MnO_{2(s)} + 4\ H^{+}_{(l)} \quad \text{.....(Equation 2.6)}$$

Below are the description of water and the impurities of the water. The worldwide ground and surface water as well as industrial waste water discharge characteristics are also described. The elements discussed are only those of the studied elements i.e. copper, manganese, zinc and nickel.

2.3 Water and the impurities

The quality of water rests on the physical, chemical and biological characteristics of the water. There is no absolutely pure water found in nature (Al-Layla et al., 1978; McGhee, 1991). The impurities in water are the result of contact with the air, soil and wastewater from both of domestic and industrial areas (Al-Layla et al., 1978).

2.3.1 Worldwide ground water characteristics

Impurities found in ground water rest on the characteristics of the underground strata (Al-Layla et al., 1978). Table 2.1 shows that manganese, copper, zinc, and/or nickel occurred in the ground water worldwide.

2.3.2 Surface water characteristics worldwide

Impurities present in the surface water (rivers, lakes and ponds) rest on the watershed. The river body receiving water from nearby domestic and/or industrial areas may contain substances derived from the effluents of those domestic and/or industrial activities. Table 2.1 depicts that either copper, manganese and/or zinc occurred in the surface water in Indonesia and/or UK.

2.3.3 Industrial waste water discharge characteristics worldwide

Table 2.1 illustrates that industrial waste water discharge contained copper, manganese, zinc, and/or nickel.

2.4 Elements and their concentrations to be removed by AUSF

Copper, manganese, zinc and nickel were studied in this work as they are commonly found in ground water, surface water and industrial waste water. Table 2.1 shows the concentrations of copper, manganese, zinc, and nickel to be treated in the ground water, surface water, and industrial waste water.

2.5 Technologies capable of removing these metals

There are many alternatives to remove these metals, nevertheless, WHO (2006) described a qualitative ranking of treatment processes with regards to their degree of difficulty. Simple chlorination and plain filtration (rapid sand, slow sand) were both in rank 1. Pre-chlorination followed by filtration, and aeration were both in rank 2.

Table 2.1 Elements to be treated and their concentrations worldwide

Element	Concentration (mg/L)		
	Ground water	Surface water	Industrial waste water
Copper	0.0278-0.19476 (1), 0.0156-0.0741 (2)	<0.02 (3), 0.002437-0.007294 (4)	0.6 and 0.2 (5), 0.1 (6), 20.3 (7), 11.780 (8)
Manganese	1.00 (9), 0.5 (10), 0.5 (11), 0.025-1.08 (1), 0.179-1.928 (2), 0.15-1.76 (12)	0.0037-0.2586 (4)	0.38-7.53 (13), 0.061 (8)
Zinc	0.03547-0.105 (1), 0.254-3.085 (2)	0.02 (3), 0.00493-0.03704 (4)	0.2 (6), 0.6135 (8)
Nickel	0.00085-0.00291 (1)		0.7 (6), 94.2 (7), 0.81 (8)

Notes:
(1) Finland's wells water (Vaaramaa and Lehto, 2003)
(2) Bangladesh's ground waters (Halim et al., 2009)
(3) Cikembang River in Purwakarta, West Java (Indorama, 2003)
(4) (dissolved) Studies conducted in the UK for the water quality of rivers draining into the North Sea from the eastern UK (Neal and Robson, 2000). The data cover rivers ranging from the rural Tweed in southeastern Scotland, to the urban and industrially impacted Wear and Humber rivers in the north and central England and two agriculturally impacted rivers in the south of England-Great Ouse and Thames
(5) Effluent samples (decantation pool (DP) and acidic mine drainage (AMD) effluent samples) collected from the intense coal mining operations held in Sider'opolis, Southern Brazil (Laus et al., 2007)
(6) Waste water from a nonferrous company after a neutralisation and precipitation process (Diels et al., 2003)
(7) Wastewater acquired from a local electroplating facility in northern Taiwan (Chen et al., 2007b)
(8) Electro plating waste water in China (Wang et al., 2007b)
(9) Ground water in Bandung, Indonesia (Paramarta et al., 1988)
(10) Raw (tap) water of Louisiana, USA (Teng et al., 2001)
(11) Korean's ground water (Choo et al., 2005)
(12) Ground water in the in the city of Avellaneda and Las Garzas in the province of Santa Fe, Argentina (Pacini et al., 2005)
(13) Textile effluent in Islamabad (Ali et al., 2009)

Rank 3 was occupied by chemical coagulation and process optimization for control of disinfection by products (DBPs). Granular activated carbon (GAC) treatment and ion exchange (IE) were in rank 4, followed by ozonation in rank 5, and advanced oxidation processes and membrane treatment in rank 6 respectively. The more difficult the technical plant/operation and the more expensive the treatment, the ranking will be higher.

Apart from the ranking of treatment processes shown by the WHO above, chemical precipitations, ion-exchange, reverse osmosis and solvent extraction were the usual techniques to remove metal ions from water. Nevertheless, there were drawbacks of applying these processes, for instance, partial metal removal, excessive reagent and energy necessity, toxic sludge or other waste production requiring disposal (Sekhar et al., 1998).

Below are the characteristics, occurrences, applications, effects and exposure pathways of each element studied along with the technologies capable of treating these elements. Manganese was described first as manganese was studied before using the AUSF. Then nickel, copper and zinc were reviewed.

2.5.1 Manganese

2.5.1.1 Characteristics, occurrences, applications, effects and exposure pathways of manganese

Elemental manganese is a transition metal located in Group 7B in the periodic table of elements (Kotz, 2006). Manganese exists in a number of different oxidation states ranging from 0 to +7, yet manganese is nearly always occurred in the oxidation state of +2, +3, and +4 state naturally. Manganese (II) is easily soluble in water; whereas manganese (III) is more unstable and likely to precipitate or dissociate to manganese (II) or manganese (IV) unless if chelators (ligands that form coordinate bonds with a single central atom) are present. Manganese (IV) is insoluble and easily noticed by the occurrence of a brown or black precipitate that is visible in neutral solutions (Tekerlekopoulou et al., 2008).

The oxidation of manganese (II) to manganese (IV) only by aeration is a slow process and much more difficult than iron unless the pH is increased > 7 (Tekerlekopoulou and Vayenas, 2007; Tekerlekopoulou et al., 2008).

Manganese is used in batteries (Kotz, 2006; USATSDR, 2009) and as a significant part of steel (Winter, 2009), of some ceramics, pesticides, fertilizers, and nutritional supplements (USATSDR, 2009). Manganese is an inorganic naturally occurring element (WHO, 2006; USATSDR, 2009).

Manganese is an essential trace element for the human body (USATSDR, 2009; Winter, 2009) as manganese is required for the development and functioning of the brain (Atsushi, 2003), for the normal functioning of several physiological processes, i.e. macromolecular metabolism (Hernandez-Bonilla et al., 2011), for the utilisation of vitamin B (Winter, 2009), and acts as a coenzyme that assists a range of metabolic processes in the body (Atsushi, 2003; Hernandez-Bonilla et al., 2011).

Excess of manganese, however, can lead to neurological disorders (USATSDR, 2009; Hernandez-Bonilla et al., 2011) similar to Parkinson's disease (Atsushi, 2003) and was linked to lower the cognitive performance of the children (Hernandez-Bonilla et al., 2011); while lack of manganese may affect manganese homeostasis in the brain and leads to convulsions (Atsushi, 2003). Therefore, the recommended daily intake (RDI) for manganese was set at 5 mg/day (Lenntech B.V., 2009). Ingestion of contaminated ground or surface water, dermal contact (USATSDR, 2009), and inhalation (Hernandez-Bonilla et al., 2011) are identified as the pathway exposure of manganese for human.

Manganese contributes to water hardness (Al-Layla et al., 1978; Alley, 2007). The WHO guideline value for manganese is 0.4 mg/L which is four times above the acceptability threshold of manganese. Manganese is in fact generally tolerable to consumers at below 0.1 mg/L. Nevertheless, beyond that, manganese presence in water supplies results in unpleasant taste and odours, and colours sanitary fixtures and laundry. Above 2.0 mg/L, manganese may accumulate as deposit in the drinking water distribution system (WHO, 2006). The precipitates of manganese are generally more difficult to remove than those of iron (Alley, 2007).

2.5.1.2 Manganese removal

Manganese can be removed basically through 3 methods: 1) Precipitation and filtration, 2) Ion exchange (IE), and 3) Stabilization with dispersing agents. The last one is usually limited to systems without filtration, and manganese water content is less than 1 mg/L (Al-Layla et al., 1978).

Three systems are used in the precipitation and filtration method (Al-Layla et al., 1978). The first and most common system uses aeration followed by sedimentation (short contact method) then filtration (Al-Layla et al., 1978; Logsdon et al., 1999; Chinn, 2003). For complete oxidation of manganese (and iron), this short detention time has to be provided although the precipitates are locked in the filter surface (not settled) and even when chlorine and potassium permanganate as strong oxidants are employed. Besides oxidizing manganese, aeration reduces the CO_2 content of groundwater hence raising the pH value (Al-Layla et al., 1978). Aeration generally occurs in a contact reactor (Sarikaya, 1990). A sedimentation tank and/or filter are then required after the aerator to remove manganese.

The second system basically is a chemical precipitation where the precipitation system employs chlorine, chlorine dioxide, potassium permanganate, ozone, or lime ($Ca(OH)_2$) and lime-soda ($Ca(OH)_2$–Na_2CO_3) softening (Al-Layla et al., 1978; Logsdon et al., 1999; Chinn, 2003; WHO, 2006). In this system, a retention tank is used followed by filtration and no aerator is employed (Al-Layla et al., 1978; Chinn, 2003; WHO, 2006). Chemical precipitation can also remove nickel (Fu et al., 2007). Lime softening may also remove nickel and zinc (Noyes, 1994a; Logsdon et al., 1999). Coagulation is merely a type of chemical precipitation. Following coagulation, dissolved air flotation (DAF) can also be used instead of sedimentation. After DAF, filtration is then employed (Logsdon et al., 1999).

The third system uses calcined magnesite (MgO) to oxidize manganese (and iron). This compound together with diatomaceous earth are located before a rapid mix tank (Al-Layla et al., 1978) with 5-10 minutes contact time, then passed through a diatomaceous filter (Al-Layla et al., 1978; Broder and Byron, 2005) or a precoat filter (Logsdon et al., 1999).

The second method employs ion exchange (IE) (Al-Layla et al., 1978; Noyes, 1994b; Vaaramaa and Lehto, 2003). IE resins can effectively discard manganese (and iron) when they are less than 5 mg/L and when there is no dissolved oxygen. Higher concentrations may reduce the effectiveness of the resin due to the oxide precipitates of these metals resulting in saturation of the resin, therefore two modifications have been employed i.e. an intermittent regeneration process and a continuous process using manganese treated greensand (zeolite) as the oxidant and the filter media (Al-Layla et al., 1978).

In the first process, water passes through the mineral bed and manganese (and iron) is oxidized. The major weaknesses of this process are economic and manganese leakages near the end of the cycle. Huge quantities of potassium permanganate ($KMnO_4$) are needed to regenerate the manganese treated greensand as well as huge volumes of water to wash the excess potassium permanganate from regenerated greensand (Al-Layla et al., 1978). In the second process, potassium permanganate is put in continuously to the filter consisting of anthracite coal filter media and manganese treated greensand. The potassium permanganate in solution oxidizes manganese (and iron) better than the manganese treated greensand that both serves as a reserve oxidant and a filter (Al-Layla et al., 1978).

Besides treating manganese and iron, IE can also treat copper (Vaaramaa and Lehto, 2003), nickel (Noyes, 1994b; Logsdon et al., 1999; Alyuz and Veli, 2009; Dizge et al., 2009; Nilchi et al., 2009), and zinc (Logsdon et al., 1999; Alyuz and Veli, 2009).

The third method generally uses sequestering agents such as sodium silicate (Chinn, 2003), sodium tripolyphosphate or sodium hexametaphosphate, that will tie up metals like manganese (and iron) and keep them in solution. There are disadvantages of using these agents. First, they do not perform better in stabilizing the precipitates so as they have to be put in before the manganese and iron oxidized. Second, once the water is heated, polyphosphate reverts to orthophosphate and does not disperse manganese (and iron) anymore (Al-Layla et al., 1978).

Other methods can also be used to treat manganese as follows.

Chemical coagulation, magnetic seeding and high gradient magnetic filtration were used to treat manganese (and iron) as well as zinc and copper in waste waters until below Japan's effluent standards (Terashima et al., 1986). The whole processing operation was claimed to be faster than the usual chemical precipitation. This process is, however, basically the same as that of chemical precipitation described above.

Manganese can also be treated by adsorption using: (a) dead waste such as chicken feathers (Sayed et al., 2005); (b) carbon nano tubes (Shamspur and Mostafavi, 2009); (c) naturally occuring materials such as clinoptilolite (Erdem et al., 2004; Doula, 2006); and (d) surface modified adsorbents such as ferric chloride impregnated granular activated carbon (GAC-Fe) (Mondal et al., 2007) and Clinoptilolite–Fe oxide (Doula, 2006; 2009). Clinoptilolite (Erdem et al., 2004) and Clinoptilolite–Fe oxide (Doula, 2009) can also be used to treat copper and zinc.

Choo et al (2005a) studied the removal of various levels of manganese (and iron) together with chlorine dosages from lake water used for drinking water by employing different ultra-filtration (UF) membrane systems. Manganese can be removed as well by employing reverse osmosis, electrodialysis, activated carbon adsorption (Erdem et al., 2004) and hollow fiber micro-filter (Teng et al., 2001b).

A biological process is also employed to treat manganese as follows: By using (a) bio filter such as trickling filters (Pacini et al., 2005; Tekerlekopoulou and Vayenas, 2007) and biological filtration column (Stembal et al., 2005; Burger et al., 2008)); and (b) sulphate reducing bacteria (SRB) (Medircio et al., 2007).

The removal of manganese (and iron) from ground waters in northern Croatia studied by Stembal et al (2005) used quartz sand coated with a naturally formed layer of MnO_2 and a bio-film consisting microorganism as filter media. Although this method used bio-filters as the filter media, the method basically employed aeration, sedimentation and filtration processes.

2.5.2 Nickel

2.5.2.1 Characteristics, occurrences, applications, effects and exposure pathways of nickel

Nickel is a transition metal located in Group 8B in the periodic table of elements (Kotz, 2006). Metallic nickel is a hard and silvery white metal. Nickel commonly exists in two oxidation states i.e. 0 and +2, yet other oxidation states of -1, +1, +3 and +4 can also occur (Eisler, 2007).

Nickel comes into the environment naturally and through human activities. Nickel's cycle occur in the environment resulting from chemical, physical and biological processes (Eisler, 2007). Nickel is reportedly vital for normal growth of several species of microorganisms, plants, animals and humans (Eisler, 2007; Fu et al., 2007); however, there is no proof of a nickel deficiency syndrome or that nickel is vital for humans (Eisler, 2007).

Human sources of nickel are mining, smelting, refining, electroplating (Eisler, 2007; Fu et al., 2007; Yang et al., 2009), fossil fuel combustion (Eisler, 2007; Carvalho et al., 2008) and waste incineration activities. Natural sources of airbone nickel are soil dust, sea salt, volcanoes, forest fires, and plants exudates. Industrial and municipal waste discharge transport nickel into near water body. The releasing of nickel from wastewater to natural waterways is occurred due to nickel is difficult to remove by treatment process (Eisler, 2007).

Metallic nickel is used to manufacture stainless steel and other nickel alloys with high corrosion and temperature resistance. These alloys are employed in ship building (Eisler, 2007), coins (Kotz, 2006; Dizge et al., 2009), kitchenware, electronics, electroplating, battery, inks, jewellery, pigments, zippers, detergents, and ceramics. Some nickel compounds are preferably used for example, in nickel cadmium battery (Eisler, 2007) used in calculators and similar devices (Carvalho et al., 2008).

Nickel is seldom found naturally in the elemental form (Alley, 2007); generally nickel occurs in nature as oxide and sulphide ores (Wentz et al., 1998).

Metallic nickel is insoluble in water, soluble in dilute nitric acid or aqua regia and slightly soluble in hydrochloric acid (Eisler, 2007).

Three natural sources of nickel occur in surface waters are particulates from rainwater, dissolution of primary bedrock material and from secondary soil phase. In waters, nickel is present in the form of soluble salts that are adsorbed onto clay particles, organic or other matters. In natural waters, nickel occurs largely as the octahedral, hexahydrate ion $(Ni(H_2O)_6)^{2+}$ at pH 5-9. Nickel nitrate is less soluble in water (45.0 g/L). Although nickel produces strong, soluble complexes with OH^-, SO_4^{2-} and HCO_3^- these species are insignificant compared with hydrated Ni^{2+} in surface and ground water. The occurrence of nickel in fresh and marine water is influenced by the pH, ionic strength and the availability of solid surface for adsorption (Eisler, 2007).

Pathway exposure of nickel is through ingestion, inhalation and skin contact (Eisler, 2007; Dizge et al., 2009). The chemical and physical forms of nickel and salts of nickel highly affect biovailability and toxicity. Nickel compounds usually are of low hazard once ingested. Ingestion of nickel is high compared to other trace metals due to nickel existing in utensils and food processing machinery. Toxic effects of nickel to humans are identified for respiratory, gastrointestinal, dermal, neurological and reproductive systems, to name a few (Eisler, 2007). Metallic nickel and nickel salts are relatively non toxic once ingested due to homeostatic mechanisms that rule nickel metabolism and limited intestinal absorption. The most generally identified toxic reaction to nickel and nickel compounds in humans is through skin contact. Nickel absorption onto the skin is increased by sweat and detergents. A reaction of dermatitis (that leads to vesicular hand eczema) occurs in persons sensitive to nickel once a minimal contact is formed. Nickel is the main allergen for women. The amount of nickel in drinking water may be raised resulting from the corrosion of nickel-containing alloys and nickel-plated faucets employed in the water distribution system (Eisler, 2007). The WHO identifies nickel compounds as human carcinogen and metallic nickel as possible human carcinogen (Eisler, 2007; Dizge et al., 2009); yet, this carcinogen classification is applied once humans are exposed through respiratory route.

Generally, nickel is not considered as an immediate threat to plants, animals and humans at environmentally exposure levels, except for nickel carbonyl. Lack of nickel is not concerned due to daily ingestion usually above 170.000μg of nickel. Nickel usually occurs in human tissues. Nickel occurs in abundant quantities in tea, cereals, vegetables and fish. The solubility of nickel increases with an increase in acidity (Eisler, 2007).

Considering the above effects, the RDI for nickel was then set < 1mg/day (Lenntech B.V., 2009). Meanwhile, the health-based guideline value for nickel in drinking water is 0.07 mg/L. It should be noted that increasing pH to prevent corrosion of other materials may decrease the leaching of nickel in water (WHO, 2006).

At the cellular level, nickel impedes the enzymatic function of manganese and zinc. Binding of nickel to DNA is reduced by salts of copper, manganese and zinc. Individual metal is less toxic than mixtures of metals (copper, zinc, arsenic etc.) containing nickel salts to fish. Nickel toxicity is reduced by treating with zinc, which is likely occurred by competition between these metals in binding to DNA and proteins. Substitution between these metals is possible as ionic nickel has a similar ionic radius to Zn^{2+} (Eisler, 2007).

2.5.2.2 Nickel removal

Other than those technologies described in other technologies and manganese removal, nickel can be also treated as follows. Reverse osmosis and electrodialysis (ED) reversal can be used to treat nickel as well as zinc (Logsdon et al., 1999). Electro-coagulation using aluminium electrodes could also be used to treat nickel (2+), copper (2+), and zinc (2+) (Heidmann and Calmano, 2008). Granulated lime ($Ca(OH)_2$) and calcium carbonate ($CaCO_3$) were also proved well to be used as coagulants to treat nickel and zinc from ground water (Lee et al., 2007). This method was, however, basically used coagulation process as chemical precipitation method.

Furthermore, nickel could be removed by adsorption using (a) naturally occurring materials i.e. natural absorbents (Choksi and Joshi, 2007), chitosan (Paulino et al., 2007); (b) surface modified absorbent i.e. silylated clays (Carvalho et al., 2008), activated carbon (Ghaedi et al., 2007), thiourea-modified magnetic chitosan microspheres (Zhou et al., 2009b); and (c) carbon nanotubes (Yang et al., 2009); (d) waste i.e. grape stalks wastes (Villaescusa et al., 2004); and (e) biosorption using algae (Chen et al., 2008).

Despite being able to remove nickel, some of those technologies could also treat other metals. Activated carbon (Ghaedi et al., 2007), thiourea-modified magnetic chitosan microspheres (Zhou et al., 2009b), grape stalks wastes (Villaescusa et al., 2004) and algae (Chen et al., 2008) were also able to treat copper.

2.5.3 Copper

2.5.3.1 Characteristics, occurrences, applications, effects and exposure pathways of copper

Copper is abundant in the environment and vital for normal growth and metabolism of all living organisms (Kotz, 2006; Eisler, 2007; Zhou et al., 2009a). Copper deficiency is regarded as a nutritional deficiency; while excess in copper intake may become acutely toxic. Copper occurs naturally as un-combined metal and in many minerals. Copper discharges to the environment mainly from anthropogenic activities (Eisler, 2007) i.e. mining and smelting, industrial activities, municipal wastes and sewage sludge (Eisler, 2007; Wang et al., 2007a; Bouzid et al., 2008; Zhou et al., 2009a). Natural sources of copper are those of sea salt sprays, windblown dusts, volcanogenic particles and decaying vegetations (Eisler, 2007). Copper compounds are extensively used as biocides and in fertilizers, in electrical equipment, in pipe, in machinery, in veterinary and medical products, in the food industry, as a preservative of wood and other materials, and in coin manufacture (Kotz, 2006; Alley, 2007; Eisler, 2007). Copper is a transition metal located in Group 1B in the periodic table of elements (Kotz, 2006). Copper has an atomic number of 29 and is a soft heavy metal.

Copper is present in four oxidation states i.e. Cu^0, Cu^{1+}, Cu^{2+} and Cu^{3+}. The cupric ion (Cu^{2+}) is the one commonly found in water. In solution, cupric ions are co-ordinated with six water molecules. Although the free cupric ion is mainly readily available and toxic inorganic species of copper in freshwater, seawater and sediment interstitial waters, the free cupric ion is susceptible to complexation and is less available to aquatic biota if natural organic chelators and high salinities occur. Cupric ions occur as total dissolved copper for approximately 1% in seawater and < 1% in freshwater. Trivalent copper (Cu^{3+}) is not likely to be occurred in nature (Eisler, 2007).

Copper interacts with several compounds generally occurring in natural waters. The amounts of the various copper compounds and complexes occur in solution, and the solubility of copper salt in freshwater are affected by water pH and temperature, to name by a few. The chemical form of copper in freshwater is essential to control geochemical and biological processes; however, there are doubts about the characteristic of known copper species due to insufficiencies in information about the adsorption characteristics of most cupric ion complexes. $Cu(CO_3)_2^{2-}$ and $CuCO_3$ are the main chemical species of copper in freshwater. Although ionic copper (Cu^{2+}) and some copper hydroxyl species are regarded as highly toxic to aquatic life, these carbonato species are much less toxic than other copper complexes. At pH < 6 cupric ion is the major toxic copper species. Cupric salts dissolve eagerly in freshwater to form the aquo ion, $Cu(H_2O)_6^{2+}$. Divalent copper carbonate will precipitate from solutions or produce colloidal suspensions once cupric ions occur in excess; while copper nitrate is extremely soluble in water (Eisler, 2007).

Copper is part of some important enzymes responsible for melanin (mainly responsible for determining human skin colour) production, cathecolamine (hormones produced in response to stress) production, free radical detoxification and iron conversion (Eisler, 2007).

The toxicity of copper in the complexed, precipitated or adsorbed form of copper is not as much as the free ionic form. Copper homeostasis is important in preventing copper toxicity. The competition for binding sites with zinc may interfere with copper absorption in mammals.

The pathway for the entry of copper is through ingestion and inhalation. Wilson's disease and Menkes' syndrome are two inherited human diseases that correspond to abnormal copper metabolism. Menkes' syndrome is distinguished by a progressive brain disease and abnormally low copper levels in the body's organs. This syndrome has the same symptoms as those of copper deficiency. Wilson's disease is the only important example of copper toxicity in humans (Eisler, 2007). Wilson's disease is a rare inherited disorder in which copper present excessively in the body's tissues (National Centre for Biotechnology Information, 2011). Hepatic, renal lesions and haemolytic anemia are systemic manifestations of Wilson's disease. Nevertheless, there is no proof that persons with normal metabolism are exposed to any chronic degenerative disorder caused by copper poisoning. Uncommonly vulnerable humans to copper poisoning are those suffered with Wilson's disease, infants and children under one year old, those with liver disruption and chronic renal disease, and those undergoing dialysis (Eisler, 2007).

In mammals, copper absorption is reduced by high input of zinc. Copper and copper compounds are not carcinogenic. Foods that are especially rich in copper are oysters, beef and lamb livers, nuts, dried vine and cocoa. Copper occurs in every tissue analysed in humans (Eisler, 2007).

Lack of copper may result in slow growth, hair loss, anemia, weight loss, edema, immune response disruption, detraction of the nervous system, decreased fetal absorption and finally death (Kotz, 2006; Eisler, 2007). Excess exposure to copper in drinking water may cause vomiting, diarrhea, stomach cramps, nausea, greenish or bluish stools and saliva (Eisler, 2007); and may have severe effect in the brain and liver of people with Wilson's disease (Eisler, 2007; Bojic et al., 2009). Deliberately elevated intake of copper may cause liver (Eisler, 2007; Wang et al., 2007a; Bouzid et al., 2008) and kidney damage, and sometimes death, particularly in children (Eisler, 2007). Considering the above effects the recommended daily intake (RDI) for copper was thus set at 2 mg/day (Lenntech B.V., 2009).

Copper is also toxic to aquatic organisms, even at extremely low levels (Wang et al., 2007a; Bouzid et al., 2008), for example 0.1–0.2 mg/L of copper (II) are lethal to fish (Zhou et al., 2009a). Meanwhile, copper in drinking water may raise the corrosion of galvanized iron and steel fittings.

This in turn may blue or green stain sanitary fixtures and laundry (for level of copper above 1 mg/L), lead to tasty but acceptable water (if it is about 2 mg/L) and make water blue and produce objectionable taste (if it exceeds 5 mg/L) (WHO, 2006). Long term consumption of water consisting 2.2–7.8 mg/L Cu(II) may result in stomach pain, vomiting and hepatocirrhosis (liver disruption) (Zhou et al., 2009a). Adverse effect of copper occurs in human infants at drinking water concentrations > 3.0 mg/L (Eisler, 2007). The WHO has therefore set the health-based guide line value for copper in drinking water at 2 mg/L (WHO, 2006).

2.5.3.2 Copper removal

Other than those technologies described in other technologies, manganese, and nickel removal, copper can be treated with technologies shown as follows. For that of IE method, copper can be treated using cationic exchange resin (Hamdaoui, 2009; Jha et al., 2009) and using natural zeolites (Calvo et al., 2009). Copper can be removed as well by co-precipitation (Khosravi and Alamdari, 2009).

Copper can also be treated by membranes, i.e. (a) highly porous chitosan/cellulose acetate blend hollow fiber membranes (Liu and Bai, 2006); (b) anion exchange membrane (Noyes, 1994b); and (c) by ultra filtration (Petrov and Nenov, 2004; Cojocaru and Zakrzewska-Trznadel, 2007).

Electrochemical process can also be used to treat copper as follows: by (a) photo reduction (electrochemically using UV lamp) (Canterino et al., 2008); (c) electrolysis with an ultrasonic field (Farooq et al., 2002); and (d) by spontaneous reduction–coagulation using micro-alloyed aluminium composite (MAlC) (Bojic et al., 2009).

Three flotation systems have been used to treat copper i.e. (a) ion flotation using xanthates as flotation collectors, (b) precipitate flotation producing copper hydroxide, and (c) sorptive flotation employing zeolites as sorbent material (Lazaridis et al., 2004).

Copper can also be removed by adsorption (Bouzid et al., 2008; Papageorgiou et al., 2009) using (a) naturally occurring materials such as bentonite (Eren and Afsin, 2008), zeolite (Panayotova, 2001), kaolinite (Alkan et al., 2008), and phosphate rock (Sarioglu et al., 2005); (b) surface modified adsorbents such as acid activated bentonite (Eren and Afsin, 2008), manganese oxide coated bentonite (Eren, 2008), modified zeolite (Panayotova, 2001), manganese oxide coated sand (Lee et al., 2004), manganese oxide coated zeolite (Han et al., 2006b), activated clay (Chen et al., 2007a), DETA-functionalized polymeric adsorbent (Liu et al., 2008); (c) waste such as fly ash (Papandreou et al., 2007; Wang et al., 2007a), water clarifier sludge in a fluidized-bed reactor (FBR) (Lee et al., 2006), nitrifying biofilm from an ultra-compact biofilm reactor (UCBR) (Lee et al., 2008), vegetal compost (Gibert et al., 2005), red mud (Nadaroglu et al., 2009), dried sunflower leaves (Benaissa and Elouchdi, 2007), dry plant leaves (mulch) (Salim and Abu El-Halawa, 2002), furnace slag (Xue et al., 2009); and (d) biosorption using microorganism (Zhou et al., 2009a), biomass (Solisio et al., 2006), and seaweeds (Murphy et al., 2007).

Despite treating copper, some of those technologies are also able to treat other metals. For instance, natural zeolites can also be used to treat zinc and lead (Calvo et al., 2009). Vegetal compost (Gibert et al., 2005) and MAlC (Bojic et al., 2009) are also able to remove zinc. Furnace slag can also be used to treat zinc, cadmium and lead (Xue et al., 2009).

2.5.4 Zinc

2.5.4.1 Characteristics, occurrences, applications, effects and exposure pathways of zinc

Zinc is a transition metal that is located in Group 2B in the periodic table of elements (Kotz, 2006). Zinc is a bluish-white metal which dissolves easily in high acidity. Zinc occurs as a sulphide, oxide or carbonate naturally. Zinc is divalent in solution and can produce hydrated Zn^{2+} in acids and zincated anions (possibly $Zn(OH)_4^{2-}$) in strong bases (Eisler, 2007).

Zinc is majorly used in the manufacture of noncorrosive alloys, brass, and in galvanised steel and iron products (Datta and Sarkar, 2005; Eisler, 2007) and for the negative plates in some electric batteries (Sarkar et al., 2007). Zinc experiences oxidation on the surface, hence keeping underlying metal from damage. Galvanised products are majorly employed in construction materials, automobile parts and households' utensils (Eisler, 2007). Zinc is also used in coins (Kotz et al, 2006). In humans, zinc is employed in the treatment of zinc deficiency, several skin diseases, wound and pain healing (Eisler, 2007). Moreover, a variety of zinc salts are applied in wood preservatives, accelerators for rubber vulcanisation, fertilizers, ceramics, textiles, and pigments (Perez-Quintanilla et al., 2009).

Zinc is released to the environment largely from human activities. Significant sources of these activities are electroplating, smelting, and mining activities, domestic and industrial waste water, combustion of fossil fuels and solid waste (Eisler, 2007; Perez-Quintanilla et al., 2009).

Dissolved zinc in aquatic environment generally contains the toxic aquo ion ($(Zn(H_2O)_6)^{2+}$) and several organic and inorganic complexes. These aquo ions and other toxic species have highest effects under low pH, low dissolved oxygen and high temperatures. Zinc ligands are soluble in neutral and acidic solutions, thus in most natural waters, zinc is mobile. Zinc mobility in waters is affected by dissolved iron and manganese levels, pH, concentrations of complexing ligands, and the concentration of zinc. Zinc is most soluble in low pH and low alkalinity (Eisler, 2007).

In water, the free zinc ion is believed to coordinate with six water molecules to form the octahedral aquo ion $(Zn(H_2O)_6)^{2+}$ without the presence of other complexing or adsorbing agents. Zinc occurs generally as the aquo ion at pH = 4 - 7 in fresh water (Eisler, 2007).

At pH = 6, the major forms of dissolved zinc are the free ion (98%) and zinc sulphate (2%); at pH = 9, the major forms are the monohydroxide ion (78%), zinc carbonate (16%) and the free ion (6%). 90% of zinc exists as aquo ion and the remaining are $ZnHCO_3^+$, $ZnCO_3$ and $ZnSO_4$ in river waters (Eisler, 2007).

Soluble chemical species of zinc are mainly bioavailable and toxic to aquatic organisms. The aquo ion is the most toxic and predominates over other dissolved species; yet the concentrations of the aquo ion reduce as alkalinity and salinity are raised, and at pH > 7.5. Suspended $Zn(OH)_2$ is moderately non toxic; while suspended $ZnCO_3$ is possibly toxic, yet the toxicity of suspended $ZnCO_3$ reduces under conditions suitable to zinc hydroxide production. $ZnCO_3$ is the predominant species at high pH and high alkalinity and only about < 1% of the dissolved zinc at low pH and low alkalinity (Eisler, 2007).

In solution, zinc is adsorbed by inorganic adsorbing agents such as hydrous oxides of manganese. Formation of zinc-ligand complexes raises the solubility of zinc and is likely to increase the adsorption of zinc. An increase in pH results in zinc sorption to particulates regardless the level of water salinity or hardness. The majority of zinc discharged into waters is sorbed onto hydrous iron and manganese oxides and finally separated into the sediments. Sorption to sediments was insignificant at pH < 6, yet this sorption was complete at pH > 7 (Eisler, 2007).

Zinc is an important trace element for all living organisms (Datta and Sarkar, 2005; Kotz, 2006; Eisler, 2007; Bojic et al., 2009). Zinc is a substance of many metalloenzimes and other metabolic compounds; and is essential in the metabolism of proteins and nucleic acids, and for the synthesis of DNA and RNA (Eisler, 2007; Sarkar et al., 2007). Zinc is abundant in read meat, milk, egg yolks, shellfish, liver, whole grain cereals, peas, beans and rice (Eisler, 2007).

Zinc deficiency in humans seems impossible as zinc is ubiquitous in the environment; nevertheless, zinc-associated dwarfism and hypogonadism (occurs once sex glands produce little or no sex hormones) in adult males are proven (Eisler, 2007). Lack of zinc may also result in delayed sexual maturation in adult males; disruption of growth of hair, skin and bone; impaired vitamin A metabolism, abnormal immune function and taste acuity (Kotz, 2006; Eisler, 2007).

High level of administered zinc limits copper uptake in humans. Human zinc intoxication may result from consuming lengthy storage of acidic foods or beverages in galvanised containers. The recommended daily allowance of zinc was that set at 15.00 mg Zn/day (Eisler, 2007).

Although there are many health problems associated to zinc, there is no health concern for zinc at levels usually occurring in water; thus no health-based guideline value has been set. However, there are some effects of zinc to water as follows. Zinc produces an objectionable taste to water at taste threshold level at around 4 mg/L. In addition, water consisting zinc at level above 3-5 mg/L may look 'opalescent' and create an oily film in heating. Even though drinking water with zinc level above 0.1 mg/L is rare, the concentration of zinc in tap water may be by far higher due to the use of zinc in older galvanized plumbing fixtures (WHO, 2006).

2.5.4.2 Zinc removal

Other than those technologies described in other technologies, manganese, and copper removal, zinc can be also treated as follows. Zinc could be treated by IE using clin-Fe system (Dimirkou, 2007). In addition, zinc could be removed by adsorption using (a) naturally occurring materials i.e. chinese loess (Tang et al., 2009) (b) surface modified adsorbents i.e. pillared clays (Guerra et al., 2008), lateritic clay (Sarkar et al., 2007); and (c) synthetic material i.e. mesoporous silica (Perez-Quintanilla et al., 2009).

Elemental concentrations to be treated and their guideline values are then depicted in Table 2.2.

Below is the comparison between AUSF and other technologies available to remove the studied metals. Conclusions are defined afterwards as to why AUSF was considered potential to remove the studied metals.

Table 2.2 Elements concentrations to be treated and their guideline values

Targeted element	Input concentrations (mg/L) (*)			Guide -line value (ppm)	Acceptable threshold level (ppm) (**)
	Groundwater	Surface water	Industrial wastewater		
Manganese (Mn),	0.025-1.928	0.0037-0.2586	0.061-7.53	0.4 (C)	< 0.1 mg/l : tolerable > 0.1 mg/l: tasted objectionable in beverages, colored sanitary fixtures etc > 2 mg/l: produces a black layer precipitate on pipes
Copper (Cu),	0.0156-0.19476	0.00101 9-0.02	0.1-20.3	2	> 1 mg/l: staining of laundry etc 2 mg/l: tasty acceptable water
Zinc (Zn),	0.03547-3.085	0.00493-0.03704	0.2-0.6135		4 mg/l (as zinc sulphate): objectionable taste to water > 3-5 mg/l: 'opalescent' water, oily film in heating
Nickel (Ni),	0.00085-0.00291	0.00031-0.04537	0.81-94.2	0.07	

Notes:
(*) Summarised from Table 2.1
(**) (WHO, 2006)
C: at levels below the guideline value, it may affect the appearance, taste or odour of water thus resulting in consumer complaints (WHO, 2006)

2.6 Comparison between AUSF and other technologies available to remove the studied metals

Table 2.3 summarises the technologies used to remove the studied elements. Table 2.3 shows that aeration, sedimentation and filtration system were used to remove manganese.

Table 2.3 Other technologies to remove the analysed elements

Flotation			√		
Oxidation/reduction		√			
Coagulation-flocculation				√	√
	Electrolysis		√		
	Spontaneous reduction–coagulation		√	√	
	Electrocoagulation		√	√	√
Electrochemicall process	Photo reduction		√		
	Sulfate reducing bacteria (SRB)	√			
Biological process	Trickling /bio filters	√	√	√	
	Anion/cation exchange membrane		√		
	Ultrafiltration	√	√		
	Electrodialysis	√		√	√
	hollow fiber micro-filter	√	√		
	Reverse osmosis	√	√	√	√
Membrane process	Membrane process	√	√	√	√
	Synthetic materials (Synthetic goethite, amorphous aluminium oxide, chelating resins		√	√	
	Carbon nao tubes	√			
	Naturally occurring materials (sea nodule, chitosan,, dolomite powder	√	√	√	√
	Biosorption		√		√
	Surface-modified adsorbents	√	√	√	√
	Waste (dead industrial biomass,chicken feathers, ash, orange peels, dry plant leaves (mulch), furnace slag	√	√	√	√
Adsorption	Adsorption	√	√	√	√
Solvent extraction		√	√	√	√
Stabilization with dispersing agents		√			
Ion exchange		√	√	√	√
	Calcined magnesite, manganese	√			
	Chemical precipitation	√	√	√	√
Precipitation and filtration	Aeration, sedimentation,	√			
Element		Manganese	Copper	Zinc	Nickel

Note: Concluded from Section 2.5

AUSF similarly used precipitation and filtration method that was aeration followed by sedimentation then filtration. AUSF also used sand as filter media, and potassium permanganate to activate the filter media. Moreover, AUSF combined those 3 processes, i.e. aeration, sedimentation and filtration, in one single unit. Although there were similarities of method, processes, and media between AUSF and others stated in Section 2.5, AUSF, however, had a unique technology i.e. using "dry sand". In addition, there is no aerator used in the AUSF, there was simply natural air designed to come through the AUSF.

All the studied metals could be treated by chemical precipitation as depicted from Table 2.3. Similarly with the chemical precipitation system, AUSF used potassium permanganate. There is a significant difference between the AUSF and this system, however, as this system do not use oxygen as an oxidant (no aeration process) (Al-Layla et al, 1978), while in the AUSF, oxygen plays an important part to reduce manganese and iron (Equation 2.1 and 2.4). Moreover, the chemical precipitation system usually uses separate sedimentation and filtration tank unit (Al-Layla et al, 1978), whereas AUSF simply used one tank that unites aeration, precipitation and filtration process.

Calcined magnesite, manganese dioxide/birm or diatomaceous earth is used to treat iron and manganese as shown in Table 2.3. AUSF, on the other hand, did not use these substances; rather AUSF used air or oxygen along with potassium permanganate to reduce iron and manganese. In addition, there was no rapid mix tank employed in the AUSF as that used in the diatomaceous earth system (Al-Layla et al, 1978); AUSF simply combined all processes in one single unit.

IE could remove all the studied metals as described in Table 2.3. However, there is a significant difference between IE and AUSF, as oxygen was the most important element in the AUSF, while IE resins could effectively operate once there was no dissolved oxygen (Al-Layla et al, 1978).

In addition, despite the similarity of using potassium permanganate, yet this potassium permanganate was applied differently in AUSF and IE methods.

In IE, the potassium permanganate was not only used to soak and regenerate the sand but also put in solution into the treated water, while in AUSF, the potassium permanganate was only used to soak and activate the sand. Moreover, although IE could be used to remove the studied metals, the higher cost of IE and the much more complicated technology compared to AUSF (WHO, 2006), surpasses the IE's benefit.

Stabilization with dispersing agents could treat iron and manganese as shown in Table 2.3. AUSF is much better to remove iron and manganese compared to the uses of sequestering agents, as AUSF could treat these substances up to 10 mg/L each, while sequestering agents were usually limited to systems with iron and manganese water content < 1 mg/L (Al-Layla et al, 1978). In addition, using these agents would prevent iron to precipitate, which is definitely opposed to AUSF as in AUSF iron was objected to precipitate in order to be further filtered.

Solvent extraction could remove all the studied metals as depicted in Table 2.3. Although solvent extraction was usually applied to reuse/recover the solvent chemicals, the incomplete separation of solvent extraction results in a post treatment which is required afterwards (Noyes, 1994c). Moreover, solvent extraction was mostly appropriate to only remove solutes in high concentrations due to for extremely dilute solutions the cost of power becomes highly expensive (Lazaridis et al, 2004). Hence, compared to AUSF, solvent extraction is much more expensive and difficult to perform.

All the studied metals could be treated by adsorption as can be seen in Table 2.3. Although the most effective technique for removing heavy metals is that of adsorption, the high cost of the adsorption technique in providing adsorbents, particularly those of activated carbon, outweighs the benefit. However, this is overcome by using natural materials as adsorbents. These natural adsorbents were claimed to be cheap, efficient for dilute concentrations, generating little sludge, not requiring additional nutrients and having the possibility of bio-sorbent regeneration and metal recovery (Lesmana et al, 2009).

Despite aeration, precipitation and filtration processes that claimed to occur in the AUSF, adsorption seemed to be also responsible in the AUSF's reaction process as the AUSF used sand that is activated by potassium permanganate. In this case, however, AUSF is much simpler in terms of the media preparation practically.

Membrane technology especially reverse osmosis, may remove all the studied metals as shown in Table 2.3. Compared to the use of membranes, however, AUSF that employed principally a simple aeration, precipitation and filtration method was much cheaper and easier to conduct (WHO, 2006). In addition, as membranes used very fine or small openings, they usually required careful pre-treatment in order to avoid fouling, such as that for reverse osmosis (Ning, 2005). AUSF, in the other hand, did not require such pre-treatment.

Table 2.3 depicts that almost all the studied metals except nickel could be treated by using biological process. Although biological process had the benefit of not requiring addition of chemicals and generating smaller quantity of sludge compared to that of chemical process (Tekerlepoulou and Vayenas, 2007), the biological process was, however, compared to AUSF, much more complicated and expensive to perform as this process required bacterial/microorganism handling.

Electrochemical processes could be used to remove iron, copper, zinc and nickel as shown in Table 2.3. These techniques had several benefits, such as did not require the addition of chemicals and produced smaller quantity of sludge compared to other conventional methods (Heidmann and Calmano, 2008). However, as these processes still required filtration as the next process, AUSF is much easier as AUSF unites three processes of aeration, precipitation and filtration in one tank.

Coagulation-flocculation can be used to treat zinc and nickel as depicted in Table 2.3. Compared to AUSF, however, coagulation-flocculation still required further treatment such as sedimentation and filtration to treat those metals. Thus, AUSF is considered much simpler as AUSF unites aeration, sedimentation and filtration in one single unit.

As all the studied metals could be treated by chemical precipitation, oxidation/reduction could thus treat manganese as well as shown in Table 2.3.

However, oxidation/reduction reactions usually produce precipitates. As a result, these reactions may hence not be applied alone and require further treatment processes. AUSF, in contrast, employed precipitation and filtration after the aeration (oxidation) processes. Therefore, AUSF is likely to be much more appropriate to remove manganese than that of oxidation/reduction method.

Copper could be removed by flotation as depicted from Table 2.3. However, flotation requires further treatment i.e. filtration. Hence, AUSF that unites aeration, sedimentation and filtration in one single unit is likely much simpler to perform than that of flotation method.

2.7 Conclusion

Many technologies are available for removing the investigated metals. Each technology has the benefits as well as the drawbacks. Therefore, choosing the best technology to treat the metals will depend on the raw water quality, the required quality of the treated water, the characteristics of the metals, the level of the metals to be removed and the resultant costs.

As chemical precipitation could be used to remove all the studied metals, AUSF that used precipitation as the basic principle may be employed to treat the metals. In addition, given the simplicity of the AUSF that unites aeration, precipitation and filtration in one single unit, and the low cost of AUSF; AUSF is likely to be applied for removing the studied metals.

CHAPTER 3

MATERIALS AND METHODOLOGY

Experiments on removing metals (i.e. copper, manganese, zinc and nickel) were done in order to achieve the aims and objectives outlined in Chapter 1. This chapter illustrates in detail the materials, equipment, experimental procedures, analytical methods as well as the data analysis and modelling that have been used in this research.

3.1 Experimental set up

3.1.1 Sand preparation

Quartz sand was used in this work as quartz sand was employed in the previous studies (Paramarta et al., 1988; Rachmawati et al., 2006a) and is generally and easily found worldwide. The filter media used in this research was natural, uncrushed silica sand fractions B (1.18mm-600μm) and C (600μm-300μm) (standard sand BS 1881-131:1998 from David Ball Specialist Sand, UK). There are mainly four processes involved in preparing the sand before being used as the media, i.e.: sieving, drying, soaking and washing. These processes are described below.

3.1.1.1 Sand sieving

Four sacks (total weight = 100 kg) of fractions B and C sand were sieved by using Russell Sieve (Russell Finex, Model 17300 Unit No. A 2347, Direct on line starter 5.5 KW – 415 V control). Appendix 3.1 shows the sieving procedure.

3.1.1.2 Sand soaking and drying

Activated sand was produced by soaking the silica sand with potassium permanganate ($KMnO_4$) 0.01 N for about 24 hours (Paramarta et al., 1988; Teng et al., 2001).

The detailed procedure to make activated sand is depicted in Appendix 3.2; whereas $KMnO_4$ solution was made according to the procedure stated in Appendix 3.3. $KMnO_4$ solutions were prepared using Milli-Q water (Q-H2O, Millipore Corp. with resistivity of 18.2mΩ_cm). $KMnO_4$ was purchased from Fisher Scientific, UK, and was of reagent grade (purity: 99%).

3.1.1.3 Sand washing

The activated sand was then cooled to room temperature and washed with Milli-Q water in order to free the sand from excess $KMnO_4$. The coated sand was then dried again at 105°C in an oven for about 24 hours (Paramarta et al., 1988; Teng et al., 2001a) then cooled to room temperature and stored in plastic containers before being used.

3.1.2 Batch studies

3.1.2.1 Equilibrium isotherms

Equilibrium isotherms were determined by conducting batch studies. A fixed mass of manganese coated sand (50 g) was contacted with 50 mL of copper solution (pH = 5) in 250 mL Fisherbrand conical flask. A range of copper concentrations (5 – 20 mg/L) were studied. The solution pH was adjusted using 1 M HNO_3 and NaOH solution. A series of such flasks (10 flasks) was then stirred using Innova 44 Incubator Shaker series (New Brunswick Scientific Co, Inc.) at a constant speed of 150 rpm and temperature of 25.6°C. At predetermined intervals of time (15 – 240 minutes), samples were taken and filtered through Millex GP Filter 0.22 μm Milipore Express PES Membrane using 10 mL Syringe BD Plastipak.

The filtrates were then diluted (four times) with milipore water and placed into 50 mL plastic tube Fisherbrand. Finally, the filtrates were analysed for copper concentration with Varian AA240FS Fast Sequential Atomic Absorption Spectrometry (Varian AA240FS AAS).

The equilibrium data were modelled with the Langmuir and Freundlich models. Five different linear types of the Langmuir isotherms and the linear form of Freundlich (Ghodbane et al., 2008) were used in this study.

3.1.2.2 Kinetics

Initial concentration of copper solution, manganese to sand ratio, mass of sand, pH and dissolved oxygen (DO) content was 20 mg/L, 0.0709 mg Mn/g sand, 50 g, 5, and 8.95 mg/L for all experiments respectively, except for those implemented to study the effect of these factors on the removal of copper by manganese coated sand. 50 mL of copper solution was stirred for 4 hours at 150 rpm and set at 25.6°C for all experiments. For kinetic studies, the batch method was employed due to the simplicity of the method (Ghodbane et al., 2008). The procedures for copper removal kinetic experiments were the same as those for equilibrium isotherms stated above in Section 3.1.2.1.

In the sorption experiments implemented to study the effect of pH, for pH $\geq$ 6, the solutions were filtered before shaking. This was done as based on theoretical calculations, copper of 20 mg/L might precipitate as hydroxides at pH 5.92 (Section 5.4).

Sorption experiments were also carried out to investigate the effect of sorbent dosage, dissolved oxygen (DO) content and the effect of coating the sand. For studying the effect of DO content on the kinetic of copper sorption by manganese coated sand, conical flasks were covered by double parafilm and tightened by selotape or wrist rubber to minimise the influence from the air. Nitrogen (N_2) gas was passed through the copper solution to remove oxygen until the targeted oxygen concentration was reached. N_2 gas (Oxygen free, Size W, purity: 99.998%) was obtained from BOC Gases. A needle valve was used to regulate the flow rate.

In order to obtain the DO level of 0.29 mg/L, N_2 gas (0.1 bar) was passed through the solution for 60 min. To achieve the DO level of 17.08 mg/L, pure O_2 gas (0.2 bar, 0.8 mL/min) was passed through the solution for 5 min. The O_2 gas cylinder was purchased from BOC Oxygen (Size W, purity: Oxygen = 99.5%). The sample was put on the magnetic stirrer (Fisher Scientific) and stirred at 150 rpm. The DO content was measured by Hach Luminescent Biochemical Oxygen Demand (LBOD) 101 probe connected to HQ30d portable meter.

In order to study the kinetics of adsorption of copper on the manganese coated sand, several kinetic models, such as pseudo-first-order, pseudo-second order, Bangham and intraparticle diffusion model of Weber and Morris were used. Pseudo-second order was evaluated using six different linear forms (Ghodbane et al., 2008).

3.1.3 Column built up

A schematic diagram of the AUSF is depicted in Figure 3.1. The filter used in this research was made of a QVF glass column of 40 mm internal diameter and 610 mm height. Sand was transferred into the column until the expected height (150, 250, 350, or 450 mm height) of the sand bed was obtained. Water was pumped from the 20L tank through a 5 mm diameter plastic hose to the filter. The filter was equipped with two perforated plates; one was placed at the top of the column and the other at the bottom. These perforated plates were utilized so as to provide air in the column naturally. The water was introduced at the top of the filter through a perforated plastic sheet in order to distribute water evenly through the cross sectional area at the inlet of the column. The perforated plate at the bottom was equipped with an aluminium screen (hole diameter: 2mm, thickness: 75mm) to support the sand bed and avoid the sand escaping the column. Sample collection was made at the outlet of the filter. Photographs of this AUSF along with the AUSF's accessories are shown in Appendix 3.4.

Filter media was arranged in uniform composition. The largest height of sand was 450 mm as the height of glass column was only 610 mm. There was a space provided between the top of the sand and the spray to allow a height fall for the water coming out from the spray. This height fall would provide a detention time.

This detention time was not only provided by the height fall but also by the journey through the void of the sand.

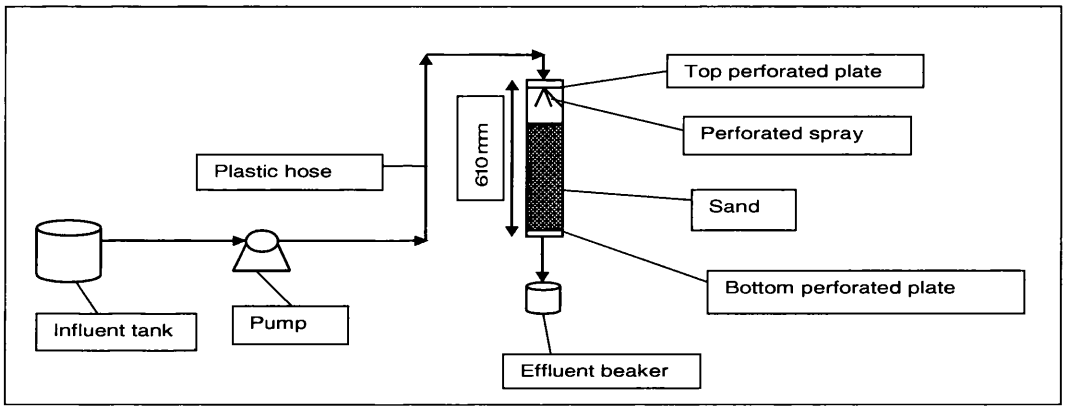

Figure 3.1 A schematic diagram of the AUSF

3.1.3.1 Flow arrangement

Before arranging the flow, the flow rate of pump had to be defined first as described in Appendix 3.5. The flow rate was then calculated as (Tchobanoglous et al., 2004):

Q (Flow rate, L/min) = V (Volume, L) : t (time, min)... (Equation 3.1)

For pump capacity calculation and flow rate regulation, a beaker of 5L volume is used replacing the input of 20L water tank in order to simplify the process. The pump used in this work was Tuthill Pump Serial No. 1224545, Model No. DGS.80PPVNN00000 (D- Series, magnetic coupled external gear pump, non-pulsing flow, positive displacement, leak free, accurate, chemical resistant, long life). Time was measured by a Fisherbrand Traceable Waterproof/Shockproof Stopwatch FB 70240.

Next, the porosity of sand was defined by the following procedures (water evaporation method). First, the sand was dried at 105 °C in an oven for about 12 hours (Bowles, 1979; Liu and Evett, 1997). After allowing the sand to be cool in room temperature (Liu and Evett, 1997), the sand was then placed in 500ml beaker and weighed. Next, the sand was saturated with water and weighed. The difference of weight between saturated sample and dried sample reflects the porosity (Foth, 1990).

The porosity was then calculated with (Foth, 1990):

% porosity = [[(wet weight-dry weight): density of water]: volume of sample] x 100%....(Equation 3.2)

Flow rate of the AUFS was measured as the water flows down the sand in the column. The procedure is basically the same as that for the pump capacity measurement and described in Appendix 3.6. The flow rate was then calculated with Equation 3.1.

Various input water flows were arranged so as the void was not fully filled with water. In order to measure the volume of water per volume of void, the amount of time passing through the AUSF had to be defined first. The procedure for measuring this is described in Appendix 3.7. Appendix 3.7 shows that t_1 (min) = time of water initially discharging from the spray, and t_2 (min) = time of water initially discharging from the filter (sand). The amount of time of water passing through the filter/sand is thus:

t (min) = t_2 (min) - t_1 (min).... (Equation 3.3)

The volume of water in the sand column can then be calculated as:

$$V = t * Q \text{ ..... (Equation 3.4)}$$

where: V = Volume of water in the sand (mL), t = time (min), and Q = flow rate of AUSF (mL/min).

As the volume of void in the sand column can be defined as:

$V_v = \varepsilon * V_s$ ....(Equation 3.5)

where: V_v = volume of void in the sand (mL), ε = porosity (%), and V_s = volume of sand column (mL),

and the volume of sand column can be calculated by:

$V_s = \pi r_c^2 H$.....(Equation 3.6),

where: r_c = radius of coloumn = 20 mm, and H = height of sand (mm).

Then the volume of water per volume of void can be calculated by:

V/V_v (%) = (V : V_v) *100%.....(Equation 3.7).

3.1.3.2 Elements and their concentrations arrangement

Four elements were studied in this research i.e. copper, manganese, zinc and nickel. These elements were investigated each of them specifically as a single element, and as multi elements mixed together. Copper, manganese, zinc and nickel were chosen as they were likely to be found globally in ground water, surface water and industrial wastewater as described in Section 2.3 and 2.4. In addition, as in nature the trivalent copper is hardly ever formed (Eisler, 2007); thus Cu^{2+} is not likely to be reduced to Cu^{3+}, hence the reactions occurred in the AUSF are expected to be rather different from that of the reactions for iron and manganese removal. The same case is applied as well to zinc and nickel as they are divalent in solution (Eisler, 2007), thus the oxidation of Zn^{2+} and Ni^{2+} is not likely their route of removal. For manganese, however, the processes occurred may be similar to those stated in Section 2.2.2.

All chemicals were purchased from Fisher Scientific, UK, and were of reagent grade. Each analyzed metal was made in solution (diluted in Milli-Q water (Q-H_2O, Millipore Corp. with resistivity of 18.2mΩ_cm)).

Copper, manganese, zinc and nickel solutions were prepared from copper (II) nitrate ($Cu(NO_3)_2.3H_2O$), manganese (II) nitrate ($Mn(NO_3)_2.4H_2O$), zinc (II) nitrate (Zn $(NO_3)_2.6H_2O$), and nickel (II) nitrate (Ni $(NO_3)_2.6H_2O$). The procedure to make, for instance, 20 mg/L copper solution is described in Appendix 3.8. Milipore water was used in all experiments. All solutions were prepared at initial pH and metal concentrations so that the solubility products of the metal hydroxides (p^cK_{so}) at 25°C = 19.66, 16.70, 15.00, 12.80 for $Cu(OH)_2$, $Zn(OH)_2$, $Ni(OH)_2$, and $Mn(OH)_2$ respectively (Table 6.3) were not exceeded to avoid precipitation.

Only copper was studied to find out the optimal conditions for AUSF as copper was assumed to be fairly representative for all the studied metals. Various concentrations of copper of 3, 4, 5, 10, 15 and 20 mg/L were used to find out the effect of input concentrations to the copper removal.

20 mg/L was selected as the maximum copper input concentration as this 20 mg/L copper was represented the waste water acquired from electroplating facility (Chen et al., 2007a). 3 mg/L was used as the minimum copper input concentration as the WHO guide line value for copper is 2 mg/L (WHO, 2006).

For the optimal conditions, 20 mg/L was then used as input concentration for all elements (copper, manganese, nickel and zinc), either as a single element or multi elements, as the value of 20 mg/L was thought to be fairly representative for mimicking the maximum value that might be encountered in waters (Table 2.1).

For artificial waste water, the concentrations of the elements were the same as the actual raw electroplating waste water examined by Wang et al (2007b). Considering this raw waste water contained all the metals (copper, manganese, nickel and zinc) studied in this research, this raw waste water was then selected to be used in this study. The concentration of copper, manganese, nickel and zinc in this waste water is 11.7800, 0.061, 0.6135 and 0.8100 mg/L respectively.

3.1.3.3 Water collection

Each sample was taken from the filter to be analyzed in terms of parameters' concentration.

3.2 Analytical methods

3.2.1 Characterisation of sand particles and sand bed

Characterisation of sand particles and sand bed is the initial essential step required in a process concerning sand particles in a bed column (Yang, 2005). The necessary characterisation of sand particles comprises those of the basic static parameters (such as size, surface area, surface area morphology, elemental analysis of sand particles, resistance towards acid and alkali, point of zero charge, effect on pH, and the ratio of manganese to the amounts of sand) and their dynamic conduct in relation to fluid flow (such as porosity); whereas the characterisation of sand bed includes the flow hydrodynamic characterisation.

3.2.1.1 Sand particles characteristics

a. Sand particles size

Sieve analysis was used to characterise particle size as sand particles were coarse. In addition, the sieve analysis offers a fairly accurate value for the mean particle size and is commonly used (Allen, 1975). Moreover, this analysis is relatively easy to be performed than that of gravity and centrifugal sedimentation techniques.

b. Sand particles surface area

The surface area of the prepared sand was investigated by the Brunauer, Emmet, Teller (BET) method and nitrogen adsorption at 77.3 K technique using NOVA 2000e Surface Area and Pore Analyzer interfaced with Quantachrome Instruments version 11.0 software. This equipment is basically run based on a continuous-flow gas-gravimetric method. The procedure for using this equipment is described in Appendix 3.9. d_{sand} for this analysis = 0.710 mm.

Degassing or surface cleaning to free the sample's surface from contaminants, such as water and oils, was done by inserting the sample in a glass cell and heating the cell under vacuum or flowing gas. The sample was then taken to a constant temperature by using an external bath. Small amounts of gas as the adsorbate are then passed into the evacuated sample chamber.

Gas molecules that attached into the surface of the solid (adsorbent) were thought to be adsorbed and were likely to produce a thin layer that coated the whole adsorbent surface. This resulting monolayer capacity (V_m) was then multiplied by the area occupied by one molecule to determine the samples' surface area (Quantachrome Instruments, 2011).

The BET equation used to calculate the surface area of sand is as follows (Allen, 1975):

$$\frac{P}{V\,(P_0 - P)} = \frac{1}{V_m\,c} + \frac{c-1}{V_m\,c}\,\frac{P}{P_o} \quad \text{.....(Equation 3.8)}$$

where: V = the volume of N_2 adsorbed at 77 K, V_m = the volume of N_2 necessary for the formation of a monolayer, P/P_o = the relative pressure, and c = the constant of BET equation.

A plot of $P/V\ (P_o - P)$ against P/P_o leads to a straight line with a slope of $(c - 1)/V_m\ c$. High values of c are important for precise V_m values. This resulted in the inclination for employing nitrogen at liquid nitrogen temperature as at liquid nitrogen temperatures with all studied solids, this gas shows high c values (Allen, 1975).

The resulting monolayer capacity (V_m) was then multiplied by the area occupied by one molecule to determine the samples' surface area as follows (Allen, 1975):

$S_w = \frac{N\ \sigma\ V_m}{M_v}$ .....(Equation 3.9).

where: S_w = specific surface area (m^2g^{-1}), N = Avogrado number (= 6.023 x 10^{23} molecules/g molecule), σ = area occupied by one adsorbate molecule (=16.2 x 10^{-20} m^2 for nitrogen), V_m = monolayer capacity (mL), and M_v = gram molecule volume (= 22410 mL).

$$Sw = \frac{(6.023\ x\ 10^{23})(16.2\ x\ 16^{-20})}{22410}\ V_m = 4.35\ V_m$$

for nitrogen at liquid nitrogen temperature.

c. Sand particles surface area morphology

Sand particles external surface area morphology are characterised by a scanning electron microscopy (SEM) (Hitachi S-4800 Type II). This type of instrument uses cold cathode field emission (CFE) electron source and 0.5-30kV voltage range. Samples for SEM were placed on a circular carbon film (9 mm diameter) and/or silver paint (Agar G302 quick drying silver paint, Agar Scientific, UK) to avoid influence of any charge effect and sample movement during the SEM operation.

For all SEM/energy dispersive X-ray scpectroscopy (EDX) experiments, 0.710mm diameter of sand was used; and for the coated sand, the ratio of manganese to sand used was 0.0709 mg manganese/g sand. Millipore water was used to make all the solutions except for the waste water bearing coated sand analysis inwhich tap water was used.

SEM is particularly useful to obtain images that have lots of surface relief such as those found on fracture surfaces. SEM basically works as follows (Figure 3.2). Field emission gun is generally used as the electron source (gun). The electrons are accelerated to an energy of 1-30keV so as they can travel towards and hit the sample surface. The electron beam is then demagnified by two or three condenser lenses until, as the beam heats the sample, the diameter of the beam is only 2-10nm. In older apparatus, the scan coils scan the fine beam of electrons across the sample; whereas, the number of low energy secondary electrons, or other radiation, revealed from each point on the surface are counted up by a detector. Simultaneously, the spot of cathode ray tube (CRT) is scanned across the screen, whereas the amplified current from the detector modulates the brightness of the spot. The similar effect is obtained in modern instruments by digitally managing the beam position on the specimen, and the resultant image is shown on a computer screen (Goodhew et al., 2001).

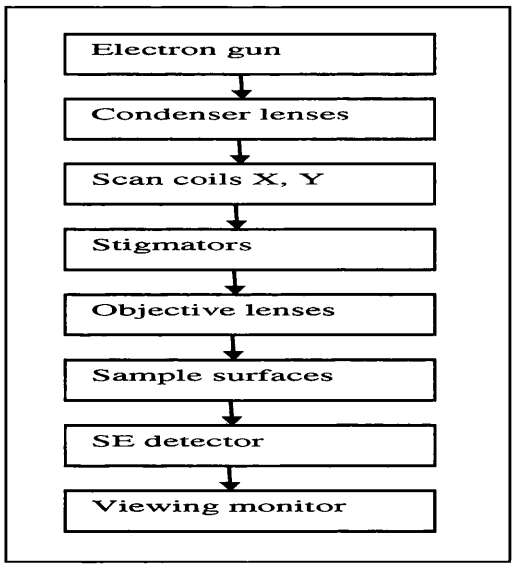

Figure 3.2 SEM components (Hitachi, 2002)

There are generally three types of signals produced once the electron beam hits the sample that are used in an SEM/EDX as shown in Figure 3.3.

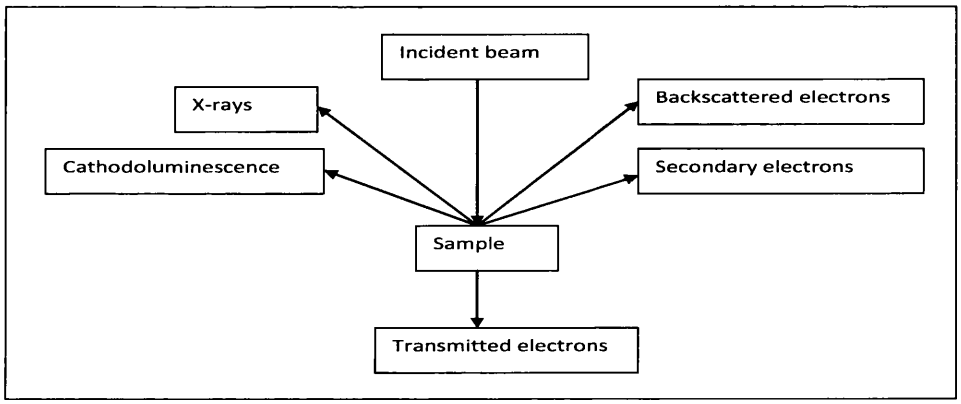

Figure 3.3 Signals produced in an SEM (Skoog et al., 2007)

The area the electrons go through the sample, or the volume within which approximately 95% of the primary electrons are absorbed, is known as the interaction volume. Even though radiation is produced within this volume; this radiation will not be identified unless the radiation escapes from the specimen. As X-rays are difficult to be absorbed, thus most of them escape. The backscattered electrons will not escape if they have gone through more than a fraction of a micrometer. The backscattered signal thus comes from a much smaller volume. The secondary electron signal comes from a section that is on the order of the diameter of the incident electron beam. Secondary electron signals are thus able to produce much higher spatial resolution than the other signals, and are the most extensively used signals in the SEM system (Skoog et al., 2007). Figure 3.4 shows the interaction volume and the regions from which each type of SEM signal arises.

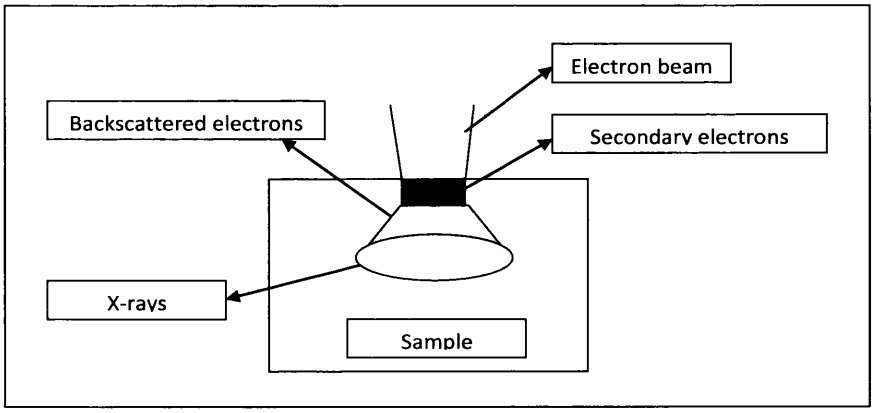

Figure 3.4 The interaction volume and the volumes from which each type of SEM signal is generated (Skoog et al., 2007)

d. Elemental analysis of sand particles

The distribution of elemental concentrations for the sand samples was investigated using the SEM of the same instrument as stated above in 3.2.1.3 equipped with the Energy Dispersive X-ray Spectroscopy (EDX) of Oxford Instruments interfaced with INCA Energy Software. SEM/EDX was chosen because of the availability of the SEM/EDX as well as the SEM/EDS provides not only images but also qualitative and quantitative analysis on the surface of the solid sample. Qualitative analysis was carried out through spectra analysis, mapping analysis and line scanning. Quantitative analysis was also performed by the SEM/EDX eventhough this analysis was extremely difficult due to several factors such as atomic number effect, absorption effect and fluorescence effect to name it in a few (Goodhew et al., 2001).

The identification of element in SEM/EDX is carried out as follows. If a localized electron has been ejected from an atom, the atom is in an excited or high energy state. Once the vacant electron state is filled, the atom will relax, releasing the excess energy as a secondary effect. A secondary effect is an effect brought by the primary beam which can be identified outside the sample. The characteristic X-ray is emitted once a single outer electron filled the inner shell vacancy (Figure 3.5). The difference between the energies of the two excited states is thus the energy of the X-ray. This X-ray energy is distinctive for the particular atomic species and the wavelength of this X-ray can be measured as follows (Goodhew et al., 2001):

$\lambda = \frac{h_P c}{\Delta E}$ ....(Equation 3.10)

where: λ = X-ray wavelength (A^0 or m), h_P = Planck constant = 6.63 x 10^{-34} Js, c = velocity of light (m/s), and ΔE = the energy difference between two excited states (J).

These energy and wavelength are dissimilar for each atomic species and by identifying them, the elements which must have been contained in the specimen can be defined. This is actually the foundation of analytical electron microscopy and electron probe microanalysis (Goodhew et al., 2001).

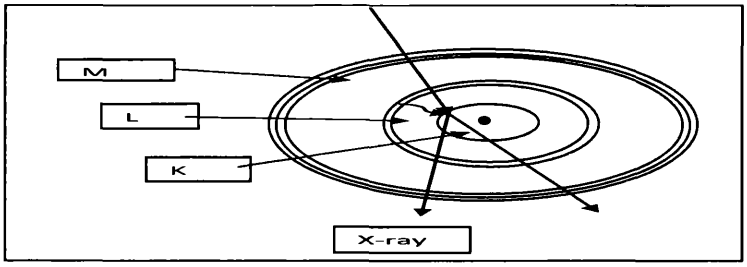

Figure 3.5 Emission of a characteristic X-ray (Goodhew et al., 2001)

EDX or Energy dispersive analysis (EDS) is employed to obtain X-rays data (Goodhew et al., 2001). The detector commonly contains a small piece of semiconducting silicon or germanium held in such a position so that as many as possible of the X-rays generated from the sample fall upon this piece. The detector has to be located in the line of sight of the sample as X-rays cannot be deflected. Thus in a SEM, this detector usually is placed in the same position as the secondary electron detector. In addition, the silicon has to be practicably close to the sample so as many X-rays as possible can be collected. A simplified energy-dispersive analysis system is shown in Figure 3.6.

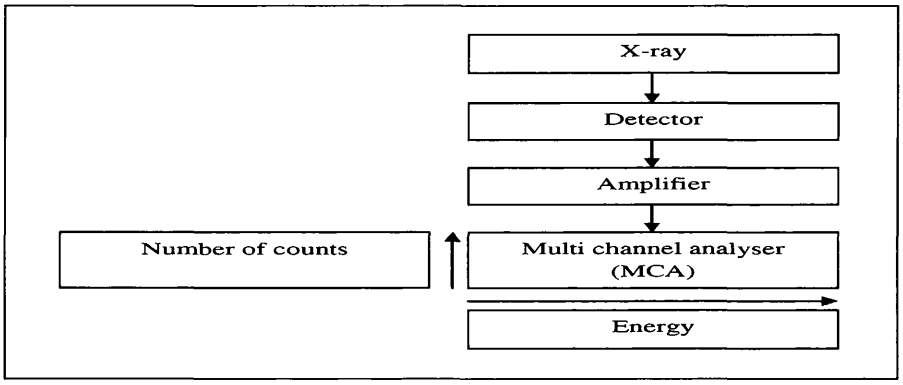

Figure 3.6 Energy-dispersive analysis system (Goodhew et al., 2001)

The EDX spectra are illustrated using x and y axis. The x axis shows the energy (keV) of the emitted X-rays; while the y axis illustrates the intensity of the X-rays. Table 3.1 depicts the energy and associated wavelength of the strongest K, L and M lines of the elements. The most efficient generation of X-rays commonly happen once the energy of electron beam are approximately three times the X-ray energy. As Table 3.1 shows that all elements have at least one strong X-ray line with energy < 10keV, the analysis for all elements using a SEM with 25-30keV energy would be no difficult at all (Goodhew et al., 2001).

Table 3.1 The energy and related wavelength of the strongest K, L and M lines of the elements (Goodhew et al., 2001)

Element	Atomic number Z	Relative atomic mass	Kα1		Lα1		Mα1	
			E_e (keV)	λ (nm)	E_e (keV)	λ (nm)	E_e (keV)	λ (nm)
Carbon	6	12.0	0.28	4.47				
Oxygen	8	16.0	0.52	2.36				
Magnesium	12	24.3	1.25	0.99				
Aluminium	13	27.0	1.49	0.83				
Silicon	14	28.1	1.74	0.71				
Sulphur	16	31.1	2.31	0.54				
Chlorine	17	35.5	2.62	0.47				
Potassium	19	39.1	3.31	0.37				
Calcium	20	40.1	3.69	0.34	0.34	3.63		
Manganese	25	54.9	5.90	0.21	0.64	1.94		
Iron	26	55.8	6.40	0.19	0.70	1.76		
Nickel	28	58.7	7.48	0.17	0.85	1.46		
Copper	29	63.5	8.05	0.15	0.93	1.33		
Zinc	30	65.4	8.64	0.14	1.01	1.23		
Molybdenum	42	95.9	17.48	0.07	2.29	0.54		
Gold	79	197.0	68.79	0.02	9.71	0.13	2.12	0.58

Quantitative analysis results of SEM/EDX are revealed in a table showing the percentage by weight (weight%) and the percentage by number of atoms (atomic%) of each of the elements detected. The letter K (e.g. Si K) after each element relates to the characteristic K shell X-ray wavelength due to the energy emitted by an electron jumping from one shell to an inner shell of the atom. Each element can produce a number of characteristic peaks, but usually only the strongest is examined (Goodhew et al., 2001). The process by which the atomic % of each element is determined is shown in Figure 3.7 and described as follows. The peak shapes of the sample spectrum and the standard profiles are compared and are adjusted to the same resolution. A digital top hat filter then removes backgrounds from the sample spectrum and standard profiles. A least square routine is then used to fit the standard profiles to the sample spectrum. The apparent concentration is then calculated as follows (Oxford Instruments, 2009):

$$Apparent\ concentration = \frac{Intensity\ sample}{Intensity\ of\ standard} \times Weight\%\ Standard \quad \text{.....(Equation 3.11)}$$

Fit indices are then calculated and are a means of the fitting performance of the standard profiles to the sample spectrum.

Intensity correction using XPP correction method (Pouchou and Pichoir, 1991) is then used to correct the apparent concentration. XPP means *x*-coordinates of image corrected by pixel projection method (Fahim, 2009). XPP has a good quality under conditions of difficult absorption i.e. the analysis of light elements in a heavy matrix and for samples that are tilted with regard to the electron beam. An iterative process is used in order to obtain the apparent concentrations as the correction factors are affected by the composition of the sample. The apparent concentration is employed to get a first estimate of correction. This correction is then put into the apparent concentration to obtain a first estimate of element weight%. This estimate is next applied to obtain a second estimate of correction. This second estimate is then applied to the apparent concentration to get a second estimate of element weight%. This iterative process runs continuously until consecutive estimates in weight% differ by less than 0.1%. In short, weight% is roughly calculated by dividing the apparent concentration by the intensity correction. The atomic% is then calculated by dividing the weight% with the atomic weight (Oxford Instruments, 2009).

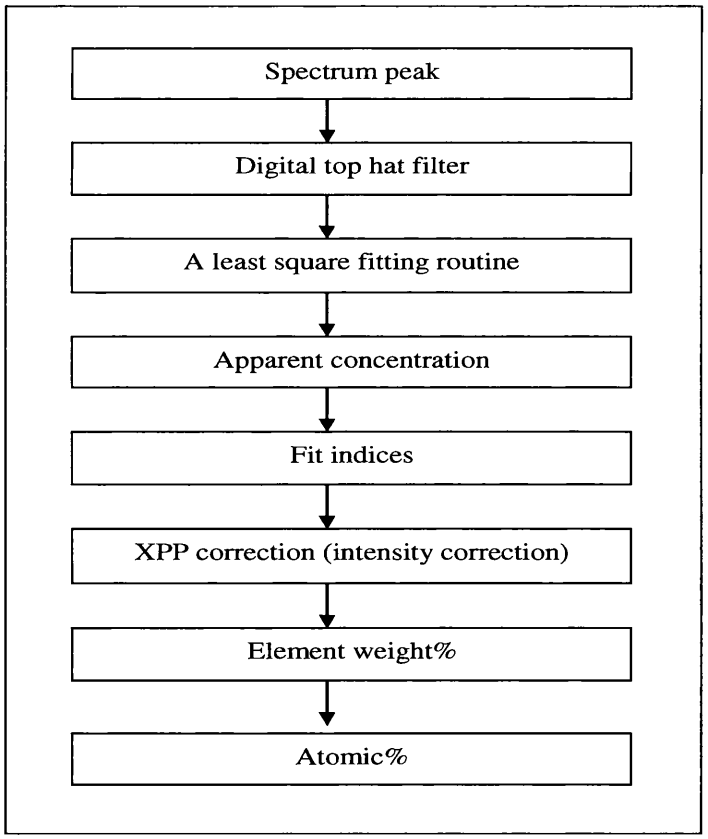

Figure 3.7 The schematic process of elemental analysis by EDX (Oxford Instruments, 2009)

e. Sand particles resistance towards acid and alkali

The characteristic of sand particles may change resulting from the exposure of the sand particles towards acid and/or alkali condition.

At some points (usually measured by the pH of the sand particles), the sand particles may retain the virgin/previous properties of the particles, yet by adding acid and/or alkali solutions, the sand particles may lose the previous characteristics of the particles (usually the intrinsic elements of the sand particles or any elements under studied) (Hu et al., 2004).

Acid and alkali resistance tests were carried out by soaking the $KMnO_4$ coated sand in Milli-Q water at room temperature for 24 hours at pH values adjusted in the range 2 to 11 ± 0.1 using nitric acid (HNO_3) and sodium hydroxide (NaOH) (Hu et al., 2004). Samples were put on the magnetic stirrer (Minor 2, Voss Instruments Ltd, Maldon Essex) and shaked at a speed adequate enough (7 – 8) to mix the samples. The samples were taken after 24 hours and analysed with FAAS. The procedure of acid and alkali resistance tests is shown in Appendix 3.10. pH was measured using Jenway 3540 pH meter. 3 g of 0.710 mm diameter of sand with 0.0709 mg manganese/g sand was used for these experiments.

f. Sand particles point of zero charge

The point of zero charge is a suitable index to measure the tendency of the surface of the particle to become either positively or negatively charged as a function of pH (Noh and Schwarz, 1989).

pH drift i.e. mass titration (Noh and Schwarz, 1989) was used to determine the point of zero charge (pzc) of sand particles. Briefly, the method involves adding certain amounts of sand (0.01%, 0.1%, 1%, 5%, 10%, 20%, 30%, 40%, 50% and 60%) to Milli-Q water in a beaker. This beaker was sealed and placed on a shaker for 24 hours. The resulting pH values were measured at the end of the experiment. The shaker and pH meter used were the same as those used in Section 3.2.1.1.e.

The detailed procedure of determining the pzc of sand particles is shown in Appendix 3.11. 0.710 mm diameter of sand with 0.0709 mg manganese/g sand was used for obtaining the point of zero charge.

g. Sand particles effect on pH

The effect of sand particles on pH was measured by passing through milipore water and copper solution to the filter column containing uncoated or manganese coated sand. Sand particles effect on pH was studied using d_{sand} = 0.710mm, H = 450 mm, m_{sand} = 881.46 g, Q = 80.69 mL/min. The $m\ Mn/\ m\ sand$ = 0.0709 mg/g for the coated sand.

h. Sand particles porosity

The measurement of porosity of sand particles was discussed in Section 3.1.3.1.

i. Manganese content on coated sand

The amount of manganese on the surface of the coated sand was measured through acid digestion analysis. The principle of the digestion process is to release the metal from the solid matrix to the acid solution during extraction process (Guven and Akinci, 2011). The procedure of acid digestion analysis is described in Appendix 3.12. Briefly, 10 mL of 50% HNO_3 was put into 50 mL conical flask (Fisherbrand) containing 1 g sand (d_{sand} = 0.710mm). The flask was then heated to 95°C (using Fisherbrand Scientific magnetic stirrer) and stirred at 100 rpm without boiling, then refluxed for 10 minutes. After cooling, the sample was refluxed with 5 mL of 65% HNO_3 for 30 minutes. The sample was then cooled and refluxed again with 10 mL of 36% HCl for 15 minutes. The digestate obtained was filtered through 150 mm diameter of Whatman TM filter paper (Cat No 1001-150), diluted to 100 mL with Milli-Q water and analysed with FAAS. This procedure is a modification of the Environmental Protection Agency (EPA)'s Acid Digestion Procedure (EPA 3050B) (Guven and Akinci, 2011).

In order to observe the strength of manganese coating onto the surface of the sand, acid digestion analysis was also done for fresh coated sand and for coated sand that has been used to treat 10 mg/L copper in AUSF. The diameter of sand used in these experiments was 0.400mm.

3.2.1.2 Sand bed characterisation

Flow hydrodynamic characterisation of reactors used in water/wastewater treatment is required so as to provide the performance of the reactors particularly in relation to chemical reactions occurring within the reactors. A tracer study is used to measure the hydraulic performance of reactors (Tchobanoglous et al., 2004). Pulse input tests were carried out for the tracer study as feeding the tracer chemical into the reactor is easy and the validity checks are assured (Teefy, 1996). The procedure of this tracer study is depicted in Appendix 3.13. A pulse of 10 mL at 100 mg/L sodium chloride (NaCl) was used as a tracer and injected using 10 mL Syringe BD Plastipak into the influent end of the AUSF. The tracer experiments were carried out at various flow rates (81.9, 74.4, 55.0, 37.8, and 16.4 mL/min).

a. Conductivity measurement

The capability of a solution to carry out an electrical current is defined as the electrical conductivity (EC) of that solution. As the electrical current is due to migration of ions in solution, the conductivity increases as the concentration of ions increase (Tchobanoglous et al., 2004). Conductivity is the reverse of resistivity and is expressed in micromhos per centimetre (μmhos/cm) or millisiemens per meter (ms/m) (Company, 1990).

In this tracer study, the conductivity of the tracer was measured, thus the corresponding concentration value could be determined. Conductivity was first calibrated using 11 points (100, 90, 80, 70, 60, 50, 40, 30, 20, 10, and 0 mg/L Na Cl). Conductivity was measured by Jenway 3540 pH -and Conductivity Meter.

b. Temperature measurement

As the conductivity of solutions increases as temperature increases at a rate of about 2% per degree Celcius (C), temperature must also be stated when reporting conductivity (Company, 1990). Temperature was measured by Jenway 3540 pH and Conductivity Meter.

3.2.2 Element concentrations

Elements concentrations were measured by flame atomic absorption spectrometry (FAAS) and colorimetri method (Hach). Hach was used once FAAS was not available. FAAS was employed due to the availability of FAAS and lower detection limits are not required for targeted metals. In addition, FAAS is a quite sensitive method, and free from spectral or radiation interference by co-existing elements and no pre-treatment is required (WHO, 2006).

3.2.2.1 Flame atomic absorption spectrometry (FAAS)

Flame atomic absorption spectrometry (FAAS) works based on the fact that the atom in the ground state absorbs the light of wavelength that are specific to each element when light is passed through the atoms in the vapour state. Due to the absorption of light lies on the concentration of atoms in the vapour, the level of the measured element in the water sample is defined from the computed absorbance. The correlation of concentration and absorbance is depicted in the Beer-Lambert law (WHO, 2006).

In order to obtain atomic optical spectra, the substances of a sample have to be converted to gaseous atoms which can then be defined by absorption measurements. Thus, initially a sample in solution has to be introduced into the atomiser (for example: flame) in which the sample is converted to gaseous atoms; hence ground state metal atoms are produced.

These ground state atoms are then excited as they absorb the light (excitation process) of the same element as the studied metal passed from the light source (a hollow cathode lamp). The number of these ground state atoms will define the amount of light absorbed in the excitation process. In order to selectively amplifying light produced from the source and ignoring emission from the sample cell, a chopper is utilised between the source and the sample cell. A wavelength selector (for example: a monochromator) is utilised to disperse the various wavelength of light which are produced from the light source and to isolate the specific line of interest (Skoog et al., 2007).

This specific wavelength is then directed to the detector, a photomultiplier tube which generates an electrical current reliant on the light intensity. This electrical current is then amplified and processed by instrument electronics to form a signal which is a computation of the light attenuation present in the sample. This signal is then processed to generate a read out in absorbance (Skoog et al., 2007). Figure 3.8 shows the main components of FAAS.

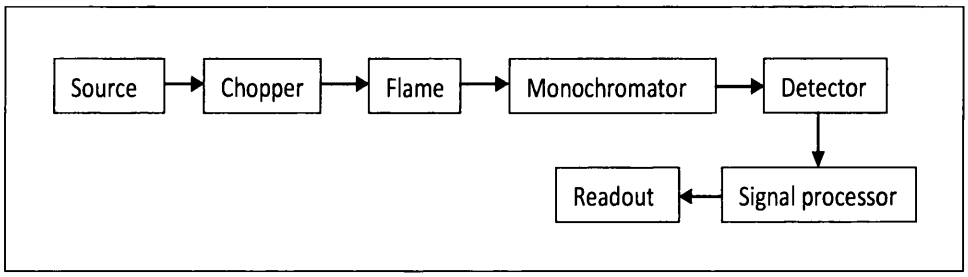

Figure 3.8 FAAS components (Skoog et al., 2007)

a. Flame atomisation

Individual atoms have to be generated from the ions solution (sample) so as the atomic absorption process can occur. FAAS that is used in this experiment employed flame atomisation. Processes involve in flame atomisation are shown in Figure 3.9.

Process		Type of matter	Process	Type of matter
	$M^+ + A$	Solution		
	↓			
Nebulisation	$M^+ + A$	(spray) Aerosol		
	↓			
Desolvation	MA	Solid aerosol		
	↓			
Volatilisation	MA	Gas molecules	→	Excited molecules
	↓			
Dissociation (reversible)	$M^0 + A^0$	Atomic gas	→	Excited atoms
	↓			
Ionisation (reversible)	$M^+ + e^-$	Atomic ions	→	Excited ions
			Excitation	

Figure 3.9 Flame atomisation process (Skoog et al., 2007)

The metal bearing solution sample is first aspirated to the burner chamber where the sample mixes with the fuel and oxidant gases to produce a fine aerosol. This process is known as nebulisation. In this stage, the metal is still in solution in the fine aerosol droplets (Skoog et al., 2007).

As the droplets are exposed into the flame, desolvation or evaporation occurred in which the solvent is removed and little solid particles of the sample are left. More heat application will then change this solid matter to gas matter. This process is known as volatilisation. In this stage, the analyte (the analyzed metal) is still in the molecule form, bounding with some anion. Therefore some more heat is required to dissociate this molecule into its individual atoms. This process is known as atomisation/dissociation. In this process, the ground state atoms are generated. These atoms will then absorb light energy and become excited state atoms (excitation process). The amount of light absorbed will be defined by the number of ground state metal atoms produced in atomisation. Concentration of the analysed metal can then be measured by comparing the absorbance of the sample to the known standard concentration (Skoog et al., 2007).

For copper, the FAAS employed was that of air-acetylene flame Perkin – Elmer 272 Atomic Absorption Spectrometry (AAS) and/or Varian AA240FS Fast Sequential Atomic Absorption Spectrometry. Varian AA240FS AAS is equipped with Varian SPS3 Autosampler and connected to Varian SpectAA Worksheet Oriented AA Software Version 5.1 Pro. Other metals and mixed metals were analysed only using Varian AA240FS AAS.

In this FAAS, ethyne or acetylene gas dissolved in solvent (acetone) was used as a fuel, and air was used as an oxidant gas (air-acetylene flame AAS). Procedure of using the Perkin – Elmer 272 AAS is given in Appendix 3.14; whereas procedure of using Varian AA240FS AAS is shown in Appendix 3.15.

For copper, manganese, nickel and zinc analysis using Varian AA240FS, the wavelength, slit width and lamp current were 324.8nm, 279.5 nm, 232.0 nm and 213.9 nm; 0.5nm, 0.2 nm, 0.2 nm and 0.1 nm; 4 mA, 5mA, 4mA, and 5mA subsequently. The air flow, acetylene flow and burner height were 13.50 L/min, 2 L/min and 13.5nm subsequently. The standard calibration method was linear. The correlation coefficient limit was 0.998 and instrument detection limit was 0.0030 mg/L.

b. Standard solutions

Standard solutions for desired concentrations have to be prepared for AAS calibration. The procedure to make these standard solutions is described in Appendix 3.16. To stabilize the metal ion, for example copper, so the metal would not precipitate again, HNO_3 (10%) was added to the solution. Appendix 3.17 shows the procedure to make the stabilized standard solutions.

c. Determining concentration by the AAS

The absorbance generated from the readout of signal in AAS is directly proportional to the concentration of the absorbing species. This is shown by Beer's Law equation as follows (Skoog et al., 2007):

$A = a_c L_b C_a$.....(Equation 3.12)

where: A = absorbance, a_c = absorptivity constant (L/mg/cm), L_b = the path length through the flame (cm), and C_a = concentration of the absorbing species (mg/L).

This straight proportional performance among absorbance and concentration is examined in atomic absorption.

A calibration relationship like that of shown in Figure 3.10 is defined once absorbances of standard solutions consisting known concentrations of analyte are analysed and the absorbance data are plotted against concentration. The figure shows that the calibration forms a straight line over the region where Beer's Law is examined. This line then forms a curve as a deviation from linearity occurs as the concentration and the absorbance increase resulting in a non ideal performance in the absorbance process (Sommerfield and Cooper, 2009).

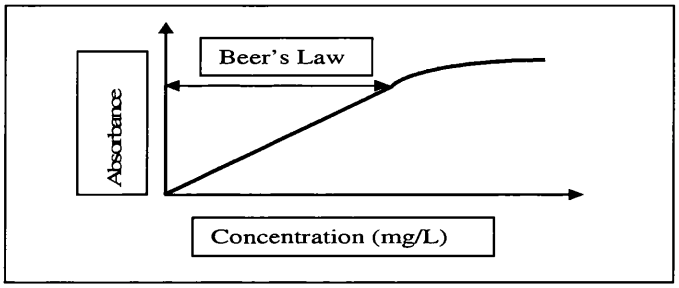

Figure 3.10 Relationships between absorbance and concentration (Sommerfield and Cooper, 2009)

d. AAS calibration

Before commencing the analysis, calibrations had to be made for the AAS. Procedure for making the standard calibration graph to analyse copper using the Perkin – Elmer 272 AAS is stated in Appendix 3.18. The equation line was defined by using a least square regression line. The least square regression line was measured by Microsoft Office Excel 2007 programme. Self calculation of standard calibration to analyse concentration using Varian AA240FS AAS was not required as the calibration was performed by the instrument.

3.2.2.2 Hach

Hach DR/2400 (Method 8506, Bicinchoninate method, concentration range 0.04 to 5.00 mg/L, CuVer® Reagent Powder Pillow, wavelength range 400-880nm, automatic wavelength selection) was used only for experiments involving 5 mg/L copper concentrations i.e. comparison between saturated and unsaturated conditions, and effect of diameters to AUSF performances. This method is a US EPA approved method for the determination of copper.

In this method, the copper is determined by the reaction with a salt of bicinchoninic acid (2,2-biqunoline-4,4-dicarboxylic acid) contained in CuVer® 1 reagant to produce a purple coloured complex in proportion to the copper concentration. The coloured complex is then measured by the spectrophotometer. The accuracy of the Hach method was checked with a Varian 240FS AAS and the correlation factor R^2 was 0.9904. pH sample was adjusted to 4-6 using HNO_3 and NaOH before Hach analysis as copper may precipitate at pH > 6 (Hach Company, 2010).

3.2.3 The solubility of metal hydroxides

The pH at which metal may precipitate was calculated as a function of its solubility product as explained as follows. If metal hydroxide (solid) is in equilibrium with free metal ions in solution (Stumm and Morgan, 1996):

$M(OH)_{z(s)} \rightleftarrows M^{z+} + zOH^-$ .... (Equation 3.13)

The conventional solubility product is:

${}^cK_{so} = [M^{z+}]\,[OH^-]^z\ mol^{(z+1)}\ L^{-(z+1)}$... (Equation 3.14)

Since the equilibrium activity in solution is independent of the amount of $M(OH)_z$, and the activity of $M(OH)_z$ is a constant at fixed temperature and pressure then $[M(OH)_z]$ is assumed to be unity. Same reasons apply to H_2O in the following reaction.

As the equilibrium concentrations of OH^- ions may be extremely small, the solubility is thus expressed in terms of reaction with protons:

$M(OH)_{z(s)} + zH^+ \rightleftarrows M^{z+} + zH_2O$ .... (Equation 3.15)

The solubility equilibrium is then:

${}^{c*}K_{so} = \frac{[M^{z+}]}{[H^+]^z}\ mol^{-(z-1)}\ L^{(z-1)}$ ... (Equation 3.16)

From Equation 3.14:

$$[M^{z+}] = \frac{^{c}K_{so}}{[OH^{-}]^{z}} \ldots \text{(Equation 3.17)}$$

Arranging Equation 3.17 into Equation 3.16:

$$^{c*}K_{so} = \frac{^{c}K_{so}}{[OH^{-}]^{z}\,[H^{+}]^{z}} \ldots \text{(Equation 3.18)}$$

$$^{c*}K_{so} = \frac{^{c}K_{so}}{K_{w}^{z}} \ldots\ldots \text{(Equation 3.19)}$$

From Equation 3.16:

$$\log {}^{c*}K_{so} = \log[M^{z+}] - \log[H^{+}]^{z} \ldots \text{(Equation 3.20)}$$

$$\log[M^{z+}] = \log {}^{c*}K_{so} - z\,pH \ldots \text{(Equation 3.21)}$$

Arranging Equation 3.19 into Equation 3.21:

$$\log[M^{z+}] = \log {}^{c}K_{so} - \log K_{w}^{z} - z\,pH \ldots. \text{(Equation 3.22)}$$

$$\log[M^{z+}] = \log {}^{c}K_{so} - (-\text{zp}\,K_{w}) - z\,pH$$

$$\log[M^{z+}] = \log {}^{c}K_{so} + \text{zp}\,K_{w} - z\,pH$$

$$\log[M^{z+}] = -\text{p}\,{}^{c}K_{so} + \text{zp}\,K_{w} - zpH$$

$$\log[M^{z+}] = \text{zp}\,K_{w} - \text{p}\,{}^{c}K_{so} - z\,pH \ldots. \text{(Equation 3.23)}$$

The concentration of metal at which the metal may precipitate at certain pH can then be calculated using Equation 3.23 by taking the value of $p^{c}K_{so}$ at 25°C.

3.3 Data analysis

3.3.1 Tracer test parameters

Tracer test parameters required for analysing tracer data are as follows.

The theoretical mean residence time, $\bar{t}_c$, is stated as the centroid of a pulse input tracer curve and was determined as below (Tchobanoglous et al., 2004):

$$\bar{t}_c = \frac{\int_0^\infty tC(t)dt}{\int_0^\infty C(t)dt} \quad \text{.....(Equation 3.24)}$$

The spread of the distribution measured by the variance σ^2_c was determined as below (Tchobanoglous et al., 2004):

$$\sigma_c^2 = \frac{\int_0^\infty t^2C(t)dt}{\int_0^\infty C(t)dt} - \left(\bar{t}_c\right)^2 \quad \text{.....(Equation 3.25)}$$

where: $\bar{t}_c$ = mean detention time obtained from the tracer curve (min), t = time (min), and $C(t)$ = tracer concentration at time t (mg/L).

In the case of the concentration versus time curve is measured by a series of discrete time step measurements, the theoretical mean residence time was approximated by the equation as below (Levenspiel, 1999):

$$\bar{t}_{\Delta c} \approx \frac{\sum_{i=1}^{i=n} t_i C_i \Delta t_i}{\sum_{i=1}^{i=n} C_i \Delta t_i} \quad \text{.....(Equation 3.26)}$$

where: $\bar{t}_{\Delta c}$ =mean residence time based on discrete time step observations (min), C_i= concentration at ith observation (mg/L), t_i = time at ith observation (min), Δt_i = the constant sampling interval selected (min), and n = the total number of data points selected.

The mean residence time calculated from Equation 3.26 should be compared to the hydraulic detention time, τ. Variance in $\bar{t}_{\Delta c}$ and τ value might reflect the occurrence of dead water zones and corresponding flow short-circuiting, erroneousness in water flow rate measurement and reactor volume estimation, or problems in tracer concentration observation (Teefy, 1996).

The variance, σ^2, as an indicator of the extent of back-mixing was defined by a series of discrete time step measurements as follows (Levenspiel, 1999):

$$\sigma_{\Delta c}^2 = \frac{\sum_{i=1}^{i=n} t_i^2 C_i \Delta t_i}{\sum_{i=1}^{i=n} C_i \Delta t_i} - \bar{t}_{\Delta c}^{\,2} \quad \text{.....(Equation 3.27)}$$

where: $\sigma_{\Delta c}^2$ = variance based on discrete time observation, min^2.

This expression is actually the variation between the tracer curve (the first term in the equation) and the mean residence time (the second term in the equation). A variance of 0 would indicate that no back-mixing occurs in the reactor (Teefy, 1996).

The total mass of salt measured at the reactor effluent, m_{salt}, was determined by integration (Equation 3.28) and compared to the total mass of salt injected.

$$m_{salt} = Q\int_0^{\infty} C(t)dt \quad \text{.....(Equation 3.28)}$$

where: m_{salt} = the total mass of salt measured at the reactor effluent (mg), and Q = the volumetric flow rate (mL/min).

This mass was approximated by a series of discrete time measurements as follows (Teefy, 1996):

$$m_{salt} = Q \sum_{i=1}^{i=n} C_i \Delta t_i \quad \text{.....(Equation 3.29)}$$

Calculated $m_{T,out}$ should then be compared to actual mass of tracer added, $m_{T,in}$. Discrepancies between calculated mass and actual mass of tracer added indicates the occurrence of dead water zones and corresponding flow short-circuiting, incorrect water flow rate measurement and reactor volume estimation, problems in measuring the tracer mass, or difficulties in concentration measurements (Teefy, 1996).

One of the major shortcomings to a pulse input test is the peak tracer concentration reaching the outlet of the reactor is not measured correctly. Theoretically, the peak concentration would be occurred near the hydraulic or theoretical detention time, τ (volume/flow rate).

Nevertheless, the peak tracer concentration may occur much sooner in practice. Thus, effluent concentration was measured at the same time as the tracer was added to the reactor.

The hydraulic performances of non ideal reactors were modelled as an open system by taking dispersion into account. For an open system, with larger amounts of dispersion, the output curve becomes gradually more non-symmetrical, thus the performance of a reactor was approximated by using a normalised effluent concentration versus time curve obtained from a unit pulse input (Levenspiel, 1999):

$$C_\theta = \frac{1}{2\sqrt{\pi\,\theta(\frac{D}{uL})}}\exp[-\frac{(1-\theta)^2}{4\,\theta(\frac{D}{uL})}] \quad \text{.....(Equation 3.30)}$$

where: C_θ = normalised tracer response C/C_0 (unitless), θ = normalised time t/τ (unitless), t = travel time (s), τ = theoretical detention time (V/Q, s), D = coefficient of axial dispersion (m^2/s), u = velocity of fluid (m/s), and L = length (m).

The related mean and variance were calculated as follows (Tchobanoglous et al., 2004):

$$\bar{\theta} = \frac{\bar{t}_c}{\tau} = 1 + 2\,\frac{D}{uL} \quad \text{.....(Equation 3.31)}$$

$$\sigma_\theta^2 = \frac{\sigma_c^2}{\tau^2} = 2\,\frac{D}{uL} + 8\,(\frac{D}{uL})^2 \quad \text{.....(Equation 3.32)}$$

where: $\bar{\theta}$ =normalised mean detention time ($\bar{t}_c/\tau$, unitless) and σ_θ^2 = variance of normalised tracer response C curve (s^2).

The mean obtained from Equation 3.31 is larger than the hydraulic detention time due to the forward movement of the tracer resulting from dispersion (Tchobanoglous et al., 2004).

The unit-less dispersion number below was used to estimate the dispersion (Tchobanoglous et al., 2004):

$$d_n = \frac{D}{uL} = \frac{Dt}{L^2} \quad \text{...(Equation 3.33)}$$

where: d_n = dispersion number (unitless).

To weigh up the level of axial dispersion, the following dispersion values were used (Tchobanoglous et al., 2004):

- No dispersion, $d_n = 0$ (ideal plug flow)
- Low dispersion, $d_n < 0.05$
- Moderate dispersion, $d_n = 0.05\text{-}0.25$
- High dispersion, $d_n > 0.25$
- Complete mix, $d_n = \infty$

3.3.2 Adsorption isotherm

The amount of adsorbate adsorbed by an adsorbent is a function of the concentration and characteristics of adsorbate and the temperature (Tchobanoglous et al., 2004). The important characteristics of the adsorbate are those of solubility, molecular weight and molecular structure. The quantity of adsorbate taken up is usually defined as a function of the concentration at a constant temperature. The resulting function is termed as an adsorption isotherm. Adsorption isotherms are made by exposing a fixed amount of adsorbent to a given amount of adsorbate in a fixed volume of liquid.

The quantity of adsorbate remaining in the solution is measured at the end of every test period. The adsorbent phase concentration after equilibrium was then calculated as (Srivastava et al., 2006):

$$q_e = \frac{(C_{in} - C_e)V}{w} \quad \text{.....(Equation 3.34)}$$

where: q_e = equilibrium adsorption uptake (mg of adsorbate/ g of adsorbent), C_{in} = initial adsorbate concentration (mg/L), C_e = equilibrium adsorbate concentration (mg/L), V = the solution volume (L), and w = adsorbent mass (g).

3.3.2.1 Freundlich isotherm

The Freundlich adsorption isotherm, which assumes that adsorption takes place on heterogenous surfaces, was measured as follows:

$q_e = K_f C_e^{1/r_a}$ .....(Equation 3.35)

where: q_e = mass of adsorbate adsorbed per unit mass of adsorbent (mg adsorbate/ g adsorbent), K_f= Freundlich capacity factor (mg adsorbate/g adsorbent)*(L water/mg adsorbate)$^{1/r}$, C_e = adsorbate equilibrium concentration in solution after adsorption (mg/L), $1/r_a$ = Freundlich intensity parameter, and r_a = rate of adsorption (Sen and Sarzali, 2008).

K_f and $1/r_a$ (the constants) in the Freundlich isotherm was defined by plotting log q_e versus log C_e as:

$\log\ (q_e) = \log K_f + \frac{1}{r_a} \log C_e$ .....(Equation 3.36)

$1/r_a$ gives information about surface heterogeneity and surface affinity for the solute. If it approaches zero ($1 < r_a < 10$) the degree of favourableness increases (Chutia et al., 2009).

$1/r_a$ also provides information about the deviation from the linearity of the adsorption. The adsorption is linear once $1/r_a$ is equal to unity. Once $1/r_a < 1$, this shows that the increased adsorption modifies the adsorbent in a way that increases the sorption capacity such as forming new sites. Once $1/r_a > 1$ or becomes greater ($1/r_a \gg 1$), the adsorption bond will become weak and the q_e will vary considerably with small changes in C_e (Balkaya and Cesur, 2008).

3.3.2.2 Langmuir isotherm

The Langmuir isotherm was made by assuming (Tchobanoglous et al., 2004):

1) A fixed number of accessible sites, all have the same energy, are available on the surface of the adsorbent
2) Adsorption is reversible

The Langmuir isotherm was determined as:

$$q_e = \frac{q_m C_L C_e}{1+C_L C_e} \quad \text{.....(Equation 3.37)}$$

where: q_e = mass of adsorbate adsorbed per unit mass of adsorbent (mg adsorbate/g adsorbent), C_L = empirical constants related to the binding energy of the sorption system (Sen and Sarzali, 2008), q_m = the maximum sorption capacity (mg/g), and C_e = adsorbate equilibrium concentration in solution after adsorption (mg/L).

q_m and C_L were obtained by plotting $C_e/(q_e)$ vs C_e:

$$\frac{C_e}{(q_e)} = \frac{1}{q_m C_L} + \frac{1}{q_m} C_e \quad \text{.....(Equation 3.38)}$$

The important characteristics of the Langmuir isotherm can be stated by a dimensionless constant separation factor or equilibrium parameter, R_L, as follows (Ghodbane et al., 2008):

$$R_L = \frac{1}{1+C_L C_{in}} \quad \text{....(Equation 3.39)}$$

where: C_L = the Langmuir constant (L/mg), and C_{in} = the initial concentration of copper (mg/L).

The parameter R_L expresses the shape of isotherm as follows:

- $R_L > 1$ unfavorable
- R_L = linear
- $0 < R_L < 1$ favorable
- $R_L = 0$ irreversible

3.3.3 Kinetics of adsorption

In order to study the mechanism of adsorption, especially potential rate-controlling step, the behaviour of metal adsorption process was analysed using the pseudo-first-order Lagergren equation, pseudo-second-order, intraparticle diffusion and Bangham models.

3.3.3.1 Pseudo-first-oder model

The metal ion adsorption kinetics based on the pseudo-first-order Lagergren equation was calculated as follows (Sen and Sarzali, 2008):

$$\frac{dq}{dt} = K_1(q_e - q_t) \quad \text{.....(Equation 3.40)}$$

where: q = the amount of copper sorbed at any time, t, (mg/g), q_e = the amount of copper sorbed at equilibrium (mg/g), K_1 = the pseudo-first-order (adsorption) rate constant (1/min), and t = contact time (min).
Integrating Equation 3.40 for the boundary conditions $t = 0$ to $t = t$ and q = 0 to $q = q_t$ leads to:

$$\ln(q_e - q) = \ln q_e - K_1 t \quad \text{.....(Equation 3.41)}$$

Hence the adsorption rate constant K_1 was obtained from the plot of ln $(q_e - q)$ against t.

3.3.3.2 Pseudo-second order model

The metal ion adsorption kinetics based on the pseudo-second-order equation was calculated as follows (Sen and Sarzali, 2008):

$$\frac{dq}{dt} = K_2(q_e - q_t)^2 \quad \text{.....(Equation 3.42)}$$

where: K_2 = the pseudo-second-order rate constant (g/(mg.min)).

Integrating Equation 3.42 for the boundary conditions $t = 0$ to $t = t$ and q = 0 to $q = q_t$ leads to:

$$q = \frac{K_2 q_e^2 t}{1 + K_2 q_e t} \ldots.$$ (Equation 3.43)

The initial sorption rate, h, was calculated as follows (Ghodbane et al., 2008):

$$h = K_2 q_e^2 \ldots.$$(Equation 3.44)

where: h = The initial sorption rate (mg/(g. min)).

3.3.3.3 Weber and Morris model

Intra-particle diffusion is an essential phenomenon for sorption processes in porous materials.

The initial rate of intra-particle diffusion was estimated using the following expression (Weber and Moris, 1963):

$$q_t = k_{id}\, t^{0.5} + C_{WM} \ldots..$$(Equation 3.45)

where: k_{id} = intra-particle diffusion rate constant (mg/g.min$^{1/2}$), q_t = the amounts of metal ion adsorbed per unit mass (mg/g) at time t (min), and C_{WM} = Weber-Morris constant (mg/g) that gives idea about the thickness of the boundary layer.

This model expects that the plot of q_t versus $t^{0.5}$ should be linear if intra-particle diffusion is occurred in the sorption process. If the line passes through the origin, intra-particle diffusion would be the only rate limiting controlling the process. On the other hand, if the data shows multi-linear plots, then two or more stages may influence the sorption process. In addition, the larger the value of C_{WM}, the greater the boundary layer effect is expected, or if the plot deviates from linearity then the boundary layer (film) controls the sorption process (Srivastava et al., 2006).

The mathematical dependence of the uptake of sorbate on $t^{1/2}$ is achieved once the adsorption process is assumed to be influenced by diffusion in the cylindrical or spherical and convective diffusion in the sorbate solution. The external resistance to mass transfer surrounding the particles is assumed to be significant merely in the initial steps of sorption. This is indicated by first sharper part. The second linear part is the gradual sorption step in which intra-particle diffusion is dominating (Srivastava et al., 2006).

3.3.3.4 Bangham's model

Bangham's equation was used to check as to whether pore diffusion is the only rate-controlling step.

Bangham's equation is given as follows (Srivastava et al., 2006):

$$\log\log\left(\frac{C_{in}}{C_{in}- q_t m}\right) = \log\left(\frac{K_o\, m}{2.303\, V}\right) + \propto \log\,(t) \quad \text{.....(Equation 3.46)}$$

where: C_{in} = initial metal concentration (mg/L), q_t = the amounts of metal ion adsorbed per unit mass (mg/g) at time t (min), m = mass of adsorbent per liter of solution (g/L), K_o= constant (L/gL), α = constant (<1), and V = solution volume (L).

The adsorption kinetics is limited by the pore diffusion once the experimental data are represented by Equation 3.46. On the other hand, if the experimental data are not well fitted by Equation 3.46, this indicates that the pore diffusion is not the only rate-controlling process. The effect of diffusion process on the whole sorption could be ignored with an increase in the contact times (Srivastava et al., 2006).

3.4 Batch and AUSF performance parameters

AUSF important parameters, such as the removal rate of element R (%), the hydraulic detention time τ, the time at which the metal removal is 95% t_{95}, the mass of element retained in the sand column m_r, and the removal capacity q, can be analysed mathematically. R, t_{95}, m_r, q, and removal efficiency, E were calculated in batch studies. These parameters along with their analysis technique are described below.

3.4.1 The removal rate of element, R (%)

The removal rate of element, R (%), is defined as (Tiwari et al., 2011):

$R = 100 \times (C_{in} - C)/C_{in}$ .....(Equation 3.47)

where: R = the removal rate (%), C = the effluent element concentration (mg/L) measured at a time t (min), and C_{in} = the input element concentration (mg/L).

3.4.2 t_{95}

The time, t_{95}, at which the metal removal is 95% (i.e. $C/C_{in} = 0.05$) can also be used to measure the performance of AUSF.

3.4.3 The mass of element retained in the sand column (m_r)

The quantity of mass retained in the sand column can be calculated by using the mass balance principle i.e. the rate of accumulation of metal within the sand column is equal to the rate of flow of metal into the sand column minus the rate of flow of metal out of the sand column.

Suppose Q is the flow rate of the water containing metal, C_{in} is the feed concentration of water containing metal, C is the effluent of the filter, the mass balance can then be written as (Tchobanoglous et al., 2004):

$$Q\,C_{in} - Q\,C = \frac{dm_r}{dt} \text{ .....(Equation 3.48)}$$

where: dm_r/dt = the rate of accumulation of mass in the sand column within a period of time (mg/s), Q = the flow rate of the water containing metal (mL/s), C_{in} = the feed concentration of water containing metal (mg/L), and C = the effluent of the filter (mg/L).

From Equation (3.48), the mass retained in the sand column can then be calculated by:

$$\int_0^{m_r} dm_r = \int_0^t (Q\,C_{in} - Q\,C)dt$$

$$m_r = Q\,C_{in} \int_0^t (1 - \frac{C}{C_{in}})\,dt \text{.....(Equation 3.49)}$$

In order to calculate the mass, the integration part has to be done first. This integration is a definite integration as there is a range of limit from *0* (the lower limit) to *t* (the upper limit).

As integration is simply a process of measuring the area of a function plotted on the graph as shown in Figure 3.11, therefore to estimate the value of this integration, the integration is then simplified to a form below:

$$I = \int_a^b f(x)dx \text{.....(Equation 3.50)}$$

where $f(x)$ = the integrand, a = lower limit of integration, and b = upper limit of integration.

The value of this integration can be estimated by using the trapezoidal rule (Kaw and Keteltas, 2009). Trapezoidal rule is based on the Newton-Cotes formula that says that if the integrand is approximated by an *n*th order polynomial then the integral of the function is approximated by the integral of that *n*th order polynomial. Integrating polynomials is an easy task and is based on the calculus formula.

According to the trapezoidal rule, if we want to estimate the value of the integral in Equation 3.50, we assume that $f(x) \approx f_n(x)$ where

$f_n(x) = a_0 + a_1 x + \cdots + a_{n-1} x^{n-1} + a_n x^n$ .....(Equation 3.51)

where $f_n(x)$ is a *nth* order polynomial.

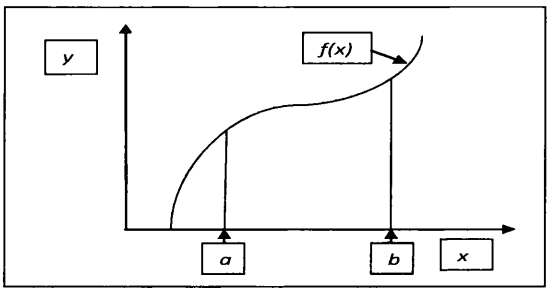

Figure 3.11 Integration of a function

As the trapezoidal rule assumes $n = 1$, meaning that the integral is estimated by a linear polynomial (straight line), then

$$\int_a^b f(x)dx \approx \int_a^b f_1(x)dx = \int_a^b (a_0 + a_1 x)\, dx = \int_a^b a_0\, dx + \int_a^b a_1 x\, dx$$

As

$$\int_a^b a_0\, dx = a_0 (b-a) \text{ and } \int_a^b a_1 x^n\, dx = a_1 \left(\frac{b^{n+1} - a^{n+1}}{n+1}\right), n \neq -1$$

Then

$$\int_a^b a_0\, dx + \int_a^b a_1 x\, dx = a_0 (b-a) + a_1 \left(\frac{b^2 - a^2}{2}\right) \text{.....} \quad \text{(Equation 3.52)}$$

a_0 and a_1 are derived from:

Let $(a, f(a))$ and $(b, f(b))$ as the two points to estimate $f(x)$ by a straight line from a to b, then $f(a) = a_o + a_1 a$ and $f(b) = a_0 + a_1 b$

Those two equations are then solved to obtain a_0 and a_1,

$$f(b) - f(a) = a_1 (b-a)$$

$$a_1 = \frac{f(b) - f(a)}{(b-a)} \text{.....(Equation 3.53)}$$

$$f(b) = a_0 + a_1 b = a_0 + \frac{f(b) - f(a)}{(b-a)}\, b$$

$$a_0 = f(b) - \frac{f(b)\,b}{(b-a)} - \frac{f(a)\,b}{(b-a)} = \frac{(b-a)f(b) - f(b)\,b + f(a)\,b}{(b-a)}$$

$$a_0 = \frac{f(a)\,b - f(b)a}{b-a} \text{.....(Equation 3.54)}$$

Therefore from Equation (3.52)

$$\int_a^b f(x)dx = a_0(b-a) + a_1\left(\frac{b^2 - a^2}{2}\right)$$

$$= f(a)\,b - f(b)a + \left(\frac{f(b) - f(a)}{(b-a)}\,\frac{b^2 - a^2}{2}\right)$$

$$= f(a)\,b - f(b)a + \left(\frac{f(b) - f(a)}{(b-a)}\,\frac{(b+a)(b-a)}{2}\right)$$

$$= f(a)\,b - f(b)a + \left((f(b) - f(a))\frac{(b+a)}{2}\right)$$

$$= f(a)\,b - f(b)a + \frac{f(b) - f(a) - f(a)b - f(a)a}{2}$$

$$= \frac{f(a)\,b - f(b)a + f(b)b - f(a)a}{2}$$

$$\int_a^b f(x)dx = (b-a)\left(\frac{f(a) + f(b)}{2}\right) \text{....(Equation 3.55)}$$

3.4.4 The removal capacity, *q*

The removal capacity, q, at a particular time is defined as the mass of metal removed, m_r, over the mass of sand, m_{sand}, thus:

$q = m_r/m_{sand}$....(Equation 3.56)

3.4.5 The removal efficiency, E

The removal efficiency, E, is calculated as the ratio between the mass retained, m_r, to the mass coming into the filter $QC_{in}t$, hence:

$E = m_r/QC_{in}t$.....(Equation 3.57)

3.4.6 The ratio of maximum metal adsorbed to the amounts of manganese, q_{Mmax}/q_{Mn}

The maximum metal adsorbed onto the sand, q_{Mmax}, is calculated as the ratio between the mass retained, m_r, to the mass of the coated sand, m_{sand}; while the amounts of manganese on the sand, q_{Mn}, is measured by acid digestion analysis. Thus, the ratio of maximum metal adsorbed to the amounts of manganese, q_{Mmax}/q_{Mn}, can then be calculated. q_{Mmax} is also sometimes defined as the maximum or saturation capacity of the filter (q_{sat}).

3.4.7 Equilibrium adsorption uptake, q_e

Equilibrium adsorption uptake, q_e, is calculated by Equation 3.34.

3.4.8 Empty-bed contact time (EBCT)

Empty-bed contact time is defined as (Tchobanoglous et al, 2004):

$\text{EBCT} = \frac{V_b}{Q}$.....(Equation 3.58)

where: EBCT = empty-bed contact time (min), V_b = bed volume (cm^3), and Q = flow rate (cm/min).

3.5 Column modelling

The Bohart-Adams equation was employed to describe the behaviour of metal removals within the AUSF. Bohart-Adams model assumes plug flow (Ruthven, 1984) and that surface reaction is the rate limiting step (Kundu and Gupta, 2007; Mohan and Sreelakshmi, 2008; Chu, 2010). In order to understand the Bohart-Adams model for a packed bed column, consider that this column is an isothermal column packed with adsorbent through which metal solution flows with constant linear velocity. The differential mass balance for the column is then (Chu and Hashim, 2007):

$$v\frac{\partial C}{\partial z}+\frac{\partial C}{\partial t}+\left(\frac{1-\varepsilon}{\varepsilon}\right)\frac{\partial q}{\partial t}=D_L\frac{\partial^2 C}{\partial z^2} \quad \text{.....(Equation 3.59)}$$

where: C = metal concentration in solution (mg/cm^3), q = metal concentration in adsorbent (mg/g), v = interstitial velocity (cm/sec), D_L = axial dispersion coefficient (cm^2/sec), ε = column void fraction, z = column axial coordinate (cm), and t = time (sec).

The original and boundary conditions for the column that at first free of metal and subjected to a step change in metal concentration at the column inlet at time zero are:

$$t=0,\ C=q=0\ ;\ z=0,\ \frac{D_L}{v}\frac{\partial C}{\partial z}=C-C_{in};\ z=L,\ \frac{\partial C}{\partial z}=0$$

where: C_{in} = the initial metal concentration (mg/cm^3), and L = the column length (cm).

The term $\partial q/\partial t$ in Equation 3.59 corresponds to the local rate of adsorption between the fluid and adsorbent phases. The Bohart-Adams model believes that adsorption can be illustrated by a quasi-chemical kinetic rate expression:

$$\frac{\partial q}{\partial t}=r_{BA}C\ (q_{sat}-q) \quad \text{....(Equation 3.60)}$$

where: q_{sat} = the saturation capacity of the adsorbent (mg/g), and r_{BA} = Bohart-Adams rate constant (cm^3/mg.sec).

The analytical solution to Equation 3.59 and 3.60, initially found by Bohart and Adams (1920) by ignoring axial dispersion, is:

$$\frac{C}{C_{in}} = \frac{\exp\left(r_{BA}C_{in}\left(t-\frac{L}{v}\right)\right)}{\exp\left(r_{BA}C_{in}\left(t-\frac{L}{v}\right)\right)+\exp\left(\frac{bq_sL}{v}\left(\frac{1-\varepsilon}{\varepsilon}\right)\right)-1} \quad \text{.....(Equation 3.61)}$$

By assuming that $t \gg L/v$ and neglecting the "1" term in the denominator (Cooney, 1998) then:

$$\frac{C}{C_{in}} = \frac{1}{1+\exp\left(r_{BA}\left(a_{qs}\frac{L}{u}- C_{in}\,t\right)\right)} \quad \text{.....(Equation 3.62)}$$

where: u = the superficial velocity (cm/sec) ($u = \varepsilon v = Q/S$; where Q = flow rate (cm/sec), and S = column surface area (cm^2) = πd^2/4, d = diameter of the column (cm)), a_{qs} = the saturation capacity of the adsorbent per unit volume of the packed bed (mg/g) ($a_{qs} = q_{sat}(1-\varepsilon)$).

Equation 3.62 is then arranged as the followings:

$$\frac{C_{in}}{C} = e^{\left(\frac{a_{qs}L}{u}- C_{in}t\right)r_{BA}} + 1$$

$$\frac{C_{in}}{C} - 1 = e^{\left(\frac{a_{qs}L}{u}- C_{in}t\right)r_{BA}}$$

$$\frac{C_{in}}{C} - 1 = e^{\left(\frac{a_{qs}L}{u}r_{BA}\right)- r_{BA}\,C_{in}t}$$

$$\ln\left(\frac{C_{in}}{C}-1\right) = \left(\frac{a_{qs}L}{u}\,r_{BA}\right) - r_{BA}\,C_{in}t$$

$$\frac{1}{r_{BA}}\ln\left(\frac{C_{in}}{C}-1\right) = \frac{a_{qs}L}{u} - C_{in}t$$

$$C_{in}t - \frac{a_{qs}L}{u} = -\frac{1}{r_{BA}}\ln\left(\frac{C_{in}}{C}-1\right)$$

$$C_{in}t = \frac{a_{qs}L}{u} - \frac{1}{r_{BA}}\ln\left(\frac{C_{in}}{C}-1\right)$$

$$t = a_{qs}\,\frac{L}{u\,C_{in}} - \frac{1}{r_{BA}}\,\frac{\ln\left(\frac{C_{in}}{C}-1\right)}{C_{in}} \quad \text{.....(Equation 3.63)}$$

As stated by Equation 3.63, plotting experimental data with regard to t versus $ln\ (C_{in}/C - 1)/C_{in}$ will lead to straight lines and the two parameters of a_{qs} and r_{BA} can be calculated from the corresponding intercepts and slopes subsequently.

Due to the experimental results did not conform to the linearized Bohart-Adams model, the saturation capacity of the adsorbent per unit volume of the packed bed, a_{qs} and the Bohart-Adams constant rate, r_{BA} were estimated by fitting directly the Bohart-Adams equation to the experimental data by using Data Solver function in Microsoft Excel 2007. Parameter t_{calc}, a_{qs}, r_{BA}, and C/C_{incalc} were obtained by using Data Solver. t_{calc} and C/C_{incalc} are calculated time and calculated C/C_{in}. t_{calc} was calculated with Equation 3.63 and with this t_{calc}, parameter a_{qs} and r_{BA} can be obtained. These parameters were then put in Equation 3.62 to obtain C/C_{incalc}. C/C_{incalc} was then plotted in the graph along with C/C_{inexp} that obtained from the experiment.

3.6 Statistics

3.6.1 Sample mean

The mean of the sample is the average value of all the observations. If there are n observations in a sample that are represented by x_1, x_2, …, x_n, the sample mean was then calculated by (Montgomery et al., 2007):

$$\bar{x} = \frac{x_1 + x_2 + \ldots + x_n}{n} \quad \text{....(Equation 3.64)}$$

The sample mean does not provide all of the information about a sample of data, even though the sample mean is useful. It is the sample variance or the sample standard deviation that shows the variability or scatter in the data.

3.6.2 Sample variance

If there are n observations in a sample that are represented by x_1, x_2, ..., x_n, the sample variance was then calculated by (Montgomery et al., 2007):

$$s^2 = \frac{\sum_{i=1}^{n}(x_i - \bar{x})^2}{n-1} \quad \text{.....(Equation 3.65)}$$

If s^2 is large, the dispersion or variability is comparatively large; on the other hand, if s^2 is small, the variability is reasonably small. It should be noted that the divisor for the sample variance is (n-1). If the divisor is n then the variability obtained, on the average, would be consistently smaller than the true population variance, σ^2.

3.6.3 Sample standard deviation

Standard deviation of a sample is the positive square root of the sample variance (Montgomery et al., 2007):

$$s = \sqrt{\frac{\sum_{i=1}^{n}(x_i - \bar{x})^2}{n-1}} \quad \text{.....(Equation 3.66)}$$

3.6.4 Standard error

The standard error provides some information about the precision of estimation (Montgomery et al., 2007). For instance, if the mean of the sample, $\bar{x}$ is used to estimate the population mean, μ, the standard error of $\bar{x}$ measures how precisely $\bar{x}$ estimates μ.

If sampling is done from a normal distribution with mean, μ, and variance σ^2, then the distribution of $\bar{x}$ is normal with mean μ, and variance σ^2/n, so the standard error of $\bar{x}$ is:

$$\sigma_{\bar{x}} = \frac{\sigma}{\sqrt{n}} \quad \text{.....(Equation 3.67)}$$

If σ is not known and s is substituted into the above equation, the estimated standard error of $\bar{x}$ is:

$\hat{\sigma}_{\bar{x}} = \frac{s}{\sqrt{n}}$ .....(Equation 3.68)

This estimated standard error can then be compared to the sample mean to obtain the precise of the point of estimate of the sample.

CHAPTER 4

SAND PARTICLES AND SAND BED CHARACTERISATION

Sand particles and sand bed characterisation is the important step that is required to be carried out initially in this work in which a process concerning sand particles in a bed column is involved. By characterising sand particles, the characteristic of the sand particles can be obtained, thus the processes that might occur within these particles can be assessed. Similarly, by characterising sand bed, the sand bed behaviour can be estimated, thus the flow patterns within the bed can be defined, hence AUSF can be determined as to be representative enough to describe the observed experimental results.

4.1 Sand particles characterisation

4.1.1 Sand particles size

Sand was sieved using a Russell Finex Sieve. 0.850mm sieve was chosen as the greatest size. Then smaller diameters i.e. 0.710 mm, 0.500mm and 0.400mm of sieve were used. The 0.850 mm diameter fraction was selected based on the previous research (Rachmawati et al., 2006a). Decreasing diameters of sands were utilised based on the same research above that showed that activated unsaturated sand filter (AUSF) performed better for smaller diameter. Time spent for sieving this 200 kg sand is about 9 days (53 hours 30 minutes).

According to David Ball Specialist Sand (2009) this standard sand was already washed, dried and graded. There was no silt, clay or organic matter in the sand. The particle shape was rounded to sub-rounded. The colour was light brown or pale silver to brown.

4.1.2 Sand particles surface area by Brunauer, Emmet, Teller (BET) analysis

Surface area for sand samples were studied using Brunauer, Emmet, Teller (BET) analysis. In order to see the effect of metal on the coated sand after the coated sand was used for treating water containing metal, copper bearing coated sand was analysed using BET method. Copper bearing coated sand was derived from 0.0709 mg manganese/g sand that was used to treat 20 mg/L copper solution by AUSF. Other metals studied in this research were not analysed by BET method due to time and instrument availability constraints. This may not affect the analysis of sand particles surface area since this work was carried out to merely confirm as to whether the metal was adsorbed (or attached) into the surface area of the sand since the metal was removed by the AUSF discussed later in Chapter 5-6.

Table 4.1 lists specific surface areas for uncoated, coated, and copper bearing coated sand. The surface area of sand increased by 21% from 0.302 to 0.365 m^2/g sand after coating the sand with potassium permanganate (0.0709 mg manganese/g sand). This is in agreement with Han et al. (2006a) who also observed an increase in surface area after potassium permanganate coating of sand but by only 6%. This indicates that coating the sand would result in increased adsorption sites hence giving better removal.

In contrast, for copper bearing coated sand, the surface area was almost halved (=0.163 m^2/g-sand), a result which is also in agreement with Han et al. (2006a). This reduction in surface area may be due to blockage of the adsorption sites by the adsorbed copper hydroxide.

BET surface area measurements also revealed that the surface area of copper bearing coated sand taken from the experiment where the sand was not fully submerged in water or with aeration (0.084 m^2 /g-sand) was about half than that taken from the experiment where the sand was fully submerged in water or without aeration (0.163 m^2 /g-sand). This is direct proof that aeration reduces the surface area and results in better removal of copper. These BET results support the assumed mechanism of copper removal as discussed later, i.e. surface attachment through precipitation and adsorption (electrostatic attraction) process, and possible surface complexation.

Table 4.1 Specific surface area of sand at different conditions

Condition	Surface area (m^2/g-sand)
Uncoated sand	0.302±0.088
Coated sand	0.365±0.123
Copper bearing coated sand under saturated condition	0.163±0.008
Copper bearing coated sand under unsaturated condition	0.084±0.058

4.1.3 Surface area morphology of sand particles by scanning electron microscope (SEM) analysis

4.1.3.1 Uncoated and coated sand

SEM images of uncoated and coated sand are shown in Figures 4.1 - 4.4. These images were taken at various magnifications to investigate the surface morphology of the sand particles. Figure 4.1, obtained at 10,000x magnification, shows that the uncoated sand had a fairly uniform and smooth surface with small fractures giving a lightly rough surface. This morphology of sand particles was also observed by other studies (Han et al., 2006a; Wan et al., 2010).

In contrast, the coated sand, shown in Figure 4.2 (taken at 10,000x magnification), emerged as a rough surface due to the coating layer. The coated sand surfaces were likely inhabited by newborn manganese oxides which were formed during the coating process. The presence of manganese in the form of insoluble oxides was indicated by dark coloured (brown-black) precipitates of the coated sand samples. The occurrence of manganese on the sand surface was confirmed later in the SEM-EDX analysis. The attachment of the manganese on the sand surface was also supported by acid alkali resistance test described later (Section 4.1.5). Figure 4.2 also shows no visible uniform sites apart from the potential crystalline manganese oxides, formed in clusters, and appeared on occupied surfaces.

These clusters are clearly shown through higher magnification of 13,000x (Figure 4.3) and 50,000x (Figure 4.4). Han et al. (2006a) and Hu et al. (2004) have also shown similar clusters as those presented in Figures 4.2 - 4.4.

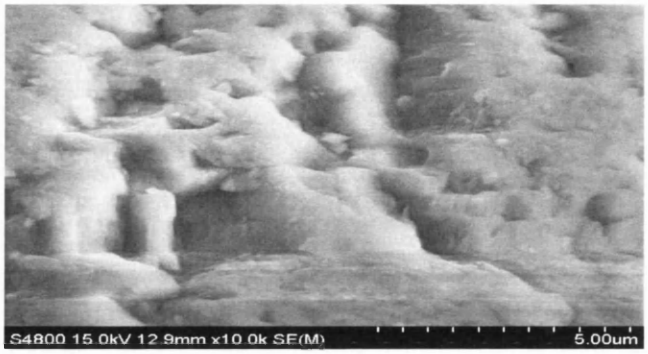

Figure 4.1 SEM micrographs for uncoated sand at 10,000x magnification (d_{sand} = 0.710mm)

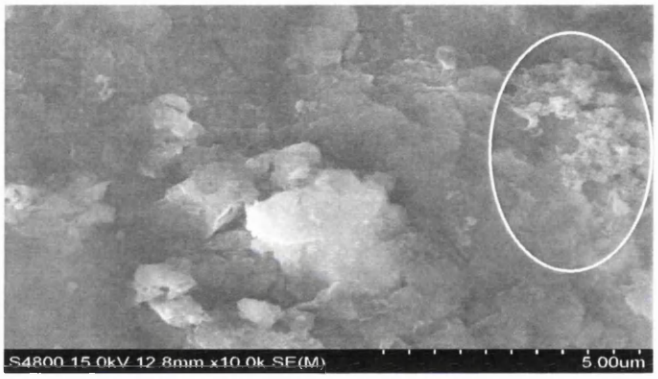

Figure 4.2 SEM micrographs for coated sand at 10,000x magnification (d_{sand} = 0.710mm, q_{Mn}/q_{sand} = 0.0709 mg Mn/g sand)

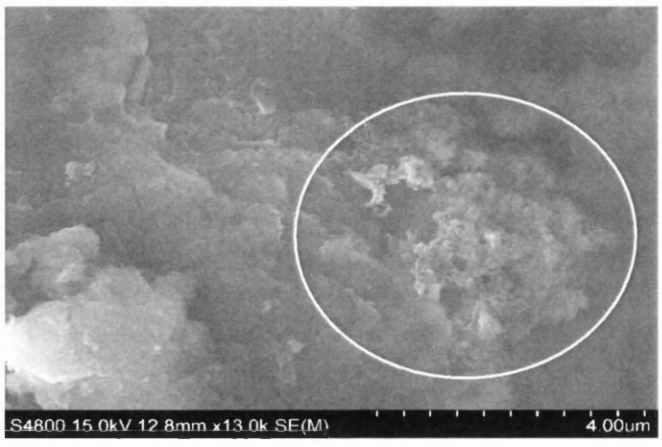

Figure 4.3 SEM micrographs for coated sand at 13,000x magnification (d_{sand} = 0.710mm, q_{Mn}/q_{sand} = 0.0709 mg Mn/g sand)

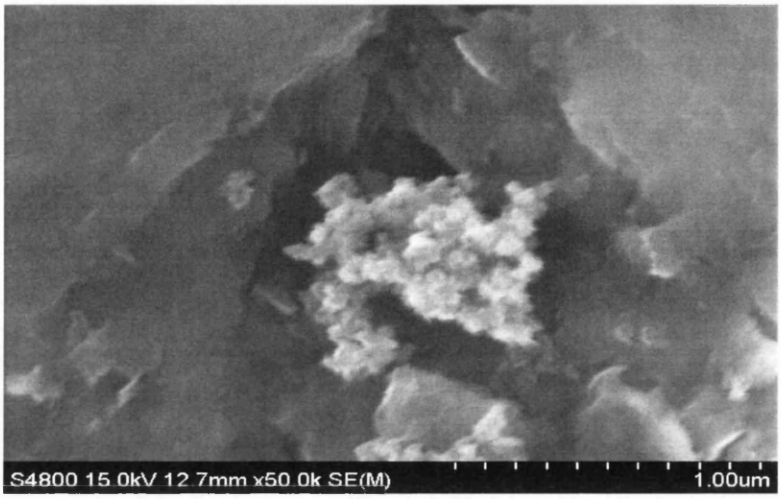

Figure 4.4 SEM micrographs for coated sand at 50,000x magnification (d_{sand} = 0.710mm, q_{Mn}/q_{sand} = 0.0709 mg Mn/g sand)

4.1.3.2 Copper bearing coated sand

SEM images of the coated sand that was used to treat copper bearing water (20 mg/L copper solutions) were taken at various magnifications, and are shown in Figures 4.5 - 4.7. The coated sand surface appeared as a fracture and some clusters occurred on the surface. These clusters were likely those of the newborn copper hydroxides. The form of the clusters was different from the manganese oxides clusters shown in Figures 4.2 - 4.4. Whilst the manganese oxide clusters consisted of many uniformly rounded shapes, the copper hydroxides clusters had a long shape with blossomed wings as that clearly seen through higher magnifications (Figures 4.6 – 4.7).

Figure 4.5 SEM micrographs for copper bearing coated sand at 1,000x magnification (d_{sand} = 0.710mm, q_{Mn}/q_{sand} = 0.0709 mg Mn/g sand, $C_{Cu\text{-}in}$ = 20 mg/L)

Figure 4.6 SEM micrographs for copper bearing coated sand at 3,000x magnification (d_{sand} = 0.710mm, q_{Mn}/q_{sand} = 0.0709 mg Mn/g sand, C_{in} = 20 mg/L)

Figure 4.7 SEM micrographs for copper bearing coated sand at 5,000x magnification (d_{sand} = 0.710mm, q_{Mn}/q_{sand} = 0.0709 mg Mn/g sand, C_{in} = 20 mg/L)

4.1.3.3 Manganese bearing coated sand

SEM images of the coated sand that was used to treat manganese bearing water (20 mg/L manganese solution) were taken at various magnifications and energies of electron beam, and are shown in Figures 4.8 - 4.10. Fractures were evidently seen across the surface of the sand particularly through lower energy of the beam (Figures 4.9 – 4.10). There was a cluster of possibly the newborn manganese hydroxides that occupied the coated sand surfaces. The cluster was somewhat different from the manganese oxides cluster found in Figures 4.2 – 4.4.

The manganese hydroxide clusters had rounded shapes and were seemed much smaller than the manganese oxide clusters.

Increasing the energy of the electron beam (kV) would result in decreasing quality of topographic image as shown in Figures 4.8 - 4.10. Figures 4.9 and 4.10 show the same site at different beam energies. Lower beams (1 – 5 keV) are used to improve the image quality and topographical information; whereas higher beam (30 keV) is employed for EDX analysis in order to increase the X-ray counts. At high energies, surface information is lost.

Figure 4.8 SEM micrographs for manganese bearing coated sand at 35,000x magnification (d_{sand} = 0.710mm, q_{Mn}/q_{sand} = 0.0709 mg Mn/g sand, $C_{Mn\text{-}in}$ = 20 mg/L)

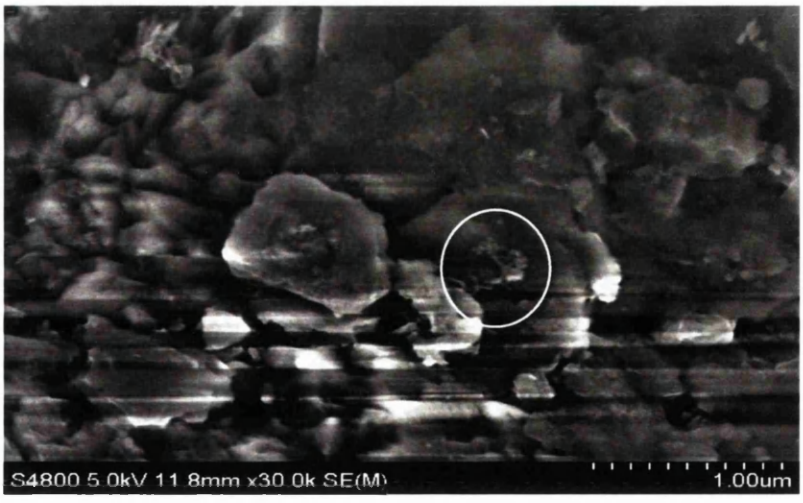

Figure 4.9 SEM micrographs for manganese bearing coated sand at 30,000x magnification (d_{sand} = 0.710mm, q_{Mn}/q_{sand} = 0.0709 mg Mn/g sand, $C_{Mn\text{-}in}$ = 20 mg/L)

Figure 4.10 SEM micrographs for manganese bearing coated sand at 20,000x magnification (d_{sand} = 0.710mm, q_{Mn}/q_{sand} = 0.0709 mg Mn/g sand, $C_{Mn\text{-}in}$ = 20 mg/L)

4.1.3.4 Zinc bearing coated sand

Figures 4.11 - 4.12 show SEM images of the coated sand that was employed to treat zinc bearing water (20 mg/L zinc solution) at two magnifications. Fractures appeared across the sand surface. The possibly newborn zinc hydroxides were found in a cluster. This cluster was identified at higher magnification (Figure 4.12).

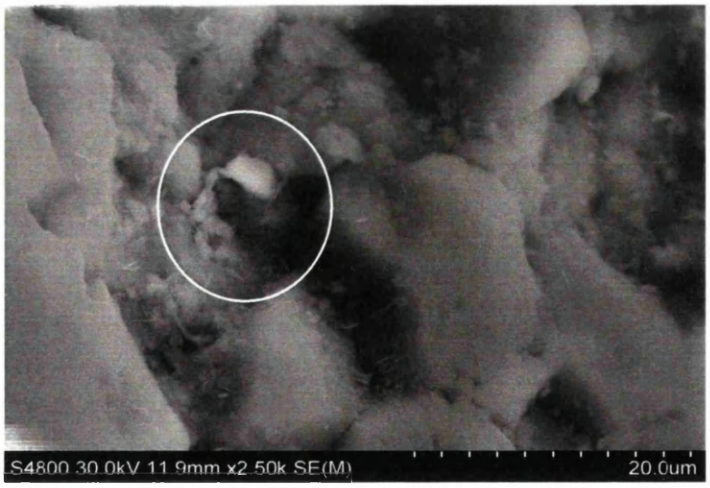

Figure 4.11 SEM micrographs for zinc bearing coated sand at 2,500x magnification (d_{sand} = 0.710mm, q_{Mn}/q_{sand} = 0.0709 mg Mn/g sand, $C_{Zn\text{-}in}$ = 20 mg/L)

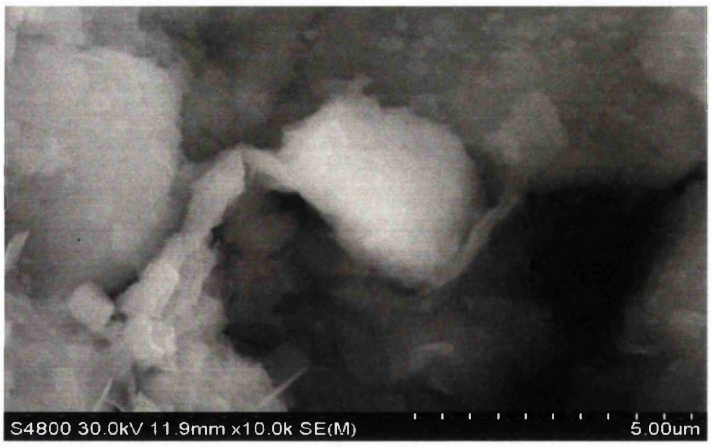

Figure 4.12 SEM micrographs for zinc bearing coated sand at 10,000x magnification (d_{sand} = 0.710mm, q_{Mn}/q_{sand} = 0.0709 mg Mn/g sand, $C_{Zn\text{-}in}$ = 20 mg/L)

4.1.3.5 Nickel bearing coated sand

SEM images of the coated sand that was used to treat nickel bearing water (20 mg/L nickel solution) are illustrated in Figures 4.13 - 4.15. A rough surface was clearly noticed on the sand surface. A cluster that is likely to be newborn nickel hydroxides was seen occupying the surface of the manganese coated sand. Figures 4.13 – 4.15 were taken at the same site but at different beam energy. Figure 4.13 taken at 1.0 keV electron beam clearly shows that the cluster was attached onto the surface of the coated sand.

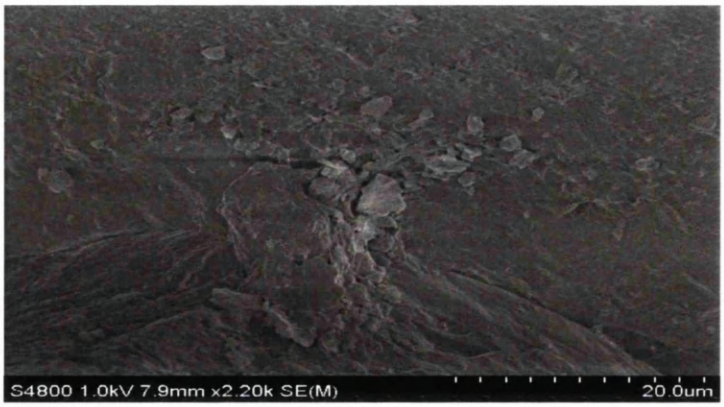

Figure 4.13 SEM micrographs for nickel bearing coated sand at 2,200x magnification and 1.0kV (d_{sand} = 0.710mm, q_{Mn}/q_{sand} = 0.0709 mg Mn/g sand, $C_{Ni\text{-}in}$ = 20 mg/L)

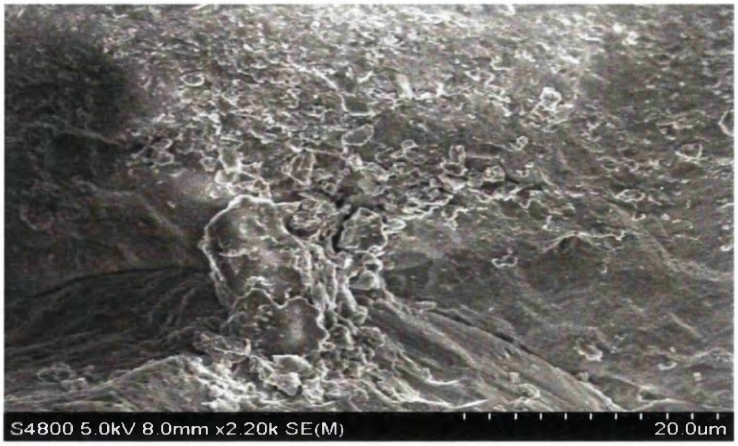

Figure 4.14 SEM micrographs for nickel bearing coated sand at 2,200x magnification and 5.0kV (d_{sand} = 0.710mm, q_{Mn}/q_{sand} = 0.0709 mg Mn/g sand, $C_{Ni\text{-}in}$ = 20 mg/L)

Figure 4.15 SEM micrographs for nickel bearing coated sand at 2,200x magnification and 30.0kV (d_{sand} = 0.710mm, q_{Mn}/q_{sand} = 0.0709 mg Mn/g sand, $C_{Ni\text{-}in}$ = 20 mg/L)

4.1.3.6 Mixed metals bearing coated sand

SEM images of the coated sand that was applied to treat mixed metals (i.e. 20 mg/L of copper, manganese, zinc and nickel solution) bearing water were taken at various magnifications, and are shown in Figures 4.16 - 4.17. The sand surface was not smooth yet fractures were evidently seen on the sand surface. The possibly metal hydroxides occurred as a cluster and inhabited the sand surface.

This cluster looked like a blossom flower was clearly seen attached to the rough sand surface particularly at higher magnification (Figure 4.16).

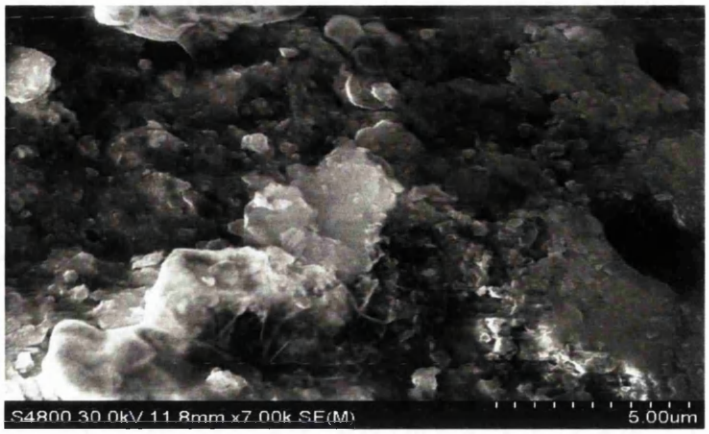

Figure 4.16 SEM micrographs for mixed metals bearing coated sand at 7,000x magnification (d_{sand} = 0.710mm, q_{Mn}/q_{sand} = 0.0709 mg Mn/g sand, C_{in} = 20 mg/L)

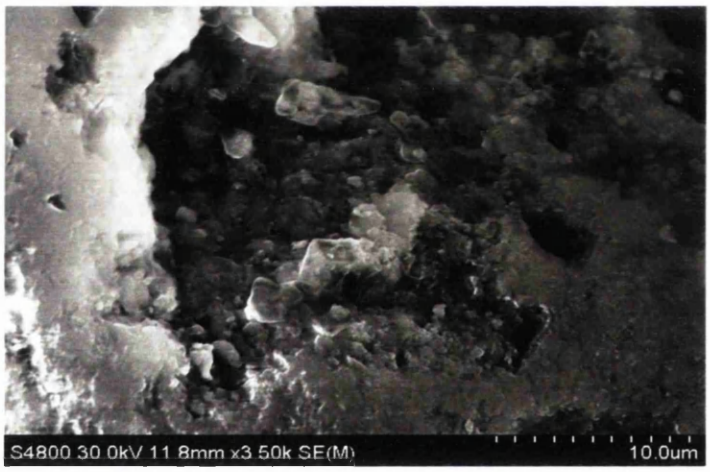

Figure 4.17 SEM micrographs for mixed metals bearing coated sand at 3,500x magnification (d_{sand} = 0.710mm, q_{Mn}/q_{sand} = 0.0709 mg Mn/g sand, C_{in} = 20 mg/L)

4.1.3.7 Waste water bearing coated sand

SEM images of the coated sand that was employed to treat waste water containing metals (11.78 mg/L, 0.061 mg/L, 0.6135 mg/L and 0.81 mg/L copper, manganese, zinc and nickel solution respectively) were taken at two magnifications, and are shown in Figures 4.18 - 4.19. These mixed metals were dissolved in tap water.

Fractures were clearly noticed on the coated sand surface. The manganese coated sand surface was like a bee hive that was evidently seen in higher magnification SEM images (Figure 4.18). The coated sand surfaces were apparently occupied by clusters that were possibly newborn metal hydroxides. These clusters were clearly different from the metal hydroxides clusters shown in Figures 4.16 – 4.17. The waste water bearing coated sand clusters were like cotton plumps and evidently attached on the bee hive like manganese coated sand surface.

All these SEM results support the results of the metals removal and the hypothesis that metals may well be removed by precipitation and adsorption on the surface of the manganese coated sand as discussed later in Chapter 5 - 6. The presence of the metals on the coated sand surface was proven with SEM-EDX analysis below.

Figure 4.18 SEM micrographs for waste water bearing coated sand at 7,000x magnification (d_{sand} = 0.710mm, q_{Mn}/q_{sand} = 0.0709 mg Mn/g sand, $C_{Cu\text{-}in}$ = 11.78 mg/L, $C_{Mn\text{-}in}$ = 0.061 mg/L, $C_{Zn\text{-}in}$ = 0.6135 mg/L, $C_{Ni\text{-}in}$ = 0.81 mg/L)

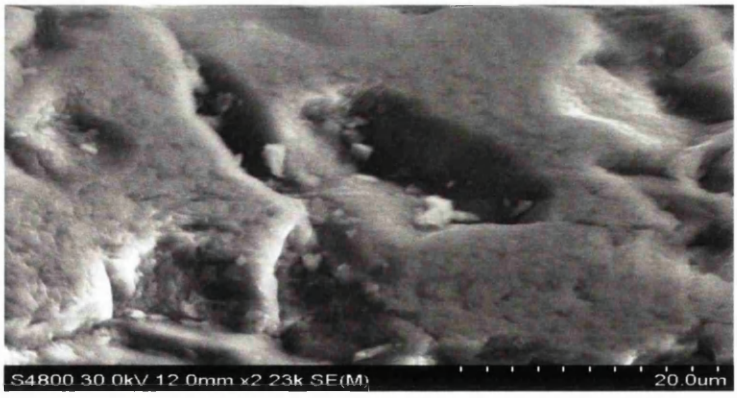

Figure 4.19 SEM micrographs for waste water bearing coated sand at 2,230x magnification (d_{sand} = 0.710mm, q_{Mn}/q_{sand} = 0.0709 mg Mn/g sand, $C_{Cu\text{-}in}$ = 11.78 mg/L, $C_{Mn\text{-}in}$ = 0.061 mg/L, $C_{Zn\text{-}in}$ = 0.6135 mg/L, $C_{Ni\text{-}in}$ = 0.81 mg/L)

4.1.4 Elemental analysis of sand particles by energy dispersive x-ray spectroscopy (EDX)

SEM/EDX analysis was made to determine and confirm the elements on uncoated, coated and elements bearing coated sand. Qualitative analysis such as spectra analysis, dots mapping analysis and line scanning were performed using the SEM/EDX system. The peak heights in the EDX spectra and line scanning are a measure of the intensity of X-rays emitted of all elements detected; while the dot density in mapping analysis is a qualitative spatial measure of the detected elements. Although direct quantification is difficult, this SEM/EDX analysis was carried out in order to confirm the occurrence of the metals on the sand surface. The quantitative analysis shows the composition of metals on the sample. The elemental analysis described throughout this section is based on the atomic% of element as this reflects the number of atoms detected in the sample as described in Section 3.2.1.1.d (Figure 3.7).

4.1.4.1. Uncoated sand

The EDX spectra for uncoated sand are shown in Figure 4.20. The x axis shows the energy (keV) of the emitted X-rays; while the y axis illustrates the intensity of the X-rays. An extremely high level of oxygen and silica could be observed as oxygen K_α X-rays emitted with the energy of 0.52 keV and silica K_α X-rays with the energy of 1.74 keV were detected. Silica and oxygen are known as the principal elements of quartz sand (Styriakova et al., 2003). High level of carbon was also appeared as carbon K_α X-rays with the energy of 0.28 keV were identified. This carbon is likely to be due to beam induced deposition of carbon on the surface of the sample. The carbon results from contamination within the SEM chamber. High calcium L_α X-rays with the energy of 0.34 keV were also detected. Calcium X-rays were also emitted from the K shell (with the energy of 3.69 keV). The peak height of the calcium L_α X-rays is higher than the calcium K_α X- rays as the electron beam energy required to excite K shell electrons are higher than that of the energy to excite L shell electrons, thus the X-rays from L shell emission are more likely to occur and more detected.

This is also true for other elements which have K, L and even M lines (Goodhew et al., 2001). Significant level of aluminium appeared as aluminium K_α X-rays with 1.49 keV. The peaks of iron X-rays were detected as these X-rays were emitted from K shell (K_α X-rays) and L shell (L_α X-rays) with the energy of 6.40 keV and 0.70 keV respectively.

Even more, magnesium and potassium were identified as the magnesium K_α X-rays and the potassium K_α X-rays with the energy of 1.25 and 3.31 keV respectively. Knowing that the sand used in this study originated from Lower Greensand (Leighton Buzzard, Beds, UK) (David Ball SpecialistSands, 2009), the detected calcium, aluminium, iron, magnesium and potassium possibly come from glauconite (Thompson and Hower, 1975), which is occasionally detected in the Lower Greensand (Whiteley, -). Finally, sulphur appeared as sulphur K_α X-rays emitted with 2.31 keV energy.

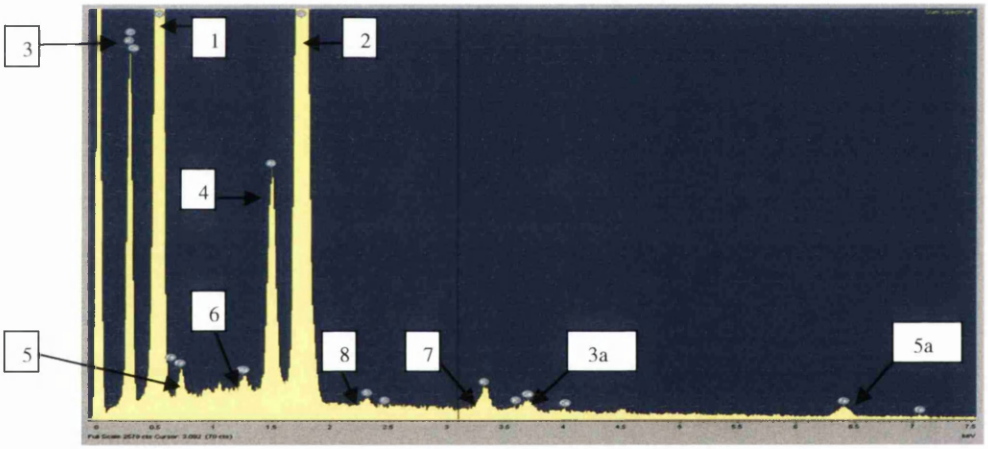

Figure 4.20 EDX spectra for uncoated sand (d_{sand} = 0.710mm): 1 = O K_α X-rays (0.52 keV), 2 = Si K_α X-rays (1.74 keV), 3 = C K_α X-rays (0.28 keV), Ca L_α X-rays (0.34 keV), 3a = Ca K_α X-rays (3.69 keV), 4 = Al K_α X-rays (1.49 keV), 5 = Fe L_α X-rays (0.70 keV), 5a = Fe K_α X-rays (6.40 keV), 6 = Mg K_α X-rays (1.25 keV), 7 = K K_α X-rays (3.31 keV), 8 = S K_α X-rays (2.31 keV).

Figure 4.21 illustrates the image used for elemental analysis of uncoated sand. All elements occurred in the spectra are listed in Table 4.2. Table 4.2 depicts that oxygen (atomic percentage = 55.44%) was the most significant element of the uncoated sand. This atomic percentage throughout this report was calculated as described in Section 3.2.1.1.d (Figure 3.7).

The amount of oxygen in this elemental analysis is in line with the EDX spectra that show the peak of oxygen X-rays is the highest. Carbon and silica came second and third with the atomic percentage of 32.25% and 10.70% subsequently. This is in contrast with the EDX spectra. The higher amount of carbon may be due to as carbon is the lightest element in the sample, the X-rays emitted by carbon may come from both the direct excitation by electrons surrounding carbon and the excitation by X-rays from higher elements (flouresence effect). In addition, EDS systems have worse peak-to-background ratios for lighter elements thus this worse ratios will affect the XPP correction performed (Goodhew et al., 2001). Iron, potassium, magnesium, calcium and sulphur were also detected with the atomic percentage of 0.21%, 0.16%, 0.09%, 0.08%, and 0.05% respectively. The amounts of atoms obtained for these elements were in line with the peak heights of their EDX spectra.

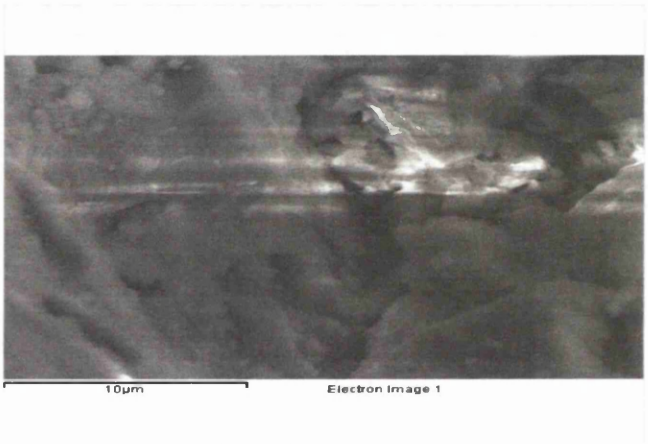

Figure 4.21 SEM image for elemental composition for uncoated sand (d_{sand} = 0.710mm)

Table 4.2 Elemental composition of uncoated sand (d_{sand} = 0.710mm)

Element	Weight %	Atomic %
C K	23.80	32.25
O K	54.51	55.44
Mg K	0.13	0.09
Al K	1.70	1.03
Si K	18.47	10.70
S K	0.09	0.05
K K	0.39	0.16
Ca K	0.20	0.08
Fe K	0.71	0.21
Totals	100.00	100.00

4.1.4.2 Coated sand

The EDX spectra for coated sand are shown in Figure 4.22. Apart from other signals described above in the uncoated sand, manganese signal can be clearly observed. The manganese X-rays were emitted from the K shell (manganese K_α X-rays) and L shell (manganese L_α X-rays) with the energy of 5.90 and 0.64 keV subsequently. However, since a strong peak of Si is observed in the EDX spectra of coated sand, manganese clearly did not coat the entire surface of sand. This is confirmed by EDX elemental distribution mapping shown in Figure 4.23. Silica signal on this coated sand (Figure 4.22) was seen greater than that of on the uncoated sand (Figure 4.20). This may be due to the amount of silica was greater (Table 4.3) than that of on the uncoated sand (Table 4.2). There was no sulphur detected as identified in the uncoated sand as shown in section 4.1.4.1. The elemental composition within the uncoated sand cannot be guaranteed the same for all the sand samples, except for silica and oxygen as they are the main elements of quartz sand, therefore sulphur as the least element previously detected in the uncoated sand was not appeared in this coated sand sample. The figure is, however, in good agreement with other studies (Hu et al., 2004; Han et al., 2006a). The EDX spectra thus prove the attachment of manganese oxide to the surface of sand. The strength of this coating was confirmed later with acid and alkali resistance test (Section 4.1.5).

In addition, the EDX elemental distribution mapping for the coated sand is illustrated in Figure 4.23. Bright points are produced each time an X-ray photon from the element is counted; thus the dot density indicates the qualitative measure of the concentration of the element being studied. The figure reveals that manganese was concentrated only on certain areas of the sand surface, its distribution was not uniform, and at lower amount than Si. The figure also shows that bright points of manganese apparently correlated to the manganese cluster, which is likely to be the manganese oxide clusters, shown ((a)). On the other hand, no bright points correlated to cluster (b). This may be due to the topographical effect occurred on a rough surface of the sand sample. As X-rays, contrast to secondary electrons, travel in straight lines from the sample to the detector, X-rays from the area of the sample which are not in the line of sight of the detector will not be detected (Goodhew et al., 2001).

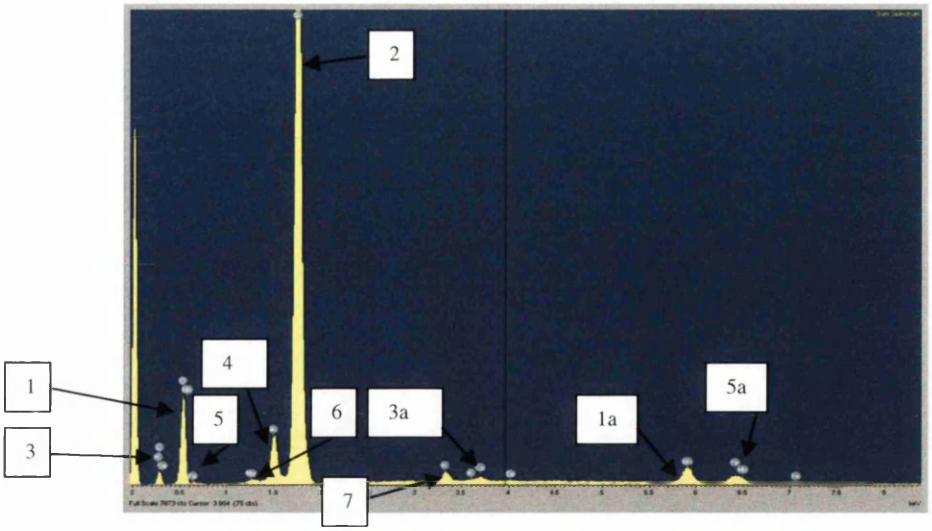

Figure 4.22 EDX spectra for coated sand (d_{sand} = 0.710mm, q_{Mn}/q_{sand} = 0.0709 mg Mn/g sand): 1 = Mn L_α X-rays (0.64 keV), O K_α X-rays (0.52 keV), 1a = Mn K_α X-rays (5.90 keV), 2 = Si K_α X-rays (1.74 keV), 3 = C K_α X-rays (0.28 keV), Ca L_α X-rays (0.34 keV), 3a = Ca K_α X-rays (3.69 keV), 4 = Al K_α X-rays (1.49 keV), 5 = Fe L_α X-rays (0.70 keV), 5a = Fe K_α X-rays (6.40 keV), 6 = Mg K_α X-rays (1.25 keV), 7 = K K_α X-rays (3.31 keV)

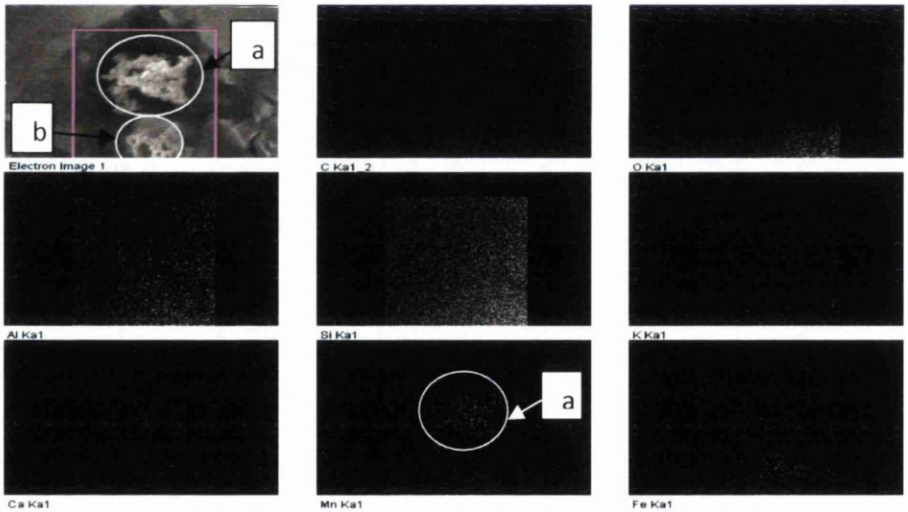

Figure 4.23 EDX elemental distribution mapping for the coated sand (d_{sand} = 0.710mm, q_{Mn}/q_{sand} = 0.0709 mg Mn/g sand)

Nevertheless, bright points from (a) give evidence that manganese was an essential part of the coated sand sample which is also clearly shown by the SEM/EDX line scanning in Figure 4.24. X axis in the line scanning figure represents the distance of the scanning sample; while y axis shows the X-rays energy. Figure 4.24 shows that manganese covered the surface of the sand.

The cluster shown in both figures results from manganese as clearly evidenced by the peak of manganese signal (as shown in Figure 4.24) giving an insight into the way manganese is attached to the sand surface.

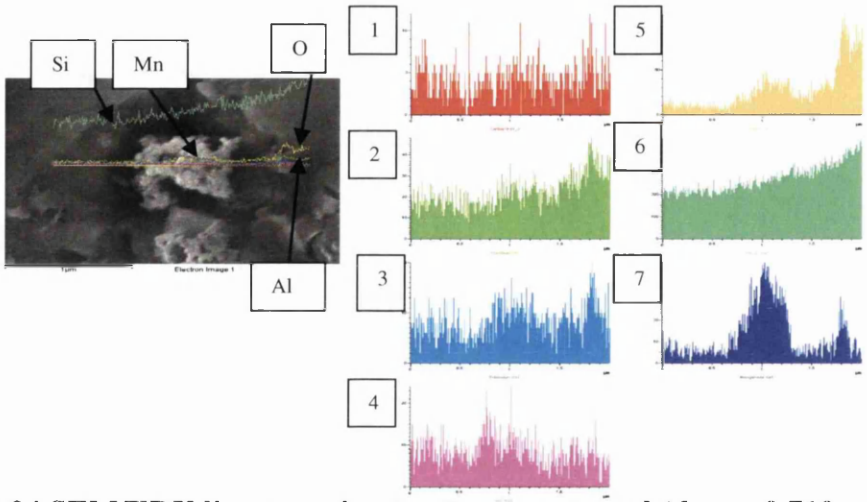

Figure 4.24 SEM/EDX line scanning for the coated sand (d_{sand} = 0.710mm, q_{Mn}/q_{sand} = 0.0709 mg Mn/g sand): 1 = C, 2 = Al, 3 = K, 4 = Fe, 5 = O, 6 = Si, 7 = Mn

Moreover, Table 4.3 shows the elemental composition of the coated sand. This composition was taken from the same image shown in Figures 4.23 – 4.24. Apart from the elements listed in uncoated sand, manganese was occurred significantly (2.84%). Although this manganese composition evidently supports the attachment of manganese into the sand surface, the value of this composition cannot be used as exact measure of composition because of the rough variable sample surface and difference in atomic number of the various elements.

Table 4.3 Elemental composition of coated sand (d_{sand} = 0.710mm, q_{Mn}/q_{sand} = 0.0709 mg Mn/g sand)

Element	Weight %	Atomic%
C K	15.24	26.96
O K	23.65	31.41
Mg K	0.15	0.13
Al K	2.78	2.19
Si K	44.73	33.83
K K	1.42	0.77
Ca K	0.57	0.30
Mn K	7.33	2.84
Fe K	4.12	1.57
Totals	100.00	100.00

4.1.4.3 Copper bearing coated sand

The EDX spectra for copper bearing coated sand are shown in Figure 4.25. Besides all elements discussed above in the coated sand, Figure 4.25 clearly shows the appearance of copper signal. Copper X-rays were both emitted from the K and L shells with the energy of 8.05 and 0.93 keV respectively. The occurrence of these copper counts indicates that the coated sand was effective in removing copper possibly through precipitation and adsorption mechanisms. Han et al. (2006a) have also shown (by SEM/EDX) the appearance of copper on their used sand in a batch system.

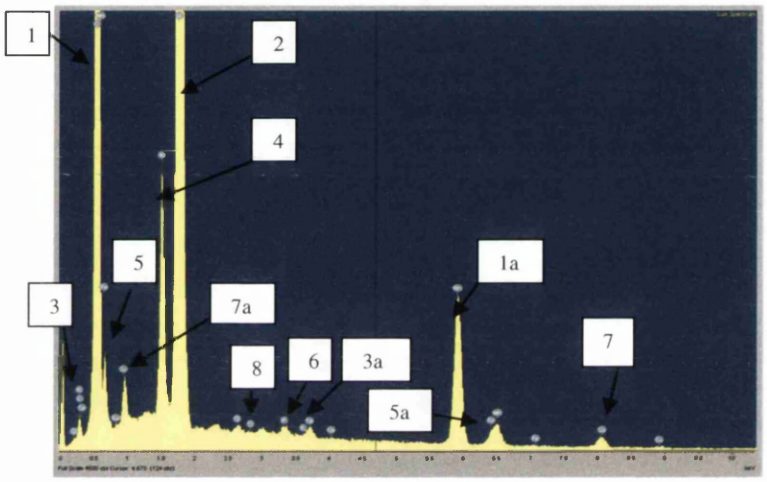

Figure 4.25 EDX spectra for copper bearing coated sand (d_{sand} = 0.710mm, q_{Mn}/q_{sand} = 0.0709 mg Mn/g sand, $C_{Cu\text{-}in}$ = 20 mg/L):1 = Mn L_α X-rays (0.64 keV), O K_α X-rays (0.52 keV), 1a = Mn K_α X-rays (5.90 keV), 2 = Si K_α X-rays (1.74 keV), 3 = C K_α X-rays (0.28 keV), Ca L_α X-rays (0.34 keV), 3a = Ca K_α X-rays (3.69 keV), 4 = Al K_α X-rays (1.49 keV), 5 = Fe L_α X-rays (0.70 keV), 5a = Fe K_α X-rays (6.40 keV), 6 = K K_α X-rays (3.31 keV), 7 = Cu K_α X-rays (8.05 keV), 7a = Cu L_α X-rays (0.93 keV), 8 = Cl K_α X-rays (2.62 keV)

Figure 4.25 also shows peaks of manganese indicating that not all manganese sites were occupied (or masked) by copper. Indeed calculation showed that only 13% of the active sites were potentially occupied by copper (Table 5.31, Figure 5.66 (d), Section 5.3.2.1). Figure 4.25 also shows the chlorine signal (Cl K_α X-rays = 2.62 keV). This may be due to contamination from tap water that was used to clean the beaker in the experiment before the beaker was washed by milipore water.

Figure 4.25 does not show the magnesium signal as shown in the coated sand sample (Figure 4.22). This may be due to the amount of magnesium was very small (Table 4.3).

Moreover, SEM/EDX line scanning, as shown in Figure 4.26, shows a significant level of copper alongside manganese within a cluster (which is evidently supported by its peak), proving the attachment of copper to the activated sand surface.

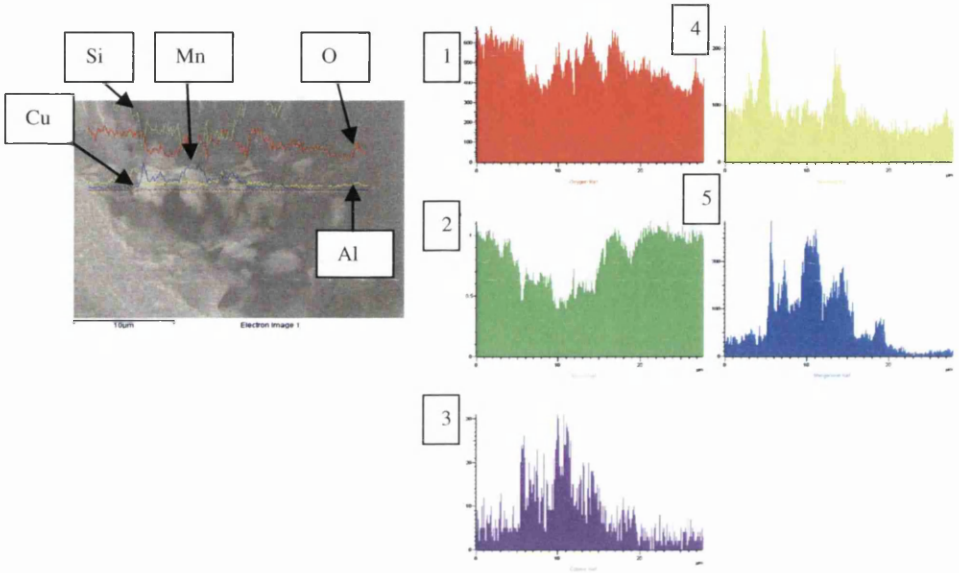

Figure 4.26 SEM/EDX line scanning for copper bearing coated sand (d_{sand} = 0.710mm, q_{Mn}/q_{sand} = 0.0709 mg Mn/g sand, $C_{Cu\text{-}in}$ = 20 mg/L):1 = O, 2 = Si, 3 = Cu, 4 = Al, 5 = Mn

The elemental composition of copper bearing coated sand is depicted in Table 4.4. This composition was derived from the same image as shown in Figure 4.26. Copper was occurred in quite high amount (0.14%) in the sample. This clearly evidences the attachment of copper into the sand surface. Manganese was also significant at 1.15% within the sand sample.

Table 4.4 Elemental composition of copper bearing coated sand (d_{sand} = 0.710mm, q_{Mn}/q_{sand} = 0.0709 mg Mn/g sand, $C_{Cu\text{-}in}$ = 20 mg/L)

Element	Weight%	Atomic%
C K	4.49	6.82
O K	66.27	75.54
Al K	2.23	1.50
Si K	22.54	14.64
Cl K	0.08	0.04
K K	0.10	0.04
Ca K	0.12	0.05
Mn K	3.47	1.15
Fe K	0.24	0.08
Cu K	0.48	0.14
Totals	100.00	100.00

4.1.4.4 Manganese bearing coated sand

Figure 4.27 depicts the EDX spectra for manganese bearing coated sand. The signals obtained were almost similar to that of the coated sand as discussed above. The manganese X-rays were emitted from both K and L shells. The manganese signal specifies that the coated sand was effective in removing manganese which likely occurred through precipitation and adsorption processes. Nevertheless, both calcium and magnesium signals were not detected in Figure 4.27 as they were in the coated sand sample (Figure 4.22). This may be due to the amounts of magnesium and calcium were very small as shown in Table 4.3.

In addition, Figure 4.28 shows the EDX elemental distribution mapping for the manganese bearing coated sand. The figure shows that manganese was spread over the surface of the coated sand. This gives a confirmation that manganese was attached to the activated sand surface, which is evidently shown as well by the SEM/EDX line scanning in Figure 4.29. This figure shows the manganese cluster as clearly supported by the peak of manganese signal.

Moreover, Table 4.5 depicts the elemental composition of manganese bearing coated sand. Manganese occurred within the sample only in a small concentration (0.05%). However, this small concentration of manganese is sufficient to prove that manganese was adsorbed onto the activated sand surface.

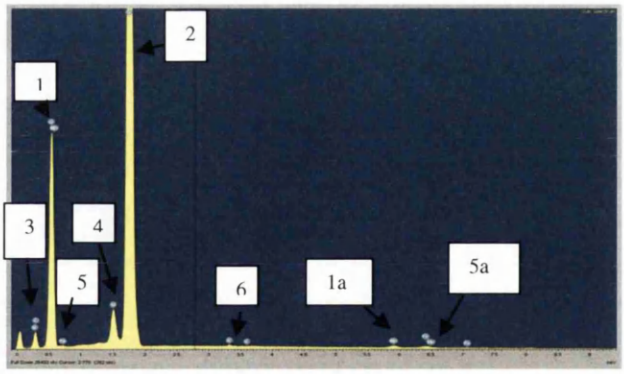

Figure 4.27 EDX spectra for manganese bearing coated sand (d_{sand} = 0.710mm, q_{Mn}/q_{sand} = 0.0709 mg Mn/g sand, $C_{Mn\text{-}in}$ = 20 mg/L): 1 = Mn L_α X-rays (0.64 keV), O K_α X-rays (0.52 keV), 1a = Mn K_α X-rays (5.90 keV), 2 = Si K_α X-rays (1.74 keV), 3 = C K_α X-rays (0.28 keV), 4 = Al K_α X-rays (1.49 keV), 5 = Fe L_α X-rays (0.70 keV), 5a = Fe K_α X-rays (6.40 keV), 6 = K K_α X-rays (3.31 keV)

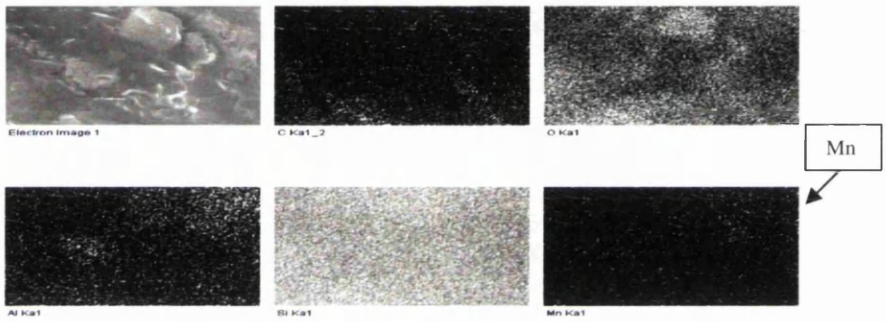

Figure 4.28 EDX elemental distribution mapping for manganese bearing coated sand (d_{sand} = 0.710mm, q_{Mn}/q_{sand} = 0.0709 mg Mn/g sand, $C_{Mn\text{-}in}$ = 20 mg/L)

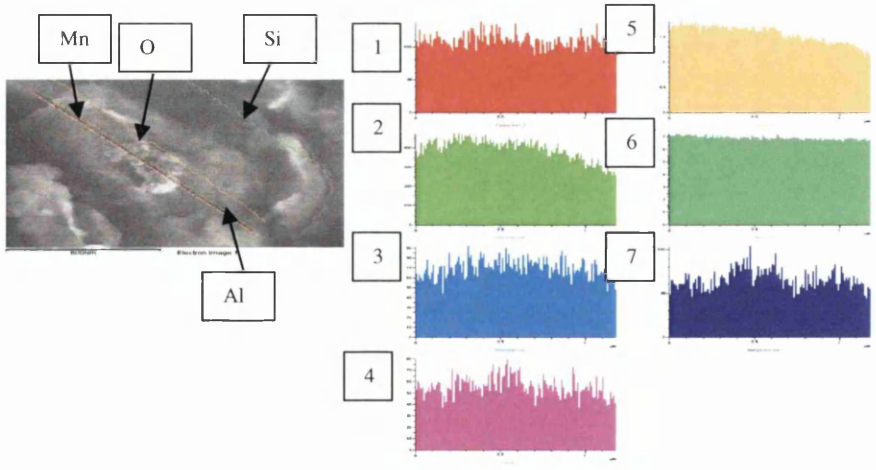

Figure 4.29 SEM/EDX line scanning for manganese bearing coated sand (d_{sand} = 0.710mm, q_{Mn}/q_{sand} = 0.0709 mg Mn/g sand, $C_{Mn\text{-}in}$ = 20 mg/L): 1 = C, 2 = Al, 3 = K, 4 = Fe, 5 = O, 6 = Si, 7 = Mn

Table 4.5 Elemental composition of manganese bearing coated sand (d_{sand} = 0.710mm, q_{Mn}/q_{sand} = 0.0709 mg Mn/g sand, $C_{Mn\text{-}in}$ = 20 mg/L)

Element	Weight%	Atomic%
C K	16.73	23.66
O K	57.04	60.54
Al K	1.24	0.78
Si K	24.68	14.92
K K	0.05	0.02
Mn K	0.15	0.05
Fe K	0.11	0.03
Totals	100.00	100.00

4.1.4.5 Zinc bearing coated sand

The EDX spectra for zinc bearing coated sand are shown in Figure 4.30. Apart from all elements discussed above in the coated sand, Figure 4.30 clearly shows the appearance of zinc signal. The zinc K_α X-rays and zinc L_α X-rays were both emitted with the energy of 8.64 and 1.01 keV respectively. This zinc signal indicates that the coated sand was effective in removing zinc possibly through precipitation and adsorption mechanisms. However, both potassium and magnesium signals were not detected in Figure 4.30 as they were in the coated sand sample (Figure 4.22). This may be due to the amount of magnesium and calcium was very small as shown in Table 4.3.

In addition, the EDX elemental distribution mapping for the zinc bearing coated sand is illustrated in Figure 4.31. The figure shows that zinc was identified within the cluster shown in the figure. This provides evidence that zinc was adsorbed to the activated sand surface. This is also supported by the SEM/EDX line scanning shown in Figure 4.32. This figure shows the zinc cluster as evidently confirmed by the peak of zinc signal. Figure 4.32 also illustrates the peaks of other cations i.e. calcium, iron and aluminium were in accordance with the peak of manganese. This supports the proposed theory of electrostatic attraction between the negatively charged manganese oxide with the positively charged cations as discussed in Chapter 6.

The amount of zinc within the sand sample was shown in Table 4.6 quantitatively. Zinc is appeared within the sample although in a very small amount (0.04%).

Nevertheless, this small amount of zinc is adequate to support the proposed theory of adsorption of zinc into the activated sand surface as discussed in Chapter 6.

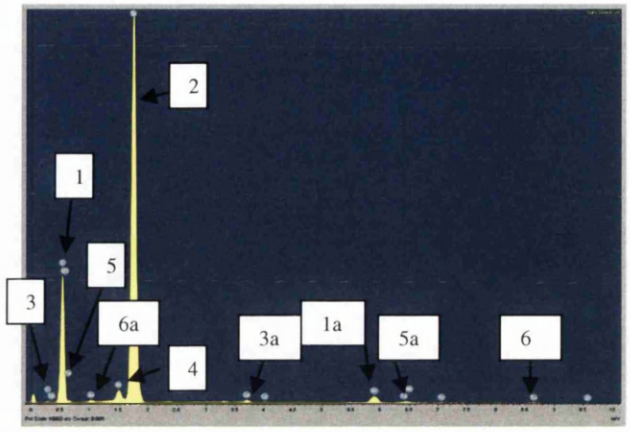

Figure 4.30 EDX spectra for zinc bearing coated sand (d_{sand} = 0.710mm, q_{Mn}/q_{sand} = 0.0709 mg Mn/g sand, $C_{Zn\text{-}in}$ = 20 mg/L): 1 = Mn L_α X-rays (0.64 keV), O K_α X-rays (0.52 keV), 1a = Mn K_α X-rays (5.90 keV), 2 = Si K_α X-rays (1.74 keV), 3 = C K_α X-rays (0.28 keV), Ca L_α X-rays (0.34 keV), 3a = Ca K_α X-rays (3.69 keV),4 = Al K_α X-rays (1.49 keV), 5 = Fe L_α X-rays (0.70 keV), 5a = Fe K_α X-rays (6.40 keV), 6 = Zn K_α X-rays (8.64 keV), 6a = Zn L_α X-rays (1.01 keV)

Figure 4.31 SEM/EDX elemental distribution mapping for zinc bearing coated sand (d_{sand} = 0.710mm, q_{Mn}/q_{sand} = 0.0709 mg Mn/g sand, $C_{Zn\text{-}in}$ = 20 mg/L)

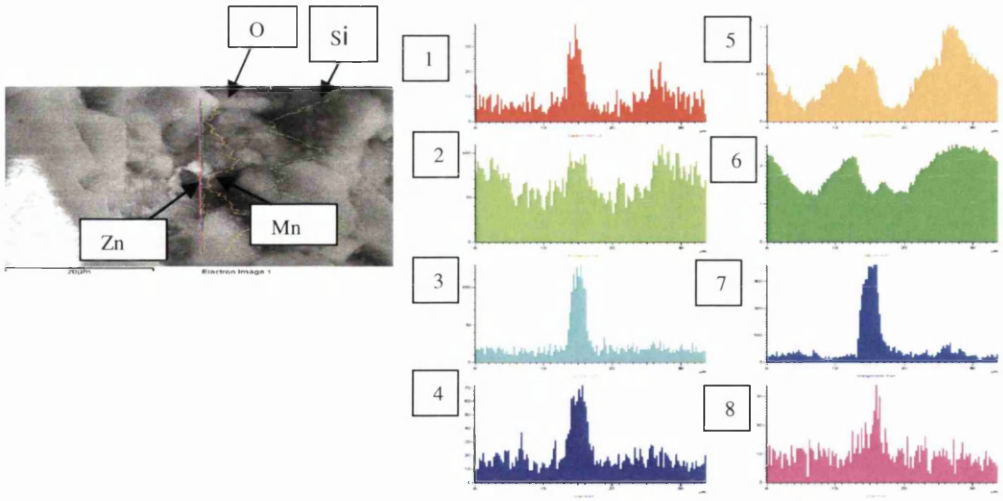

Figure 4.32 SEM/EDX line scanning for zinc bearing coated sand (d_{sand} = 0.710mm, q_{Mn}/q_{sand} = 0.0709 mg Mn/g sand, $C_{Zn\text{-}in}$ = 20 mg/L): 1 = C, 2 =Al, 3 = Ca, 4 = Fe, 5 = O, 6 = Si, 7 = Mn, 8 = Zn

Table 4.6 Elemental composition of zinc bearing coated sand (d_{sand} = 0.710mm, q_{Mn}/q_{sand} = 0.0709 mg Mn/g sand, $C_{Zn\text{-}in}$ = 20 mg/L)

Element	Weight%	Atomic%
C K	5.06	7.76
O K	61.57	70.83
Al K	0.89	0.61
Si K	30.95	20.28
Ca K	0.15	0.07
Mn K	1.06	0.35
Fe K	0.17	0.06
Zn K	0.14	0.04
Totals	100.00	100.00

4.1.4.6 Nickel bearing coated sand

Figure 4.33 shows the EDX spectra for nickel bearing coated sand. This figure evidently depicts the occurrence of nickel signal apart from all elements discussed above in coated sand. Both of the K and L shells of nickel emitted nickel X-rays with the energy of 7.48 and 0.85 keV respectively. Thus the coated sand was effective in removing nickel which likely occurred through precipitation and adsorption mechanisms.

The EDX elemental distribution mapping for the nickel bearing coated sand is also shown in Figure 4.34. The figure depicts that nickel was detected within the cluster shown. This clearly gives evidence that nickel was attached to the activated sand surface. Moreover, SEM/EDX line scanning (Figure 4.35) shows a significant level of nickel within a cluster (which is clearly confirmed by the peak of nickel signal) proving the attachment of nickel to the activated sand surface. Sharp peaks on the very left of the graphs for silica, manganese and carbon shown in Figure 4.35 may be due to anomaly. The figure also shows the decreasing intensity of X-rays counts for all the elements. This cannot be claimed as the decrease in the amounts of element of interest as it may occur due to the topographical effect (Goodhew et al., 2001).

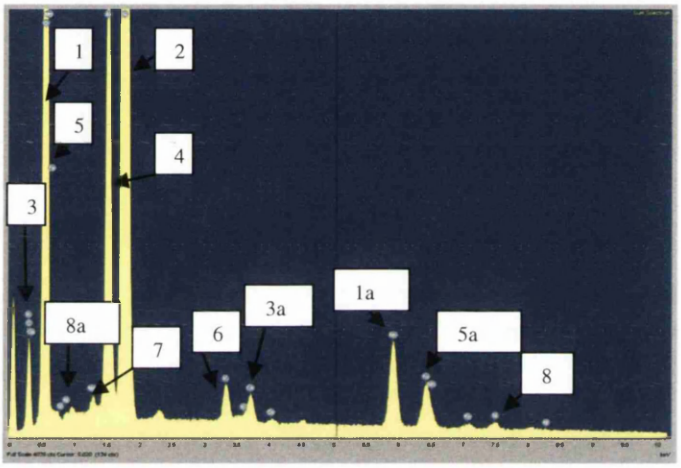

Figure 4.33 EDX spectra for nickel bearing coated sand (d_{sand} = 0.710mm, q_{Mn}/q_{sand} = 0.0709 mg Mn/g sand, $C_{Ni\text{-}in}$ = 20 mg/L): 1 = Mn L_α X-rays (0.64 keV), O K_α X-rays (0.52 keV), 1a = Mn K_α X-rays (5.90 keV), 2 = Si K_α X-rays (1.74 keV), 3 = C K_α X-rays (0.28 keV), Ca L_α X-rays (0.34 keV), 3a = Ca K_α X-rays (3.69 keV),4 = Al K_α X-rays (1.49 keV), 5 = Fe L_α X-rays (0.70 keV), 5a = Fe K_α X-rays (6.40 keV), 6 = K K_α X-rays (3.31 keV), 7 = Mg K_α X-rays (1.25 keV), 8 = Ni K_α X-rays (7.48 keV), 8a = Ni L_α X-rays (0.85 keV)

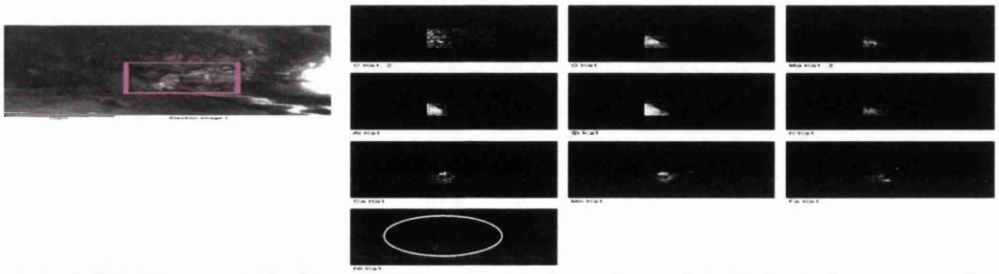

Figure 4.34 Elemental distribution mapping for nickel bearing coated sand (d_{sand} = 0.710mm, q_{Mn}/q_{sand} = 0.0709 mg Mn/g sand, $C_{Ni\text{-}in}$ = 20 mg/L)

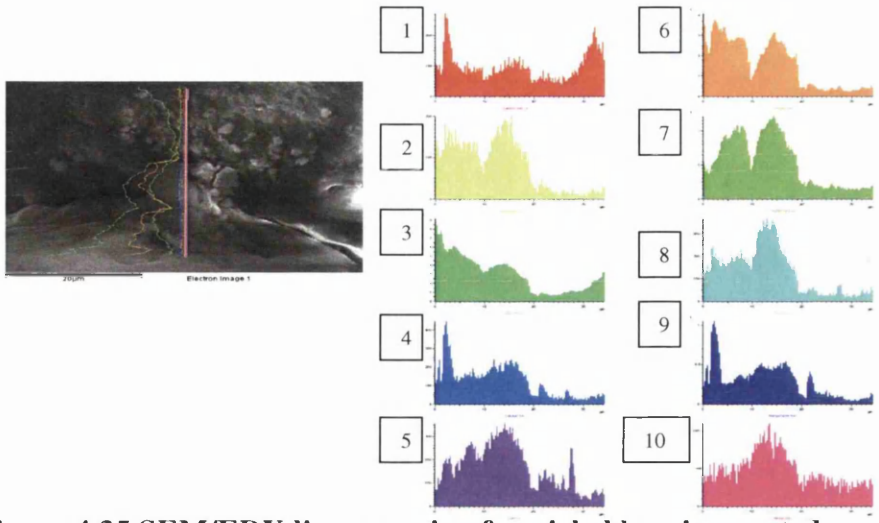

Figure 4.35 SEM/EDX line scanning for nickel bearing coated sand (d_{sand} = 0.710mm, q_{Mn}/q_{sand} = 0.0709 mg Mn/g sand, $C_{Ni\text{-}in}$ = 20 mg/L): 1 = C, 2 = Mg, 3 = Si, 4 = Ca, 5 = Fe, 6 = O, 7 = Al, 8 = K, 9 = Mn, 10 = Ni

Furthermore, the appearance of nickel within the sand sample was identified through the elemental analysis and is depicted in Table 4.7. Nickel occurred only in a very small amount (0.06%) in the sample. Nevertheless, this small amount of nickel is sufficient to confirm the attachment of nickel into the activated sand surface.

Table 4.7 Elemental composition of nickel bearing coated sand (d_{sand} = 0.710mm, q_{Mn}/q_{sand} = 0.0709 mg Mn/g sand, $C_{Ni\text{-}in}$ = 20 mg/L)

Element	Weight%	Atomic%
C K	18.13	25.50
O K	58.26	61.52
Mg K	0.20	0.14
Al K	6.59	4.13
Si K	11.74	7.06
K K	0.41	0.18
Ca K	0.42	0.18
Mn K	2.84	0.87
Fe K	1.21	0.37
Ni K	0.19	0.06
Totals	100.00	100.00

4.1.4.7 Mixed metals bearing coated sand

Figure 4.36 shows the EDX spectra for mixed metals bearing coated sand. This figure clearly shows the occurrence of all metals (copper, manganese, zinc and nickel) signals within the sample. Both K and L shell atoms emitted the detected X-rays. The presence of these metal signals thus indicates that the coated sand was effective in removing these mixed metals, which likely occurred through precipitation and adsorption mechanisms, from the water. Figure 4.36, however, does not show magnesium signal as shown in the coated sand sample (Figure 4.22). This may be due to the amount of magnesium was very small as shown in Table 4.3.

In addition, the EDX elemental distribution mapping for the mixed metals bearing coated sand is illustrated in Figure 4.37. Only copper, manganese, and zinc were detected within the cluster shown in the figure. Nickel was not identified in the figure. This may occur as the removal of nickel was low compared to the other elements as discussed later in Chapter 6. The bright points of copper, manganese, and zinc noticeably confirm that these elements were adsorbed onto the manganese coated sand surface. On the other hand, SEM/EDX line scanning, shown in Figure 4.38 shows a significant level of nickel together with the other elements within a cluster (which is clearly confirmed by its peak), proving the attachment of mixed metals to the activated sand surface. Nickel was more readily detected using a line scan concentrated onto the nickel rich area rather than the mapping over a larger area which would dilute the signal. The scan times were the same thus the electron beam is concentrated onto the nickel less when mapping over an area, hence the small quantity of nickel was not detected.

Moreover, the appearance of mixed metals within the sand sample was listed in the quantitative analysis shown in Table 4.8. All metals occurred in the list. Manganese came first with 0.48%. Copper came second with 0.24% followed by zinc and nickel with the amount of 0.03% and 0.01% respectively. Copper was actually removed in a greater quantity than manganese as discussed later in Chapter 6. This high amount of manganese occurred as manganese was the constituent or the coated material of the activated sand. Zinc and nickel that were the third and fourth most abundant in this quantitative analysis is supported by the results discussed later in Chapter 6 in which zinc and nickel came third and forth in the removal of mixed metals.

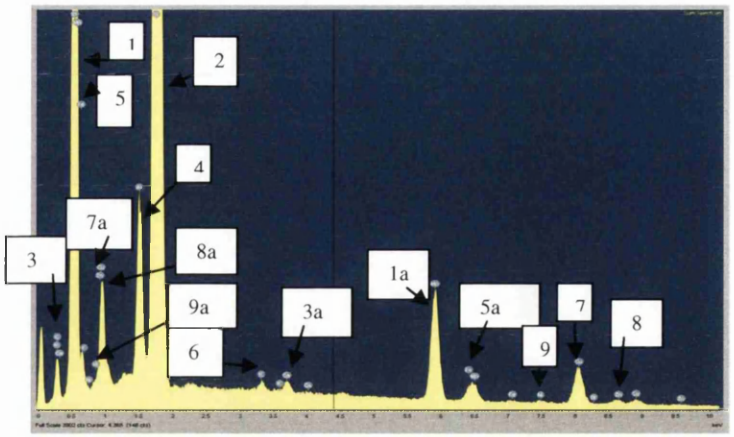

Figure 4.36 EDX spectra for mixed metals bearing coated sand (d_{sand} = 0.710mm, q_{Mn}/q_{sand} = 0.0709 mg Mn/g sand, C_{in} = 20 mg/L): 1 = Mn L_α X-rays (0.64 keV), O K_α X-rays (0.52 keV), 1a = Mn K_α X-rays (5.90 keV), 2 = Si K_α X-rays (1.74 keV), 3 = C K_α X-rays (0.28 keV), Ca L_α X-rays (0.34 keV), 3a = Ca K_α X-rays (3.69 keV),4 = Al K_α X-rays (1.49 keV), 5 = Fe L_α X-rays (0.70 keV), 5a = Fe K_α X-rays (6.40 keV), 6 = K K_α X-rays (3.31 keV), 7 = Cu K_α X-rays (8.05 keV), 7a = Cu L_α X-rays (0.93 keV), 8 = Zn K_α X-rays (8.64 keV), 8a = Zn L_α X-rays (1.01 keV), 9 = Ni K_α X-rays (7.48 keV), 9a = Ni L_α X-rays (0.85 keV)

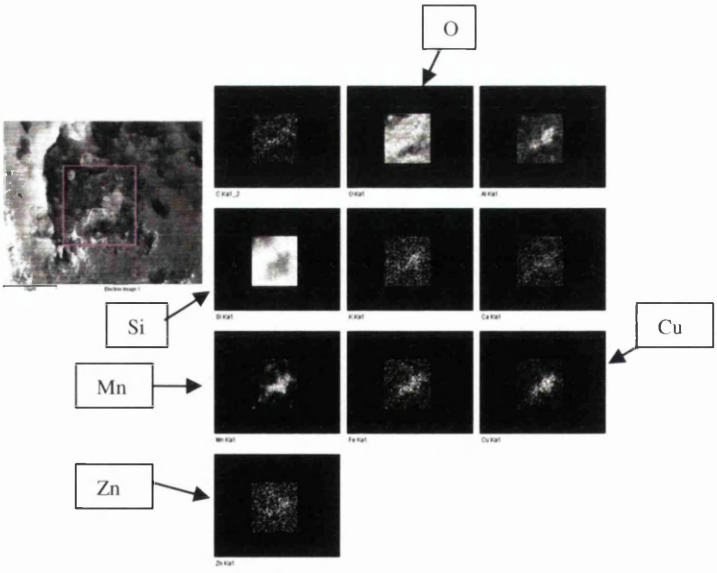

Figure 4.37 Elemental distribution mapping for mixed metals bearing coated sand (d_{sand} = 0.710mm, q_{Mn}/q_{sand} = 0.0709 mg Mn/g sand, C_{in} = 20 mg/L)

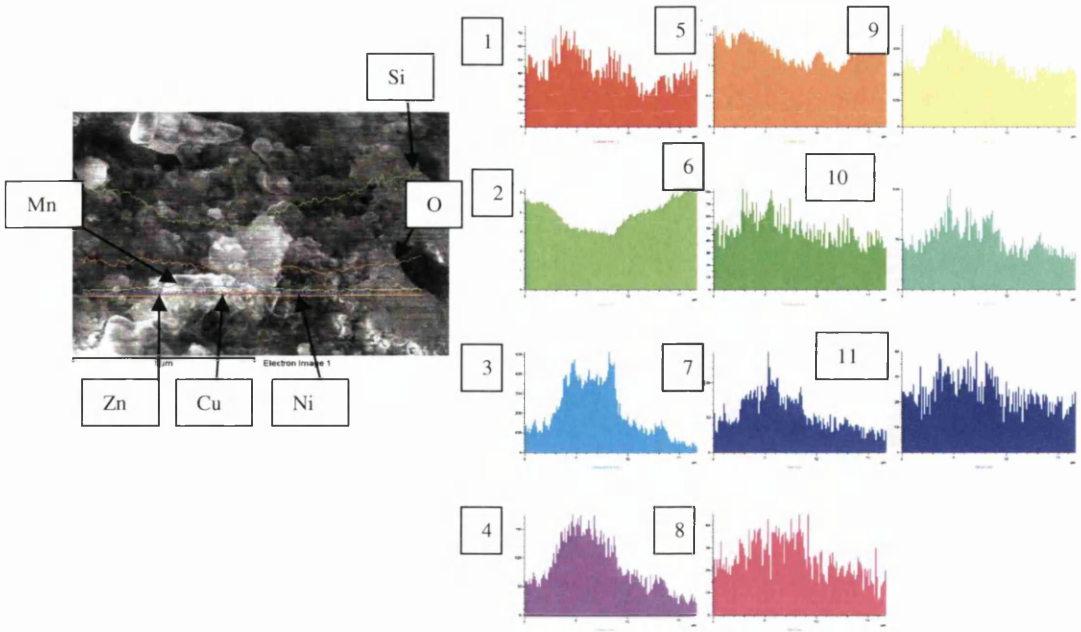

Figure 4.38 SEM/EDX line scanning for mixed metals bearing coated sand (d_{sand} = 0.710mm, q_{Mn}/q_{sand} = 0.0709 mg Mn/g sand, C_{in} = 20 mg/L): 1 = C, 2 = Si, 3 = Mn, 4 = Cu, 5 = O, 6 = K, 7 = Fe, 8 = Zn, 9 = Al, 10 = Ca, 11 = Ni

Table 4.8 Elemental composition of mixed metals bearing coated sand (d_{sand} = 0.710mm, q_{Mn}/q_{sand} = 0.0709 mg Mn/g sand, C_{in} = 20 mg/L)

Element	Weight%	Atomic%
C K	10.53	15.48
O K	61.35	67.71
Al K	1.40	0.91
Si K	23.88	15.01
K K	0.06	0.03
Ca K	0.09	0.04
Mn K	1.49	0.48
Fe K	0.16	0.05
Ni K	0.04	0.01
Cu K	0.88	0.24
Zn K	0.11	0.03
Totals	100.00	100.00

4.1.4.8 Waste water bearing coated sand

EDX spectra for waste water bearing coated sand are depicted in Figure 4.39. The figure shows that besides other elements occurred in the coated sand sample such as oxygen, silica, aluminium, potassium and calcium (Figure 4.22), only copper and manganese signals were detected. Other elements signals, such as zinc and nickel, were not detected. This may be because of the removal of these metals was lower compared to copper and manganese as shown and discussed later in Chapter 6. Magnesium was also not detected in Figure 4.39 as was in the coated sand sample (Figure 4.22). This may be due to the amount of magnesium was very small as shown in Table 4.3.

In addition, the EDX elemental distribution mapping for the waste water bearing coated sand is illustrated in Figure 4.40. Only copper and manganese contained in the waste water were detected within the cluster shown in the figure. Both zinc and nickel were not identified. This is most likely because the amounts in the sample were lower than the detection limit. This supports the results that zinc and nickel removals were lower compared to the other elements (i.e. copper and manganese) as discussed later in Chapter 6. The bright signals of copper and manganese distinctly verify that these elements were attached onto the manganese coated sand surface. Moreover, SEM/EDX line scanning, shown in Figure 4.41, merely shows a significant level of copper and manganese. This is apparent by the distinct peak, confirming the attachment of these metals to the activated sand surface. There was neither zinc nor nickel detected by the line scanning. This again may result from their low removal by the AUSF. Furthermore, the only attachment of copper and manganese into the sand surface was also shown in Table 4.9. This table illustrates the quantitative analysis for the waste water bearing coated sand. Copper was detected in small amounts (0.01%) on the sample; while manganese was detected at a greater quantity (0.11%). The higher amount of manganese may possibly occur due to manganese not only being contained in the water sample but also in the coated sand material. In addition, Chapter 6 shows that copper was removed preferentially over manganese.

Nickel and zinc which were actually removed by the AUSF although only in small amounts (Chapter 6) were not listed in the quantitative analysis table. This is possibly due to their concentrations were being very small so they were difficult to detect (Goodhew et al., 2001).

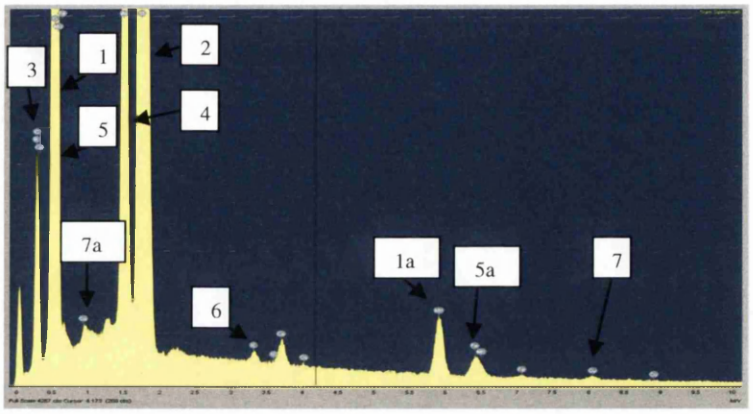

Figure 4.39 EDX spectra for waste water bearing coated sand (d_{sand} = 0.710mm, q_{Mn}/q_{sand} = 0.0709 mg Mn/g sand, $C_{Cu\text{-}in}$ = 11.78 mg/L, $C_{Mn\text{-}in}$ = 0.061 mg/L, $C_{Zn\text{-}in}$ = 0.6135 mg/L, $C_{Ni\text{-}in}$ = 0.81 mg/L): 1 = Mn L_α X-rays (0.64 keV), O K_α X-rays (0.52 keV), 1a = Mn K_α X-rays (5.90 keV), 2 = Si K_α X-rays (1.74 keV), 3 = C K_α X-rays (0.28 keV), Ca L_α X-rays (0.34 keV), 3a = Ca K_α X-rays (3.69 keV),4 = Al K_α X-rays (1.49 keV), 5 = Fe L_α X-rays (0.70 keV), 5a = Fe K_α X-rays (6.40 keV), 6 = K K_α X-rays (3.31 keV), 7 = Cu K_α X-rays (8.05 keV), 7a = Cu L_α X-rays (0.93 keV)

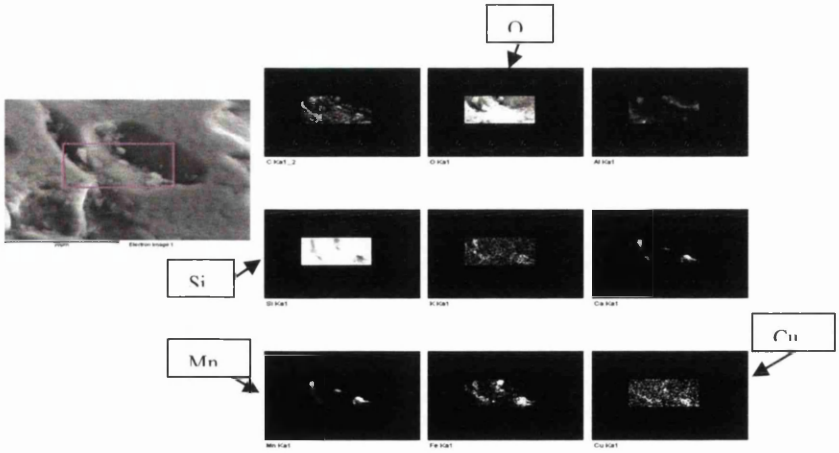

Figure 4.40 SEM/EDX elemental distribution mapping for waste water bearing coated sand (d_{sand} = 0.710mm, q_{Mn}/q_{sand} = 0.0709 mg Mn/g sand, $C_{Cu\text{-}in}$ = 11.78 mg/L, $C_{Mn\text{-}in}$ = 0.061 mg/L, $C_{Zn\text{-}in}$ = 0.6135 mg/L, $C_{Ni\text{-}in}$ = 0.81 mg/L)

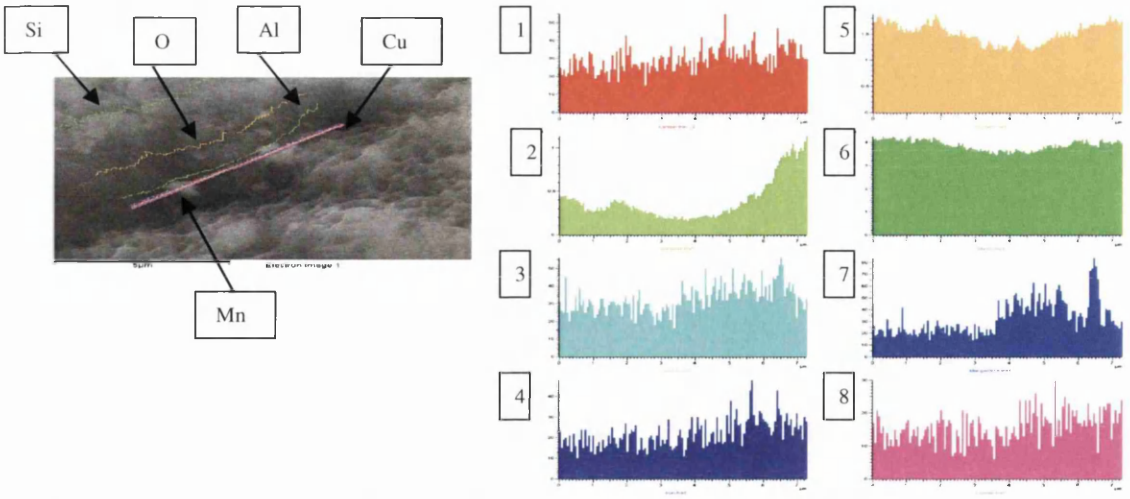

Figure 4.41 SEM/EDX line scanning for waste water bearing coated sand (d_{sand} = 0.710mm, q_{Mn}/q_{sand} = 0.0709 mg Mn/g sand, $C_{Cu\text{-}in}$ = 11.78 mg/L, $C_{Mn\text{-}in}$ = 0.061 mg/L, $C_{Zn\text{-}in}$ = 0.6135 mg/L, $C_{Ni\text{-}in}$ = 0.81 mg/L): 1 = C, 2 = Al, 3 = Ca, 4 = Fe, 5 = O, 6 = Si, 7 = Mn, 8 = Cu

Table 4.9 Elemental composition of waste water metals bearing coated sand (d_{sand} = 0.710mm, q_{Mn}/q_{sand} = 0.0709 mg Mn/g sand, $C_{Cu\text{-}in}$ = 11.78 mg/L, $C_{Mn\text{-}in}$ = 0.061 mg/L, $C_{Zn\text{-}in}$ = 0.6135 mg/L, $C_{Ni\text{-}in}$ = 0.81 mg/L)

Element	Weight%	Atomic%
C K	19.25	26.18
O K	61.45	62.72
Al K	2.27	1.37
Si K	16.36	9.52
K K	0.04	0.01
Ca K	0.09	0.04
Mn K	0.38	0.11
Fe K	0.12	0.04
Cu K	0.04	0.01
Totals	100.00	100.00

4.1.5 Sand particles resistance towards acid and alkali

3 g of 0.710 mm diameter of sand with 0.0709 mg manganese/g sand was used for each pH for these experiments. Figure 4.42 shows the results from the acid and alkali resistance tests. These tests are very important as they describe the attachment strength between manganese and sand surface.

The figure indicates that as the pH decreased from about 4.5 to 2, a significant release of manganese into the aqueous solution was observed. Manganese concentration as high as 1.8 mg/L, was measured at pH 2. Higher pH values than 4.5 gave almost no release of manganese into solution. This clearly indicates that pH affects the attachment of manganese on the sand surface and a careful control of pH higher than 4.5 assures high resistance to manganese leaching. Hu et al. (2004) have also observed similar results.

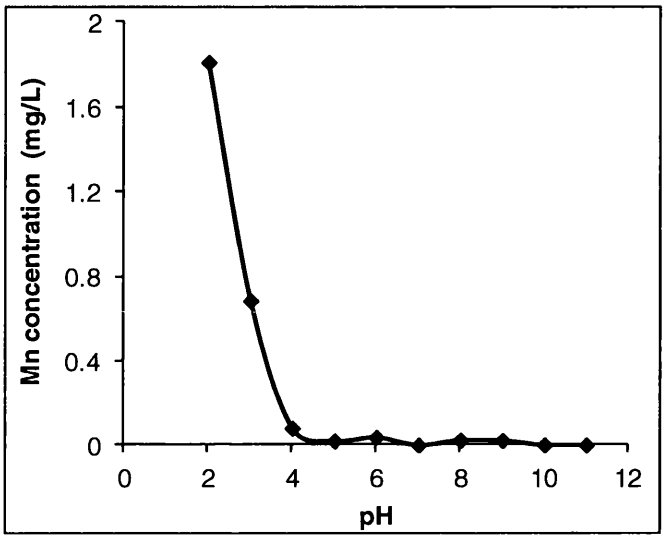

Figure 4.42 Acid and alkali resistance tests (d_{sand} = 0.710 mm, m Mn/m sand = 0.0709 mg Mn/g sand)

4.1.6 Sand particles point of zero charge

0.710 mm diameter of sand with 0.0709 mg manganese/g sand was used for obtaining the point of zero charge. Figure 4.43 shows that the point of zero charge (pzc) for the coated sand occurred at pH = 7.75. The pH was not altered once more coated sand was added to the solution.

4.1.7 Sand particles effect on pH

Sand particles effect on pH was studied using d_{sand} = 0.710mm, H = 450 mm, m_{sand} = 881.46 g, Q = 80.69 mL/min, and $m\ Mn/\ m\ sand$ = 0.0709 mg/g. Figure 4.44 illustrates the results.

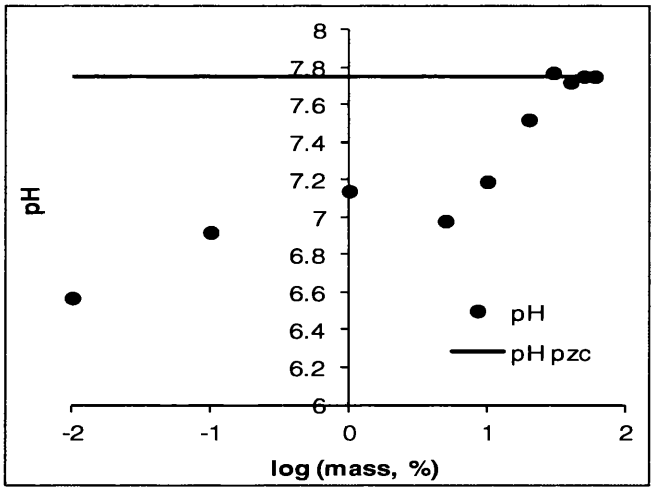

Figure 4.43 Point of zero charge (d_{sand} = 0.710 mm, m Mn/m sand = 0.0709 mg Mn/g sand)

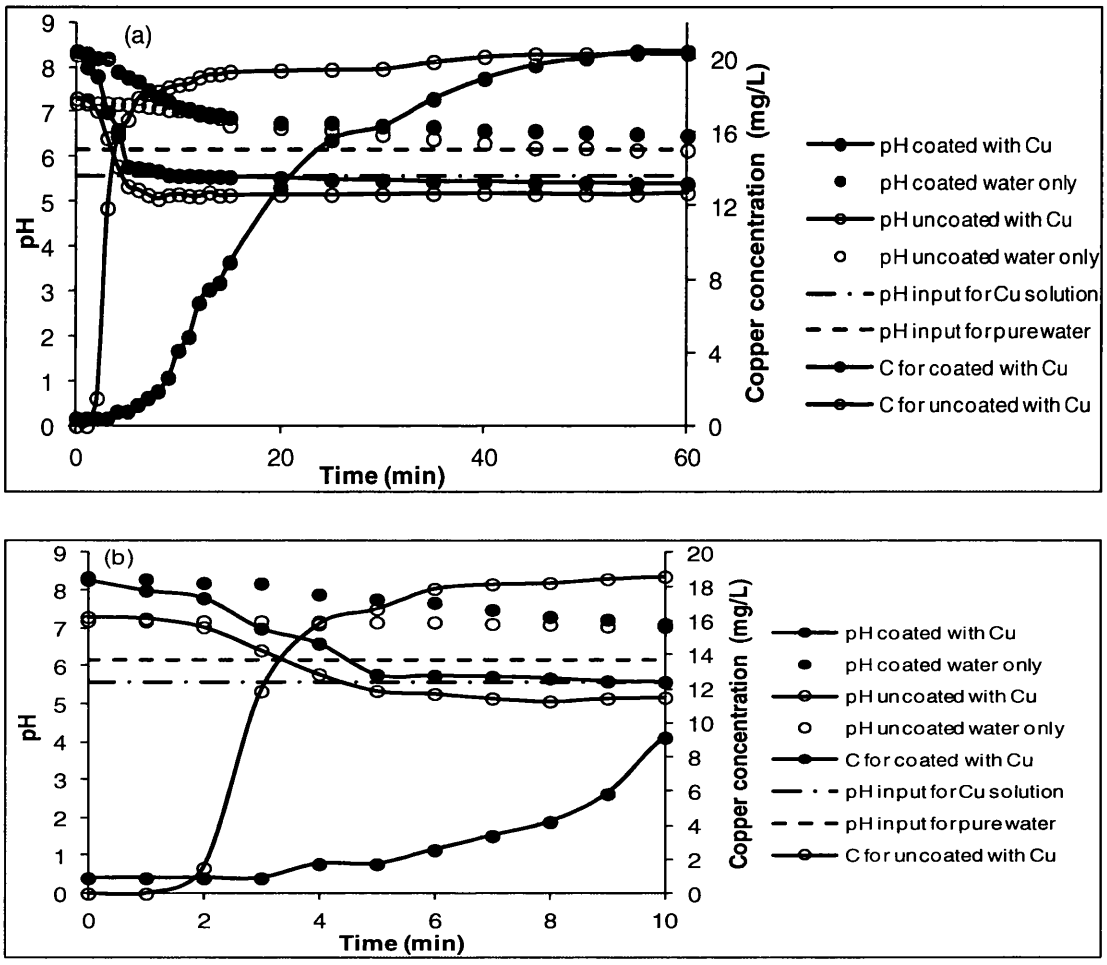

Figure 4.44 Sand particles effect on pH (d_{sand} = 0.710mm, H = 450 mm, m_{sand} = 881.46 g, Q = 80.69 mL/min, C_{in} = 20 mg/L, and $m\ Mn/\ m\ sand$ = 0.0709 mg/g) (a) Sand particles effect on pH; (b) Enlargement

The figure shows that once millipore water (pH = 6.15) was passing through the uncoated sand, the effluent pH decreased from 7.2 to 6.15. On the other hand, once this water passed through the coated sand, the effluent pH decreased from 8.35 to 6.47. The results clearly show that coating the sand resulted in increasing pH. This is also supported with the results once copper was added to the water. Once this copper solution (pH = 5.59) was passing through the uncoated sand, the pH was decreasing from 7.30 to 5.20; while once the copper solution was passing through the coated sand, the pH was decreasing from 8.28 to 5.4. This is also confirmed by batch tests of uncoated and coated sand; pH for uncoated sand was 7.3, while for the coated sand, the pH was 7.81.

It appears from the figure that initially the pH is high when either water or copper solution is passed through uncoated or coated sand. This may be due to natural air flowing through the AUSF as was also confirmed by Al-Layla (1978).

4.1.8 Sand particles porosity

The porosity of sand is measured by using the procedure described in Section 3.1.3.1. For each diameter of sand, three experiments were done. The porosity was then calculated by using Equation 3.2 and the results were shown in Table 4.10. Table 4.10 depicts that porosity of sand is in the range of (36.92-38.04) %.

Table 4.10 Porosity of sand

Diameter of sand (mm)	Porosity			Average (%)	Std dev	Error (%)
	Exp. 1	Exp. 2	Exp.3			
0.85	37.69	38.44	37.87	38.00	0.3929	0.52
0.71	37.41	37.00	36.93	37.11	0.2583	0.35
0.50	36.78	37.31	36.68	36.92	0.3363	0.46
0.40	38.81	37.47	37.82	38.04	0.6956	0.91

4.1.9 Manganese content on the coated sand

The amounts of manganese on the surface of the coated sand were measured through acid digestion analysis (Appendix 3.12).

The results from the acid digestion analysis are shown in Table 4.11 (a-c) for d_{sand} = 0.710mm and summarized in Table 4.11 (d). Table 4.11 (d) reveals that the amounts of manganese on the surface of the coated sand were 0.0709, 0.1261 and 0.1341 mg Mn/g sand respectively.

Table 4.11 (a) Ratio of manganese to mass of sand (1)

Vol initial (mL)	Final vol after digestion completed (mL)	Diluted to (mL)	*C* measured (mg/L)	*C* after digestion (mg/L)	*m*Mn (mg)	*q* (mg Mn/g sand)	*q* (micro-mol Mn/g sand)
25	15	100	0.695	4.63	0.070	0.070	1.265
25	16.5	50	1.326	4.02	0.066	0.066	1.207
25	15.5	50	1.525	4.92	0.076	0.076	1.388
			Average	4.524	0.071	**0.071**	1.287
			Std dev	0.461	0.005	0.005	0.092
			Error (%)	6	4	4	4

Note:

1. m_{sand} = 1 g, d_{sand} = 0.710mm
2. M Mn = 54.938 g/mol

Table 4.11 (b) Ratio of manganese to mass of sand (2)

Vol initial (mL)	Final vol after digestion completed (mL)	Diluted to (mL)	*C* measured (mg/L)	*C* after digestion (mg/L)	*m*Mn (mg)	*q* (mg Mn/g sand)	*q* (micromo l Mn/g sand)
25	16	100	1.23	7.71	0.123	0.123	2.244
25	16	100	1.28	7.99	0.128	0.128	2.326
25	17	100	1.27	7.46	0.127	0.127	2.308
			Average	7.72	0.126	**0.126**	2.293
			Std dev	0.26	0.002	0.002	0.043
			Error (%)	2	1	1	1

Note: Same as Table 4.11 (a)

Table 4.11 (c) Ratio of manganese to mass of sand (3)

Vol initial (mL)	Final vol after digestion completed (mL)	Diluted to (mL)	*C* measured (mg/L)	*C* after digestion (mg/L)	*m*Mn (mg)	*q* (mg Mn/g sand)	*q* (micromol Mn/g sand)
25	16.5	100	1.326	8.04	0.133	0.133	2.414
25	17	100	1.368	8.05	0.137	0.137	2.490
25	17	100	1.33	7.82	0.133	0.133	2.421
			Average	7.97	0.134	**0.134**	2.442
			Std dev	0.126	0.002	0.002	0.042
			Error (%)	1	1	1	1

Note: Same as Table 4.11 (a)

Table 4.11 (d) Summary of ratio of manganese to mass of sand

	q (mg Mn/g sand)		
	Exp. 1	Exp. 2	Exp. 3
Average	0.071	0.126	0.134
Std dev	0.005	0.002	0.002
Error (%)	4	1	1

Note:
1. Same as Table 4.11 (a)
2. Summarized from Table 4.11 (a) – (c)

The strength of manganese coating onto the surface of the sand was also observed through acid digestion analysis. 0.400mm sand particle diameter was used for this study. In this case, acid digestion analysis was done for fresh sand and for sand that has been used to treat 10mg/L copper in AUSF. The results are shown in Table 4.11 (e-f) and summarized in Table 4.11 (g). Table 4.11 (g) reveals that there was no manganese leaching from the coated sand. This is also supported by the AUSF results (Section 5.3.7).

Table 4.11 (e) Ratio of manganese to mass of sand for fresh coated sand

Vol initial (mL)	Final Vol after digestion completed (mL)	Diluted to (mL)	*C* measured (mg/L)	*C* after digestion (mg/L)	*m*Mn (mg)	*q* (mg Mn/g sand)	*q* (micromol Mn/g sand)
25	10	100	0.893	8.930	0.089	0.089	1.625
25	8	100	1.155	14.438	0.116	0.116	2.102
25	15	100	1.307	8.713	0.131	0.131	2.379
			Average	10.694	0.112	**0.112**	2.036
			Std dev	3.244	0.021	0.021	0.381
			Error (%)	18	11	11	11

Note:

1. m_{sand} = 1 g, d_{sand} = 0.400mm
2. M Mn = 54.938 g/mol

Table 4.11 (f) Ratio of manganese to mass of sand for coated sand that has been used to treat 10 mg/L copper

Vol initial (mL)	Final Vol after digestion completed (mL)	Diluted to (mL)	*C* measured (mg/L)	*C* after digestion (mg/L)	*m*Mn (mg)	*q* (mg Mn/g sand)	*q* (micromol Mn/g sand)
25	12	100	1.249	10.408	0.125	0.125	2.273
25	13	100	1.212	9.323	0.121	0.121	2.206
25	13.5	100	1.252	9.274	0.125	0.125	2.279
			Average	9.668	0.124	**0.124**	2.253
			Std dev	0.641	0.002	0.002	0.041
			Error (%)	4	1	1	1

Note:

1. m_{sand} = 1 g, d_{sand} = 0.400mm, C_{in} = 10 mg/L
2. M Mn = 54.938 g/mol

Table 4.11 (g) Summary of the amount of manganese on the surface of the sand for fresh and used coated sand

$C_{Cu\text{-}in}$ (mg/L)	after digestion
	q (mg Mn/g sand)
uncoated	0.000
0	0.112
10	0.124

Note:

1. m_{sand} = 1 g, d_{sand} = 0.400mm
2. M Mn = 54.938 g/mol
3. Summarized from Table 4.11 (f) – (g)

4.2 Sand bed characterisation

Before proceeding with sand bed characterisation, pump and AUSF flow rate have to be defined first.

4.2.1 Flow rate regulation of the AUFS

Several arrangements, especially those for the top and bottom perforated plate and the spray tube, were made for the AUSF in order to be run properly. The flow rate of the AUSF was measured with the procedure shown in Appendix 3.6 and calculated with Equation 3.1. This flow rate was measured for various heights (150, 250, 350, and 450 mm) of each diameter (0.850, 0.710, 0.500, 0.400 mm) of sand. The results are summarized in Table 4.12.

Table 4.12 AUSF flow rate

	Height of sand (mm)	Pump rotation speed (%)	Average AUSF flow rate (L/min)			
Sand diameter (mm)			0.85mm	0.71mm	0.50mm	0.40mm
	150	8	98.94	98.23	o/f	o/f
		7	83.65	80.30	79.75	o/f
		6	62.88	62.78	60.27	53.28
		5	45.02	44.59	41.88	40.31
	250	8	93.02	o/f	o/f	o/f
		7	80.19	72.20	o/f	o/f
		6	58.46	55.01	o/f	o/f
		5	39.20	37.65	37.40	o/f
	350	8	86.79	o/f	o/f	o/f
		7	77.92	o/f	o/f	o/f
		6	56.85	45.24	o/f	o/f
		5	38.51	36.24	o/f	o/f
	450	8	81.91	80.69	78.75	o/f
		7	74.40	65.35	62.98	o/f
		6	55.01	55.97	42.09	o/f
		5	37.78	37.99	38.33	25.01
		4	16.39	16.30	16.21	16.16

Note:
1. o/f = over flow
2. for uncoated sand

The maximum rotation speed of the pump was 8% as beyond that the sand was submerged with water, which for this research, has to be avoided as the condition of unsaturated sand filter will not be met. The minimum rotation speed was 4% as below that the flow rate was very small. The table depicts that as the height of sand increased, the AUSF flow rate decreased for the same rotation speed (= flow rate) of the pump. In addition, for the same rotation speed (= flow rate) of the pump, the AUSF flow rate increased as the diameter of sand increased. Moreover, as the pump rotation speed decreased, the AUSF flow rate decreased.

4.2.2 Tracer studies

Tracer studies were carried out to determine the hydraulic performance of the AUSF. From these studies, the theoretical mean detention time, $\bar{t}_c$, the spread of the distribution measured by the variance σ^2_c and the total mass of salt measured at the reactor effluent, m_{salt} were determined (Tchobanoglous et al., 2004). A pulse of 10 mL of 100 mg/L sodium chloride (NaCl) was used as a tracer and injected into the influent end of the AUSF. The tracer experiments were carried out at various flow rates (81.9, 74.4, 55.0, 37.8, and 16.4 mL/min). Conductivity calibration was initially done showing a correlation factor of ≈ 1 as shown in Figure 4.45.

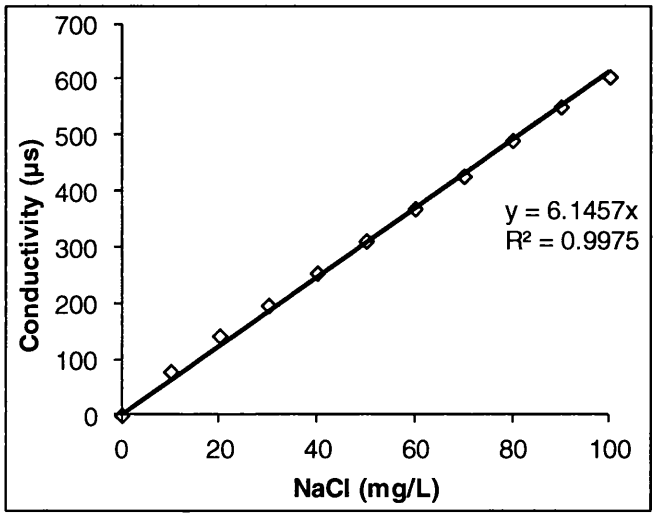

Figure 4.45 Conductivity calibration

The C-curves obtained at these different flow rates are illustrated in Figure 4.46 and their corresponding residence times and variances are summarized in Table 4.13. Consistency checks were made and showed that most of the tracer was recovered by more than 95% on average at the effluent end of the column. These checks validate the study. Figure 4.46 shows non symmetrical c-curves with tails. This indicates that the flow approaches plug flow but with dispersion. The degree of dispersion is characterised by calculating the dispersion number ($d_n = D/uL$) from σ^2 using the open-open vessel model ($\sigma^2 = 2d_n + 8d_n^2$) (Levenspiel, 1999). An average value of d_n was obtained = 0.041±0.016. The magnitude of d_n number value indicates that the flow did not deviate largely from plug flow, which validates the model used to describe the observed experimental results.

Results of the variance (Table 4.13) show that the spread of the data from the mean is about 5%, hence the mean residence time from the c-curves, $\bar{t}_c$, can be defined as the ratio of V_L/Q, where V_L represents the volume occupied by the liquid in AUSF and Q is the flow rate of water passing through AUSF. The fraction of volume occupied by liquid to the total column volume is then $\varepsilon_L=V_L/V$ and the fraction of volume occupied by the gas to the total column volume is then $\varepsilon_G = (\varepsilon - \varepsilon_L)$, where ε is the total voidage in the column having a value equal to 0.38 determined in a preliminary study. Values of ε_G are shown in Table 4.13. The results in Table 4.13 clearly shows that as the flow rate increased, the fraction of gas available in the column decreased since the more liquid is expected to occupy more pores. This relationship was confirmed by a correlation factor of 0.99 as shown in Figure 4.47. The higher the ε_G, the more unsaturated condition is expected to be, which leads to higher removal rates. As a result, operating at lower flow rates gives better removal percentages. This is confirmed by the results shown in Section 5.3.4. Moreover, the results clearly prove that when the flow was introduced at the top of the column, the sand bed was not fully submerged in water, hence the system operated under unsaturated conditions.

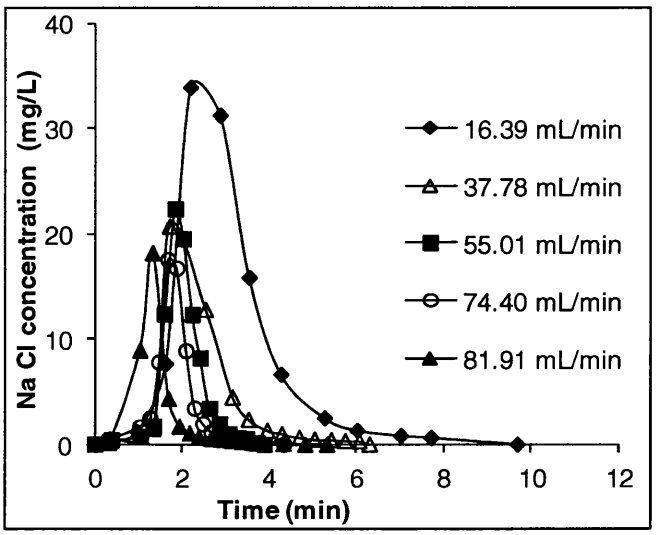

Figure 4.46 C-curves (m_{salt} = 1mg; d_{sand} = 0.850mm; H = 450 mm)

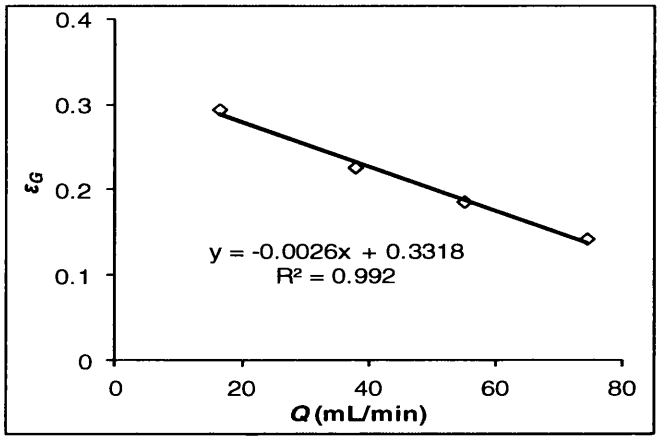

Figure 4.47 Flow rate (mL/min) vs ε_G (d_{sand} = 0.850mm,m_{sand} = 892.28 g, H = 450 mm)

Table 4.13 Hydraulic performances derived from tracer studies (m_{salt} = 1mg; d_{sand} = 0.850mm, m_{sand} = 892.28 g, H = 450 mm)

V (mL)	565.49	565.49	565.49	565.49	565.49
ε	0.38	0.38	0.38	0.38	0.38
Q (mL/min)	81.90	74.40	55.00	37.80	16.40
$\bar{t}_c$ (min)	1.38	1.80	1.99	2.29	2.95
σ^2_c (min^2)	0.24	0.18	0.19	0.68	1.13
τ (min)	2.62	2.89	3.91	5.69	13.11
m_{salt} injected/ m_{salt} integration	0.93	0.98	0.99	0.95	0.88
σ_θ^2 (min^2)	0.12	0.06	0.05	0.13	0.13
d_n (unitless)	0.05	0.03	0.02	0.05	0.05
V_L (mL)	113.02	133.92	109.45	86.56	48.38
ε_L	0.20	0.24	0.19	0.15	0.09
ε_G	0.18	0.14	0.19	0.23	0.29

4.3 Conclusions

Sand was sieved to 0.850mm, 0.710 mm, 0.500mm and 0.400mm sand particle size by a Russell Finex Sieve. The porosity of sand is in the range of (36.92-38.04) %.

The BET results support the assumed mechanism of copper removal (Section 5.4), i.e. surface attachment through precipitation and adsorption (electrostatic attraction) process, and possible surface complexation. This is shown by the increase in surface area of sand by 21% from 0.302 to 0.365 m^2/g-sand after coating, and the reduction of it (up to half to 0.163 m^2/g-sand) after the coated sand has been used to treat copper. AUSF was also proven to reduce the surface area up to half as it was 0.163 m^2 /g-sand under saturated condition and 0.084 m^2 /g-sand under unsaturated condition.

SEM image of uncoated sand showed that the sand had a fairly uniform and smooth surface with small fractures. In contrast, the coated sand emerged as a rough surface inhabited by the likely clusters of uniformly rounded shapes of newborn manganese oxides. This occurrence was confirmed in the SEM-EDX, acid alkali resistance, and digestion analysis.

SEM images of the used coated sand appeared as fractures and some unique clusters, the form of which depend on the element in the sample, occurred on the surface. The SEM/EDX analysis for uncoated sand showed that the sand contained O, Si, Ca, Al, Fe, Mg, K and S; while the coated sand contained manganese besides those elements. The EDX spectra for the used coated sand showed that the sand contained the element that was removed by the sand. The SEM/EDX results support the results of the metals removal and the hypothesis that metals may well be removed by precipitation and adsorption on the surface of the manganese coated sand (Chapter 5).

The acid and alkali resistance tests showed that pH affects the attachment of manganese on the sand surface and a careful control of pH higher than 4.5 assures high resistance to manganese leaching.

The point of zero charge (pzc) for the coated sand occurred at pH=7.75. The results of sand particles effect on pH revealed that coating the sand resulted in increasing pH (pH for uncoated sand = 7.3, for coated sand = 7.81).

The pH was initially raised once both water and copper solutions were passing through either uncoated or coated sand.

The maximum rotation speed of the pump was 8% as beyond that the sand was submerged with water; while the minimum speed was 4% as below that the flow rate was very small.

Acid digestion analysis showed that the amount of manganese on the surface of the sand was 0.0709, 0.1261 and 0.1341 mg Mn/g sand respectively. There was no manganese leaching out of the sand surface as has been proved by AUSF results (Section 5.3.7).

Tracer studies showed that the flow approaches plug flow but with low dispersion (d_n = 0.041±0.016) which validates the AUSF used to describe the observed experimental results. The studies also showed that operating at lower flow rates gives better removal percentages (as discussed later in Section 5.3.4) and proved that when the flow was introduced at the top of the column, the sand bed was not fully submerged in water, hence the system operated under unsaturated conditions.

CHAPTER 5

COPPER REMOVAL

In order to find out the optimal conditions for AUSF, copper was studied in this work as copper was assumed to be fairly representative of all the studied metals. Flame atomic absorption spectrometry (FAAS) was used to analyse the copper concentration and standard calibration has to be made prior to the analysis. This chapter thus first describes the standard calibration performed for the FAAS. Both batch and column studies were performed in this research. Batch studies were run to study the kinetic and equilibrium of the sorption of copper ions from water by coated sand. Different operating conditions were run to investigate the performance of coated sand in removing copper in batch studies. These parameters were different initial concentrations, pH values, dissolved oxygen (DO) contents, mass of sand and sand coating (mgMn/g sand). Blank samples were done for several samples in batch studies to validate the results. The attachment strength of manganese onto the coated sand was also observed in the batch studies.

For column studies, the performance of AUSF in removing copper was compared to the saturated condition. Next, various operating conditions were run to study the effect of these conditions to the performance of AUSF. These parameters were different initial concentrations, height of sand columns, flow rates, sand particle diameters, manganese to sand ratios, and reusing the sand bed material. The results from column studies are then compared to those from batch studies. Finally, the processes of copper removal that may occur within the AUSF are proposed.

5.1 Standard calibration for the FAAS

The stabilized (10% HNO_3) 0, 2, 4, 6, 8, 10, 15, 20, 25, 30, 40, and 50 mg/L standard solutions of copper were made to perform FAAS standard calibration by using the FAAS Perkin – Elmer 272.

The absorbance of each standard solution of copper for 216.5 nm - 0.2 slit, and 324.8 nm - 0.7 slit (The Perkin Elmer Corporation, 1996) were then measured and the graphs between absorbance and concentration were plotted. The results are shown in Figures 5.1 (a – b).

The results show that the relationships between absorbance and copper concentration were linear and their correlation factors were close to 1 (Figures 5.1 (a – b)). This reflects that they followed Beer's Law (Skoog et al., 2007). These graphs were then used as standard calibration graphs to measure copper concentrations with FAAS.

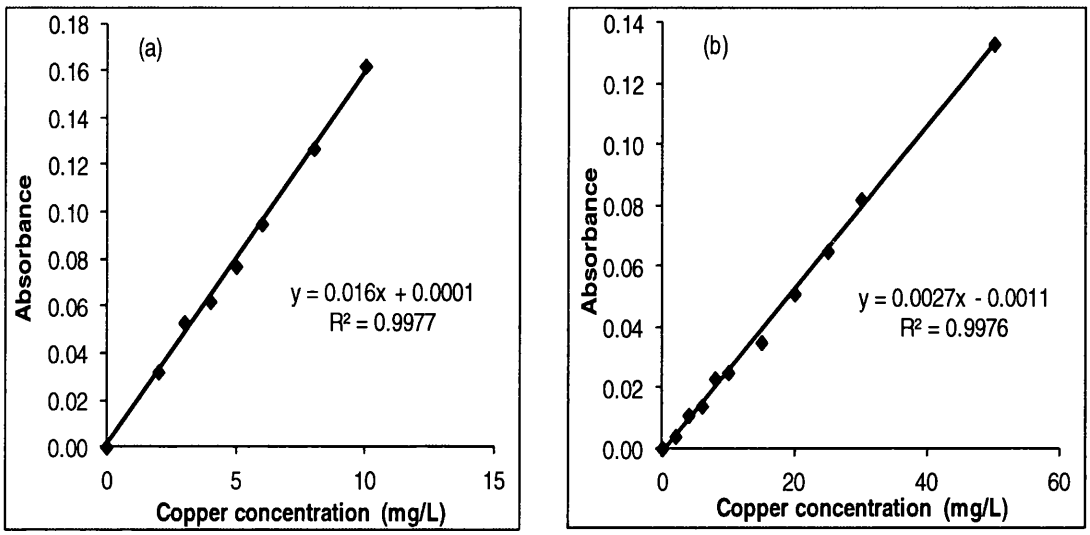

Figure 5.1 Standard calibrations for copper (a) for 3 – 5 mg/L copper: 324.8 nm, 0.7 slit (b) for 10 – 20 mg/L copper: 216.5 nm, 0.2 slit

5.2 Batch studies

The quantity of copper adsorbed onto the filter paper during the filtration was found to be less than 7% for all the m_{sand} between 7.5-100.0 g; less than 5% for all the C_{in} between 5 – 20 mg/L g and for the uncoated and coated sand; less than 4% for all the *DO* content between 0 – 20 mg/L (Table 5.1). Thus, the effect of the filter paper on adsorption by the adsorbents can be neglected during the studies. For the effect of pH on copper removal, however, the effect of the filter was significant for pH = 8 and pH =9, where this quantity was found to be = 55% for pH = 8 and 66% for pH = 9. This is confirmed with the pH values taken after filtration (Table 5.2).

Table 5.1 Percentage of reduction after filtration

	C before filtration (mg/L)	*C* after filtration (mg/L)	% reduction
pH			
3	23.76	22.81	4.01
4	23.60	23.48	0.54
5	24.20	23.32	3.65
6	23.13	23.02	0.48
7	22.93	21.29	7.15
8	21.02	9.36	55.48
9	22.26	7.56	66.06
C_{in} (mg/L)			
6.87	7.23	6.87	5.03
13.9	14.04	13.90	0.97
17.98	18.92	17.98	4.93
23.32	24.20	23.32	3.65
m_{sand} (g)			
5	23.26	21.71	6.66
7.5	22.81	21.56	5.51
10	22.81	21.56	5.51
30	24.20	23.32	3.65
50	24.20	23.32	3.65
100	26.15	25.03	4.30
DO (mg/L)			
0.29	20.14	19.78	1.77
2.4	21.86	21.41	2.07
8.95	24.20	23.32	3.65
17.08	23.78	23.09	2.93
Sand coating (mgMn/gsand)			
0	26.15	25.03	4.30
0.071	24.20	23.32	3.65

Table 5.2 shows that the pH value significantly increased after filtration for pH = 3 – 6, and decreased after filtration for pH = 7 – 9. This reflects that some of copper were removed by the filter paper for pH = 7 – 9. The pH values that increased after filtration for pH = 3 – 6 may be attributed to the influence from the millipore water, which was more alkaline (pH = 6.68), that was used to clean the filter during the experiments. Blank samples were carried out for pH = 6 – 8 to anticipate this matter. For pH 3 to pH 7, this quantity was found to be less than 7%.

Table 5.2 pH values taken before and after filtration (C_{in} = 20 mg/L)

pH	Before filtration			Average	Error (%)	After filtration			Average	Error (%)	Reduction (%)
	1	2	3			1	2	3			
3	3.02	3.02	3.01	3.02	0.56	3.19	3.12	3.01	3.11	2.98	-2.98
4	4.03	4.04	3.96	4.01	0.25	4.87	4.99	3.72	4.53	12.88	-12.88
5	5.01	5.01	4.99	5.00	0.07	5.79	5.75	5.91	5.82	16.26	-16.26
6	6.03	6.04	6.01	6.03	0.44	6.72	6.59	6.54	6.62	9.79	-9.79
7	7.02	7.06	7.01	7.03	0.43	6.67	6.68	6.28	6.54	-6.92	6.92
8	8.00	8.02	8.00	8.01	0.08	6.73	6.59	7.82	7.05	-11.99	11.99
9	9.02	8.88	9.09	9.00	-0.04	8.33	8.27	7.45	8.02	-10.89	10.89

Blank samples were carried out as a control. Blank samples were done for 5 g sand (pH = 5) and for 50 g sand (pH = 6 to 9). Table 5.3 shows the errors of blank samples were less than 4% representing the experimental data were valid. For pH 9, however, the error value was about 12%. This may be attributed to the difficulty to filter the samples.

Table 5.3 Percentage of error of blank samples

m_{sand} (g)	pH	C_{in} (mg/L)	C average (mg/L)	Error (%)
5	5	21.71	22.02	1.45
50	6	23.02	22.27	3.26
50	7	21.29	21.59	1.39
50	8	9.36	9.36	0.05
50	9	7.56	8.49	12.34

5.2.1 Equilibrium isotherms

Equilibrium isotherms of copper sorption by manganese coated sand were studied using the initial copper concentrations of 6.87, 13.90, 17.98 and 22.32 mg/L.

m_{sand}, $V_{solution}$, pH, T, and shaker speed (r) were kept constant at 50 g, 50 mL, 5, 25.6°C, and 150 rpm subsequently. The results are as follows. Figure 5.2 shows the amount of copper sorbed at 25.6°C plotted against the copper concentration in liquid phase at equilibrium (t_e = 120 min). Isotherm data obtained within a range of C_{in} showed an increase in the amount of copper sorbed at equilibrium when C_{in} was raised from 6.87 to 23.32 mg/L. This relationship is confirmed with the value of R^2 = 0.74, as shown in Figure 5.3.

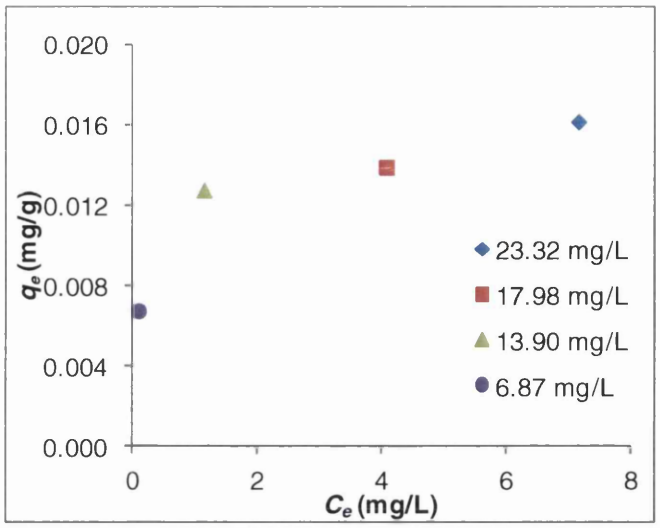

Figure 5.2 Equilibrium isotherms of copper sorption by manganese coated sand at 25.6°C (m_{sand} = 50 g, $V_{solution}$ = 50 mL, pH = 5, shaker speed = 150 rpm, t_e = 120 min)

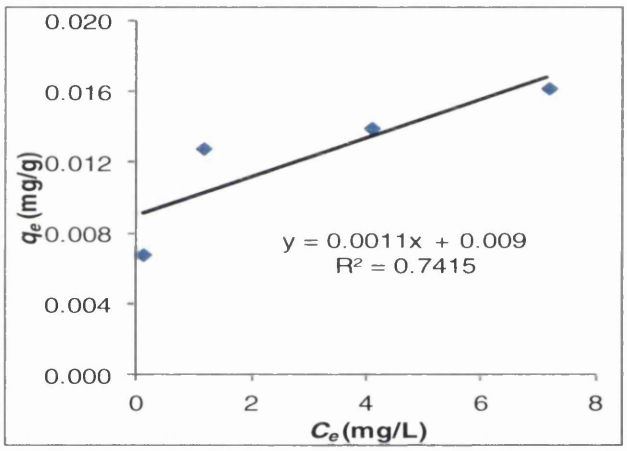

Figure 5.3 The correlation factor of equilibrium isotherms of copper sorption by manganese coated sand at 25.6°C (m_{sand} = 50 g, $V_{solution}$ = 50 mL, pH = 5, shaker speed = 150 rpm, t_e = 120 min)

Five different linear types of the Langmuir models and the linear form of the Freundlich model were used to model the equilibrium data (Ghodbane et al., 2008). These models are shown in Table 5.4. The Langmuir constants and the Freundlich parameters for the sorption of copper by manganese coated sand at 25.6°C are shown in Table 5.5. The Langmuir parameters obtained were greatly affected by linear analysis using different linear forms of the Langmuir equation as shown in Table 5.5.

Table 5.4 The linear forms of Freundlich and Langmuir isotherms (Ghodbane et al., 2008)

Isotherm	Linear form	Plot
Freundlich	$ln\ q_e = ln\ K_F + (1/r_a)\ ln\ C_e$	$ln\ q_e$ vs $ln\ C_e$
Langmuir 1	$C_e/q_e = (1/q_m)\ C_e + 1/(q_m C_L)$	C_e/q_e vs C_e
Langmuir 2	$1/q_e = (1/C_L q_m)\ (1/C_e) + (1/q_m)$	$1/q_e$ vs $1/C_e$
Langmuir 3	$q_e = -\ (1/C_L)\ (q_e/C_e) + q_m$	q_e vs q_e/C_e
Langmuir 4	$q_e/C_e = -\ C_L q_e + C_L q_m$	q_e/C_e vs q_e
Langmuir 5	$1/C_e = C_L q_m\ (1/q_e) - C_L$	$1/C_e$ vs $1/q_e$

The value of R^2 (= 0.99) obtained from the Langmuir type 1 (Table 5.5) shows that the sorption of copper by manganese coated sand clearly follows the Langmuir isotherm. The maximum uptake of copper by manganese coated sand (obtained from the Langmuir type 1) was 0.0164 mg/g; while the Langmuir constant was 3.1326 (L/mg).

Ghodbane et al (2008) also found that the equilibrium data could be better described by the Langmuir isotherm than by the Freundlich model, although they stated that the Langmuir type 2 was the best model to describe the equilibrium isotherms of the sorption of cadmium (II) ions from aqeous phase by eucalyptus bark.

The sorption favourability can be determined by calculating the R_L value (Equation 3.39). Table 5.6 shows the obtained R_L values calculated using Langmuir 1 model at different initial concentrations. Table 5.6 shows that copper sorption was found to be more favourable at higher concentration. This is confirmed by the value of the correlation factor of R_L and C_{in} (= 0.90) as shown in Figure 5.4. This trend is in line with Ghodbane et al (2008). In addition, at all initial concentrations, the obtained value of R_L ($0 < R_L < 1$) confirmed the favourable sorption of copper by the manganese coated sand.

Table 5.5 The Langmuir and Freundlich parameters obtained by using the linear method (C_{in} = 6.87 – 23.32 mg/L, m_{sand} = 50 g, $V_{solution}$ = 50 mL, pH = 5, shaker speed = 150 rpm, t_e = 120 min)

Isotherm	Parameters	
Langmuir-1	q_m (mg/g)	0.0164
	C_L (L/mg)	3.1326
	R^2	0.9920
Langmuir-2	q_m (mg/g)	0.0149
	C_L (L/mg)	8.3056
	R^2	0.9858
Langmuir-3	q_m (mg/g)	0.0150
	C_L (L/mg)	8.0775
	R^2	0.9326
Langmuir-4	q_m (mg/g)	0.0152
	C_L (L/mg)	7.5309
	R^2	0.9326
Langmuir-5	q_m (mg/g)	0.0150
	C_L (L/mg)	8.1473
	R^2	0.9858
Freundlich	r_a	4.5351
	K_F ((mg/g) (L/mg)1/n)	0.0103
	R^2	0.9890

Table 5.6 Separation factor values for copper sorption by manganese coated sand at 25.6°C (m_{sand} = 50 g, $V_{solution}$ = 50 mL, pH = 5, shaker speed = 150 rpm, t_e = 120 min)

C_{in} (mg/L)	C_L (L/mg)	R_L
6.87	3.1326	0.0444
13.90	3.1326	0.0225
17.98	3.1326	0.0174
23.32	3.1326	0.0135

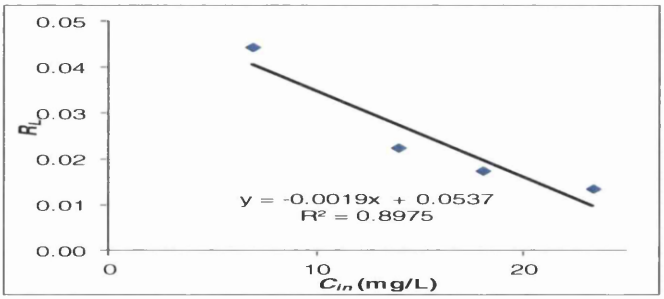

Figure 5.4 The correlation factor between R_L and C_{in} (m_{sand} = 50 g, $V_{solution}$ = 50 mL, pH = 5, shaker speed = 150 rpm, t_e = 120 min, T = 25.6°C)

5.2.2 Sorption kinetics

5.2.2.1 Effect of contact time and initial concentration of copper

The rate of metal removal is an important factor in developing sorbent-based water technology. In order to find out the equilibrium time for maximum uptake and the kinetics of sorption process, the study of the sorption of copper by manganese coated sand was done using contact times ranging from 0 – 240 min. Figure 5.5 shows that effluent copper concentration decreased as C_{in} decreased. This may be due to less copper retained per g of sand as depicted in Figure 5.6. Figure 5.7 illustrates that C/C_{in} increased with increasing C_{in}. This occurs as the more copper contained in the solution the more copper retained per g of sand hence saturation was achieved faster. A clear relationship of C/C_{in} at equilibrium was obtained as shown in Figure 5.8. Figure 5.9 shows that the removal efficiency increased as C_{in} decreased. This may be due to higher ratio of active sites available to the amount of copper in the solution. The ratio of maximum copper adsorbed to the amounts of manganese was clearly correlated to C_{in} as depicted in Figure 5.10. In addition, the mass of copper to mass of sand ratio at equilibrium was apparently correlated to C_{in} as shown in Figure 5.11. These batch results are confirmed with the column results discussed in Section 5.3.2.

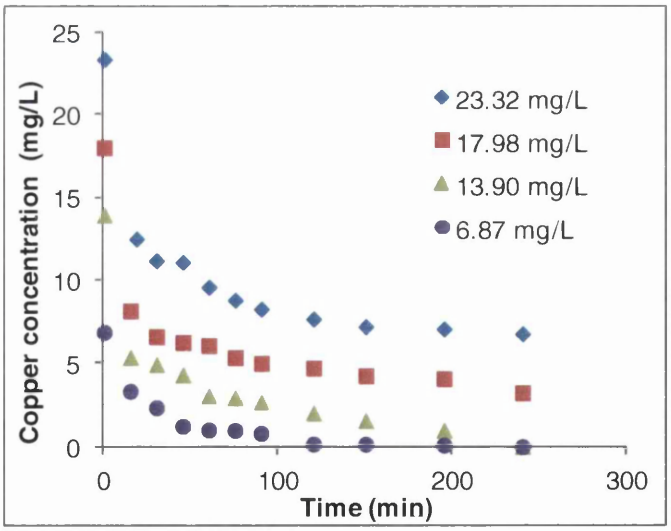

Figure 5.5 Copper concentration vs time for different C_{in} (m_{sand} = 50 g, $V_{solution}$ = 50 mL, pH = 5, shaker speed = 150 rpm, T = 25.6°C)

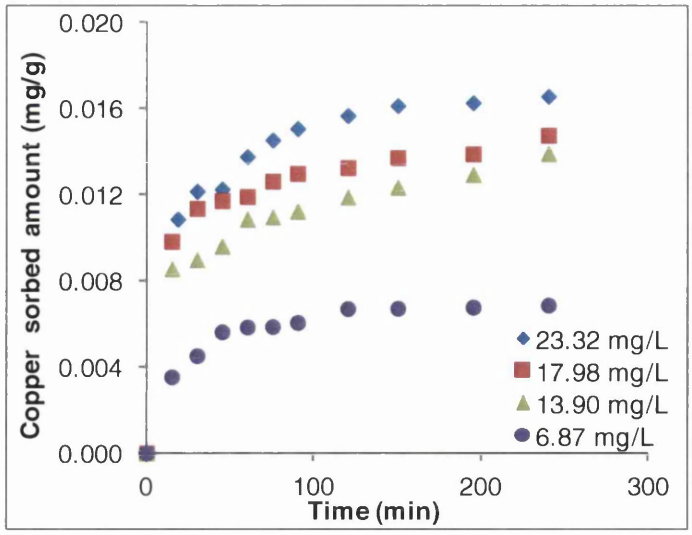

Figure 5.6 Effect of C_{in} on the sorption of copper by manganese coated sand (m_{sand} = 50 g, $V_{solution}$ = 50 mL, pH = 5, shaker speed = 150 rpm, T = 25.6°C)

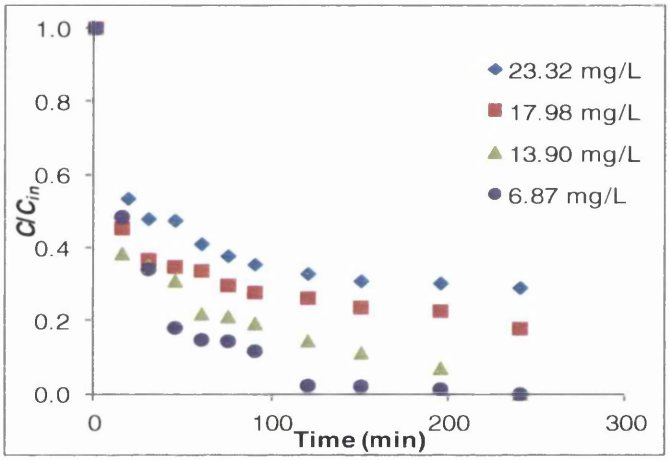

Figure 5.7 C/C_{in} vs time for different C_{in} (m_{sand} = 50 g, $V_{solution}$ = 50 mL, pH = 5, shaker speed = 150 rpm, T = 25.6°C)

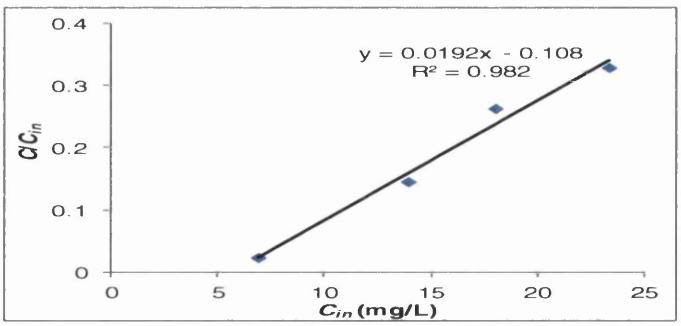

Figure 5.8 The correlation factor of C/C_{in} (at equilibrium) vs C_{in} for different C_{in} (m_{sand} = 50 g, $V_{solution}$ = 50 mL, pH = 5, shaker speed = 150 rpm, T = 25.6°C)

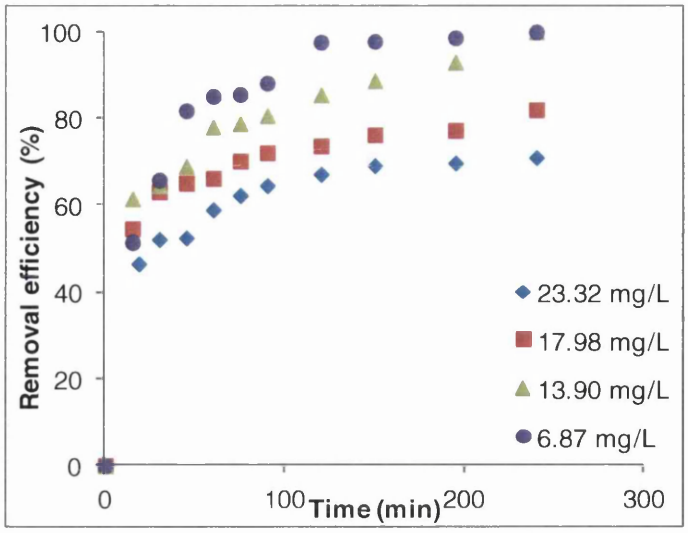

Figure 5.9 Removal efficiency vs time for different C_{in} (m_{sand} = 50 g, $V_{solution}$ = 50 mL, pH = 5, shaker speed = 150 rpm, T = 25.6°C)

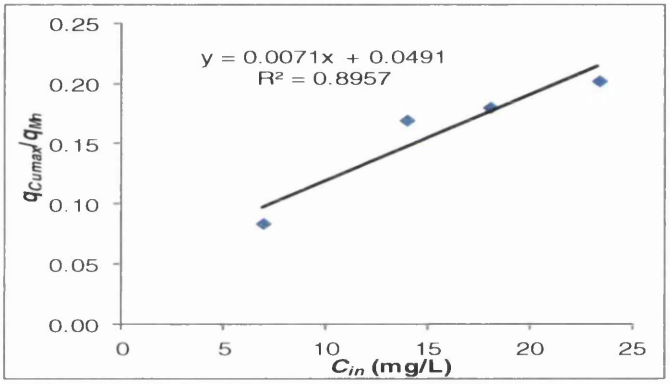

Figure 5.10 The correlation factor of q_{Cumax}/q_{Mn} vs C_{in} (m_{sand} = 50 g, $V_{solution}$ = 50 mL, pH = 5, shaker speed = 150 rpm, T = 25.6°C)

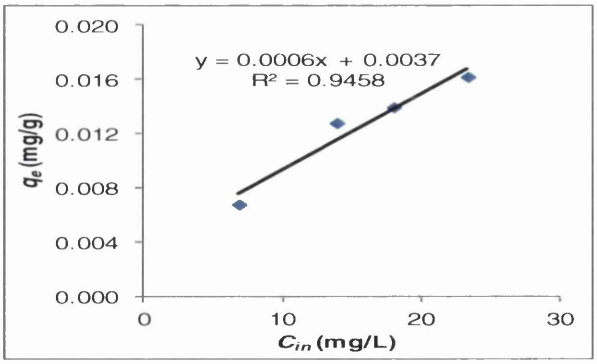

Figure 5.11 The correlation factor of q_e vs C_{in} (m_{sand} = 50 g, $V_{solution}$ = 50 mL, pH = 5, shaker speed = 150 rpm, T = 25.6°C)

Figure 5.6 depicts the sorption amount of copper increased gradually with increasing contact times and then reached a plateau. In addition, the sorption capacity of copper by manganese coated sand increased with an increase in C_{in}. Moreover, the increase in C_{in} leads to an increase in equilibrium uptake (Figure 5.2). Ghodbane et al (2008) observed similar trends in their study. This may be explained as follows. The initial concentration provides the required driving force to overcome the resistances to the mass transfer of copper between the bulk solution and solid phases (Srivastava et al., 2006; Ghodbane et al., 2008). The increase in C_{in} also signifies the reaction between copper and the manganese coated sand. Thus, the uptake of copper by the manganese coated sand increased with an increase in C_{in}. Copper removal was found to be fast during the initial 15 min and afterwards the rate of removal decreased. For all initial concentrations, the equilibrium uptake of copper adsorbed occurred within 120 min. This indicates that manganese coated sand is an effective adsorbent for the removal of copper from waters. Boujelben et al (2009) also found that the optimum time for copper removal by the natural iron oxide coated sand was 120 min. The equilibrium sorption capacity increased from 0.0078 to 0.0177 mg/g once C_{in} was raised from 6.87 to 23.32 mg/L (Figure 5.11).

The results show that the removal of copper was rapid at the early stages of the contact times, and afterwards, this removal becomes slower once closes to the equilibrium. Between these two stages of uptake, the rate of adsorption was found to be almost constant. This may be due to a large number of empty surface sites were available during the early stage, and after times, the remaining available sites were difficult to be inhabited resulted from the repulsive forces between the solute molecules on the bulk and solid phases (Srivastava et al., 2006). This kinetic experiment also shows that adsorption of copper ion onto manganese coated sand may involve a two steps process i.e. fast adsorption of copper ion to the external surface of manganese coated sand followed by possible slow intra-particle diffusion in the interior of manganese coated sand. The rapid kinetics serves as an important point practically. The faster the reaction, the smaller reactor volumes are required thus minimising cost and enhancing efficiency (Sen and Sarzali, 2008).

In order to study the kinetics of adsorption, especially potential rate-controlling step, the behaviour of copper adsorption process was analysed using the pseudo-first-order Lagergren equation, pseudo-second-order, intraparticle diffusion and Bangham models. For the pseudo-second order model, the parameters can be obtained as shown in Table 5.7 by using the six different linear forms of the pseudo-second order equation (Ghodbane et al., 2008). For the pseudo-first-order model, the adsorption rate constant K_1 can be obtained from the plot of ln $(q_e - q)$ against t. Table 5.8 depicts the pseudo-second-order and the pseudo-first-order kinetic parameters by using the linear methods for different C_{in}.

Table 5.7 The linear forms of the pseudo-second-order kinetic model (Ghodbane et al., 2008)

Type	Linear form	Plot	Parameters
Type 1	$\frac{t}{q} = \frac{1}{K_2 q_e^2} + \frac{1}{q_e} t$	t/q vs t	q_e = 1/slope K_2 = slope^2/intercept h = 1/intercept
Type 2	$\frac{1}{q} = \frac{1}{q_e} + \frac{1}{K_2 q_e^2} \frac{1}{t}$	$1/q$ vs $1/t$	q_e = 1/intercept K_2 = intercept^2/slope h = 1/slope
Type 3	$q = q_e - \frac{1}{K_2 q_e^2} \frac{q}{t}$	q vs q/t	q_e = intercept K_2 = -1/(slope x intercept) h = - intercept/slope
Type 4	$\frac{q}{t} = K_2 q_e^2 - K_2 q_e q$	q/t vs q	q_e = -intercept/slope K_2 = slope^2/intercept h = intercept
Type 5	$\frac{1}{t} = -K_2 q_e + K_2 q_e^2 \frac{1}{q}$	$1/t$ vs $1/q$	q_e = -slope/intercept K_2 = intercept^2/slope h = slope
Type 6	$\frac{1}{q_e - q} = \frac{1}{q_e} + K_2 t$	$1/(q_e-q)$ vs t	q_e = 1/intercept K_2 = slope h = slope/intercept^2

Table 5.8 shows that over all, the q_e values obtained by the pseudo-second order and the pseudo-first-order models were close to the values obtained from the experiments. Except for those values obtained by the pseudo-second-order type 6 for C_{in} = 23.32 and 17.98 mg/L, where the values were negative. This indicates that type 6 of the pseudo-second-order model was not appropriate to model the sorption kinetic of copper by manganese coated sand.

Table 5.8 The pseudo-second-order and the pseudo-first-order kinetic parameters by using the linear methods for different C_{in} (m_{sand} = 50 g, $V_{solution}$ = 50 mL, pH = 5, shaker speed = 150 rpm, t_e = 120 min)

Type	Parameters	Initial Concentration (mg/L)			
		23.32	17.98	13.9	6.87
Type-1	K_2 (g/mg.min)	4.1038	9.1130	6.8405	7.2807
	q_e (mg/g)	0.0173	0.0140	0.0128	0.0075
	h (mg/g.min)	0.0012	0.0018	0.0011	0.0004
	R^2	0.9952	0.9984	0.9951	0.9939
Type-2	K_2 (g/mg.min)	6.2888	12.7230	13.1581	8.2410
	q_e (mg/g)	0.0162	0.0135	0.0118	0.0074
	h (mg/g.min)	0.0017	0.0023	0.0018	0.0004
	R^2	0.9021	0.9593	0.8114	0.9804
Type-3	K_2 (g/mg.min)	6.0033	12.4272	12.5489	8.1279
	q_e (mg/g)	0.0164	0.0136	0.0119	0.0074
	h (mg/g.min)	0.0016	0.0023	0.0018	0.0004
	R^2	0.8560	0.9346	0.7569	0.9436
Type-4	K_2 (g/mg.min)	5.0761	11.3473	9.1207	8.0656
	q_e (mg/g)	0.0166	0.0139	0.0124	0.0070
	h (mg/g.min)	0.0014	0.0022	0.0014	0.0004
	R^2	0.8560	0.9346	0.7569	0.9436
Type-5	K_2 (g/mg.min)	5.3760	12.2702	9.7607	8.6730
	q_e (mg/g)	0.0167	0.0134	0.0124	0.0068
	h (mg/g.min)	0.0015	0.0022	0.0015	0.0004
	R^2	0.9021	0.9593	0.8114	0.9804
Type-6	K_2 (g/mg.min)	14.7630	11.6560	7.9498	14.4250
	q_e (mg/g)	-0.0047	-5.2798	0.0264	0.0082
	h (mg/g.min)	0.0003	324.9298	0.0055	0.0010
	R^2	0.8106	0.9482	0.9298	0.9698
First-order	K_1 (min^{-1})	0.0265	0.0223	0.0192	0.0331
	q_e (mg/g)	0.0115	0.0073	0.0077	0.0066
	R^2	0.9649	0.8827	0.8994	0.8946

Table 5.8 also shows that although the q_e values obtained by both the pseudo-second order models and pseudo-first-order model were generally close to the values obtained from the experiments, the pseudo-second-order kinetic model type one has the greatest R^2 average value (≈ 1) for all the initial concentrations. Thus, the kinetic of the sorption of copper by manganese coated sand can be best modelled by using the pseudo-second-order kinetic model type one. Ghodbane et al (2008) also reported the similar finding. Sen and Sarzali (2008) found also that their adsorption experiment followed the pseudo-second-order kinetic model, although they did not study several linear models of the pseudo-second-order kinetic model.

The rate of removal of copper by manganese coated sand, K_2 (obtained by the pseudo-second-order kinetic model type one), generally increased as C_{in} decreased. On the other hand, the initial sorption rate, h, and the theoretical amount of copper sorbed at equilibrium, q_e, generally decreased with a decrease in C_{in}. These relationships are confirmed by the R^2 values of 0.91, 0.98, and 0.98 for K_2, h and q_e relationships with C_{in} respectively as shown in Figures 5.12 - 5.14. The decrease of theoretical q_e with a decrease in C_{in} confirms with the experimental data. By using these trends, K_2 increased from 4.3631 to 7.6284 g/mg.min as C_{in} decreased from 23.32 to 6.87 mg/L (Table 5.9). On the other hand, h and q_e decreased from 0.0018 to 0.0002 mg/g.min and from 0.0179 to 0.0080 mg/g respectively with a decrease in C_{in} from 23.32 to 6.87 mg/L. Sen and Sarzali (2008) also found that h decreased with a decrease in C_{in}. However, they obtained that K_2 increased with an increase in C_{in}.

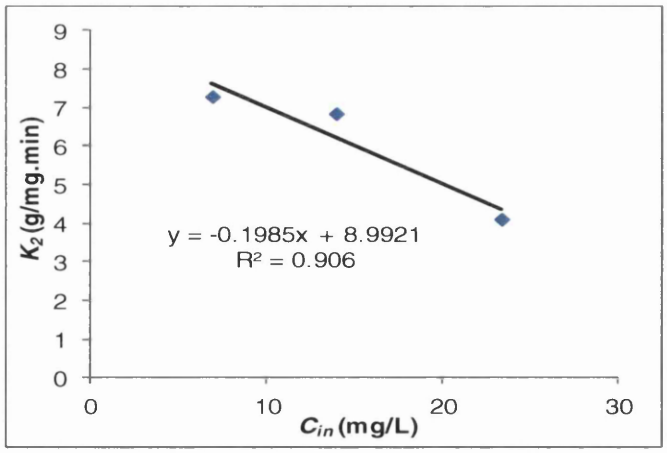

Figure 5.12 The correlation factor of K_2 vs C_{in} (m_{sand} = 50 g, $V_{solution}$ = 50 mL, pH = 5, shaker speed = 150 rpm, t_e = 120 min, T = 25.6°C)

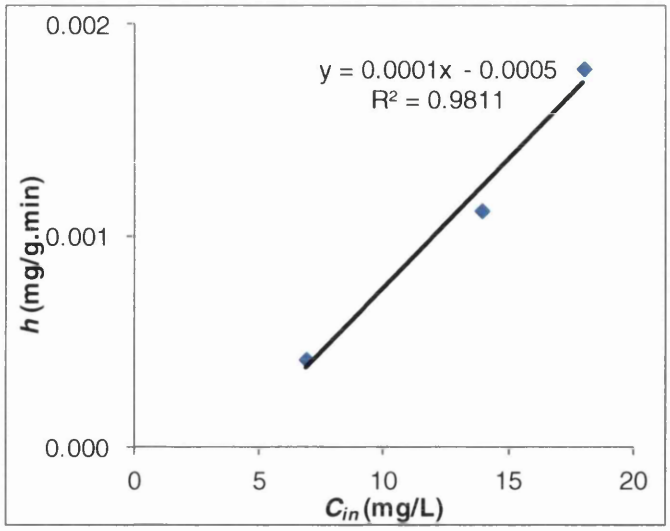

Figure 5.13 The correlation factor of h vs C_{in} (m_{sand} = 50 g, $V_{solution}$ = 50 mL, pH = 5, shaker speed = 150 rpm, t_e = 120 min, T = 25.6°C)

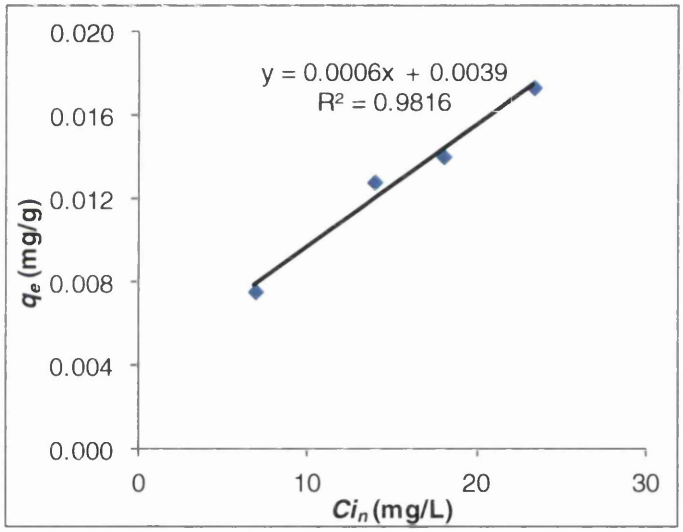

Figure 5.14 The correlation factor of theoretical q_e vs C_{in} (m_{sand} = 50 g, $V_{solution}$ = 50 mL, pH = 5, shaker speed = 150 rpm, t_e = 120 min, T = 25.6°C)

Table 5.9 The pseudo-second-order kinetic parameters obtained by using the equation in Figures 5.12 – 5.14 for different C_{in} (m_{sand} = 50 g, $V_{solution}$ = 50 mL, pH = 5, shaker speed = 150 rpm, t_e = 120 min. T = 25.6°C)

C_{in}	K_2 (g/mg.min)	h (mg/g.min)	q_e (mg/g)
23.32	4.3631	0.0018	0.0179
17.98	5.4231	0.0013	0.0147
13.90	6.2330	0.0009	0.0122
6.87	7.6284	0.0002	0.0080

The pseudo-second-order kinetic model is based on assumption that the rate-limiting step might be those of chemisorptions (Han et al., 2006a; Sen and Sarzali, 2008) involving valence forces through sharing or exchange of electrons between sorbate and sorbent (Sen and Sarzali, 2008). Hence, considering that the correlation coefficients were almost 1 (Table 5.8), the adsorption of copper ions was assumed to be occurred through chemisorptions.

The sorbate transport from the solution phase to the surface of the sorbent particles occurs in a number of stages. The whole adsorption process may be usually controlled by one or more stages, for instance, film or external diffusion, surface diffusion, pore diffusion and adsorption on the pore surface. In a fast shaked batch adsorption, the diffusive mass transfer can be expressed by a clear diffusion coefficient, which will fit the experimental sorption-rate data (Srivastava et al., 2006). In general, a process is diffusion controlled once the rate of this process is dependent on the rate at which components diffuse towards each other. The likelihood of intra-particle diffusion can be analysed by using the intra-particle diffusion of Weber and Morris (Equation 3.45). Weber and Morris stated that the plot of q_t against $t^{0.5}$ should be linear if intra-particle diffusion occurs in the adsorption process, and the line will pass through the origin if the pore diffusion is the only rate-limiting step (Weber and Moris, 1963; Wahab, 2007; Borah et al., 2009).

Figure 5.15 shows Weber and Morris intra-particle diffusion plots for all initial concentrations. The plot of q_t against $t^{0.5}$ shows that the relationship was not linear for the whole period of reaction times. However, if q_t versus $t^{0.5}$ was plotted for the initial period of the reaction only the line was linear proving that intra- particle diffusion was involved in the initial period of the reaction. Similar results also obtained by Borah et al (2009). The well fitted of Weber and Morris model (R^2 = 0.94 - $\approx$ 1 (Table 5.10)) thus suggests that the boundary layer (film) did not control the sorption process of copper onto the manganese coated sand. This is confirmed in column studies discussed later that showed that solid-phase mass transfer controls the process (Section 5.3.2.1).

These R^2 values also indicate that the Weber-Morris model shows better representation of the data than the pseudo-first order kinetic model. Table 5.10 reveals that K_{id} increased as C_{in} increased.

On the other hand, C_{WM} decreased as C_{in} increased. These relationships are supported by their R^2 values as shown in Figure 5.16 (R^2 = 0.92) and Figure 5.17 (R^2 = 0.99). By using these trends, K_{id} increased from 0.0009 to 0.0024 mg/g.min$^{1/2}$ as C_{in} increased from 6.87 to 23.32 mg/L (Table 5.11). On the other hand, C_{WM} decreased from 0.0006 to 0.0002 mg/g as C_{in} increased. Wahab (2007) found that both K_{id} and C_{WM} increased with increasing C_{in}.

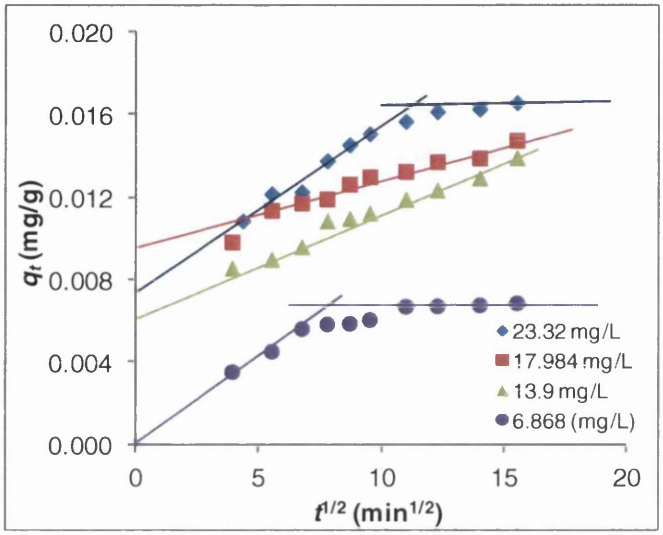

Figure 5.15 Weber and Morris intra-particle diffusion plots for different C_{in} for the whole period of times (m_{sand} = 50 g, $V_{solution}$ = 50 mL, pH = 5, shaker speed = 150 rpm, t_e = 120 min, T = 25.6°C)

Table 5.10 Kinetic parameters obtained by using Weber and Morris equation for different C_{in} (m_{sand} = 50 g, $V_{solution}$ = 50 mL, pH = 5, shaker speed = 150 rpm, T = 25.6°C)

C_{in} (mg/L)	23.32	17.98	13.9	6.87
K_{id} (mg/g. min$^{1/2}$)	0.0023	0.0022	0.0017	0.0008
C_{WM} (mg/g)	0.0002	0.0003	0.0004	0.0001
R^2	0.9885	0.9733	0.9404	0.9958

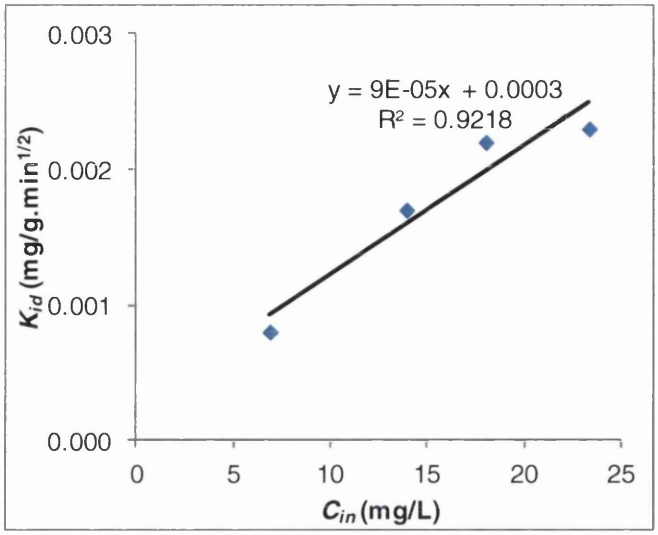

Figure 5.16 The correlation factor of K_{id} vs C_{in} for different C_{in} (m_{sand} = 50 g, $V_{solution}$ = 50 mL, pH = 5, shaker speed = 150 rpm, T = 25.6°C)

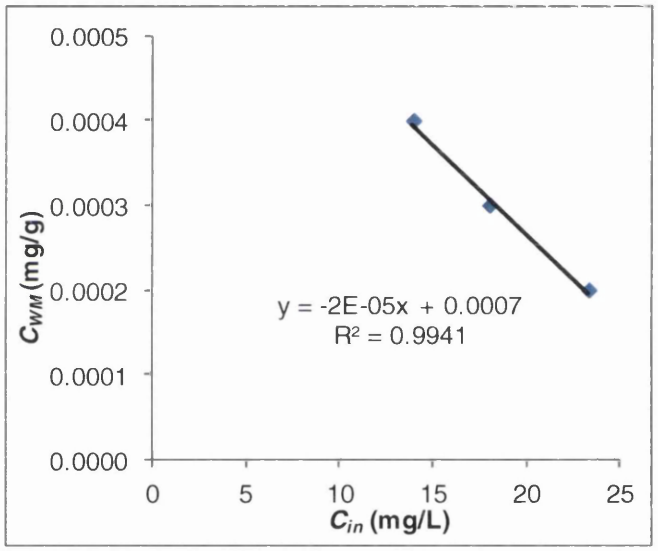

Figure 5.17 The correlation factor of C_{WM} vs C_{in} for different C_{in} (m_{sand} = 50 g, $V_{solution}$ = 50 mL, pH = 5, shaker speed = 150 rpm, T = 25.6°C)

Table 5.11The kinetic parameters of Weber and Morris obtained by using the equation in Figures 5.17 – 5.18 for different C_{in} (m_{sand} = 50 g, $V_{solution}$ = 50 mL, pH = 5, shaker speed = 150 rpm, t_e = 120 min, T = 25.6°C)

C_{in} (mg/L)	K_{id} (mg/g. min$^{1/2}$)	C_{WM} (mg/g)
23.32	0.0024	0.0002
17.98	0.0019	0.0003
13.90	0.0016	0.0004
6.87	0.0009	0.0006

Experimental data were further analysed to see as to whether pore diffusion is the only rate-controlling process by Bangham's (Equation 3.46). The results are depicted in Table 5.12. Table 5.12 shows that the values of R^2 were greater than the pseudo-first-order model indicating that the Bangham's model shows better representation of the data. This also shows that the pore diffusion is the rate-controlling process supporting the above analysis using Weber-Morris model. Srivastava et al. (2006) and Wahab (2007) found that their experimental data did not fit well with both the Bangham's equation and the Weber-Morris model.

Figure 5.18 shows that K_o increased with an increase in C_{in} (R^2 = 0.98). On the other hand, α decreased as C_{in} increased ($R^2 \approx 1$) (Figure 5.19). By using these trends, K_o increased from 2.1236E-09 to 1.3704E-08 (L/g.L) once C_{in} increased from 6.87 to 23.32 mg/L; while, α decreased from 7.1415E-01 to 1.1149E-01 once C_{in} increased (Table 5.13).

Table 5.12 Kinetic parameters obtained by using Bangham's equation for different C_{in} (m_{sand} = 50 g, $V_{solution}$ = 50 mL, pH = 5, shaker speed = 150 rpm, T = 25.6°C)

C_{in} (mg/L)	23.32	17.984	13.9	6.868
K_o (L/gL)	1.2203E-05	2.06E-05	1.68E-05	5E-06
α	0.3168	0.2474	0.3543	0.7168
R^2	0.9622	0.9749	0.9294	0.9399

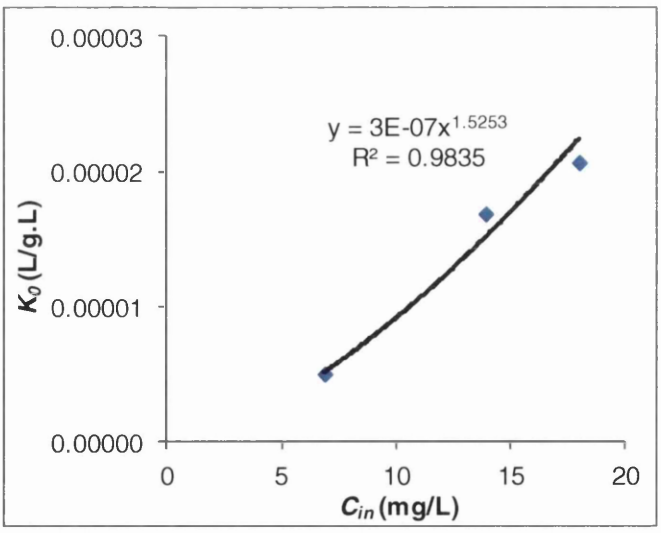

Figure 5.18 The correlation factor of K_o vs C_{in} for different C_{in} (m_{sand} = 50 g, $V_{solution}$ = 50 mL, pH = 5, shaker speed = 150 rpm, T = 25.6°C)

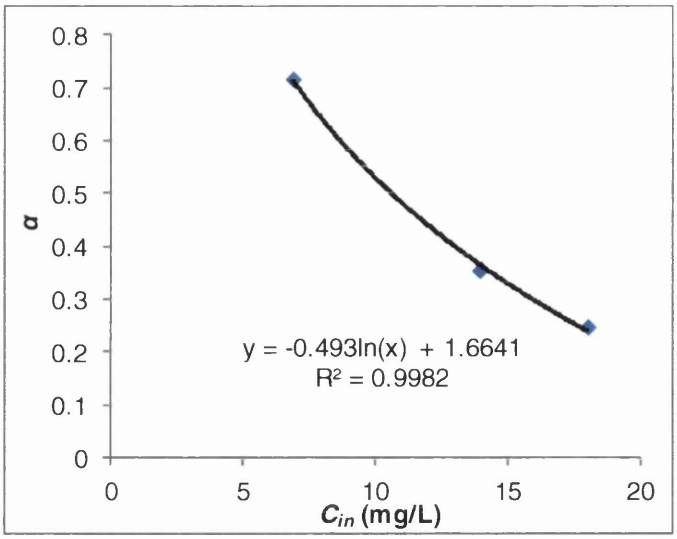

Figure 5.19 The correlation factor of α vs C_{in} for different C_{in} (m_{sand} = 50 g, $V_{solution}$ = 50 mL, pH = 5, shaker speed = 150 rpm, T = 25.6°C)

Table 5.13 The kinetic parameters of Bangham's model obtained by using the equation in Figures 5.19 – 5.20 for different C_{in} (m_{sand} = 50 g, $V_{solution}$ = 50 mL, pH = 5, shaker speed = 150 rpm, t_e = 120 min, T = 25.6°C)

C_{in} (mg/L)	K_O (L/g.L)	α
23.32	1.3704E-08	1.1149E-01
17.98	9.2200E-09	2.3959E-01
13.90	6.2243E-09	3.6658E-01
6.87	2.1236E-09	7.1415E-01

5.2.2.2 Effect of mass of sand

The effect of mass of sand variation on the kinetics of the sorption of copper on manganese coated sand was studied using 5, 7.5, 10, 30, 50 and 100 g mass of sand. C_{in}, $V_{solution}$, pH, T, and r were kept constant at 20 mg/L, 50 mL, 5, 25.6°C and 150 rpm subsequently. The results are as follows. Figure 5.20 illustrates that C/C_{in} decreased with increasing mass. This occurs as a decrease in mass resulted in a decrease in the active sites; hence the bed is saturated faster. Figure 5.21 shows that effluent copper concentration decreased with an increase in mass. This may result from an increase in sand surface area and the availability of more active sites as mass of sand increased. This in turns leads to an increase in removal efficiency, E as shown in Figure 5.22.

However, the amount of copper removed per unit mass of sand decreased with an increase in mass of sand (Figures 5.23 and 5.24). Other studies have also obtained the same trend (Ghodbane et al., 2008; Sen and Sarzali, 2008). This trend may be due to particle-particle interactions (Sen and Sarzali, 2008). High solid content may cause these interactions block some active sites resulting in a decrease in adsorption, or leading to electrostatic interferences such that the electrical surface charges on the closely packed particles reduce attractions between the adsorbate and surfaces of individual sand. This trend confirmed by the ratio of maximum copper adsorbed to the amounts of manganese on the coated sand that also decreased with an increase in mass of sand (Figure 5.25).

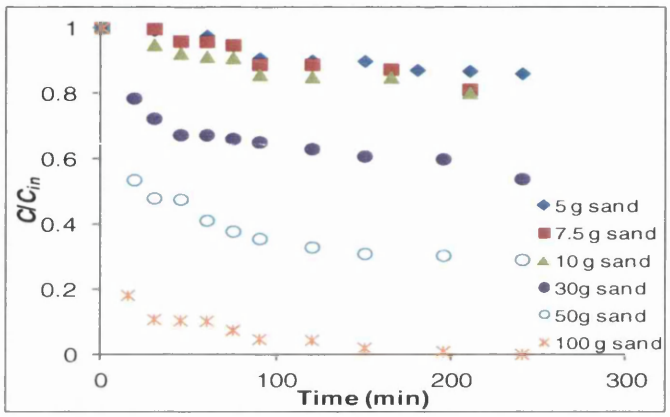

Figure 5.20 C/C_{in} vs time for different mass of sand (C_{in} = 20 mg/L, $V_{solution}$ = 50 mL, pH = 5, shaker speed = 150 rpm, T = 25.6°C)

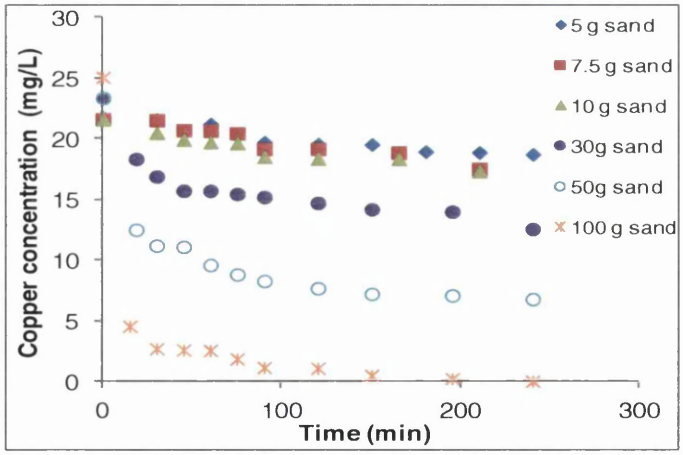

Figure 5.21 Copper concentration vs time for different mass of sand (C_{in} = 20 mg/L, $V_{solution}$ = 50 mL, pH = 5, shaker speed = 150 rpm, T = 25.6°C)

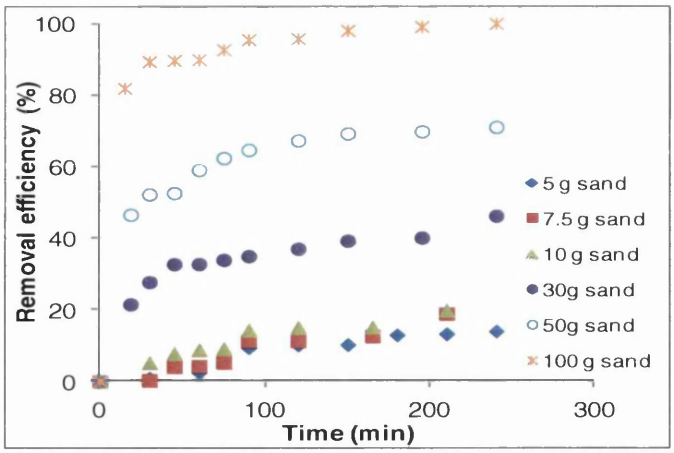

Figure 5.22 Removal efficiency, E (%) vs time for different mass of sand (C_{in} = 20 mg/L, $V_{solution}$ = 50 mL, pH = 5, shaker speed = 150 rpm, T = 25.6°C)

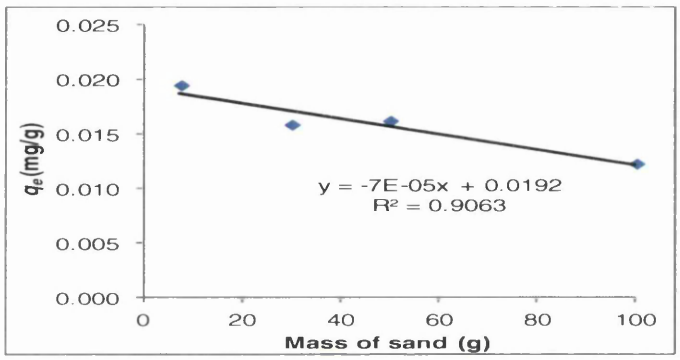

Figure 5.23 The correlation factor of q_e (mg/g) vs mass of sand (g) (C_{in} = 20 mg/L, $V_{solution}$ = 50 mL, pH = 5, shaker speed = 150 rpm, T = 25.6°C)

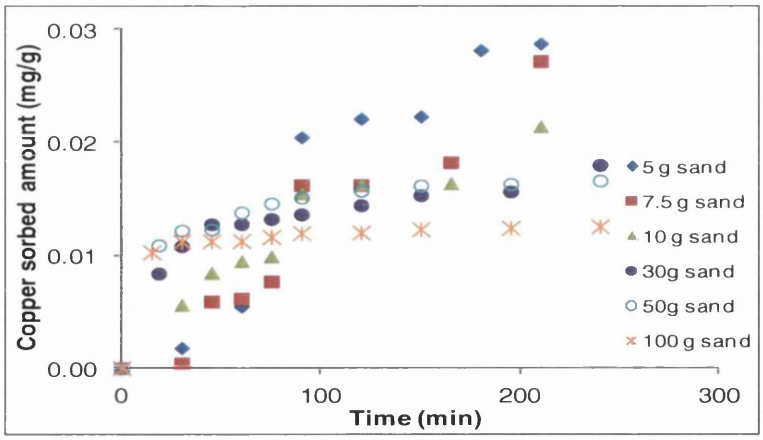

Figure 5.24 Effect of mass of sand on the sorption of copper by manganese coated sand (C_{in} = 20 mg/L, $V_{solution}$ = 50 mL, pH = 5, shaker speed = 150 rpm, T = 25.6°C)

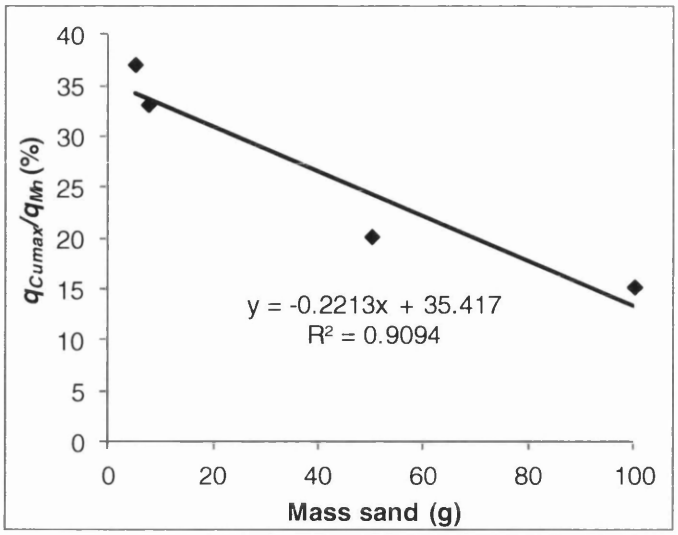

Figure 5.25 The correlation factor of q_{Cumax}/q_{Mn} (%) vs mass sand (g) (C_{in} = 20 mg/L, $V_{solution}$ = 50 mL, pH = 5, shaker speed = 150 rpm, T = 25.6°C)

Figure 5.26 shows the isotherm data obtained within a range of mass of sand. The figure depicts an increase in the amount of copper sorbed at equilibrium when the mass of sand was decreased from 100 g to 5 g. This relationship is confirmed with the value of R^2 = 0.91, as shown in Figure 5.23. The equilibrium sorption capacity increased from 0.0122 to 0.0189 mg/g once mass decreased from 100 to 5 g.

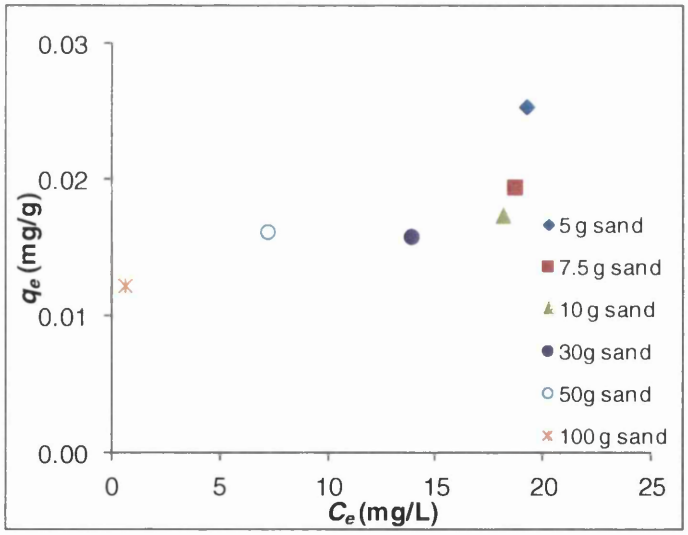

Figure 5.26 Equilibrium isotherms of copper sorption by manganese coated sand at 25.6°C for different mass of sand (C_{in} = 20 mg/L, $V_{solution}$ = 50 mL, pH = 5, shaker speed = 150 rpm)

The experimental kinetic data were fitted to the pseudo-second-order type 1 kinetic model. The results are shown in Table 5.14. The sorption of copper by manganese coated sand was found to be well represented by the pseudo-second-order kinetic equation as the correlation factor were generally close to 1. The R^2 value of m_{sand} = 7.5 g were lower (= 0.76) compared to other mass of sand. This may be due to the removal of copper was lower for lower mass of sand resulted from the sand was not strong enough to adsorb the copper. However, as the mass of sand increased the sand was able to adsorb more copper. The rate constant and the initial sorption rate increased as the mass of sand increased; while the theoretical amount of copper sorbed at equilibrium tended to decrease with an increase in the mass of sand (Figures 5.27 – 5.29). The rate constant and the initial sorption rate increased from 0.6748 to 23.4083 g/mg.min and from 0.0001 to 0.0030 mg/g.min respectively; while the theoretical amount of copper sorbed at equilibrium was likely to decrease from 0.0252 to 0.0157 mg/g with an increase in the mass of sand from 5 to 100 g. Similar trends are also observed by Sen and Sarzali (Sen and Sarzali, 2008). The trend of the theoretical amount of copper sorbed at equilibrium that tended to decrease with an increase in the mass of sand confirms the experimental data.

Ghodbane et al (2008), however, observed that the initial sorption rate decreased with increasing sorbent mass, although they also found that increasing the dose of the sorbent would enhance the rate constant and reduce the theoretical amount of sorbate sorbed at equilibrium.

Table 5.14 Kinetic parameters obtained by using pseudo-second-order kinetic model type 1 for different mass of sand (C_{in} = 20 mg/L, $V_{solution}$ = 50 mL, pH = 5, shaker speed = 150 rpm, T = 25.6°C)

Parameters	Mass of sand (g)					
	5	7.5	10	30	50	100
K_2 (g/mg.min)	1.7416	1.0967	2.9796	4.0180	4.1038	24.0501
q_e (mg/g)	0.0257	0.0139	0.0133	0.0161	0.0173	0.0122
h (mg/g.min)	0.0012	0.0002	0.0005	0.0010	0.0012	0.0036
R^2	0.9957	0.7559	0.9956	0.9974	0.9952	0.9984

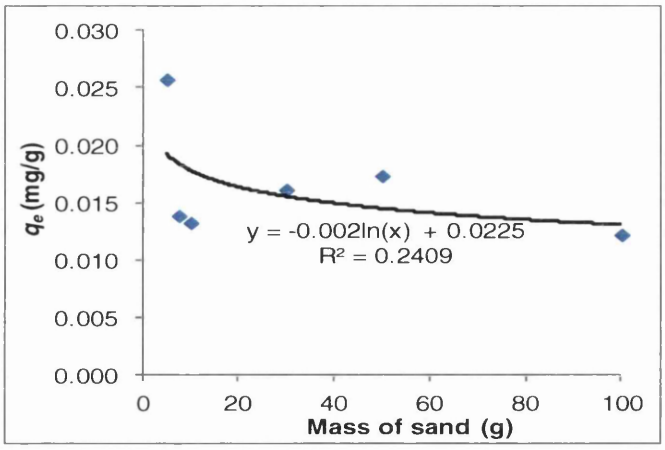

Figure 5.27 The correlation factor of theoretical q_e vs m_{sand} (C_{in} = 20 mg/L, $V_{solution}$ = 50 mL, pH = 5, shaker speed = 150 rpm, T = 25.6°C)

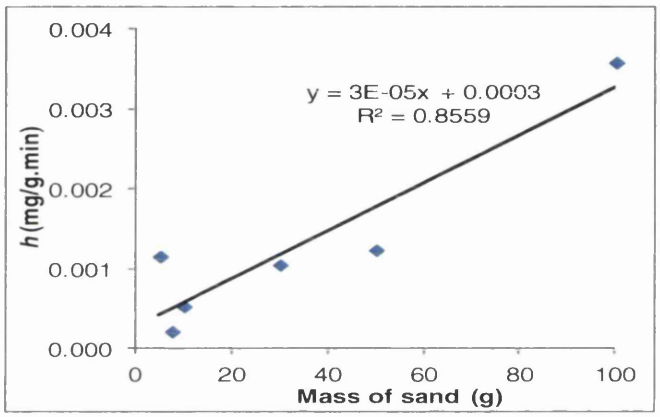

Figure 5.28 The correlation factor of h vs m_{sand} (C_{in} = 20 mg/L, $V_{solution}$ = 50 mL, pH = 5, shaker speed = 150 rpm, T = 25.6°C)

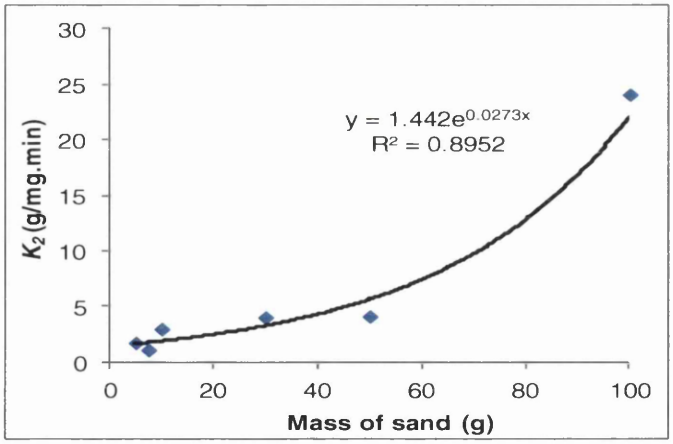

Figure 5.29 The correlation factor of K_2 vs m_{sand} (C_{in} = 20 mg/L, $V_{solution}$ = 50 mL, pH = 5, shaker speed = 150 rpm, T = 25.6°C)

Figures 5.30 (a – b) shows Weber and Morris intra-particle diffusion plots for different mass of sand. The plot of q_t against $t^{0.5}$ was linear for the initial period of the reaction proving that intra particle diffusion was involved in the initial period of the reaction. The well fitted of Weber and Morris model thus suggests that the boundary layer (film) did not control the sorption process of copper onto the manganese coated sand. The values of R^2 (Table 5.15) also indicate that the Weber-Morris model shows better representation of the data than the pseudo-first order kinetic model. Table 5.15 and Figures 5.31 – 5.32 show that K_{id} and C_{WM} increased with increasing mass of sand. Wahab (Wahab, 2007) also obtained similar trends. By using these trends, K_{id} and C_{WM} increased from 0.0009 to 0.0037 mg/g.min$^{1/2}$ and from -0.00002 to 0.00036 mg/g respectively with increasing mass of sand from 5 to 100 g.

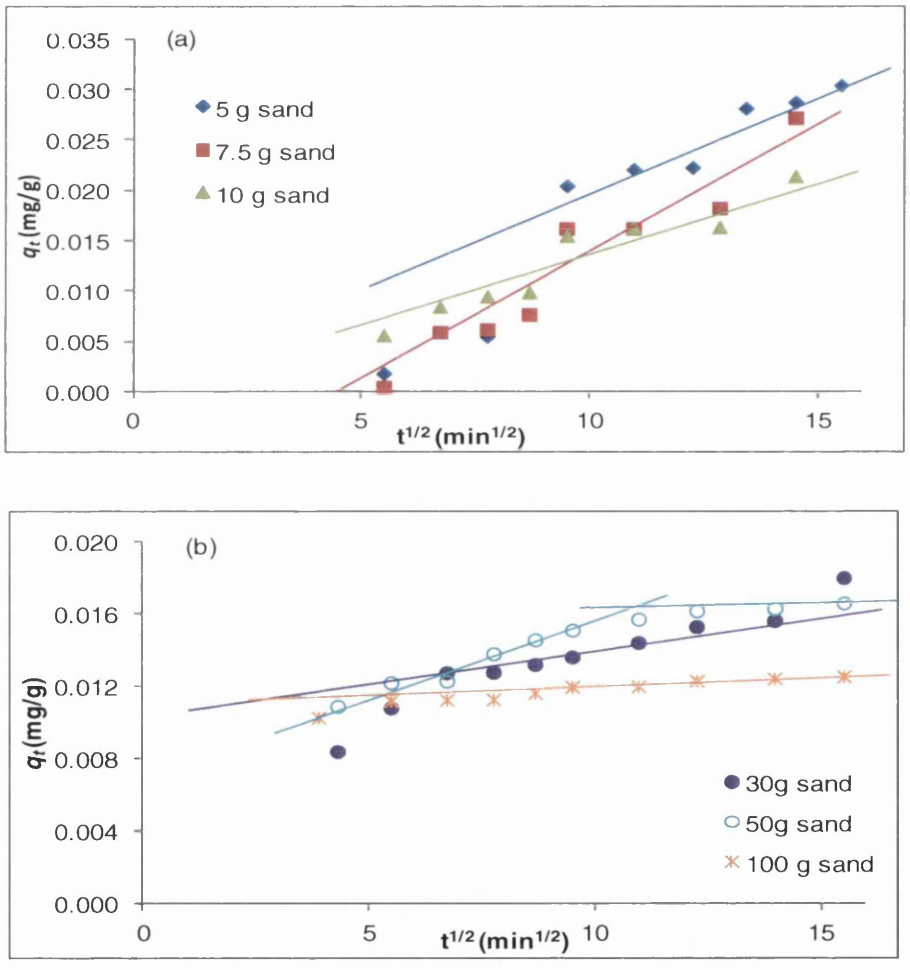

Figure 5.30 Weber and Morris intra-particle diffusion plots for different mass of sand (a) 5 - 10 g sand (b) 30 - 100 g sand (C_{in} = 20 mg/L, $V_{solution}$ = 50 mL, pH = 5, shaker speed = 150 rpm, t_e = 120 min, T = 25.6°C)

Table 5.15 Kinetic parameters obtained by using Weber and Morris for mass of sand (C_{in} = 20 mg/L, $V_{solution}$ = 50 mL, pH = 5, shaker speed = 150 rpm, T = 25.6°C)

m_{sand} (g)	5	7.5	10	30	50	100
K_{id} (mg/g. min$^{1/2}$)	0.0021	0.0008	0.0012	0.0019	0.0023	0.0022
C_{WM} (mg/g)	0.0001	0.0000	0.0002	0.0000	0.0002	0.0004
R^2	0.9968	0.9921	0.9799	0.999	0.9885	0.9549

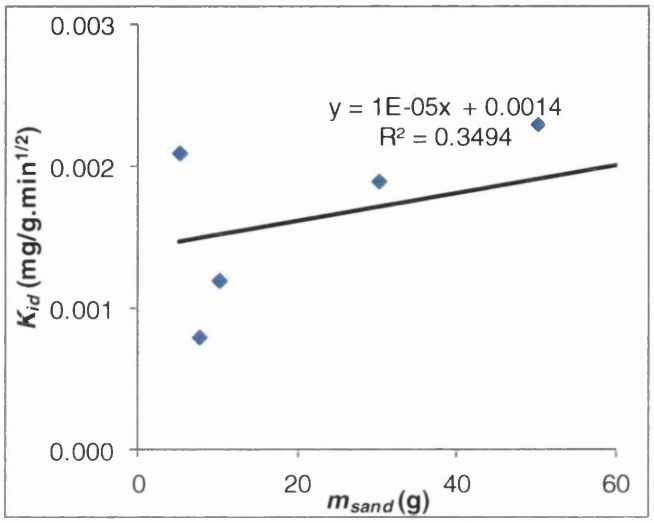

Figure 5.31 The correlation factor of K_{id} vs m_{sand} (C_{in} = 20 mg/L, $V_{solution}$ = 50 mL, pH = 5, shaker speed = 150 rpm, T = 25.6°C)

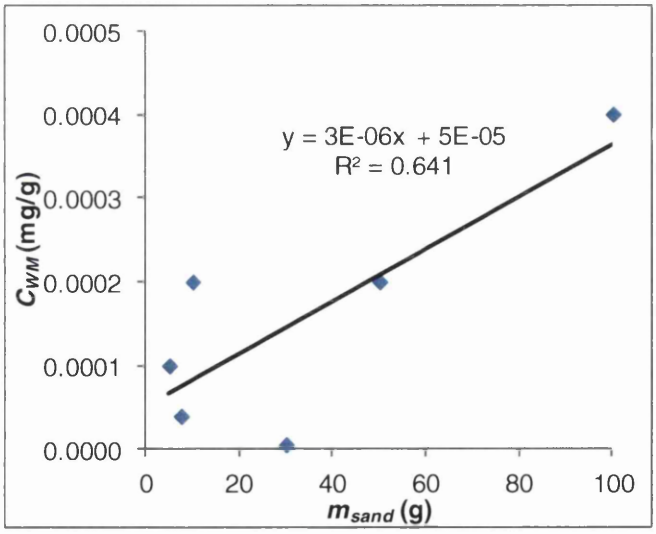

Figure 5.32 The correlation factor of C_{WM} vs m_{sand} (C_{in} = 20 mg/L, $V_{solution}$ = 50 mL, pH = 5, shaker speed = 150 rpm, T = 25.6°C)

Experimental data were further analysed to see as to whether pore diffusion is the only rate-controlling process by Bangham's equation (Equation 3.46). The results are depicted in Table 5.16. Table 5.16 shows that some of the double logarithmic plot did not give satisfactory linear curves (the values of R^2 < 0.88); however, as the average value of R^2 was 0.91, thus Bangham's model represented the data quite well. This reflects that pore diffusion is the rate limiting process as the experimental data are represented by Bangham's equation.

Figure 5.33 shows that K_o increased with an increase in mass of sand (R^2 = 0.96). On the other hand, α decreased as mass of sand increased (R^2 = 0.84) (Figure 5.34). By using these trends, K_o increased from 1E-06 to 2E-05 (L/g.L) once mass of sand increased from 5 to 100 g; while, α decreased from 2.8486 to 0.2349 once mass increased.

Table 5.16 Kinetic parameters obtained by using Bangham's equation for different mass of sand (C_{in} = 20 mg/L, $V_{solution}$ = 50 mL, pH = 5, shaker speed = 150 rpm, T = 25.6°C)

m_{sand} (g)	5	7.5	10	30	50	100
K_o (L/g.L)	2.14E-09	7.25E-11	7.82E-07	8.69E-06	1.22E-05	2.04E-05
α	2.1922	2.9598	0.8347	0.3213	0.3168	0.2759
R^2	0.959	0.8413	0.8944	0.9067	0.9622	0.8753

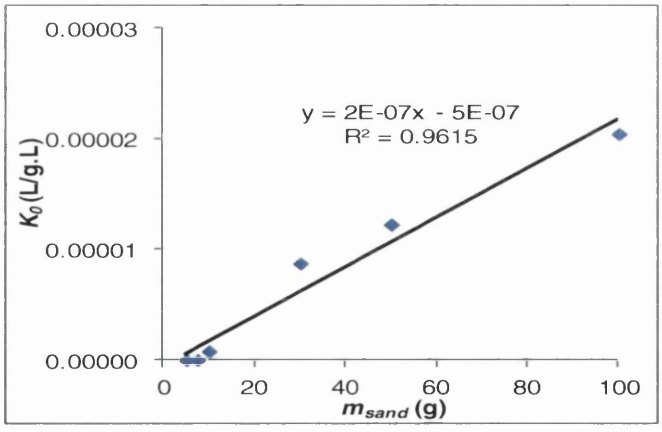

Figure 5.33 The correlation factor of K_o vs m_{sand} (C_{in} = 20 mg/L, $V_{solution}$ = 50 mL, pH = 5, shaker speed = 150 rpm, T = 25.6°C)

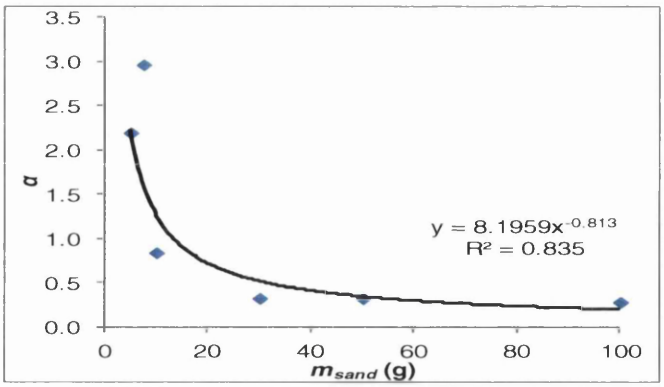

Figure 5.34 The correlation factor of α vs m_{sand} (C_{in} = 20 mg/L, $V_{solution}$ = 50 mL, pH = 5, shaker speed = 150 rpm, T = 25.6°C)

5.2.2.3 Effect of solution initial pH

The pH of metal solutions is the significant parameter controlling the metal removal process. The effect of pH on the kinetics of the sorption of copper on manganese coated sand was studied by using the initial pH of the copper solutions of 3 to 9. m_{sand}, C_{in}, $V_{solution}$, T, and r were kept constant at 50 g, 20 mg/L, 50 mL, 25.6°C and 150 rpm subsequently.

The removal of copper increased with increasing pH (Figure 5.35). In addition, the amount of copper removed per unit mass of sand generally increased with increasing pH for pH = 3 – 7 (Figure 5.36). This finding confirms other studies (Ghodbane et al., 2008; Sen and Sarzali, 2008). The lower values of q_t for pH = 8 – 9 may be attributed to the higher reduction of copper adsorbed onto the filter paper (55% for pH = 8 and 66% for pH = 9 (Table 5.1)). The increasing removal of copper with increasing pH may be explained as follows. The characteristics of the surface of manganese coated sand strongly depend on pH (Section 5.4). The pH_{pzc} of the manganese coated sand was found to be 7.75. The surface is charged positively in an acidic medium, below pH_{pzc}; while in a basic condition, above pH_{pzc}, the surface is charged negatively (Sen and Sarzali, 2008). In aqueous solution, an electric double layer is produced resulting from an electrostatic attraction between the charged manganese coated sand surface and ions of an opposite charge present in the solution. Thus, such increase in adsorption may be due to the favourable change in surface charge and to the extent of hydrolysis of the adsorbing copper ion change with different pH.

The manganese coated sand surface attracts copper cations as the surface charge becomes more negative with increasing pH (Section 5.4). In addition, as the proportion of hydrated ions increases with pH, then these ions may be more strongly attracted than unhydrated ions. Hence, these are both synergistically increasing the amount of adsorption of copper ions at higher pH. The low adsorption occurred at low pH, on the other hand, may be attributed to the high mobility and higher concentration of the H^+, which are more preferentially adsorbed than the copper ions (Sen and Sarzali, 2008). Therefore, at higher pH, higher negative surface charge of the manganese coated sand together with the lower amount of H^+ leads to more copper adsorbed onto the coated sand.

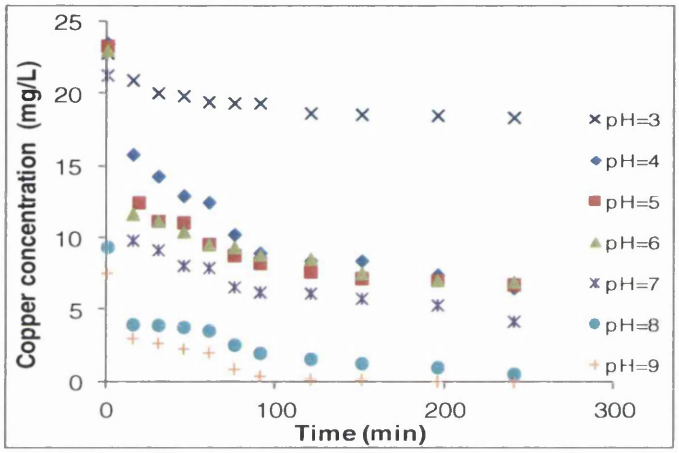

Figure 5.35 Copper concentration vs time for different initial pH (m_{sand} = 50 g, C_{in} = 20 mg/L, $V_{solution}$ = 50 mL, shaker speed = 150 rpm, T = 25.6°C)

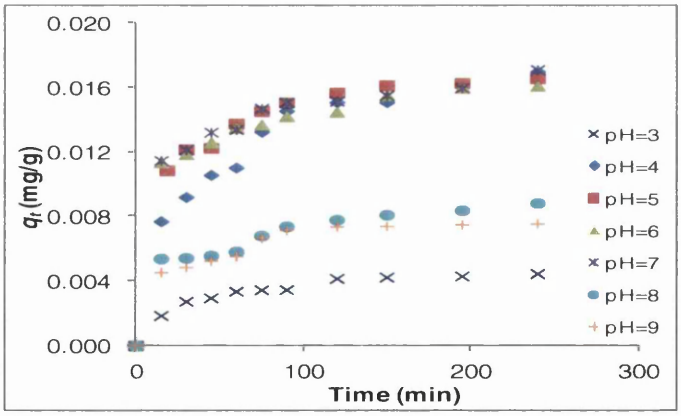

Figure 5.36 Effect of initial pH on the sorption of copper by manganese coated sand (m_{sand} = 50 g, C_{in} = 20 mg/L, $V_{solution}$ = 50 mL, shaker speed = 150 rpm, T = 25.6°C)

Figure 5.37 shows the isotherm data obtained within a range of pH. The figure depicts an increase in the amount of copper sorbed at equilibrium when the pH was increased from 3 to 7, and once the pH value went beyond 7, this amount decreased. This trend is clearly shown in Figure 5.38. q_e increased from 0.0043 to 0.0162 mg/g as pH increased from 3 to 7; once the pH value increased to 9, q_e decreased to 0.0075 mg/g.

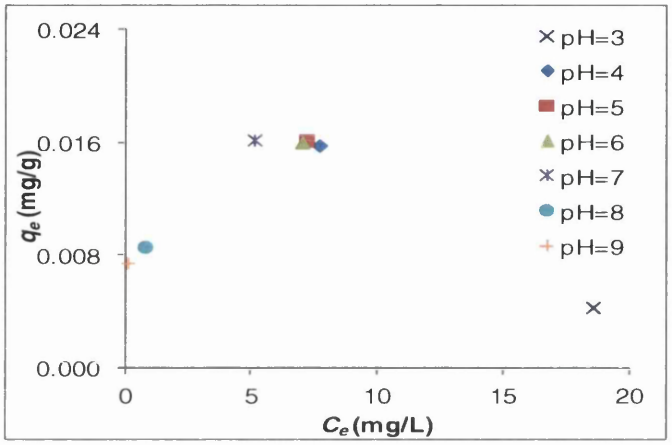

Figure 5.37 Equilibrium isotherms of copper sorption by manganese coated sand at 25.6°C for different initial pH (m_{sand} = 50 g, C_{in} = 20 mg/L, $V_{solution}$ = 50 mL, shaker speed = 150 rpm, T = 25.6°C)

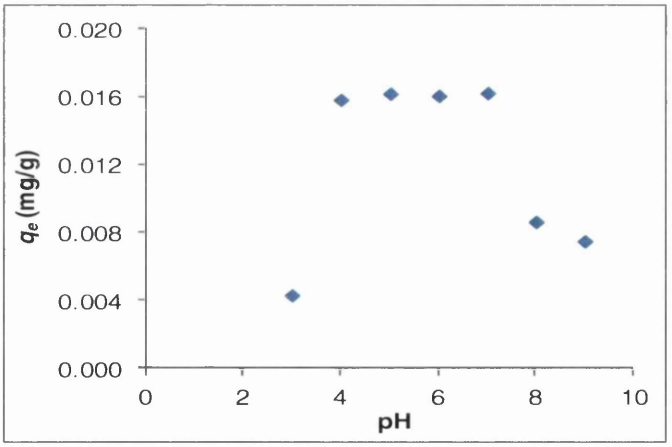

Figure 5.38 q_e vs pH (m_{sand} = 50 g, C_{in} = 20 mg/L, $V_{solution}$ = 50 mL, shaker speed = 150 rpm, T = 25.6°C)

The experimental kinetic data were fitted to the pseudo-second-order type 1 kinetic model. The results are shown in Table 5.17.

The sorption of copper by manganese coated sand was found to be well represented by the pseudo-second-order kinetic equation as the correlation factor were between 0.96 - 1. Figures 5.39 - 5.41 show the plots of K_2, h and theoretical q_e with pH. K_2 decreased from 8.2054 to 1.8328 g/mg.min as pH increased from 3 to 4; once the pH increased from 4 to 9, K_2 increased to 10.3951 g/mg.min. On the other hand, the theoretical q_e increased from 0.0048 to 0.0185 mg/g as pH increased from 3 to 4 then decreased to 0.0078 mg/g once the pH is raised from 4 to 9.

Table 5.17 Kinetic parameters obtained by using pseudo-second-order kinetic model type 1 for different initial pH (m_{sand} = 50 g, C_{in} = 20 mg/L, $V_{solution}$ = 50 mL, shaker speed = 150 rpm, T = 25.6°C)

	pH						
Parameters	3	4	5	6	7	8	9
K_2 (g/mg.min)	8.2054	1.8328	4.1038	4.4786	6.2284	6.9586	10.3951
q_e (mg/g)	0.0048	0.0185	0.0173	0.0167	0.0164	0.0088	0.0078
h (mg/g.min)	0.0002	0.0006	0.0012	0.0013	0.0017	0.0005	0.0006
R^2	0.9802	0.9696	0.9952	0.9961	0.9978	0.9799	0.9604

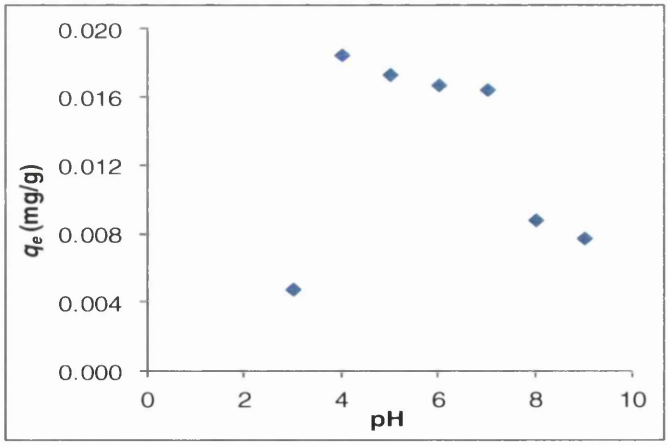

Figure 5.39 Theoretical q_e vs initial pH (m_{sand} = 50 g, C_{in} = 20 mg/L, $V_{solution}$ = 50 mL, shaker speed = 150 rpm, T = 25.6°C)

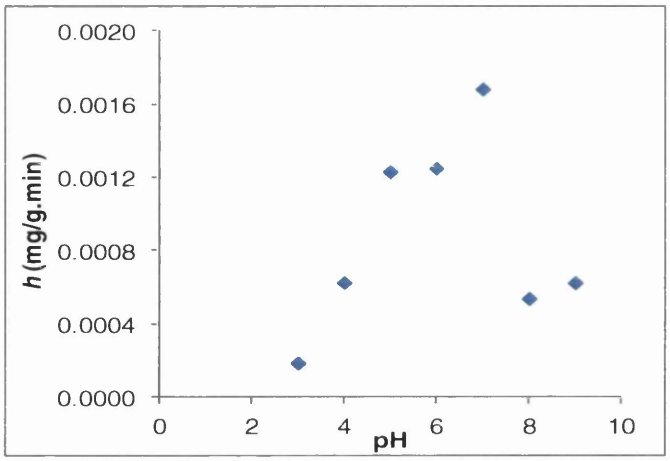

Figure 5.40 h vs initial pH (m_{sand} = 50 g, C_{in} = 20 mg/L, $V_{solution}$ = 50 mL, shaker speed = 150 rpm, T = 25.6°C)

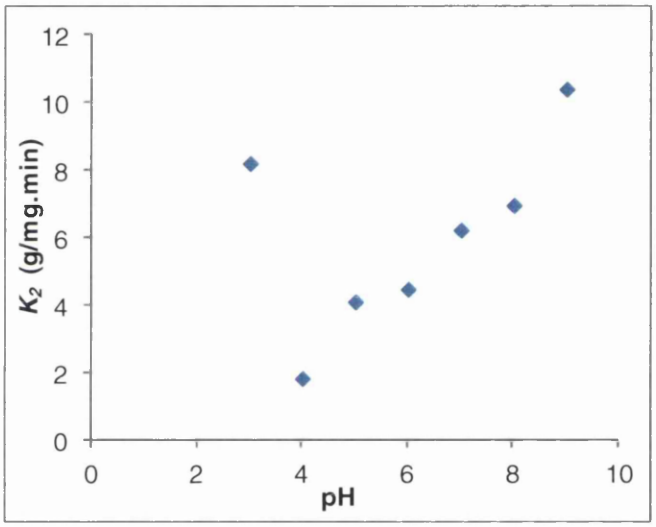

Figure 5.41 K_2 vs initial pH (m_{sand} = 50 g, C_{in} = 20 mg/L, $V_{solution}$ = 50 mL, shaker speed = 150 rpm, T = 25.6°C)

Similarly, h increased from 0.0002 to 0.0017 mg/g as pH increased from 3 to 7 then decreased to 0.0006 mg/g once the pH is raised from 7 to 9. Sen and Sarzali (2008) and Ghodbane et al (2008) found that the rate constant, the initial sorption rate and the theoretical amount of copper sorbed at equilibrium increased as the initial pH increased. The trend of the theoretical q_e with initial pH confirms the experimental data.

Figure 5.42 shows Weber and Morris intra-particle diffusion plots for different pH. The plots of q_t against $t^{0.5}$ were linear indicating that intra particle diffusion occurred.

The well fitted of Weber and Morris model thus suggests that the boundary layer (film) did not control the sorption process of copper onto the manganese coated sand. The values of R^2 (Table 5.18) also indicate that the Weber-Morris model shows better representation of the data than the pseudo-first order kinetic model. Figures 5.43 (a – b) illustrate the plots between K_{id} and C_{WM} with pH values. K_{id} and C_{WM} increased from 0.0005 to 0.0024 mg/g.min$^{1/2}$ and from 0.00002 to 0.0005 respectively as pH increased from 3 to 7, then decreased to 0.0009 mg/g.min$^{1/2}$ and 0.0002 respectively as pH increased from 7 to 9.

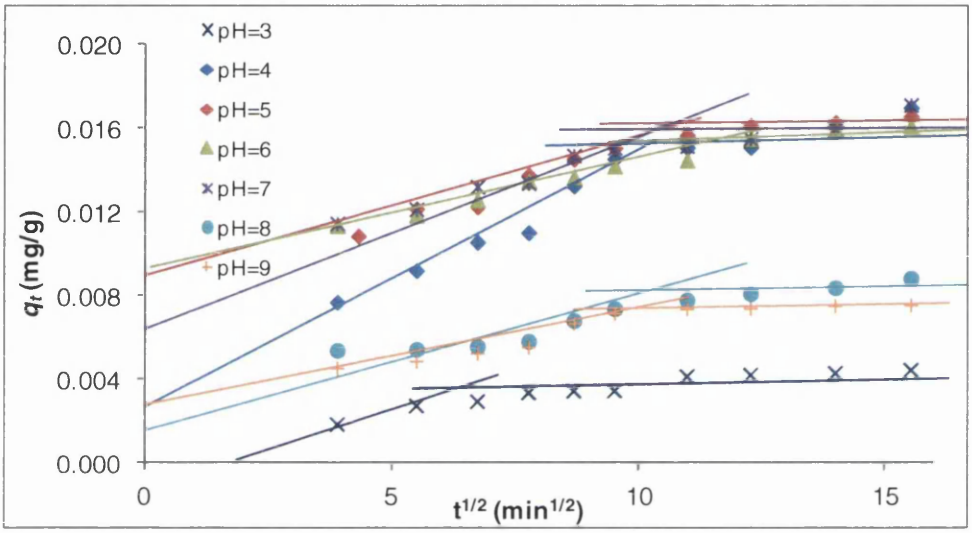

Figure 5.42 Weber and Morris intra-particle diffusion plots for different pH (m_{sand} = 50 g, C_{in} = 20 mg/L, $V_{solution}$ = 50 mL, shaker speed = 150 rpm, t_e = 120 min, T = 25.6°C)

Table 5.18 Kinetic parameters obtained by using Weber and Morris for different initial pH (m_{sand} = 50 g, C_{in} = 20 mg/L, $V_{solution}$ = 50 mL, shaker speed = 150 rpm, T = 25.6°C)

pH	3	4	5	6	7	8	9
K_{id} (mg/g. min1/2)	0.0005	0.0017	0.0023	0.0023	0.0024	0.0011	0.0009
C_{WM} (mg/g)	0.00002	0.0002	0.0002	0.0005	0.0005	0.0003	0.0002
R^2	0.9988	0.9819	0.9885	0.9379	0.9438	0.9230	0.9486

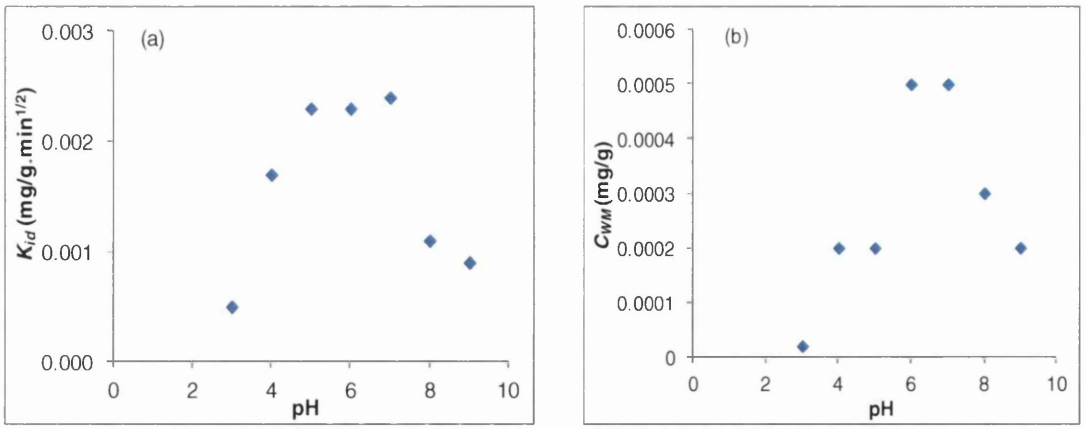

Figure 5.43 (a) K_{id} vs pH (b) C_{WM} vs pH (m_{sand} = 50 g, C_{in} = 20 mg/L, $V_{solution}$ = 50 mL, shaker speed = 150 rpm, T = 25.6°C)

Experimental data were further analysed to see as to whether pore diffusion is the only rate-controlling process by Bangham's equation (Equation 3.46).

The results are depicted in Table 5.19. The experimental data for pH = 8 and pH= 9 did not fit well with the Bangham's equation although for other pH values the R^2 values were about 0.95 – 0.96. This may be due to the higher amount of copper was adsorbed onto the filtration paper (Table 5.1). Figures 5.44 – 5.45 show the plots of K_o and α against pH. K_o increased from 1.63E-06 to 1.9E-05 L/g.L once pH increased from 3 to 7, then decreased to 5.37E-06 L/g.L once pH increased from 7 to 9 (Figure 5.47). α increased from 0.3771 to 0.4827 once pH increased from 3 to 4, then decreased to 0.2254 once pH increased from 4 to 6. Once pH increased from 6 to 9, α increased to 0.6941 (Figure 5.45).

Table 5.19 Kinetic parameters obtained by using Bangham's equation for different initial pH (m_{sand} = 50 g, C_{in} = 20 mg/L, $V_{solution}$ = 50 mL, shaker speed = 150 rpm, T = 25.6°C)

pH	3	4	5	6	7	8	9
K_o (L/g.L)	1.63E-06	5E-06	1.22E-05	1.74E-05	1.9E-05	1.04E-05	5.37E-06
α	0.3771	0.4827	0.3168	0.2254	0.2495	0.4351	0.6947
R^2	0.9554	0.9507	0.9622	0.9632	0.9487	0.8507	0.8138

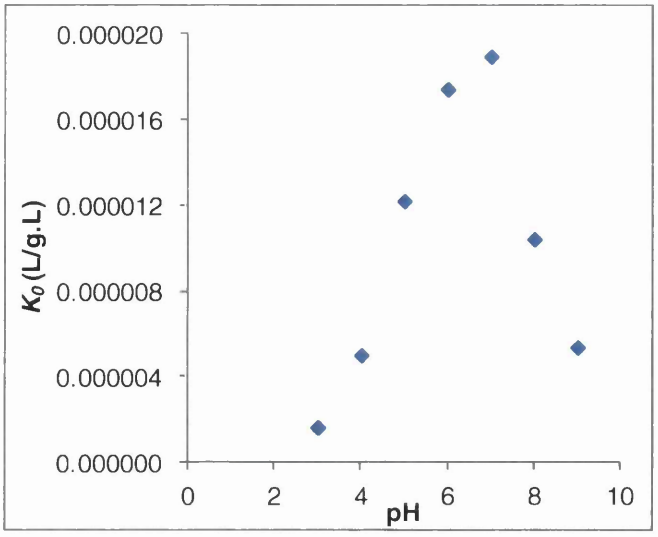

Figure 5.44 K_o vs pH (m_{sand} = 50 g, C_{in} = 20 mg/L, $V_{solution}$ = 50 mL, shaker speed = 150 rpm, T = 25.6°C)

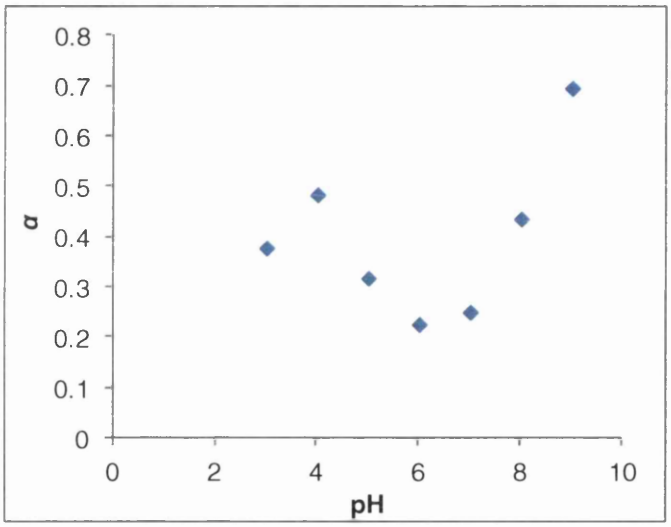

Figure 5.45 α vs pH (m_{sand} = 50 g, C_{in} = 20 mg/L, $V_{solution}$ = 50 mL, shaker speed = 150 rpm, T = 25.6°C)

5.2.2.4 Effect of DO content

The DO content is a significant parameter in AUSF system. The effect of DO on the kinetics of the sorption of copper on manganese coated sand was observed by using DO of the copper solutions of 0.29, 2.40, 8.95, and 17.08 mg/L. m_{sand}, C_{in}, $V_{solution}$,

pH, T, and r were kept constant at 50 g, 20 mg/L, 50 mL, 5, 25.6°C and 150 rpm subsequently.

Increasing DO content from 0.29 to 17.08 mg/L generally resulted in an increase in the removal of copper (Figure 5.46) and a decrease in the ratio of C/C_{in} (Figure 5.47). However, increasing the DO content from 8.95 mg/L to 17.08 mg/L did not give any significant changes. This may be attributed to a greater release of manganese from the surface of the coated sand for 17.08 mg/L DO content as discussed in Section 5.2.4. This reflects that the coated sand may best perform at natural air environment as the DO content of natural air is 8.95 mg/L. The results also show that the copper removal for the DO content of 0.29 mg/L was greater than that for the 2.4 mg/L DO level. This is confirmed by the results of the experiments done with and without manganese coated sand to observe the effect of the DO level on pH (Figure 5.48).

Figure 5.48 shows that the pH values for DO = 0 mg/L (with and without sand) were greater than that for DO = 2.37 mg/L. The greater the pH value the more negative the surface of the coated sand, hence resulted in the more copper removed by the coated sand. Figure 5.48 also shows that the pH value decreased with an increase in DO level from 0 to 2.37 mg/L, and increased with an increase in DO level from 2 to about 8 mg/L. Up to date there is no published data on this matter. This trend confirms the results obtained from tracer studies (Section 4.2.2) and column studies (Section 5.3.1). High DO content leads to higher ε_G which in turns results in higher removal rates. Moreover, higher ε_G represents the sand bed was not fully submerged in water, hence the system operated under unsaturated conditions. These batch results are confirmed with the column results discussed in Section 5.3.1.1 in which operating filter under unsaturated conditions (AUSF) gave better removal than saturated conditions. Higher removal rates for higher DO contents are confirmed with the pH values taken after shaking the samples (Figure 5.49).

Figure 5.49 reveals that the pH value after the adsorption reaction is lower for higher DO content. This lower pH value reflects more copper was adsorbed by the manganese coated sand. As discussed in Section 5.4 the more copper ions adsorbed by the manganese coated sand, the more hydrogen ions released resulting in lower pH value (Equation 5.11, 5.13, and 5.15).

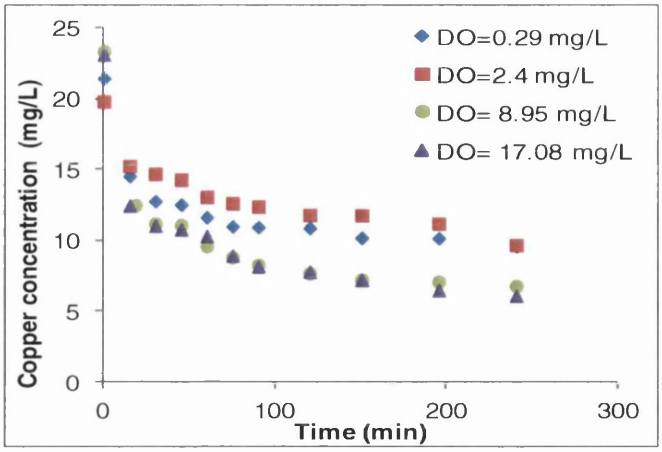

Figure 5.46 Copper concentration vs time for different DO content (m_{sand} = 50 g, C_{in} = 20 mg/L, $V_{solution}$ = 50 mL, pH = 5, shaker speed = 150 rpm, T = 25.6°C)

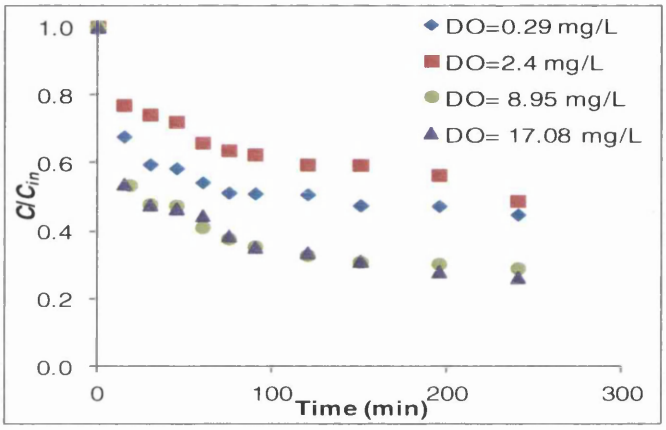

Figure 5.47 C/C_{in} vs time for different DO content (m_{sand} = 50 g, C_{in} = 20 mg/L, $V_{solution}$ = 50 mL, pH = 5, shaker speed = 150 rpm, T = 25.6°C)

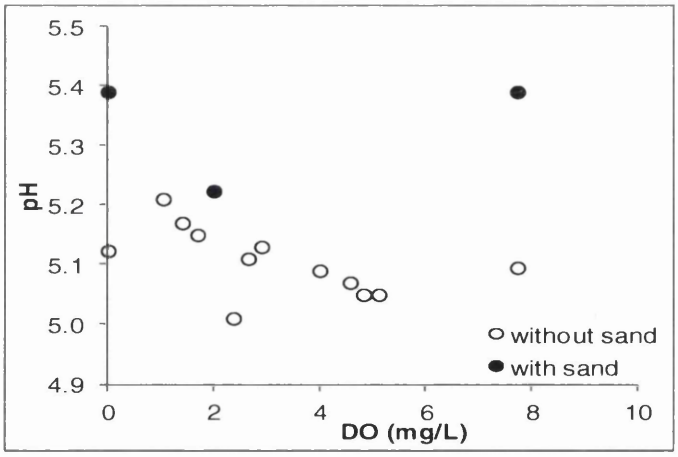

Figure 5.48 pH vs DO with and without sand (m_{sand} = 50 g, C_{in} = 20 mg/L)

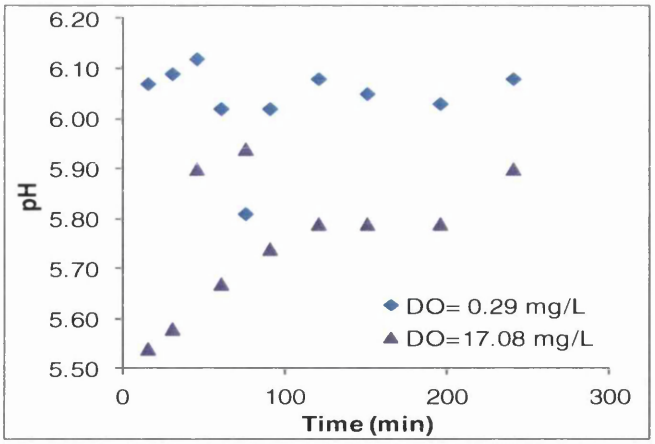

Figure 5.49 The values of pH after shaking experiments vs time for different DO contents (m_{sand} = 50 g, C_{in} = 20 mg/L, $V_{solution}$ = 50 mL, pH = 5, shaker speed = 150 rpm, T = 25.6°C)

Figures 5.50 – 5.51 show the isotherm data obtained within a range of DO content. The figures depict a decrease in the amount of copper sorbed at equilibrium (from 0.0115 to 0.0087 mg/g) when the DO content was increased from 0.29 to 2.4 mg/L, and when the DO level increased from 2.4 to 17.08 mg/L, the amount increased to 0.0168 mg/g. This trend is clearly shown in Figure 5.52.

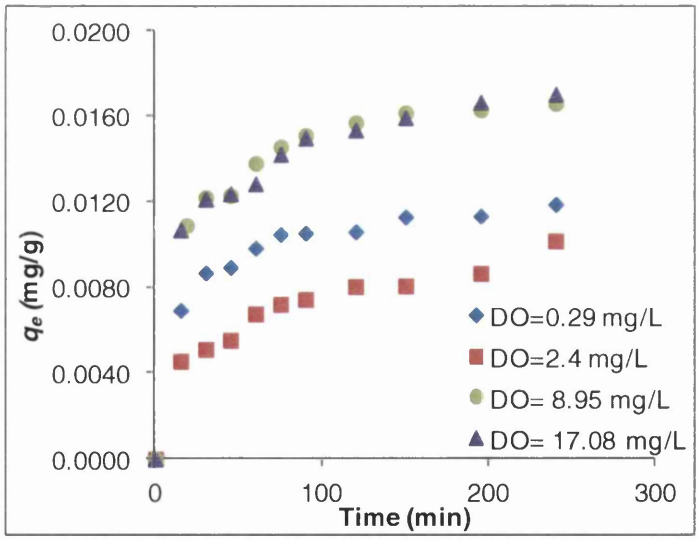

Figure 5.50 Effect of DO content on the sorption of copper by manganese coated sand (m_{sand} = 50 g, C_{in} = 20 mg/L, $V_{solution}$ = 50 mL, pH = 5, shaker speed = 150 rpm, T = 25.6°C)

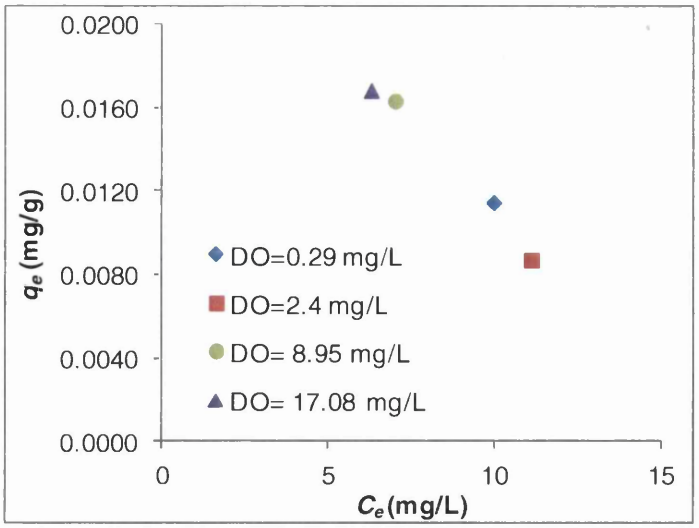

Figure 5.51 Equilibrium isotherms of copper sorption by manganese coated sand at 25.6°C for different DO content (m_{sand} = 50 g, C_{in} = 20 mg/L, $V_{solution}$ = 50 mL, pH = 5, shaker speed = 150 rpm, T = 25.6°C)

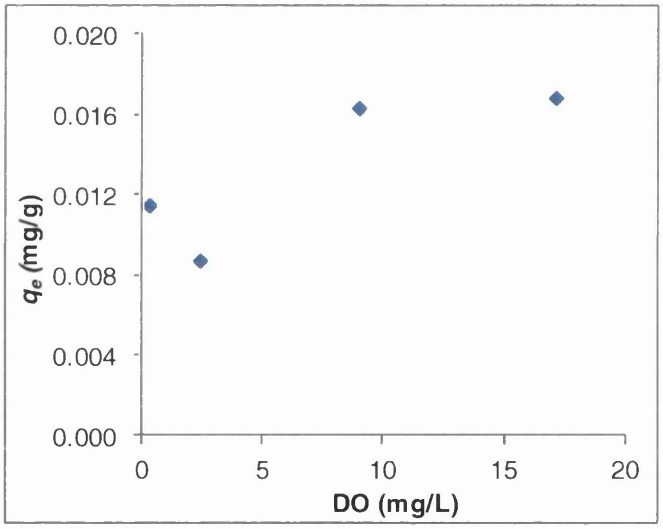

Figure 5.52 q_e vs DO (m_{sand} = 50 g, C_{in} = 20 mg/L, $V_{solution}$ = 50 mL, pH = 5, shaker speed = 150 rpm, T = 25.6°C)

The experimental kinetic data were fitted to the pseudo-second-order type 1 kinetic model. The results are shown in Table 5.20. The sorption of copper by manganese coated sand was found to be well represented by the pseudo-second-order kinetic equation as the correlation factors were between 0.98 - 1.

The rate constant decreased with increasing DO content, which is confirmed by the correlation factor $R^2 \approx 1$ as shown in Figure 5.53. By using this trend, K_2 decreased from 6.5242 to 3.3574 g/mg.min as DO level increased from 0.29 to 17.08 mg/L.

Table 5.20 Kinetic parameters obtained by using pseudo-second-order kinetic model type 1 for different DO content (m_{sand} = 50 g, C_{in} = 20 mg/L, $V_{solution}$ = 50 mL, pH = 5, shaker speed = 150 rpm, T = 25.6°C)

Parameters	DO (mg/L)			
	0.29	2.4	8.95	17.08
K_2 (g/mg.min)	6.5672	4.5500	3.7579	3.3618
q_e (mg/g)	0.0120	0.0094	0.0176	0.0177
h (mg/g.min)	0.0009	0.0004	0.0012	0.0011
R^2	0.9975	0.9832	0.9971	0.9955

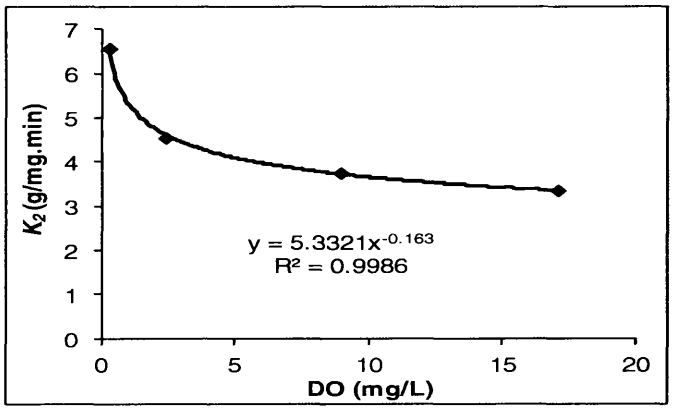

Figure 5.53 The correlation factor of K_2 vs DO content (m_{sand} = 50 g, C_{in} = 20 mg/L, $V_{solution}$ = 50 mL, pH = 5, shaker speed = 150 rpm, T = 25.6°C)

Figure 5.54 shows Weber and Morris intra-particle diffusion plots for different DO contents. The plots of q_t against $t^{0.5}$ were linear indicating that intra particle diffusion occurred. The well fitted of Weber and Morris model thus suggests that the boundary layer (film) did not control the sorption process of copper onto the manganese coated sand. The values of R^2 = 0.94 – 0.99 (Table 5.21) indicate that the Weber-Morris model shows better representation of the data than the pseudo-first order kinetic model. K_{id} increased from 0.0016 to 0.0023 mg/g.min$^{1/2}$ as the DO level increased from 0.29 to 17.08 mg/L. On the other hand, C_{WM} decreased from 0.0010 to 0.0004 mg/g with increasing DO.

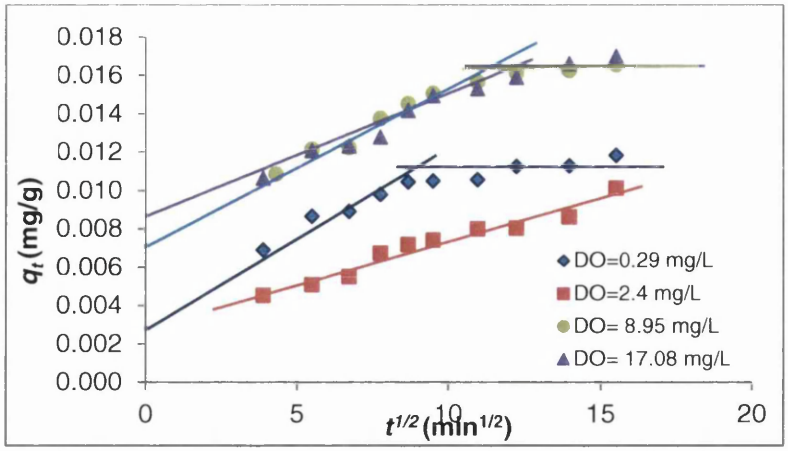

Figure 5.54 Weber and Morris intra-particle diffusion plots for different DO contents (m_{sand} = 50 g, C_{in} = 20 mg/L, $V_{solution}$ = 50 mL, pH = 5, shaker speed = 150 rpm, t_e = 120 min, T = 25.6°C)

Table 5.21 Kinetic parameters obtained by using Weber and Morris for different DO content (m_{sand} = 50 g, C_{in} = 20 mg/L, $V_{solution}$ = 50 mL, pH = 5, shaker speed = 150 rpm, T = 25.6°C)

DO (mg/L)	0.29	2.40	8.95	17.08
K_{id} (mg/g. min$^{1/2}$)	0.0016	0.0010	0.0023	0.0023
C_{WM} (mg/g)	0.0010	0.0002	0.0002	0.0004
R^2	0.9909	0.9645	0.9885	0.9379

Experimental data were further analysed to see as to whether pore diffusion is the only rate-controlling process by Bangham's equation (Equation 3.46). The results are depicted in Table 5.22. Table 5.22 shows that Bangham's equation gives better representation of the data than pseudo-first-order kinetic model as shown by the R^2 values of 0.95 – 0.97. The value of K_o tended to increase as DO increased (Figure 5.55). By using this trend, K_o increased from 9.9082E-06 to 1.0214E-04 (L/g.L) as DO increased from 0.29 to 17.08 mg/L.

Table 5.22 Kinetic parameters obtained by using Bangham's equation for different DO content (m_{sand} = 50 g, C_{in} = 20 mg/L, $V_{solution}$ = 50 mL, pH = 5, shaker speed = 150 rpm, T = 25.6°C)

DO (mg/L)	0.29	2.40	8.95	17.08
K_o (L/g.L)	9.81E-06	4.69E-06	1.24E-05	1.35E-05
α	0.2710	0.3555	0.3132	0.2905
R^2	0.9571	0.9496	0.9711	0.9619

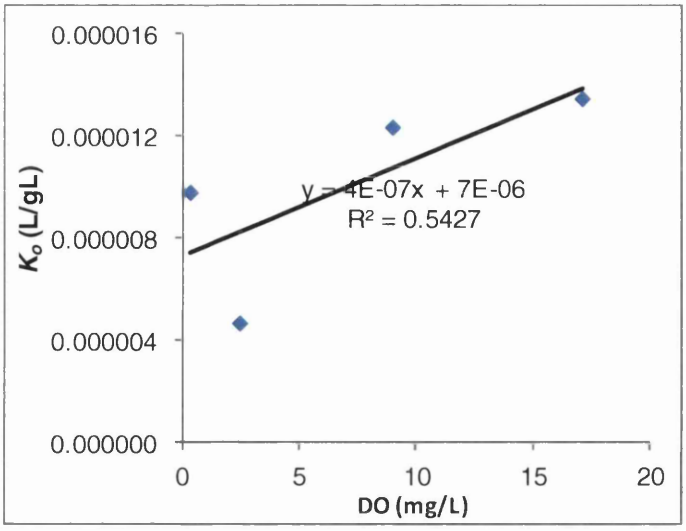

Figure 5.55 The correlation factor of K_o vs DO content (m_{sand} = 50 g, C_{in} = 20 mg/L, $V_{solution}$ = 50 mL, pH = 5, shaker speed = 150 rpm, T = 25.6°C)

5.2.2.5 Effect of sand coating

The effect of sand coating on the kinetics of the sorption of copper on manganese coated sand was studied by using sand coated with manganese 0.0709 mg Mn/g sand and uncoated sand (raw sand). m_{sand}, C_{in}, $V_{solution}$, pH, T, and r were kept constant at 50 g, 20 mg/L, 50 mL, 5, 25.6°C and 150 rpm subsequently.

Figure 5.56 illustrates that effluent copper concentration decreased as the manganese to sand ratio increased. This is likely due to more mass copper retained as shown in Figure 5.57. This may be due to as the more manganese coated the sand particles, the greater the surface area produced (Section 4.1.2) resulting in the more active sites formed. The removal efficiency, E, and the ratio of maximum copper adsorbed to the amounts of manganese on the surface of the sand also increased as the manganese to sand ratio increased (Figures 5.58 – 5.59).

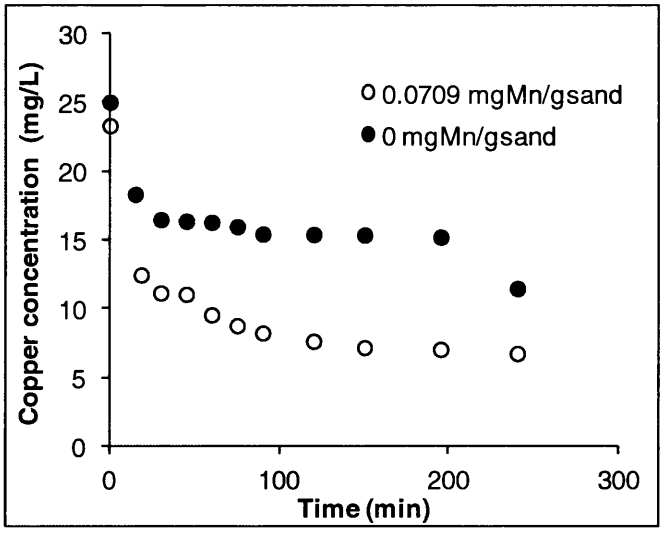

Figure 5.56 Copper concentration vs time for different coating condition (coated = 0.0709 mg Mn/g sand, uncoated = 0 mg Mn/g sand, m_{sand} = 50 g, C_{in} = 20 mg/L, $V_{solution}$ = 50 mL, pH = 5, shaker speed = 150 rpm, T = 25.6°C)

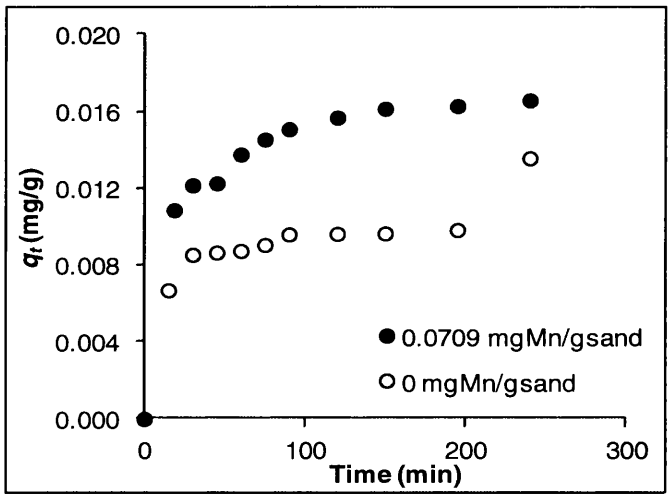

Figure 5.57 Effect of sand coating on the sorption of copper by manganese coated sand (coated = 0.0709 mg Mn/g sand, uncoated = 0 mg Mn/g sand, m_{sand} = 50 g, C_{in} = 20 mg/L, $V_{solution}$ = 50 mL, pH = 5, shaker speed = 150 rpm, T = 25.6°C)

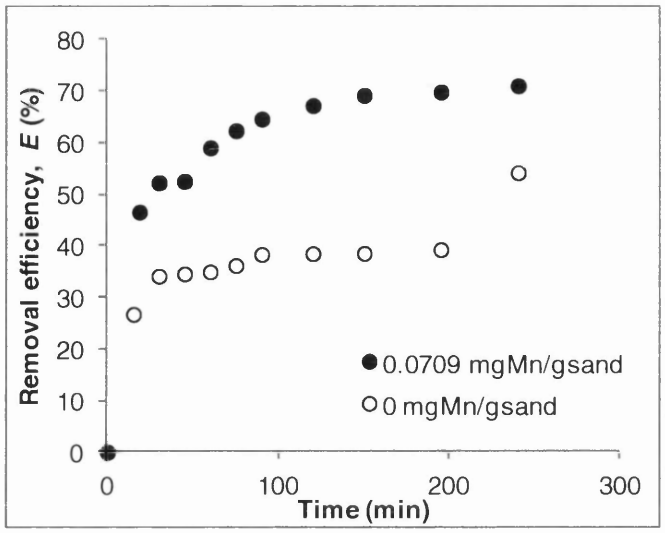

Figure 5.58 Removal efficiency, E (%) vs time for different coating condition (coated = 0.0709 mg Mn/g sand, uncoated = 0 mg Mn/g sand, m_{sand} = 50 g, C_{in} = 20 mg/L, $V_{solution}$ = 50 mL, pH = 5, shaker speed = 150 rpm, T = 25.6°C)

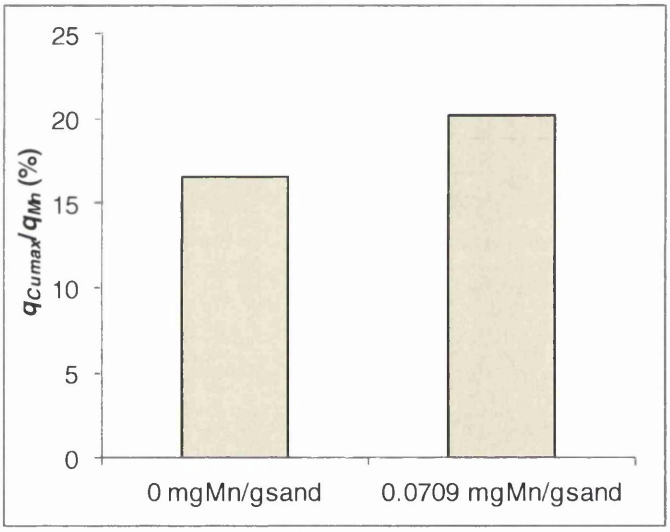

Figure 5.59 q_{Cumax}/q_{Mn} for different coating condition (coated = 0.0709 mg Mn/g sand, uncoated = 0 mg Mn/g sand, m_{sand} = 50 g, C_{in} = 20 mg/L, $V_{solution}$ = 50 mL, pH = 5, shaker speed = 150 rpm, T = 25.6°C)

Figure 5.60 shows the isotherm data obtained for sand coating. The figure depicts an increase in the amount of copper sorbed at equilibrium (from 0.0104 to 0.0159 mg/g) when coating the sand was performed (0.0709 mgMn/gsand).

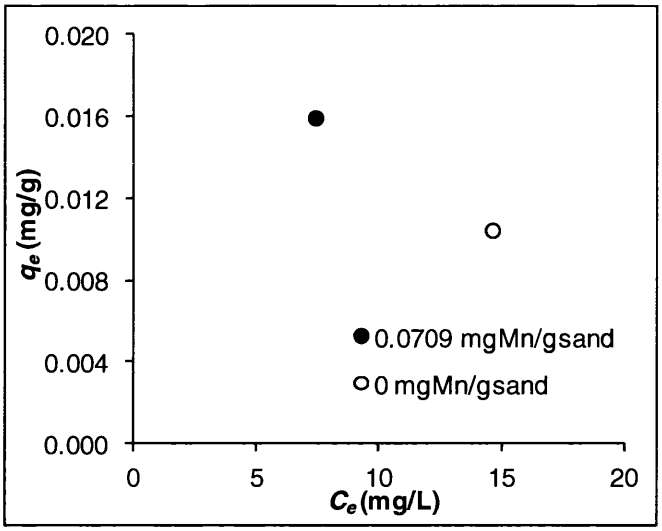

Figure 5.60 Equilibrium isotherms of copper sorption by manganese coated sand at 25.6°C for different coating conditions (coated = 0.0709 mg Mn/g sand, uncoated = 0 mg Mn/g sand, m_{sand} = 50 g, C_{in} = 20 mg/L, $V_{solution}$ = 50 mL, pH = 5, shaker speed = 150 rpm, T = 25.6°C)

The experimental kinetic data were fitted to the pseudo-second-order type 1 kinetic model. The results are shown in Table 5.23. The sorption of copper by manganese coated sand was found to be well represented by the pseudo-second-order kinetic equation as the correlation factors were close to 1. The theoretical amount of copper sorbed at equilibrium increased (from 0.0102 to 0.0169 mg/g) when sand was coated. This trend confirms the experimental data. The initial sorption rate was slightly increased (from 0.001337 to 0.001339 mg/g.min) when sand coating was performed. On the other hand, the rate constant decreased (from 12.9620 to 4.6923 g/mg.min) with coating the sand.

Table 5.23 Kinetic parameters obtained by using pseudo-second-order kinetic model type 1 for different coating conditions (coated = 0.0709 mg Mn/g sand, uncoated = 0 mg Mn/g sand, m_{sand} = 50 g, C_{in} = 20 mg/L, $V_{solution}$ = 50 mL, pH = 5, shaker speed = 150 rpm, T = 25.6°C)

Parameters	Sand coating	
	Coated	Uncoated
K_2 (g/mg.min)	4.6923	12.9620
q_e (mg/g)	0.0169	0.0102
h (mg/g.min)	0.001339	0.001337
R^2	0.9919	0.9959

Figure 5.61 shows Weber and Morris intra-particle diffusion plots for different sand coating. The plots of q_t against $t^{0.5}$ were linear indicating that intra particle diffusion occurred. The well fitted of Weber and Morris model thus suggests that the boundary layer (film) did not control the sorption process of copper onto the manganese coated sand. The values of R^2 (Table 5.24) indicate that the Weber-Morris model shows better representation of the data than the pseudo-first order kinetic model. Table 5.24 also shows that K_{id} and C_{WM} increased (from 0.0016 to 0.0023 mg/g.min1/2 and from 0.0001 to 0.0002 mg/g respectively) once sand was coated.

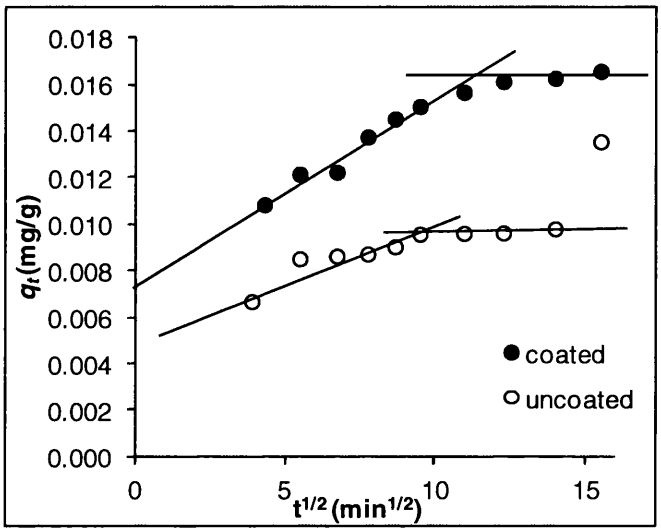

Figure 5.61 Weber and Morris intra-particle diffusion plots for different sand coating (coated = 0.0709 mg Mn/g sand, uncoated = 0 mg Mn/g sand, m_{sand} = 50 g, C_{in} = 20 mg/L, $V_{solution}$ = 50 mL, pH = 5, shaker speed = 150 rpm, t_e = 120 min, T = 25.6°C)

Table 5.24 Kinetic parameters obtained by using Weber and Morris for different sand coating (coated = 0.0709 mg Mn/g sand, uncoated = 0 mg Mn/g sand, m_{sand} = 50 g, C_{in} = 20 mg/L, $V_{solution}$ = 50 mL, pH = 5, shaker speed = 150 rpm, T = 25.6°C)

Sand coating	Coated (0.0709 mg/L Mn)	Uncoated (0 mg/L Mn)
K_{id} (mg/g. min$^{1/2}$)	0.0023	0.0016
C_{WM} (mg/g)	0.0002	0.0001
R^2	0.9885	0.9932

Experimental data were further analysed to see as to whether pore diffusion is the only rate-controlling process by Bangham's equation (Equation 3.46). The results are depicted in Table 5.25. Table 5.25 shows that the average R^2 value was 0.91 representing well fit of the model. K_0 and α increased from 9.2E-06 to 1.23E-05 L/g.L and from 0.2140 to 0.3155 once sand was coated.

Table 5.25 Kinetic parameters obtained by using Bangham's equation for different sand coating (coated = 0.0709 mg Mn/g sand, uncoated = 0 mg Mn/g sand, m_{sand} = 50 g, C_{in} = 20 mg/L, $V_{solution}$ = 50 mL, pH = 5, shaker speed = 150 rpm, T = 25.6°C)

Sand coating	Coated	Uncoated
K_o (L/g.L)	1.23E-05	9.2E-06
α	0.3155	0.2140
R^2	0.9463	0.8828

5.2.3 Summary of the kinetics parameters

Table 5.26 shows the kinetics parameters obtained from the batch studies, while Table 5.27 illustrates the correlation factors, R^2, obtained from the kinetics models used in these batch studies. Table 5.26 shows that theoretical q_e values derived from Langmuir type 1 model and pseudo second order type 1 particularly for C_{in}, DO and sand coating variation as well as for pH = 3 and 9 were almost similar. In addition these theoretical values were close to the values that obtained from the experiments. Langmuir type 1 model and pseudo second order type 1 were thus concluded to be best fitted to model the sorption of copper onto the manganese coated sand.

As Langmuir type 1 model was best fitted to model the sorption of copper onto the manganese coated sand (which is also confirmed by its value of R^2 (= 0.99) (Table 5.5)), it is thus assumed that the adsorption of copper onto the manganese coated sand was occurred in one layer (monolayer).

This favourable sorption of copper by the manganese coated sand was also confirmed by the obtained value of R_L ($0 < R_L < 1$) (Table 5.6, Section 5.2.1).

Table 5.26 Kinetic parameters obtained in batch studies

Parameter	C_{in} (mg/L)		m_{sand} (g)		pH					DO (mg/L)			sand coating (mgMn/gsand)	
	23.32	6.87	5	100	3	4	6	7	9	0.29	2.4	17.08	0	0.0709
Langmuir type 1														
q_e (mg/g)	0.0177	0.0078	0.0189	0.0122	0.0043			0.0162	0.0075	0.0115	0.0087	0.0163	0.0104	0.0159
	decreased		decreased		increased			decreased		decreased	increased		increased	
Pseudo second order type 1														
K_2 (g/mg.min)	4.3631	7.6284	0.6748	23.4083	8.2054	1.8328			10.3951	6.5242		3.3574	12.9620	4.6923
	increased		increased		decreased	increased				decreased			decreased	
h (mg/g.min)	0.0018	0.0002	0.0001	0.0030	0.0002			0.0017	0.0006	0.0009	0.0004	0.0011	0.001337	0.001339
	decreased		increased		increased			decreased		decreased	increased		increased	
q_e (mg/g)	0.0179	0.0080	0.0252	0.0157	0.0048	0.0185			0.0078	0.0120	0.0094	0.0177	0.0102	0.0169
	decreased		decreased		increased	decreased				decreased	increased		increased	
Weber and Morris model														
K_{id} (mg/g. min1/2)	0.0024	0.0009	0.0009	0.0037	0.0005			0.0024	0.0009	0.0016	0.0010	0.0023	0.0016	0.0023
	decreased		increased		increased			decreased		decreased	increased		increased	
C_{WM} (mg/g)	0.0002	0.0006	-0.00002	0.00036	0.00002		0.0005		0.0002	0.0010	0.0002	0.0004	0.0001	0.0002
	increased		increased		increased		decreased			decreased	increased		increased	
Bangham's equation														
K_o (L/g.L)	1E-08	2E-09	0.000001	0.00002	1.6E-06			2E-05	5.4E-06	9.9E-06		1E-05	9.2E-06	1.23E-05
	decreased		increased		increased			decreased		increased			increased	
α	0.1115	0.7142	2.8486	0.2349	0.3771	0.4827	0.2254		0.6947	0.2710	0.3555	0.2905	0.2140	0.3155
	increased		decreased		increased	decreased	increased			increased	decreased		increased	

In addition, chemisorptions are assumed to be involved in the removal of copper by the manganese coated sand as shown by the good fit of the pseudo second order type 1 model to model this removal. The well capability of this pseudo second order type 1 was also supported by its R^2 values (= 0.96 - ≈ 1) as shown in Table 5.27.

Table 5.27 The correlation factors, R^2, obtained from the kinetics models used in the batch studies

Parameter	Pseudo second order type 1	Weber and Morris model	Bangham's equation
	R^2 average	R^2 average	R^2 average
C_{in} (mg/L)	0.9957	0.9745	0.9516
m_{sand} (g)	0.9564	0.9852	0.9065
pH	0.9827	0.9604	0.9207
DO (mg/L)	0.9933	0.9705	0.9599
mgMn/gsand	0.9939	0.9909	0.9146

Moreover, intra particle diffusion was assumed to be involved in the removal of copper by the manganese coated sand as confirmed by the R^2 values of Weber and Morris (= 0.96 – 0.99) as well as Bangham (= 0.91 – 0.96) models as shown in Table 5.27. The well fitted of Weber and Morris model thus suggests that the boundary layer (film) did not control the sorption process of copper onto the manganese coated sand.

5.2.4 Manganese attachment strength

To find out the attachment strength of manganese onto the coated sand, manganese concentrations were measured for several samples in batch studies. Figure 5.62 shows manganese concentrations for different initial pH. A high amount of manganese released into the aqueous solution with increasing contact times was observed for all pH values.

Figure 5.62 clearly shows that at pH = 3, manganese was leached the most (up to 11.83 mg/L in 240 min). For other pH values, the amounts of manganese leached were up to 3.76 – 6.58 mg/L in 240 min.

Compared to the acid alkali resistance test in Section 4.1.5, manganese was much more leached in these batch studies. This may be attributed to the greater shaker speed (= 150 rpm) used in these batch studies.

Figure 5.63 illustrates manganese concentrations for different DO contents. For all DO contents, a significant amount of manganese leached into the solution occurred with increasing contact times. Smallest DO content (= 0.24 mg/L) released manganese the most (= 6.16 mg/L). The results reveal that the natural air environment (DO = 8.95 mg/L) leached the smallest manganese amount (= 3.76 mg/L). Increasing DO content to 17.08 mg/L, however, did not result in decreasing the amount of manganese leached from the sand.

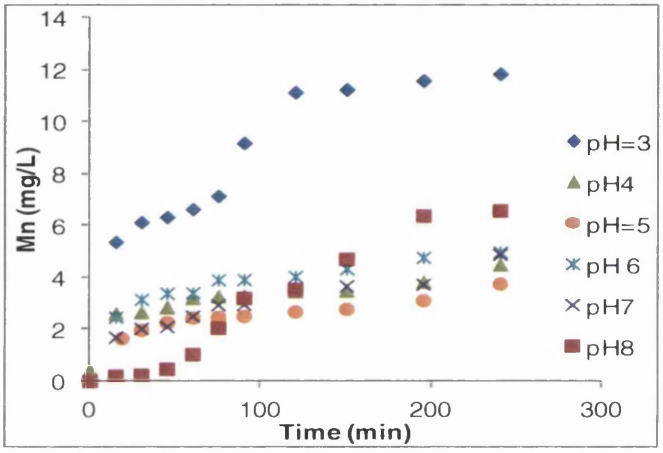

Figure 5.62 Manganese concentrations for different initial pH (m_{sand} = 50 g, C_{in} = 20 mg/L, $V_{solution}$ = 50 mL, shaker speed = 150 rpm, T = 25.6°C)

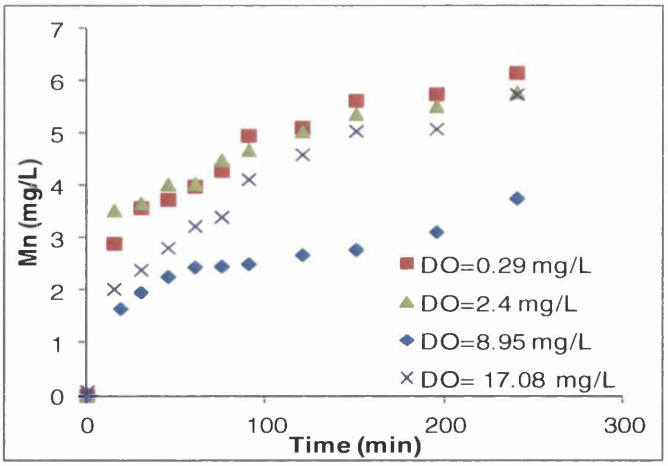

Figure 5.63 Manganese concentrations for different DO contents (pH = 5, m_{sand} = 50 g, C_{in} = 20 mg/L, $V_{solution}$ = 50 mL, shaker speed = 150 rpm, T = 25.6°C)

For all different initial concentrations, a high amount of manganese released into the aqueous solution was observed as shown in Table 5.28.

The amounts of manganese found in the solution were in the range of 3.88 – 7.31 mg/L. The results show that manganese coated sand was fragile under higher shaker speed ($r \geq 150$ rpm) and particularly at low pH (≤ 3).

Table 5.28 Manganese concentrations for several samples in batch studies

DO (mg/L)	C_{in} (mg/L)	m_{sand} (g)	pH	*C* Mn(mg/L)	*t* (min)
0.29	19.784	50	5	6.16	240
2.4	21.408	50	5	5.78	240
8.95	23.32	50	5	3.76	240
17.8	23.088	50	5	5.74	240
8.95	22.808	50	3	11.83	240
8.95	23.476	50	4	4.49	240
8.95	23.32	50	5	3.76	240
8.95	23.02	50	6	4.96	240
8.95	21.292	50	7	4.88	240
8.95	9.356	50	8	6.58	240
8.95	6.87	50	5	7.31	240
8.95	13.9	50	5	3.88	240
8.95	17.98	50	5	4.26	240

5.3 Column studies

5.3.1 Saturated and unsaturated

5.3.1.1 Comparison between saturated and unsaturated column

In this work, the performance of AUSF in removing copper was compared to the saturated condition. C_{in}, Q, H, d_{sand}, and manganese to sand ratio were kept constant at 5 mg/L, 81.9 mL/min, 450 mm, 0.850 mm, and 0.0709 mg-manganese/g-sand respectively.

Table 5.29 shows the removal of copper under saturated and unsaturated conditions obtained in this study along with the comparison of these removals with other studies.

Table 5.29 Comparison of saturated and unsaturated sand filter (AUSF) with other studies

	Saturated	Unsaturated	Lee et al (2004) aerated -and non aerated	Han et al (2006a)	Wan et al (2010)	Chu and Hashim (2007)	Boujelben et al (2009)	Han et al (2009)
Adsorbent and Carrier material	Manganese coated sand		Manganese coated sand (MCS)	Manganese oxide coated sand (MCS)	Chitosan coated sand (CCS)	PVA-immobilized seaweed biomass	Natural iron oxide-coated sand	Iron oxide-coated zeolite (IOCZ)
Preparation of adsorbent and carrier material	Sand was dried at 105 C, 24 hr, soaked in KMnO4 0.1N, washed and dried at 105C, 24 hr		Commercially purchased	Sand was soaked in 0.1 mol/L HCl, 24 hr, rinsed and dried at 373 K. Boiled KMNO4 poured over sand+ HCl, stirred 1 hr, filtered, washed, dried at room temperature	Chitosan + sand + HCl+Na OH			Zeolite + Ferric chloride+NaOH
Technology	Filter, d = 40 mm, H = 450 mm		Fluidized bed reactor, d = 30 mm, H = 1500 mm	Batch	Batch	Fixed bed, d=1.6cm, h=10cm	Batch	fixed bed column, continuous flow system, 0.95cm diameter glass column, h = 6,11, 15 cm
Diameter (mm)	0.85		1.00 ± 0.1	0.99 to 0.67	0.50	0.25-0.50	0.00063- 0.10	0.42-0.86
Flow rate	81.91 mL/min		10 m/h			1, 1.5 mL/min		8,11,14 mL/min
pH	Non adjusted: 5.99-7.15	Non adjusted: 5.86-7.83	6	4	6		5	4
C_{in} (mg/L)	5		30	0.315 mmol l–1	100	20,40	30	40,60,80
Element	Copper		Copper	Copper	Copper		Copper	Copper
Removal rate in 30 min (%) (=((C_{in}-C)/C_{in}) x 100)	Saturated: 13.25	Unsaturated: 26.32	Non aerated: 58.17 Aerated: 71.17		99.07			
Removal rate in 60 min (%)	Saturated: 0	Unsaturated: 14.88		80				

	Saturated	Unsaturated	Lee et al (2004) aerated -and non aerated	Han et al (2006a)	Wan et al (2010)	Chu and Hashim (2007)	Boujelben et al (2009)	Han et al (2009)
Removal in 120 min (%)							100	
Amount of manganese/sand (mg-Mn/g- sand)	Saturated: 0.63	Unsaturated: 0.61	Aerated and non aerated: 8.03	5.46				
Saturation time (min)	50	85	1000	90	1440	900 for Q=1ml/min 600 for Q=1.5 ml/min	120	Exhaust time (=90% *Cin*) for Q=8,11, 14 mL/min: 680, 300, 210 min; for *Cin*=40, 60, 80 mg/L: 521, 300, 160 min; for 60,110, 150 mm height: 135, 300, 460 min
t_{95} (i.e. C/C_{in} = 0.05) (min)	0.62	5.23						
Removal capacity, q (mass retained) after 50 min (mg/g sand)	0.0058	0.0092	0.70					
Ratio of maximum copper adsorbed per g-sand to the amounts of manganese per g-sand, q_{Cumax}/q_{Mn} (%)	Saturated: 7.10	Unsaturated: 12.89						

The removal rates of copper, R, in 30 min was 13.25% for saturated and doubled to 26.32% for unsaturated. This indicates that aeration (i.e. unsaturated condition) played a significant role in enhancing sand filter performances. This was consistent with Lee et al. (2004) who also obtained enhanced removal under aerated condition. As discussed earlier, BET surface area results also proved that the removal of copper was improved under unsaturated condition. The removal rates obtained in this study were much lower than that obtained by Lee et al. (2004) who reported removals up to 58.17% and 71.17% for non aerated and aerated conditions respectively. This is likely due to the amounts of manganese/sand used in this study which were much lower (= 0.0709 mg-Mn/g-sand) compared to 8.03 mg-Mn/g-sand. Moreover and possibly for the same reason, saturation times were shorter in this study (~50 min for the saturated and ~80 min for the unsaturated filter as shown in Figure 5.64 (a)) as compared to ~1000 min. The removal rate of copper (for unsaturated condition) after 60 min was 14.88% which was also lower than the 80% obtained by Han et al. (2006a). They also obtained a much longer saturation time of 90 min. This again is likely due to the higher manganese ratio of 5.46 mg-Mn/g-sand.

On the other hand, complete removal of copper and higher saturation times were obtained when smaller sand sizes (Boujelben et al., 2009) or different material (i.e. immobilized biopolymers (Chu and Hashim, 2007) and chitosan coated sand (Wan et al., 2010)) were used. Moreover, low flow rates gave longer saturation times as obtained by Han et al. (2009).

Figure 5.64 (a) shows typical breakthrough curves for copper removal on the filter operated under saturated and unsaturated (AUSF) conditions. The figure shows that the profile of the C-curves do not follow a smooth trend possibly due to changing removal mechanisms over time. Figures 5.64 (a - b) clearly show that the AUSF was more efficient than the saturated condition in removing copper. As shown in Figure 5.64 (a), saturated condition reached saturation in about 50 minutes while AUSF continued removing copper until about 80 minutes. This indicates that AUSF can operate much longer than saturated condition. Besides, t_{95} (Figure 5.64 (a) (inset)) was 0.62 min for the saturated filter and more than 8 times greater (i.e. 5.23 min) for the unsaturated filter.

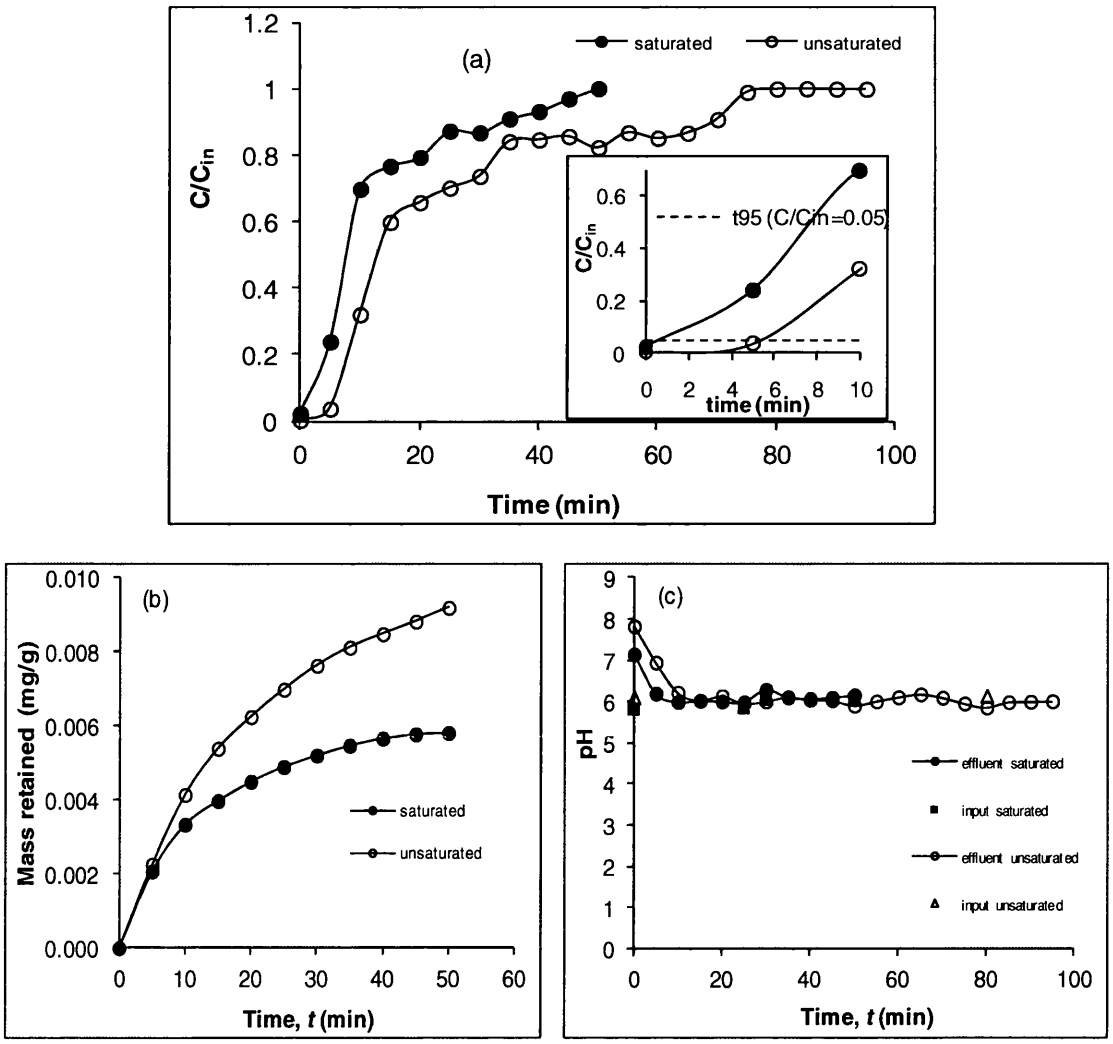

Figure 5.64 Copper removal under saturated and unsaturated conditions (C_{in} = 5 mg/L, Q = 81.9 mL/min, H = 450 mm, d_{sand} = 0.850mm, manganese to sand ratio = 0.0709 mg-manganese/g-sand) (a) C/C_{in} vs time, t (b) Mass retained (mg-copper/g sand) vs time, t (c) pH vs time, t

Moreover, the percentage ratio of maximum copper adsorbed per g-sand to the amounts of manganese per g-sand (q_{Cumax}/q_{Mn}) were observed to be 7.10% for the saturated, and 12.89% for the AUSF unsaturated filter respectively. These reflect that the unsaturated condition removed more copper than the saturated one. Up to date there is no published data on t_{95}, and q_{Cumax}/q_{Mn}.

Figure 5.64 (b) shows that the removal capacity at saturation, q_{sat} achieved in saturated filter was 0.0058 mg/g as compared to almost a double value of 0.0092 mg/g in AUSF.

This indicates that unsaturated condition (i.e. aerated) was important in enhancing the filter performance, which is in agreement with Lee et al. (2004) who have also obtained enhanced removals under aerated condition. These were lower than that of Lee et al. (2004) (0.70 mg-copper/g-MCS) since they used more manganese to coat the sand particles. Nevertheless, it is clear from these results that manganese load and aeration play important roles in the performance of manganese coated sand AUSF, which is clearly an effective technology for copper removal.

Copper may precipitate theoretically as hydroxide compounds if the pH > 5.92 (Section 5.4). Other researchers observed that it occurred once pH went beyond 6 (Lee et al., 2004; Han et al., 2006b; Lee et al., 2006; Wan et al., 2010). pH adjustments are usually made in order to achieve precipitation of the metal hydroxide using chemicals such as lime or soda caustic (Lee et al., 2004; Wan et al., 2010), which can have a drastic effect on the overall cost of the operation. In this work such pH adjustment was not needed since the pH was alkaline at the beginning of the experiment and then dropped to pH 6 at which this pH remained constant throughout the process as shown in Figure 5.64 (c).

5.3.1.2 Comparison between column and batch studies for different DO contents

Table 5.30 shows the comparison between column and batch studies for different DO contents. Table 5.30 depicts that copper removal was much better once the DO contents increased. Increasing DO contents leads to a decrease in C/C_{in} which in turns results in longer saturation time. An increase in DO contents results in an increase in removal capacity q, removal rate, removal efficiency E, t_{95}, and q_{Cumax}/q_{Mn}.

In column studies, an increase in DO contents may achieve t_{95} faster. On the other hand, in batch studies, increasing DO content may obtain t_{95} longer. This occurs as in batch studies, effluent concentration decreased with increasing contact times, whereas in coloumn studies, effluent concentration increased with increasing contact times. The results obtained for different DO contents from column studies clearly confirmed the results from batch studies.

Table 5.30 Comparison between batch and column studies for different DO contents

Parameter	DO contents (mg/L)					
	Column		Batch			
	Saturated	Unsaturated	0.29	2.4	8.95	17.08
C_{in} (mg/L)	5	5	20	20	20	20
C/C_{in}	higher	lower	decreased with increasing DO contents			
Removal rate in 30 min (%)	13.25	26.32	40.47	25.80	52.14	52.37
Removal rate in 60 min (%)		14.88	45.80	34.07	59.01	55.46
Saturation time (min)	50	80	increased with increasing DO contents			
t_{95} (min)	0.62	5.23	may achieve faster with increasing DO contents			
Removal efficiency, E (%)			55.31	51.25	71.03	73.70
q_{Cumax}/q_{Mn}	0.07	0.13	0.14	0.12	0.20	0.21
removal capacity, q (mgCu/gsand) in 50 min	0.006	0.009	0.009	0.006	0.013	0.012

5.3.2 Different input concentrations

5.3.2.1 Effect of copper input concentrations on AUSF performances

The effect of copper input concentrations on copper removal was studied by using C_{in} of 3, 4, 5, 10, 15 and 20 mg/L. Q, H, d_{sand}, and manganese to sand ratio were kept constant at 81.91 mL/min, 450 mm, 0.850 mm, and 0.0709 mg-manganese/g-sand respectively.

Table 5.31 depicts that removal rates (R), saturation time, t_{95} and the ratio of maximum copper adsorbed per g-sand to the amounts of manganese per g-sand ($q_{Cu\ max}/q_{Mn}$) increased as copper input concentration decreased. Kundu and Gupta (2007) also obtained t_{90} increased with the decrease in the input concentration in their study of a fixed bed column on arsenic removal. This may be due to the more mass copper retained as clearly shown in Figure 5.65 (c) Besides, Figure 5.65 (a) shows that the outlet concentrations followed similar trend; being low initially, indicating copper removal, and evolved until reaching the inlet concentration, C_{in}.

Table 5.31 The removal rates (R), saturation time, t_{95}, and ratio of maximum copper adsorbed to the amounts of manganese for various concentrations

C_{in} (mg/L)	Removal Rate, R (%)			Saturation time (min)	t_{95} (min)	q_{Cumax}/q_{Mn} (%)
	30 min	60 min	120 min			
20	0.00	0.00	n/a	30	0.26	13.10
15	2.38	0.00	n/a	35	0.50	15.27
10	14.23	0.00	n/a	40	0.51	15.42
5	35.11	0.00	n/a	60	16.05	15.31
4	54.77	18.78	7.82	210	25.06	22.84
3	84.48	56.97	7.86	240	25.54	24.96

Notes:

1. n/a = not available
2. Q_{in} = 80.91 mL/min, H = 450mm, d_{sand} = 0.850 mm, manganese to sand ratio = 0.62 mg-manganese/g-sand

At low C_{in} the breakthrough curves extend for longer times as compared to those at higher C_{in}, which are rapidly reached and are characterised by a sharp increase in concentration (Figure 5.65 (b)) possibly due to low ratio of active sites to the amount of copper introduced to the filter. Other researchers also found the similar tendency (Pan et al., 2005; Chu and Hashim, 2007; Kundu and Gupta, 2005; Han et al., 2009).

The calculated removal capacity, q, evolved as function of time to a maximum (or saturation) value noted as q_{sat} and the change of q_{sat} as function of the inlet copper concentration is shown in Figure 5.65 (c). Surprisingly, the figure shows that as the inlet concentration increased, the saturation removal capacity of AUSF decreased. This trend may be explained by as the inlet copper concentration increased, precipitation of copper hydroxide on the sand surface is significant, which blocks significant number of removal sites and hence reduces the overall capacity of the filter.

In contrast and for dilute concentrations, precipitation is less significant hence copper removal by adsorption prevailed. Breakthrough curves obtained at low inlet concentrations as opposed to those obtained at high inlet concentrations were steep at the beginning but concave downward with increasing operation time and asymptotically nearing complete breakthrough. This type of breakthrough curves is typical for adsorption where solid-phase mass transfer controls the process, which further supports that adsorption is significant at low inlet concentrations.

This is also supported by Figure 5.65 (d) that shows the ratio of maximum copper adsorbed to the amounts of manganese was clearly correlated to input concentration. The role of solid-phase mass transfer as the controlling step is supported also by the results from the batch studies (Section 5.2.2.1) that showed that the boundary layer (film) did not control the sorption process.

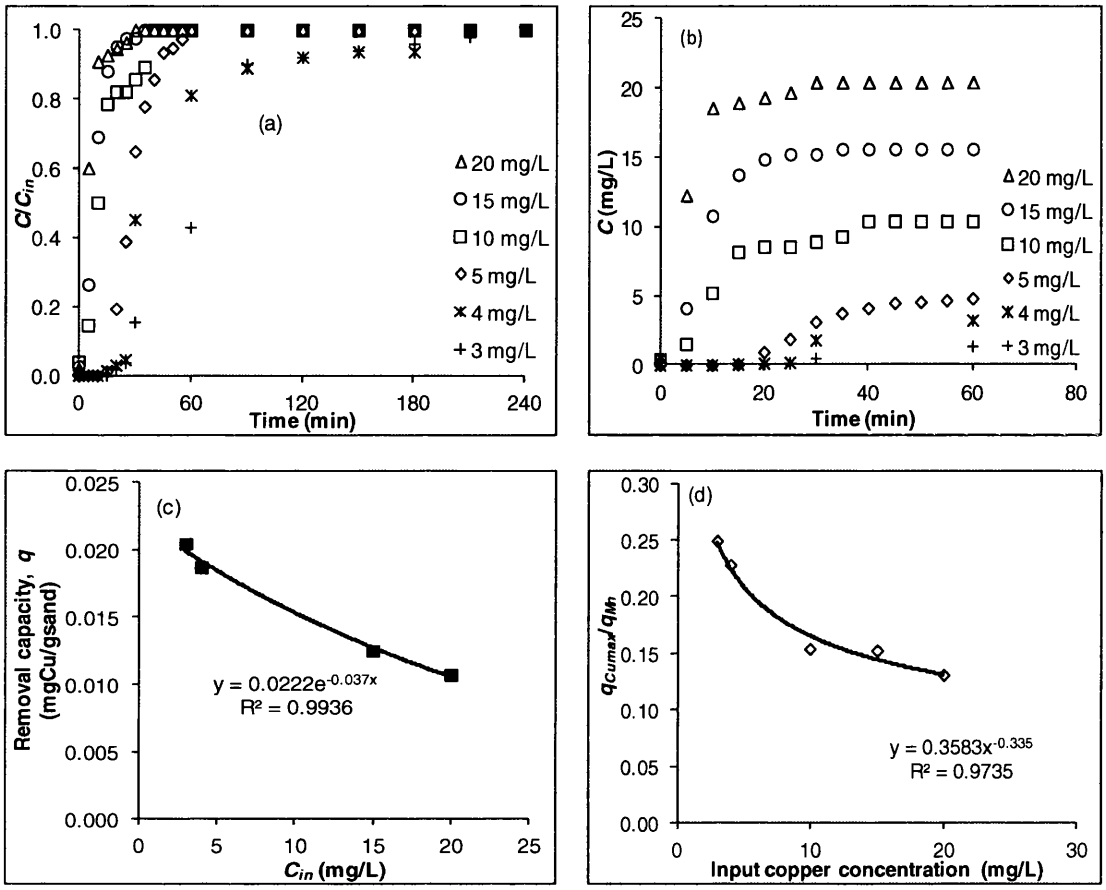

Figure 5.65 AUSF performances at different copper input concentrations (Q_{in} = 80.91 mL/min, H = 450mm, d_{sand} = 0.850 mm, manganese to sand ratio = 0.0709 mg-manganese/g-sand, m_{sand} = 891.13 g) (a) C/C_{in} vs time (b) effluent copper concentration (c) removal capacity, q vs C_{in} after saturation (d) q_{Cumax}/q_{Mn} vs C_{in}

5.3.2.2 Comparison between column and batch studies for different input concentrations

Table 5.32 illustrates the comparison between column and batch studies for different initial concentrations.

Table 5.32 Comparison between batch and column studies for different initial concentrations

Parameter	Column						Batch			
C_{in} (mg/L)	3	4	5	10	15	20	6.87	13.9	18	23.3
C/C_{in}	increased with increasing C_{in}						increased with increasing C_{in}			
C (mg/L)	increased with increasing C_{in}						increased with increasing C_{in}			
Removal capacity, q (mg/g)	decreased with increasing C_{in}						increased with increasing C_{in}			
Removal efficiency, E (%)							decreased with increasing C_{in}			
q_{Cumax}/q_{Mn}	decreased with increasing C_{in}						increased with increasing C_{in}			
Removal rate in 30 min (%)	84.48	54.77	35.11	14.23	2.38	0.00	65.87	64.60	63.21	52.14
Removal rate in 60 min (%)	56.97	18.78	0.00	0.00	0.00	0.00	85.15	78.04	66.28	59.01
Removal rate in 120 min (%)	7.86	7.82	n/a	n/a	n/a	n/a	97.67	85.50	73.73	67.20
Saturation time (min)	240	210	60	40	35	30	decreased with increasing C_{in}			
t_{95} (min)	25.54	25.06	16.05	0.51	0.50	0.26	111.51	207.82	> 240	> 240
q_{Cumax}/q_{Mn} (%)	24.96	22.84	15.31	15.42	15.27	13.10	8.38	16.96	18.01	20.21

Table 5.32 depicts that copper removal was much better once initial concentration decreased. Decreasing initial concentrations leads to a decrease in C/C_{in} which in turns results in longer saturation time. A decrease in initial concentration results in a decrease in effluent copper concentration. On the other hand decreasing initial concentration leads to an increase in removal rate and removal efficiency E. In column studies, increasing initial concentration results in a decrease in removal capacity q, and q_{Cumax}/q_{Mn}. In addition, an increase in initial concentration may achieve t_{95} faster. On the other hand, in batch studies, removal capacity q, and q_{Cumax}/q_{Mn} increased with an increase in initial concentration.

Moreover, increasing initial concentration might achieve t_{95} longer. This occurs as in batch studies, effluent concentration decreased with increasing contact times, while in column studies, effluent concentration increased with contact times. The results obtained from column studies for different initial concentrations clearly confirmed the ones from batch studies.

5.3.3 Different height of sand bed

5.3.3.1 Effect of height of sand bed on AUSF performances

The effect of height of sand bed on copper removal was studied by using different H of 150, 250, 350 and 450 mm. Q, C_{in}, d_{sand}, and manganese to sand ratio were kept constant at 80.91 mL/min, 20 mg/L, 0.850 mm, and 0.0709 mg-manganese/g-sand subsequently.

Table 5.33 shows that generally removal rates (R), saturation time, t_{95} and ratio of maximum copper adsorbed to manganese amounts (q_{Cumax}/q_{Mn}) increased slightly as height of sand bed increased. Kundu and Gupta (2005) obtained t_{90} increased with an increase in the bed depth in their study. Figures 5.66 (a - b) illustrate C/C_{in} and effluent copper concentration vs time (t) curves. The figure shows that all curves have the same shape and almost superimpose which indicates that the height of sand did not affect the mechanisms by which copper was removed. Other researchers found that C/C_{in} vs time (t) curve was steeper at lower bed depth (Pan et al., 2005; Kundu and Gupta, 2005; Mohan and Sreelakshmi, 2008; Han et al., 2009). Nevertheless, mass copper retained was correlated to the height of sand bed as depicted clearly in Figure 5.66 (c). The figure show that the removal capacity increased as the height of sand bed increased. Mohan and Sreelakshmi (2008) also obtained that the uptake of metals (i.e copper, lead, zinc and manganese) increased with the increase in the bed depth. In addition, the ratio of maximum copper adsorbed to the amounts of manganese on the coated sand was apparently correlated to the height of sand bed as shown in Figure 5.66 (d).

Table 5.33 The removal rates (R), saturation time, t_{95}, and ratio of maximum copper adsorbed to the amounts of manganese for various heights

Height of sand bed (mm)	Removal Rate, R (%)			Saturation time (min)	t_{95} (min)	q_{Cumax}/q_{Mn} (%)
	5 min	10 min	25 min			
150	0.00	0.00	n/a	5.00	0.00	11.70
250	16.33	0.00	n/a	10.00	0.00	11.94
350	19.96	7.26	0.00	15.00	0.19	11.00
450	39.93	9.07	3.63	30.00	0.26	12.94

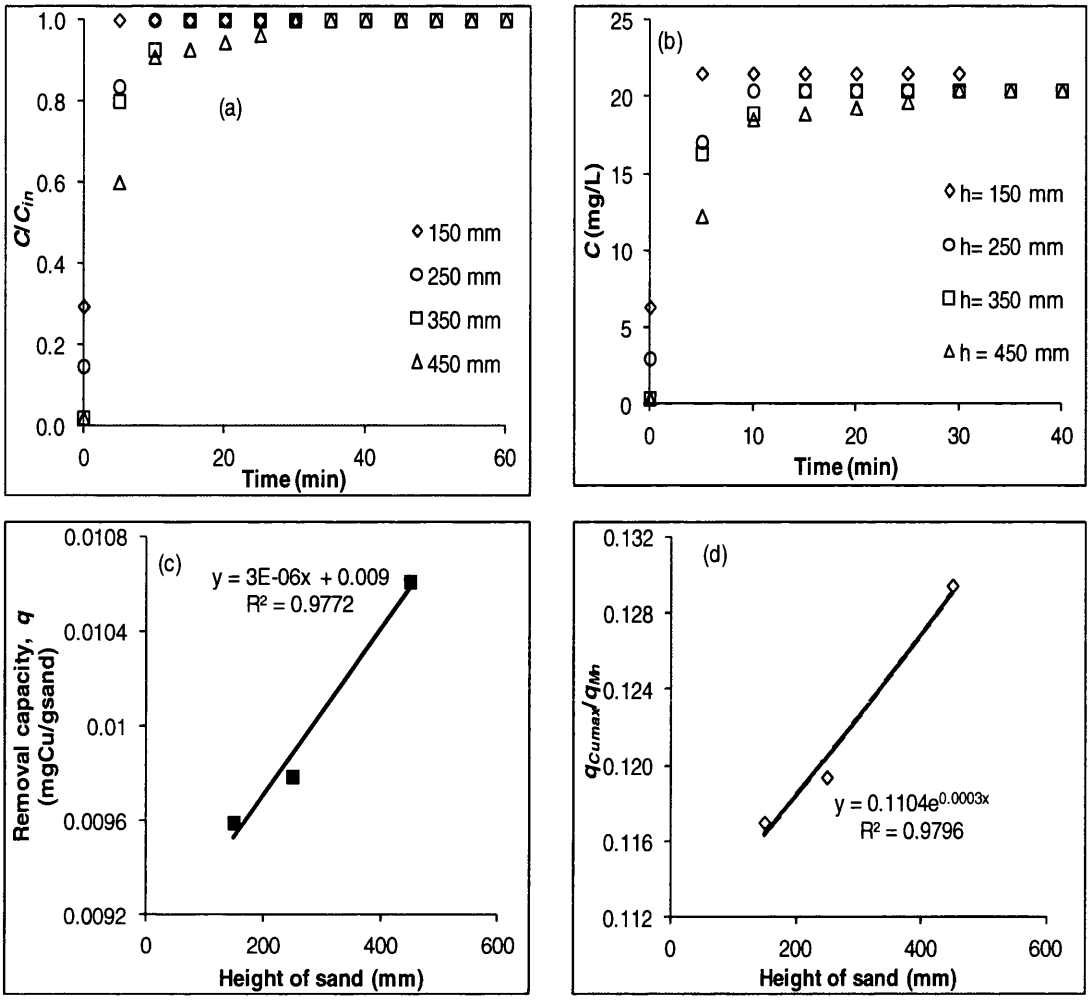

Figure 5.66 AUSF performances at different heights of sand bed (C_{in} = 20 mg/L, Q_{in} = 80.91 mL/min, d_{sand} = 0.850 mm, manganese to sand ratio = 0.0709 mg-manganese/g-sand) (a) C/C_{in} vs time (b) effluent copper concentration (c) removal capacity, q after saturation (d) q_{Cumax}/q_{Mn} vs heights of sand bed after saturation

5.3.3.2 Comparison between column and batch studies for different mass of sand

Table 5.34 shows the comparison between column and batch studies for different mass of sand. Table 5.34 reveals that copper removal was much better once mass increased. An increase in mass leads to a decrease in effluent copper concentration and thus a decrease in C/C_{in} which in turns results in longer saturation time.

On the other hand increasing mass leads to an increase removal efficiency E, and removal rate. In column studies, increasing mass resulted in an increase in removal capacity q and q_{Cumax}/q_{Mn}. In addition, increasing mass led to an increase in time to achieve t_{95}. On the other hand, in batch studies, the removal capacity q and q_{Cumax}/q_{Mn} decreased with an increase in mass. Moreover, an increase in mass may achieve t_{95} faster. This may be attributed to as in batch studies, effluent concentration decreased with increasing contact times, while in column studies, effluent concentration increased with contact times. The results of column studies for different heights clearly confirmed the batch results for different mass of sand.

Table 5.34 Comparison between batch and column studies for different mass of sand

Parameter	Column				Batch					
m_{sand} (g)	320.28	497.6	697.7	889.8	5	7.5	10	30	50	100
C/C_{in}	decreased with increasing mass				decreased with increasing mass					
C (mg/L)	decreased with increasing mass				decreased with increasing mass					
Removal efficiency, E (%)					increased with increasing mass					
Removal capacity, q (mg/g)	increased with increasing mass				decreased with increasing mass					
q_{Cumax}/q_{Mn}	increased with increasing mass				decreased with increasing mass					
Removal rate in 5 min (%)	0.00	16.33	19.96	39.93						
Removal rate in 10 min (%)	0.00	0.00	7.26	9.07						
Removal rate in 25 min (%)	n/a	n/a	0.00	3.63						
Removal rate in 30 min (%)					0.82	0.30	5.18	27.74	52.14	89.29
Saturation time (min)	5	10	15	30	increased with increasing mass					
t_{95} (min)	0.00	0.00	0.19	0.26	> 240	> 240	> 240	> 240	> 240	88
q_{Cumax}/q_{Mn} (%)	11.70	11.94	11.00	12.94	37.08	33.15	26.08	21.93	20.21	15.27

5.3.4 Effect of liquid flow rates on AUSF performances

The effect of liquid flow rates on copper removal was studied by using different flows of 81.91 mL/min, 74.40 mL/min, 55.01 mL/min and 37.78 mL/min. H, C_{in}, d_{sand}, and manganese to sand ratio were kept constant at 450 mm, 5 mg/L, 0.850 mm, and 0.0709 mg-manganese/g-sand respectively.

Table 5.35 depicts that removal rates (R), saturation time, t_{95} and ratio of maximum copper adsorbed to manganese amounts generally increased as flow rates decreased. Kundu and Gupta (2005) also obtained that t_{90} increased with the decrease in flow rate in their study.

Figure 5.67 (a) illustrates that C/C_{in} vs time (t) curve was steeper at higher flow rate. This occurs as the greater the flow rate the more void occupied by the aqueous solution thus saturation is achieved faster. Other researchers found the similar observation (Pan et al., 2005; Chu and Hashim, 2007; Kundu and Gupta, 2005; Han et al., 2009). The mass of copper to mass of sand ratio was correlated to flow rate and an apparent relationship after saturation was acquired (Figure 5.67 (b)). In addition, the ratio of maximum copper adsorbed to the amounts of manganese on the surface of the sand was clearly correlated to the flow rate as shown in Figure 5.67 (c). The change of the ratio q/q_{sat} as function of the number of equivalent bed contact time is represented in Figure 5.67 (d) at the different flow rates.

Figure 5.67 (a) shows that all curves almost superimpose, particularly for $q/q_{sat} < 0.8$. This may indicate that the liquid-film mass transfer process is not the controlling process and as shown earlier solid-phase mass transfer controls the process (Section 5.3.2.1). The removal capacity at saturation, q_{sat}, was also calculated as function of liquid flow rate and is represented in Figure 5.67 (e). The figure shows that q_{sat} reduces by about 10% as the liquid flow rate increases from 37.78 to 81.91 mL/min. The reason for this reduction may be explained by the reduction in the air fraction due to increased liquid flow rate (Table 4.13). ε_G as the flow rate increased is shown in Figure 5.67 (e). This indicates that aeration is important in copper removal by AUSF.

Table 5.35 The removal rates (R), saturation time, t_{95}, and ratio of maximum copper adsorbed to the amounts of manganese for various flow rates

Flow rates (mL/min)	Removal Rate, R (%)			Saturation time (min)	t_{95} (min)	q_{Cumax}/q_{Mn} (%)
	30 min	60 min	120 min			
81.91	35.11	0	n/a	60	16.05	15.31
74.40	65.51	6.18	n/a	80	18.93	15.69
55.01	87.61	5.01	n/a	90	23.87	16.36
37.78	100.00	97.59	n/a	95	60.21	16.67

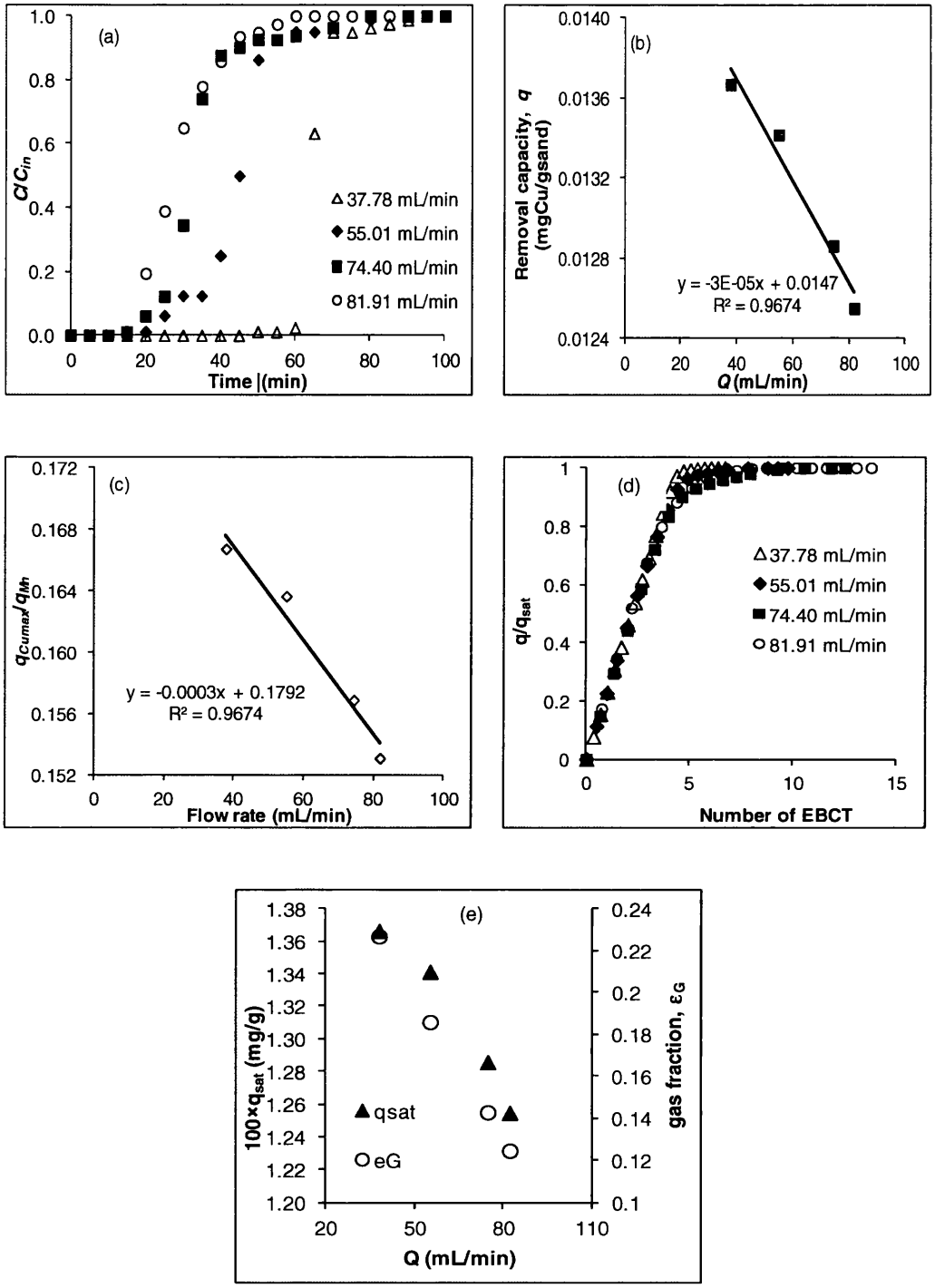

Figure 5.67 AUSF performances at different flow rates (C_{in} = 5 mg/L, H = 45 cm, m_{sand} = 920.59 g, d_{sand} = 0.850mm, manganese to sand ratio = 0.0709 mg-manganese/g-sand) (a) C/C_{in} vs time (b) removal capacity, q (c) q_{Cumax}/q_{Mn} vs flow rates after saturation (d) q/q_{sat} vs number of EBCT, (e) variation of q_{sat} and gas fraction ε_G as function of liquid flow rate.

5.3.5 Effect of sand particle diameters on AUSF performance

The effect of sand particle diameters on copper removal was studied by using different diameter of sand of 0.40, 0.50, 0.71 and 0.85 mm. H, C_{in}, m_{sand}, and manganese to sand ratio were kept constant at 450 mm, 5 mg/L and 875.51 g and 0.0709 mg-manganese/g-sand respectively.

The liquid flow rate was reduced to 25 mL/min for particle diameters of 0.40 mm to overcome the high pressure drop when the flow rate was greater as for other particle sizes.

Table 5.36 shows that removal rates (R), saturation time, t_{95} and ratio of maximum copper adsorbed to manganese amounts (q_{Cumax}/q_{Mn}) generally increased as sand particle diameters decreased.

Figure 5.68 (a) shows that effluent copper concentration decreased as diameter decreased. This is possibly due to the more copper retained as shown in Figure 5.68 (b). In addition, smaller diameter particles have a shorter diffusion path resulting in faster adsorption (Alley, 2007). Besides, the ratio of maximum copper adsorbed to the amounts of manganese on the coated sand was clearly correlated to the sand particle diameter as shown in Figure 5.68 (c).

Table 5.36 The removal rates (R), saturation time, t_{95}, and ratio of maximum copper adsorbed to the amounts of manganese for various sand particle diameters

Diameter (mm)	Removal Rate, R (%)			Saturation time (min)	t_{95} (min)	q_{Cumax}/q_{Mn} (%)
	30 min	60 min	120 min			
0.85	28.55	16.14	n/a	85	5.95	12.21
0.71	48.25	18.74	n/a	90	11.14	19.46
0.50	85.14	32.20	n/a	85	26.65	24.35
0.40	100.00	100.00	64.67	480	71.46	29.06

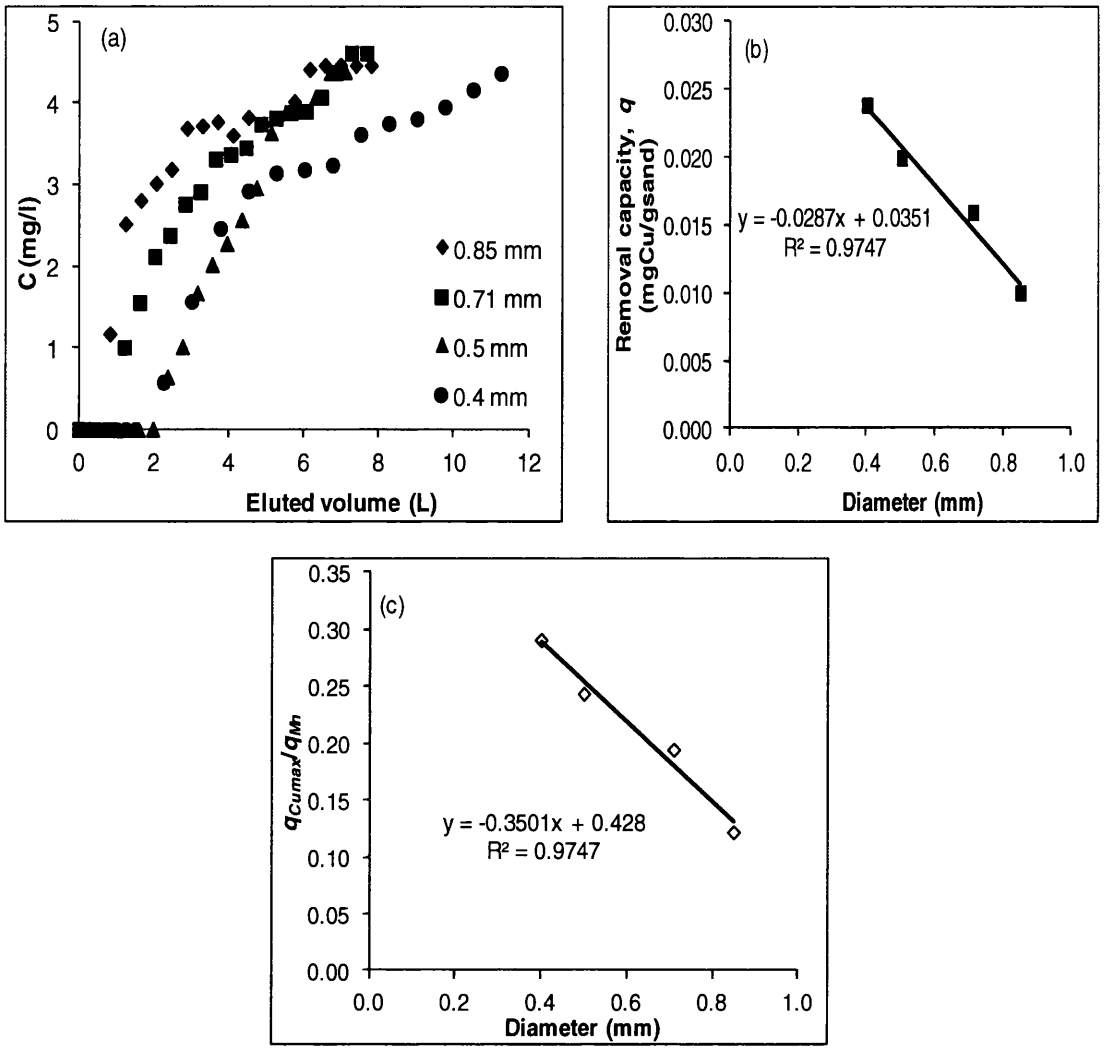

Figure 5.68 AUSF performances at different sand particle diameters (C_{in} = 5 mg/L, H = 45 cm, m_{sand} = 875.51 g, manganese to sand ratio = 0.0709 mg-manganese/g-sand) (a) effluent copper concentration (b) removal capacity (mg-copper/g-sand) vs eluted volume (L) after saturation (c) q_{Cumax}/q_{Mn} vs sand particle diameter (mm)

5.3.6 Different manganese to sand ratio

5.3.6.1 Effect of manganese to sand ratio on AUSF performances

The effect of manganese to sand ratio on copper removal was studied by using different manganese to sand ratio of 0.00, 0.0709, 0.1261 and 0.1341 mg manganese/g sand. The amount of manganese on the surface of the coated sand was measured through acid digestion analysis (Section 4.1.9).

H, Q, C_{in}, d_{sand}, and m_{sand} were kept constant at 450 mm, 80.69 mL/min, 20 mg/L, 0.710mm and 884.49 g respectively.

Table 5.37 depicts that removal rates (R), saturation time, t_{95} and the ratio of maximum copper adsorbed to the amounts of manganese (q_{Cumax}/q_{Mn}) generally increased as manganese to sand ratio increased. t_{95} for 0.1261 mg-manganese/g-sand were achieved much faster than for 0.0709 mg-manganese/g-sand due to the much longer collection (=30 min) of copper effluent. For 0.1341 mg-manganese/g-sand, the removal rate in 60 min (= 80.94%) was much better than Han et al (2006a) (= 80%). Han et al (2006a) used 5.46 mg-manganese/g-sand and 0.67 – 0.99 mm diameter of sand. The saturation time was also much longer (= 600 min) than theirs that obtained 90 min saturation time (Han et al., 2006a). In addition, the removal rate in 30 min (= 87.80%) was higher than Lee at al (2004) (= 71.17%) although they used more manganese on their sand (8.03 mg-manganese/g-sand). Their saturation time, however, was longer (= 1000 min) than this study as they apparently used more manganese.

Figure 5.69 (a) illustrates that q increased as the manganese to sand ratio increased. This occurs as the more manganese coated the sand particles the greater the surface area produced resulting in more active sites formed for copper removal. Moreover as shown in Figure 5.69 (b) and for the same reason, the maximum copper removed q_{sat} enhanced significantly as the manganese to sand ratio increased. An exponential function seems to fit well the change of q_{sat} as function of the manganese to sand ratio.

Table 5.37 The removal rates (R), saturation time, t_{95}, and ratio of maximum copper adsorbed to the amounts of manganese for various manganese to sand ratios (H = 450 mm, Q = 80.69 mL/min , C_{in} = 20 mg/L, d_{sand} = 0.710mm, and m_{sand} = 884.49 g)

Manganese to sand ratio (mg-Mn/g-sand)	Removal Rate, R (%)			Saturation time (min)	t_{95} (min)	q_{Cumax}/q_{Mn} (%)
	30 min	60 min	120 min			
0.0000	4.05	0.00	n/a	55	1.68	0.00
0.0709	44.27	0.00	n/a	60	9.36	66.00
0.1261	47.69	45.91	40.40	420	2.87	127.70
0.1341	87.80	80.94	63.50	600	12.29	267.23

On a molar basis, the amount of copper removed relative to manganese was found to be varied between almost stoichiometric ratio of 1.0 up to 2.7 mol Cu/mol Mn as the manganese to sand ratio increased from 0.071 to 0.134 mg/g (Table 5.37 and Figure 5.69 (c)). This indicates that at low manganese to sand ratio copper removal is based on the interaction with the manganese species possibly by adsorption/ion exchange but as the manganese to sand ratio increased, further mechanisms such as precipitation contributed to the overall removal process.

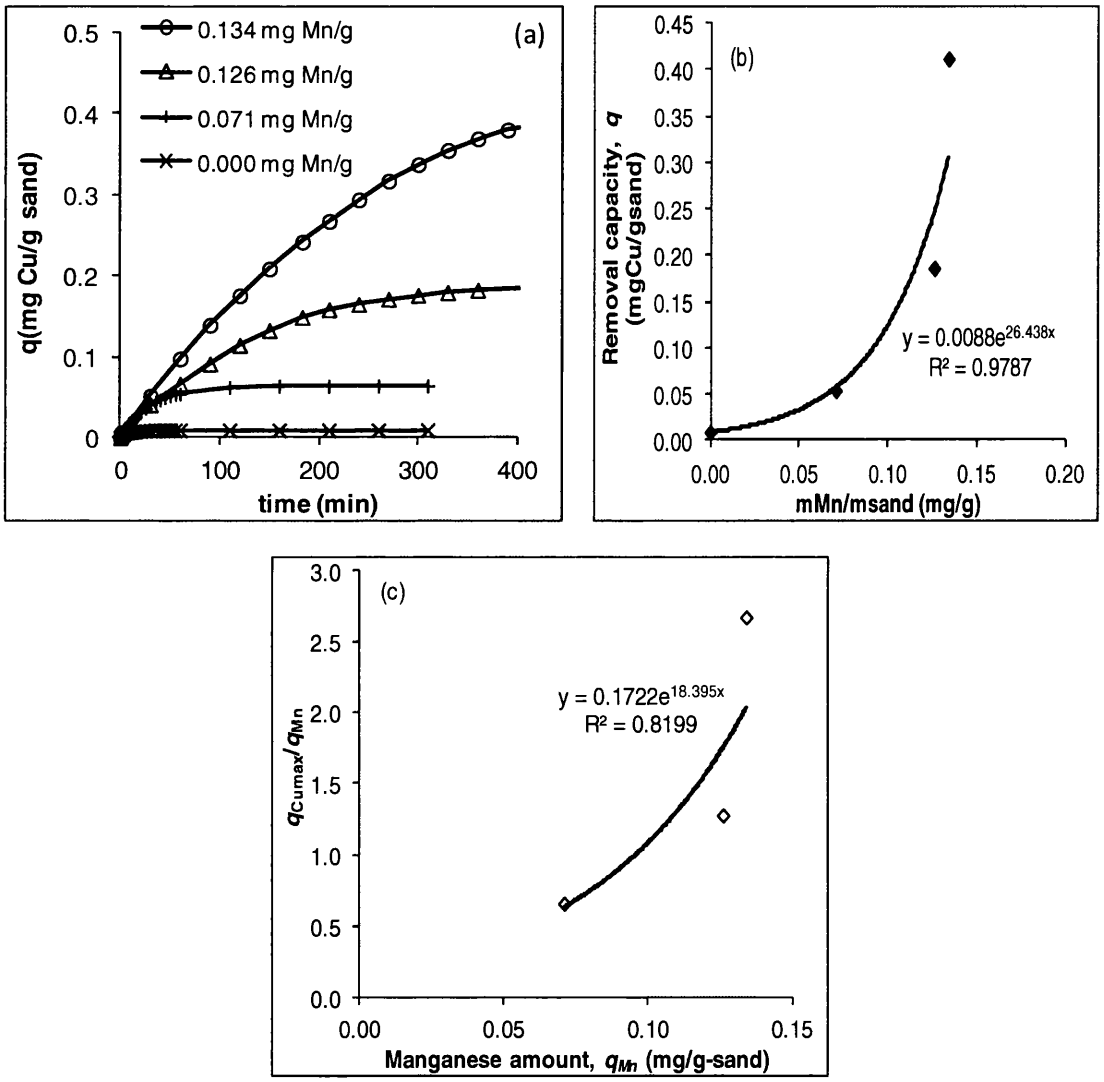

Figure 5.69 AUSF performances at different manganese to sand ratios (Q = 80.69 mL/min, C_{in} = 20 mg/L, H = 45 cm, m_{sand} = 884.49 g, d_{sand} = 0.71 mm) (a) effluent copper concentration (mg/L) (b) removal capacity (mg-copper/g-sand) vs mass manganese/mass sand (mg-manganese/g-sand) (c) q_{Cumax}/q_{Mn} vs mass manganese/mass sand

5.3.6.2 Comparison between column and batch studies for different manganese to sand ratio

Table 5.38 shows the comparison between column and batch studies for different manganese to sand ratios. Table 5.38 depicts that copper removal was much better once manganese to sand ratio increased. An increase in the ratio of manganese to sand leads to a decrease in effluent copper concentration and thus a decrease in C/C_{in} which in turns results in longer saturation time. On the other hand increasing the ratio leads to an increase in removal efficiency E, removal rate, removal capacity q and q_{Cumax}/q_{Mn}. In column studies, increasing the ratio led to an increase in time to achieve t_{95}. On the other hand, in batch studies, an increase in the ratio may obtain t_{95} faster. This may be due to as in batch studies, effluent concentration decreased with increasing contact times, while in coloumn studies, effluent concentration increased with contact times. The results of the column studies for different manganese to sand ratios clearly confirmed the results of the batch studies.

Table 5.38 Comparison between batch and column studies for different manganese to sand ratios

Parameter	Column				Batch	
Sand coating (mgMn/g sand)	0	0.071	0.126	0.134	0	0.071
C (mg/L)	decreased with increasing manganese coating				decreased with increasing manganese coating	
Removal efficiency, E (%)					increased with increasing manganese coating	
Removal capacity, q (mg/g)	increased with increasing manganese coating				increased with increasing manganese coating	
q_{Cumax}/q_{Mn}	increased with increasing manganese coating				increased with increasing manganese coating	
Removal rate in 30 min (%)	4.05	44.27	47.69	87.80	34.09	52.14
Removal rate in 60 min (%)	0.00	0.00	45.91	80.94	34.90	59.01
Removal rate in 120 min (%)	n/a	n/a	40.40	63.50	38.45	67.20
Saturation time (min)	55	60	420	600	increased with increasing manganese coating	
t_{95} (min)	1.68	9.36	2.87	12.29	may achieve faster with increasing manganese coating	
q_{Cumax}/q_{Mn} (%)	0.00	66.00	127.70	267.23	16.53	20.21

5.3.7 Effect of reusing sand bed material on AUSF performances

The effect of reusing sand bed material on copper removal was investigated by reusing sand bed for 0, 1 and 2 times. H, Q, C_{in}, d_{sand}, m_{sand}, and manganese to sand ratio are kept constant at 450 mm, 25.01 mL/min, 20 mg/L, 0.400 mm, 906.19 g and 0.0709 mg-manganese/g-sand respectively.

Table 5.39 depicts that removal rates (R), saturation time, and t_{95} decreased as reusing times increased. Figure 5.70 (a) illustrates that effluent copper concentration increased with times as reusing time of sand bed material increased. Figure 5.70 (a) also shows that manganese appeared (= 0.008 – 0.009 mg/L) at 330 min in once and second times of reusing the sand bed material. The manganese concentration increased as reusing times increased. At 480 min, the manganese concentrations were 0.24 – 0.27 mg/L. The manganese leakage was possibly occurred due to the sand was washed and dried after each usage. This manganese leakage thus resulted in decreasing AUSF performances. Figure 5.70 (b) shows that the removal capacity, q, was also correlated to the reusing times of the sand bed.

Table 5.39 The removal rates (R), saturation time, t_{95}, and ratio of maximum copper adsorbed to the amounts of manganese for various reusing times of sand bed material (Q = 25.01 mL/min, C_{in} = 20 mg/L, H = 45 cm, m_{sand} = 906.19 g, d_{sand} = 0.71 mm, manganese to sand ratio = 0.0709 mg-manganese/g-sand)

Regeneration times	Removal Rate, R (%)			Saturation time (min)	t_{95} (min)
	30 min	60 min	120 min		
0	100.00	100.00	99.92	n/a	179.94
1	90.78	80.16	72.99	n/a	16.26
2	68.86	66.75	59.03	n/a	4.82

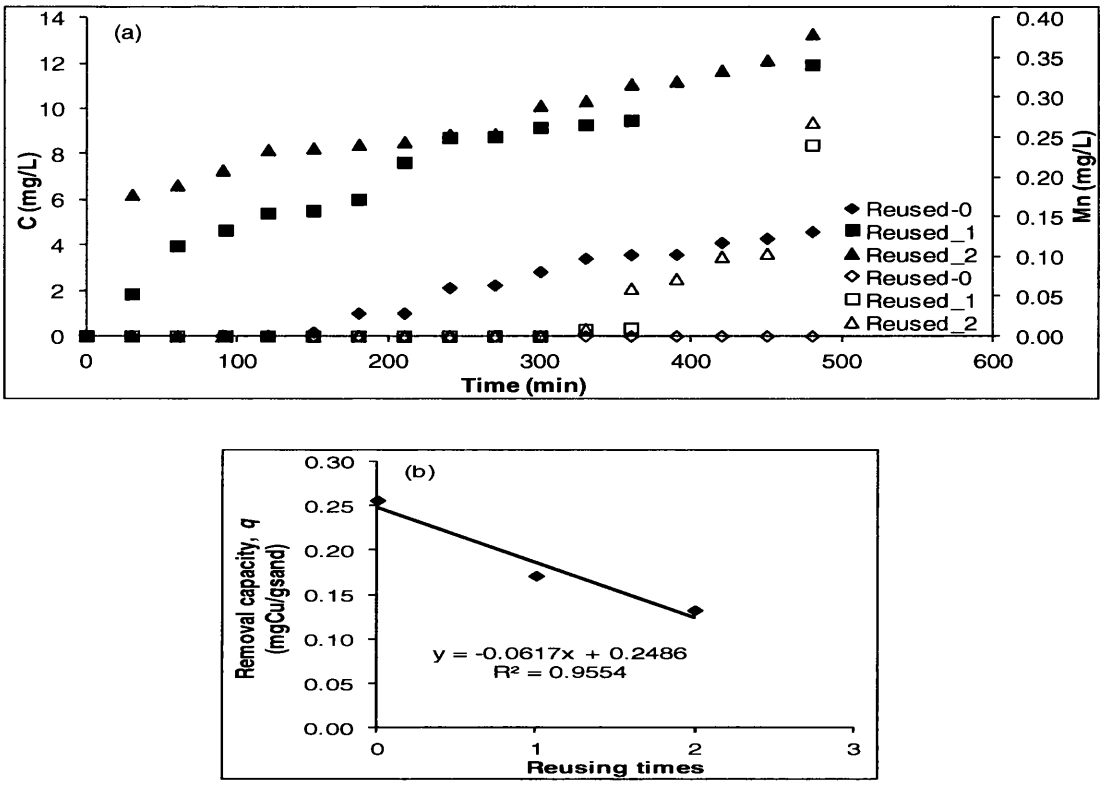

Figure 5.70 AUSF performances at different reusing times of sand bed material (Q = 25.01 mL/min, C_{in} = 20 mg/L, H = 45 cm, m_{sand} = 906.19 g, d_{sand} = 0.71 mm, manganese to sand ratio = 0.0709 mg-manganese/g-sand) (a) effluent copper and manganese concentration vs time (min) (b) removal capacity (mg-copper/g-sand) vs reusing times after 480 min

5.4 Proposed processes that occurred for copper removal

Based on the results obtained in this study, mechanisms for copper removal have been proposed. The chemical reactions for copper removal in the AUSF are somewhat different from those for iron and manganese since the trivalent copper is rarely formed naturally (i.e. cupric ion (Cu^{2+}) cannot be oxidized to Cu^{3+} under the experimental conditions used) (Eisler, 2007).

From the column studies, in the beginning, the pH of input copper solutions were weakly acidic (about 5.59) which is typical for 2+ metal ions (Figure 5.71 (a)). This is due to the fact that as once copper is dissolved in water, copper forms a complex ion of $(Cu(H_2O)_6)^{2+}$ in which water is the ligand (Winter and Andrew, 2000; Eisler, 2007).

Indeed, all metal cations in water are hydrated or form aquo complexes (Stumm and Morgan, 1996). The hexaaquacopper(II) ion, $(Cu(H_2O)_6)^{2+}$, donates a proton to a water molecule to produce the hydrated proton H_3O^+. This occurs as due to the pull of the water's O-H bond electrons towards the positive central ion, the hydrogen atoms attached to the water ligands become sufficiently positive that they can be detached in a reaction involving water molecules to produce H_3O^+, hence a drop of pH. This acidic pH is explained in Equation 5.1. as follows (Winter and Andrew, 2000):

$$[Cu(H_2O)_6]^{2+}_{(aq)} + H_2O_{(l)} \rightarrow [Cu(H_2O)_5OH]^+_{(aq)} + H_3O^+_{(aq)} \quad ...(\text{Equation 5.1})$$

Lee et al (2004) also stated that the copper species found in the solution were those of Cu^{2+} and $Cu(OH)^+$ once the pH of the solutions was below 6.01 for the initial copper concentration of 30 mg/L.

Coated sand has been made by soaking the sand in potassium permanganate solution. The presence of manganese in the form of insoluble oxides was indicated by dark coloured (brown-black) precipitates of the coated sand samples. Han et al (2006a) who prepared manganese oxide coated sand in a similar procedure with this study proved that manganese on the surface of the coated sand was in the form of manganese oxide (MnO_x).

The process by which copper removed in the AUSF may be best described as follows:

1. Precipitation

As evidenced by experiments in this work, the manganese-coated sand releases hydroxide ions in the aqueous solution ((Figures 5.71 and 5.73) – increase of effluent pH), which results in a precipitation reaction in which hydroxide ions react with the hexaaquacopper complex (in two steps Equation 5.2 and 5.3) to form a solid precipitate, hence copper removal from the solution was by precipitation (Equation 5.4).

The precipitation reaction proceed up to a point at which the ion product is less than the solubility product constant K_{sp}, which is 2.19×10^{-20} for copper hydroxide at 25°C (Tchobanoglous et al., 2004).

Based on effluent concentration and pH (Figures 5.71 and 5.73), calculation shows that precipitation proceeded up to time 4.8 min, which corresponds to the time at which effluent copper concentration started to increase from zero (i.e. breakthrough point). Moreover, based on effluent pH values, the copper removed was found to be significantly higher than the stoichiometric ratio of 2 (Table 5.37) which indicates that other mechanisms in addition to precipitation contributed to copper removal.

The occurrence of precipitation of copper hydroxide depends on the copper concentration in the solution and the pH value of the solution (Equation 3.23). The relationship between copper concentration and pH for the precipitation of copper as hydroxide is shown in Figure 5.72. Figure 5.72 shows that at greater copper concentration, the precipitation of copper as hydroxide occurs at lower pH. For copper concentration of 20 mg/L, theoretically copper will precipitate as hydroxide at pH > 5.92 (pH critical). By taking this pH critical into account and knowing that the pH value for the first 5 minutes was decreasing from 8.28 to 5.78 (Figures 5.71 and 5.73), then precipitation is assumed to be the dominant process during this period ($0 \leq t \leq 4.8$ min).

The precipitation process may be written as follows:

$[Cu(H_2O)_6]^{2+}_{(aq)} + OH^-_{(aq)} \rightleftarrows [Cu(H_2O)_5OH]^+_{(aq)} + H_2O_{(l)}$....(Equation 5.2)

$[Cu(H_2O)_5OH]^+_{(aq)} + OH^-_{(aq)} \rightleftarrows [Cu(H_2O)_4(OH)_2]_{(s)} + H_2O_{(l)}$....(Equation 5.3)

$[Cu(H_2O)_6]^{2+}_{(aq)} + 2OH^-_{(aq)} \rightleftarrows [Cu(H_2O)_4(OH)_2]_{(s)} + 2H_2O_{(l)}$....(Equation 5.4) (Winter and Andrew, 2000).

or

$Cu^{2+}_{(aq)} + 2OH^-_{(aq)} \rightleftarrows Cu(OH)_{2(s)}$....(Equation 5.5) (Tchobanoglous et al., 2004)

The release of hydroxide ions is in line with the experiment done with pure water (Section 4.1.7). Indeed the pH of influent pure water was about 6.15 and after passing through AUSF, this pH increased to 8.35 and as water passed through the column, the pH gradually reduced to 6.47 in 60 minutes (Figure 5.71 (a)).

The hydroxide ion released from the coated sand will then react with copper ion to form $Cu(OH)_2$ or $[Cu(OH)_2(OH_2)_4]$ precipitate. Lee et al (2004) stated that the precipitate $Cu(OH)_{2(s)}$ formed once pH > 6.01 for the initial copper concentration of 30 mg/L.

In short, the species of copper is assumed to be $Cu(OH)_{2(s)}$ or $[Cu(OH)_2(OH_2)_4]_{(s)}$ when pH > 5.92. On the other hand, $Cu^{2+}{}_{(aq)}$ or $[Cu(H_2O)_6]^{2+}{}_{(aq)}$ is assumed to be the dominant species when pH ≤ 5.92.

2. Electrostatic attraction

Electrostatic attraction results from the interaction between species having opposite charges and since the charge of the surface is affected by pH, point of zero charge (pzc) of the Mn-coated sand was determined. A value of pzc equal to 7.75 was obtained (Section 4.1.6). This indicates that at pH values above the pzc, the surface of the Mn-coated sand is negative (i.e. $\equiv MnO^-$ predominates; Equation 5.6), which favours removal of the positively charged hexaaquacopper complex; while at pH values less than pzc, the removal by electrostatic attraction is expected to be less significant since positive surface predominates (i.e. $MnOH_2^+$; Equation 5.7). As shown in Figures 5.71 and 5.73, the pH dropped below pzc rapidly within the first 3 minutes indicating that electrostatic attraction may contribute to copper removal only during this period of the experiment.

The electrostatic attraction results in copper adsorption as illustrated by Equations 5.8 and 5.9. Adsorption of copper may also take place on a neutral surface as illustrated by Equation 5.10.

$\equiv MnOH \rightleftarrows \equiv MnO^- + H^+$ ....(Equation 5.6)

$\equiv MnOH + H^+ \rightleftarrows \equiv MnOH_2^+$ ....(Equation 5.7)

$\equiv MnO^- + Cu^{2+} \rightleftarrows \equiv MnOCu^+$ ....(Equation 5.8)

$2(\equiv MnO^-) + Cu^{2+} \rightleftarrows (\equiv MnO^-)_2Cu^{2+}$ ....(Equation 5.9)

$\equiv MnOH + Cu^{2+} \rightleftarrows Cu(\equiv Mn\text{-}OH)^{2+}$ ....(Equation 5.10)

The increase in metal removal as the pH increases (pH = 8.28 – 7.00, $0 \leq t < 3$ min) can thus be explained on the basis of a decrease in competition between proton and copper cations for the same surface functional groups and by the increase in negative surface charge, which results in a greater electrostatic attraction between the surface and the copper ion. Lee at al (2004) also showed that positively charged copper (Cu^{2+} and $Cu(OH)^{+}$) was adsorbed by negatively charged manganese coated sand (MCS) through electrostatic attraction at $2 \leq pH \leq 6$ for initial copper concentration of 30 mg/L.

3. Adsorption/Ion exchange and surface complex formation

A further mechanism by which copper is removed from solution may involve ion exchange of H^{+} with Cu^{2+} with surface complex formation as illustrated by Equation 5.11 - 5.15. The release of hydrogen ions resulting from copper ion exchange is evidenced by the more significant drop in pH in the case of copper solution as compared to pure water (Figures 5.71 and 5.73). Figures 5.71 and 5.73 show that the pH values of the solution decreased from 8.28 to 5.40 during 60 min period. This indicates that the mechanism by which copper was adsorbed onto the coated sand might involve an exchange reaction of Cu^{2+} with H^{+} on the surface and surface complex formation.

According to the principle of ion-exchange, the more copper adsorbed onto the coated sand, the more hydrogen ions are released resulting in the decrease in the pH value. The complex reactions of Cu^{2+} with manganese oxide may be written as follows (Stumm and Morgan, 1996):

$\equiv Mn{-}OH + Cu^{2+} \rightleftarrows \equiv Mn{-}O^{-}Cu^{2+} + H^{+}$ ....(Equation 5.11)

$\equiv Mn{-}O^{-} + Cu^{2+} \rightleftarrows \equiv Mn{-}O^{-}Cu^{2+}$ ....(Equation 5.12)

$2(\equiv Mn{-}OH) + Cu^{2+} \rightleftarrows (\equiv Mn{-}O^{-})_2Cu^{2+} + 2H^{+}$ ....(Equation 5.13)

$2(\equiv Mn{-}O^{-}) + Cu^{2+} \rightleftarrows (\equiv Mn{-}O^{-})_2Cu^{2+}$ ....(Equation 5.14)

$\equiv Mn{-}OH + Cu^{2+} + H_2O \rightleftarrows \equiv Mn{-}OCuOH + 2\,H^{+}$ ....(Equation 5.15)

Equation 5.11, 5.13 and 5.15 show the hydrogen ion concentration increased with an increasing amount of copper ion adsorbed onto the coated sand.

This is in line with Figures 5.71 and 5.73 that show the adsorption of copper onto the coated sand surface was highly dependent on the pH. As the pH increased, the OH^- increased resulting in the increase in the surface activity of the coated sand. In addition, Figure 5.71 shows that the removal curve of Cu^{2+} displayed two pH patterns.

The removal amount increased rapidly with decreasing pH from 8.28 to 5.92 and increased slowly with decreasing pH from 5.92 to 5.40. When pH was > 5.92, the precipitation of $Cu(OH)_2$ occurred, and these precipitates coated the sand surface. The formation of surface complex by which copper ions were bound to the adsorbent is in line with others (Reddad et al., 2002b; Lee et al., 2004; Han et al., 2006a; Lee et al., 2006).

From this analysis, all mechanisms (i.e. precipitation, electrostatic attraction and ion exchange/adsorption accompanied by surface complexation) are suggested to be contributed to copper removal within the first 3 minutes, while removal by precipitation continued up to 4.8 minutes and removal by ion exchange and to some extent adsorption developed up to the end of the experiment (i.e. complete exhaustion of the bed). Precipitation and electrostatic attraction seem to overtake the other processes since breakthrough occurred at about the same time when they are inhibited (Figures 5.71 and 5.73).

In short, the assumed copper speciation occurred in the water at certain pH is shown in Table 5.40 and the proposed reactions occurred in the AUSF is depicted in Figure 5.74. A summary of the contribution of each mechanism during the time of the experiment alongside the change of the ratios C/C_{in} and q/q_{sat} is illustrated in Figure 5.75, which shows that about 20% of the total copper removed occurred within the first 4.8 minutes. The proposed reactions occurred in the AUSF are in line with the results obtained from the batch studies. The batch studies reveal that the process by which copper was removed from the solutions was observed to be that through adsorption particularly chemisorptions. The kinetic experiment also shows that adsorption of copper ion onto manganese coated sand may involve a two steps process i.e. fast adsorption of copper ion to the external surface of manganese coated sand followed by possible slow intra-particle diffusion in the interior of manganese coated sand (Section 5.2.1 and 5.2.2).

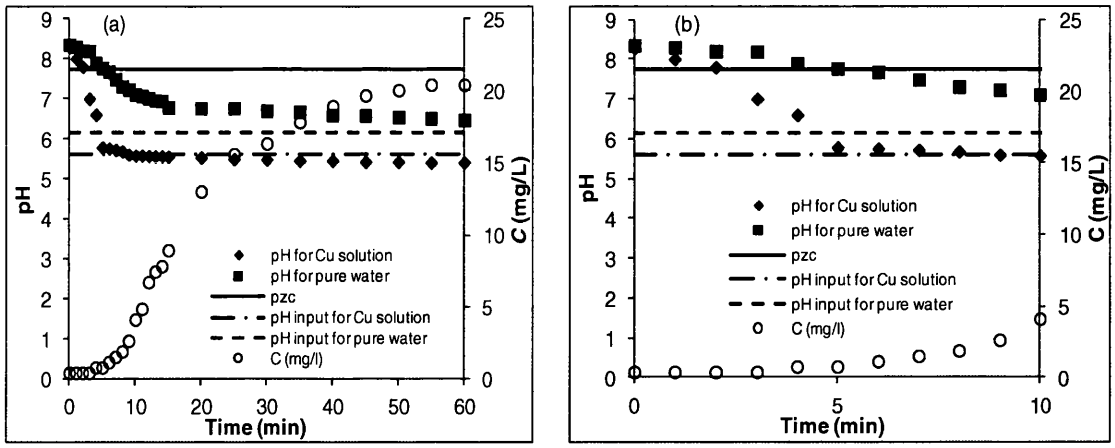

Figure 5.71 pH and point of zero charge (pzc) (d_{sand} = 0.710mm, H = 450 mm, m_{sand} = 881.46 g, Q = 80.69 mL/min, C_{in} = 20 mg/L, and $m\ Mn/\ m\ sand$ = 0.0709 mg/g) (a) pH and C vs time, t (b) enlargement

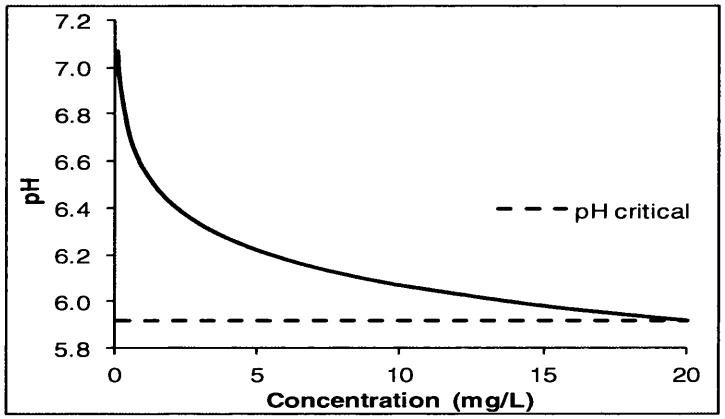

Figure 5.72 Copper concentrations as a function of pH for the precipitation of copper as hydroxide (pKs = 19.66 at 25°C (Tchobanoglous et al., 2004))

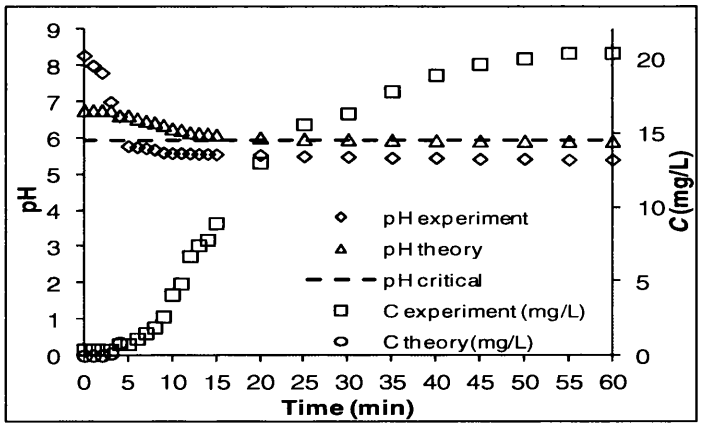

Figure 5.73 Comparison between C and pH experiment and theory for the precipitation of copper as hydroxide (d_{sand} = 0.710mm, H = 450 mm, m_{sand} = 881.46 g, Q = 80.69 mL/min, C_{in} = 20 mg/L, $m\ Mn/\ m\ sand$ = 0.0709 mg/g, and pKs = 19.66 at 25°C (Tchobanoglous et al., 2004))

Table 5.40 Assumed copper speciation at certain pH

Type of species		pH
Dominant	Other	
$Cu^{2+}_{(aq)}$ or $Cu(OH)^{2+}_{(aq)}$	$\equiv Mn-O^{-}Cu^{2+}$ or $(\equiv Mn-O^{-})_2Cu^{2+}$ or $\equiv Mn-OCuOH$	≤ 5.92
$Cu(OH)_{2\,(s)}$	$Cu^{2+}_{(aq)}$ or $Cu(OH)^{2+}_{(aq)}$ or $\equiv Mn-O^{-}Cu^{2+}$ or $(\equiv Mn-O^{-})_2Cu^{2+}$ or $\equiv Mn-OCuOH$	> 5.92

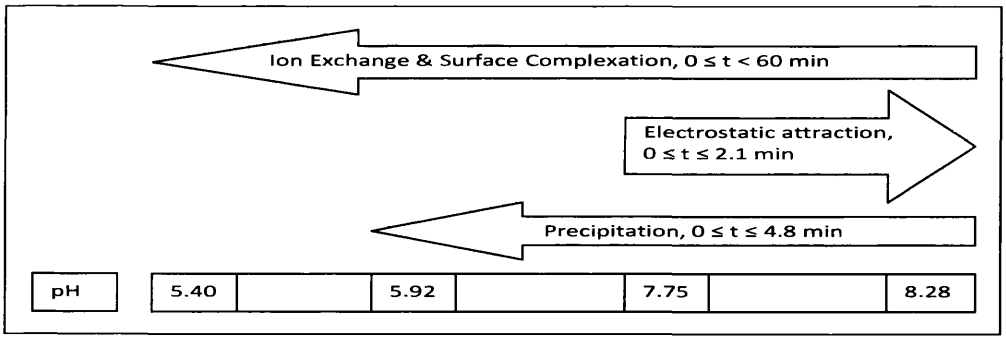

Figure 5.74 Proposed processes in the AUSF based on the pH values (d_{sand} = 0.710mm, H = 450 mm, m_{sand} = 881.46 g, Q = 80.69 mL/min, C_{in} = 20 mg/L, and *m Mn/ m sand* = 0.0709 mg/g)

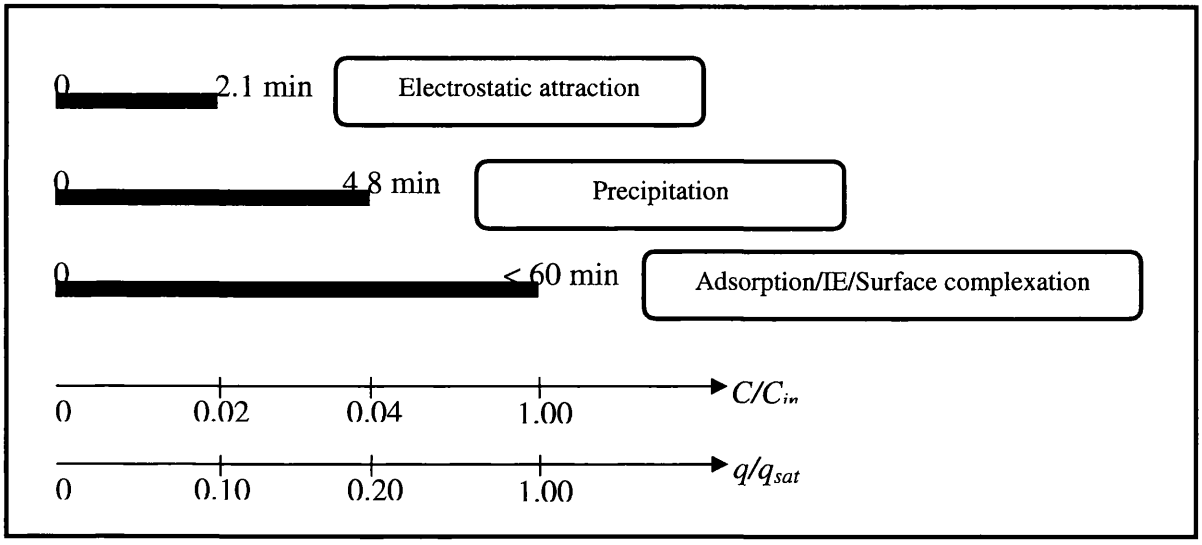

Figure 5.75 Mechanisms contributing to copper removal by AUSF along with its C/C_{in} and q/q_{sat} values (d_{sand} = 0.710mm, H = 450 mm, m_{sand} = 881.46 g, Q = 80.69 mL/min, C_{in} = 20 mg/L, and *m Mn/ m sand* = 0.0709 mg/g)

5.5 Conclusions

Adsorption of copper onto the manganese coated sand may occur in one layer as Langmuir type 1 model was best fitted to model the copper removal (R^2 = 0.99) in all cases of different initial concentrations . This favourable sorption of copper was also confirmed by the obtained value of R_L ($0 < R_L < 1$). In addition, chemisorptions were assumed to be involved in the removal of copper as shown by the good fit of the pseudo second order type 1 model (R^2 = 0.96 - $\approx$ 1) in all different conditions. Moreover, intra particle diffusion was assumed to be involved in the removal of copper as confirmed by the R^2 values of Weber and Morris (= 0.96 – 0.98). This thus suggests that the boundary layer (film) did not control the sorption process of copper onto the manganese coated sand as confirmed by the well fitted of Bangham model (R^2 = 0.91 – 0.96) and the results obtained from the column studies (Section 5.3.2.1 and 5.3.4).

The kinetic experiment also shows that adsorption of copper ion onto manganese coated sand may involve a two steps process i.e. fast adsorption of copper ion to the external surface of manganese coated sand followed by possible slow intra-particle diffusion in the interior of manganese coated sand.

The results from batch studies show that manganese coated sand was fragile under higher shaker speed (r $\geq$ 150 rpm) and particularly at low pH ($\leq$ 3) as more manganese leached compared to the acid alkali resistance test.

Aeration (i.e. unsaturated condition) played a significant role in enhancing activated sand filter performances in removing copper than the saturated condition. The AUSF system also showed advantage as no pH adjustment was necessary as it would be in the usual metal hydroxide precipitation processes.

The study also showed that the performance of AUSF increased as input concentration, flow rate, diameter of the sand particles, and reusing sand bed material decreased. Increasing the manganese to sand ratio and height of sand bed column, on the other hand, resulting in an increase in the performance of AUSF.

The decrease in the performance of the AUSF as reusing sand bed material increased may be due to the more manganese was eluted resulting from the washing and drying processes of the coated sand after each used. The results obtained from column studies confirmed the results from batch studies.

Results from the column studies showed that the type of breakthrough curves obtained at low inlet concentrations is typical for adsorption where solid-phase mass transfer controls the process. This further supports that adsorption is significant at low inlet concentrations; while precipitation is significant at greater inlet concentrations. The rule of the solid-phase mass transfer as the controlling process was also confirmed by the curves obtained from the liquid flow rate variations that showed that all curves almost superimpose, particularly for $q/q_{sat} < 0.8$, indicating that the liquid-film mass transfer process is not the controlling process. This is also supported by the results from batch studies that showed that in all cases the boundary layer (film) did not control the sorption process.

Based on the pH values, precipitation, electrostatic attraction, adsorption/ion exchange/complex ion formation were proposed to contribute to the removal of copper by AUSF. The proposed reactions occurred in the AUSF are in line with the results obtained from the batch studies.

The copper speciation in water depends on the pH at which copper precipitates at certain concentration. As copper precipitates at pH > 5.92 for concentration 20 mg/L, thus the dominant copper species at pH > 5.92 was assumed to be $Cu(OH)_2$. Other species that might be occurred at this pH were assumed to be $Cu^{2+}{}_{(aq)}$ or $Cu(OH)^{2+}{}_{(aq)}$ or $\equiv Mn{-}O^{-}Cu^{2+}$ or $(\equiv Mn{-}O^{-})_2Cu^{2+}$ or $\equiv Mn{-}OCuOH$. On the other hand, the dominant copper species at pH ≤ 5.92 was assumed to be $Cu^{2+}{}_{(aq)}$ or $Cu(OH)^{2+}{}_{(aq)}$. Other species that might be occurred at this pH were assumed to be $\equiv Mn{-}O^{-}Cu^{2+}$ or $(\equiv Mn{-}O^{-})_2Cu^{2+}$ or $\equiv Mn{-}OCuOH$.

CHAPTER 6

REMOVAL OF METALS (COPPER, MANGANESE, NICKEL AND ZINC)

6.1 Removal of metals under optimal conditions

Chapter 5 reveals that copper removal was at the greatest at lower concentration, higher sand bed depth, lower flow rate, smaller diameter of sand, greater manganese coating, and first time use of the sand bed. These conditions were then employed to study the removal of metals under optimal conditions. However, manganese to sand ratio used was that of 0.0709 mg-manganese/g-sand. In addition, metal concentration used was that of 20 mg/L as this was assumed to be the greatest concentration of metals found in waters that could be treated by AUSF.

Copper, manganese, nickel and zinc were studied first as individual element. Next, the processes that might occur within these metals in AUSF are proposed. Following this, these metals were mixed and the metal removals between individual and mixed metals were then compared. Finally, artificial electroplating waste water was used to study the performance of AUSF in removing the metals in the waste water.

6.1.1 Removal of copper, manganese, nickel and zinc as individual metal

The removal of copper, manganese, nickel and zinc individually was studied and the summaries are shown in Table 6.1 and Figures 6.1 (a – c). Q, H, m_{sand}, C_{in}, d_{sand}, and manganese to sand ratio were kept constants at 25.01 mL/min, 450 mm, 869.77 g, 20 mg/L, 0.400 mm, and 0.0709 mg-manganese/g-sand respectively.

Table 6.1 shows removal rates (R), saturation time, t_{95}, and ratio of maximum metal adsorbed to the manganese amounts on the surface of the sand (q_{Mmax}/q_{Mn}) for the metals. The order of removal rate, saturation time, t_{95} and q_{Mmax}/q_{Mn} was copper > manganese > zinc > nickel. Copper was best removed by AUSF. Copper was completely removed in 30 and 60 min; and near complete (90.51%) in 120 min.

Table 6.1 The removal rates (R), saturation time, t_{95}, and ratio of maximum metal adsorbed to the amounts of manganese (q_{Mmax}/q_{Mn}) for individual copper, manganese, nickel and zinc (Q = 25.01 mL/min, H = 450 mm, m_{sand} = 869.77 g, C_{in} = 20 mg/L, d_{sand}, and mg Mn/ g sand = 0.0709 mg/g)

Element	Removal Rate, R (%)			Saturation time (min)	t_{95} (min)	q_{Mmax}/q_{Mn} (%)
	30 min	60 min	120 min			
Cu	100.00	100.00	90.51	n/a	94.42	n/a
Mn	27.64	14.47	9.00	270	0.00	23.62
Zn	19.93	12.28	3.48	240	0.00	13.55
Ni	3.5	1.76	0.02	150	0.00	5.95

On the other hand, manganese was only removed a quarter (27.64%) in 30 min; and 14.47% and 9% in 60 and 120 min respectively. Zinc was only removed a fifth (19.93%) in 30 min; and 12.28% and 3.48% in 60 and 120 min respectively. Nickel was worst treated by AUSF. Nickel was only slightly removed by AUSF (0.02 – 3.5% in 30-120 min). No data available for copper for saturation time, as the experiment was only run in 480 min. It is then assumed that the saturation time for copper was > 480 min. t_{95} for copper was 94.42 min. t_{95} for zinc and nickel were not recorded. This is likely occurred due to the input concentration was quite high (= 20 mg/L). q_{Mmax}/q_{Mn} was the greatest for manganese (23.62%) and the worst for nickel (5.95%). For zinc, q_{Mmax}/q_{Mn} was 13.55%. As there was no saturation data available for copper, no q_{Mmax}/q_{Mn} value was obtained. However, as the removal rate for copper was the greatest, the q_{Mmax}/q_{Mn} value for copper was assumed to be the greatest among the studied metals.

Figure 6.1 (a) shows that effluent concentration decreased in the order of copper > manganese > zinc > nickel. This may result from the more mass metal retained within the bed within that order as shown in Figure 6.1 (b). Figure 6.1 (c) illustrate the removal capacity of AUSF for each element after saturation (except for copper where these removals were calculated at 480 min). The order of these removals was, again, copper > manganese > zinc > nickel. The order shows that AUSF had a stronger affinity for Cu^{2+} than Ni^{2+}. This is in line with Boujelben et al (2009) who studied the adsorption of nickel and copper (individually and mixed) onto natural iron oxide-coated sand.

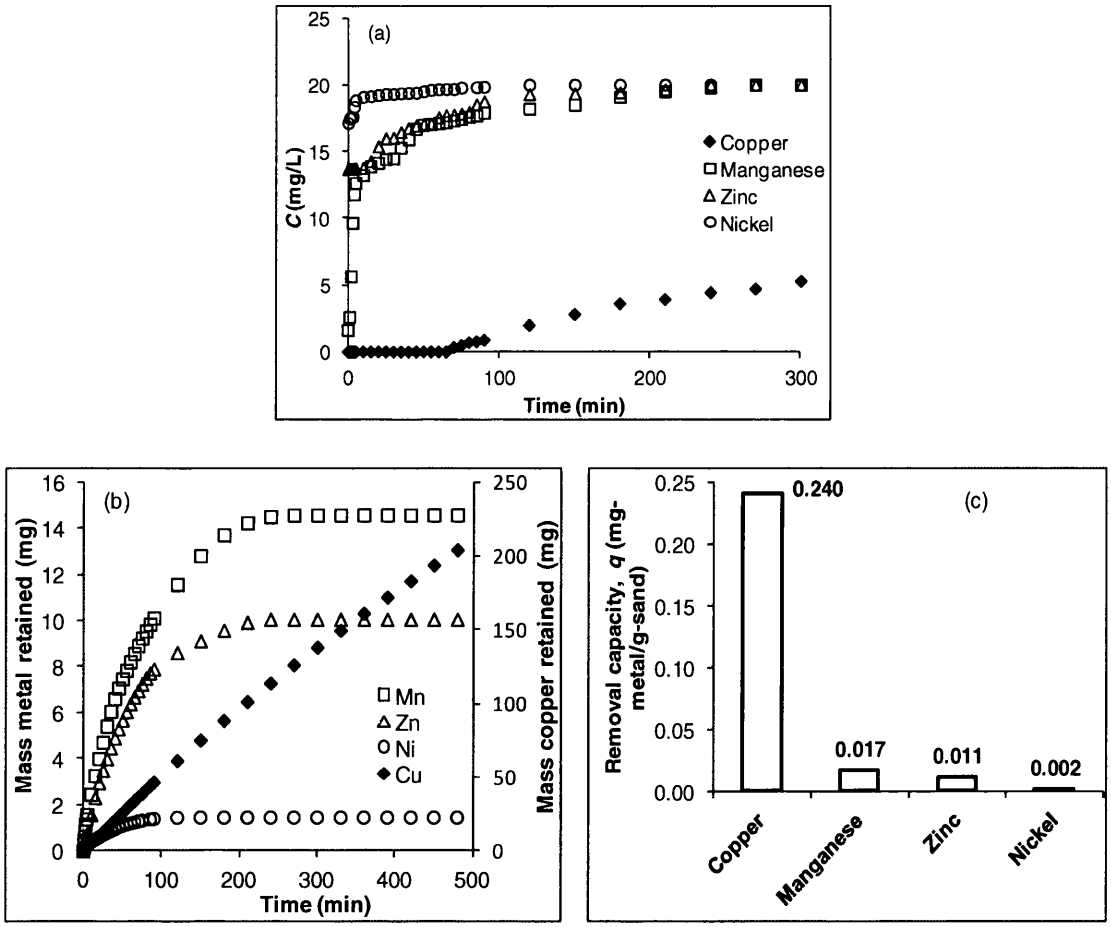

Figure 6.1 AUSF performances for individual copper, manganese, nickel and zinc (C_{in} = 20 mg/L, Q_{in} = 25.01 mL/min, d_{sand} = 0.400 mm, H = 450 mm, m_{sand} = 869.77 g, manganese to sand ratio = 0.0709 mg-manganese/g-sand) (a) effluent metal concentration (b) mass metal retained (mg) vs time (min) (c) removal capacity, q

This affinity order of copper > zinc > nickel is in good agreement with Reddad et al. (2002b) who studied these metals as mixed metals and showed that nickel was most poorly adsorbed onto the sugar beet pulp than the other metals. Previous studied revealed that the adsorbent affinity towards metal ions will vary depending on the pH value of the solution, the ionic strength (Reddad et al., 2002b) and the hydration enthalphy of the cations (Ricordel et al., 2001). The higher the ionic strength the less metal is adsorbed; while the solution pH affects the surface charge of the adsorbent which results in the occurrence of electrostatic attraction between the surface and the metal ion, hence leads to the adsorption of metal by the adsorbent (Reddad et al., 2002b).

The hydration enthalpy is the energy that allows the detachment of H_2O molecules from cations thus shows the tendency for the ion to interact with other ions. The less a cation is hydrated, the weaker the hydration enthalpy, the more the cations detach H_2O thus the more the cations can interact with the adsorbent (Ricordel et al., 2001).

The ionic strength theory cannot be applied in this study as the ionic strength was not changed in this study. The hydration enthalpy theory cannot also be used in this study as this usage would result in a different affinity order of the metal ions with that of the experimental result. By using the hydration enthalpy theory, the affinity order of the metals would be manganese > zinc > copper > nickel (Table 6.2).

There is another theory to describe the affinity order i.e. the electro-negativity of the atom. The electro-negativity is defined by Pauling as the power of an atom in a molecule to attract electrons to itself (Greenwood and Earnshaw, 1997). Thus, the greater the electro-negativity value, the more metal would be adsorbed by the adsorbent. However, this theory cannot also be applied in this case, as this application would lead to a different affinity order of the metal ions with that of the result. Based on the electro-negativity theory, the affinity order of the metals would be copper > nickel > zinc > manganese (Table 6.2).

The pH theory, on the other hand, would be more appropriate to be applied in this case, as the pH theory is more likely to affect the affinity order as discussed in the following section (Section 6.1.2).

Table 6.2 The studied metal properties

Metal	Properties	
	Hydration enthalpy (MJ/mol)*	Electronegativity (Pauling scale)**
Copper	-3.00	1.9
Manganese	-2.75	1.5
Zinc	-2.95	1.6
Nickel	-3.10	1.8

Note:
*(Jones, 2002)
**(Greenwood and Earnshaw, 1997)

6.1.2 Proposed processes for the removal of manganese, nickel and zinc

Similar to copper, manganese, zinc and nickel will form hexa-aqua complexes once they are dissolved in water (Stumm and Morgan, 1996; Winter and Andrew, 2000). These complexes donate a proton to a water molecule to produce the hydrated proton H_3O^+ as follows (Winter and Andrew, 2000):

$$[M(H_2O)_6]^{2+}_{(aq)} + H_2O_{(l)} \rightarrow [M(H_2O)_5OH]^+_{(aq)} + H_3O^+_{(aq)} \quad ...(\text{Equation } 6.1)$$

where M = metal. Therefore, they are weakly acidic in water (pH values for input copper, zinc, nickel and manganese are 5.58, 5.66, 5.71 and 5.64 respectively).

The process by which copper, manganese, zinc and nickel removed in the AUSF may be best described as follows:

1. Precipitation

The occurrence of precipitation of metal hydroxide depends on the metal concentration in the solution and the pH value of the solution (Section 3.2.4). Section 5.4 shows that for copper concentration of 20 mg/L, theoretically copper will precipitate as hydroxide at pH > 5.92 (pH critical). By taking this pH critical into account and knowing that the pH value for the 480 min operational period was decreasing from 8.48 to 7.06 (Figure 6.2 (a)), then precipitation is assumed to be the dominant process during this period ($0 \leq t \leq 480$ min).

Section 5.4 shows the precipitation process of copper hydroxides and the assumed copper speciation in the water. For other metals (manganese, zinc and nickel), the relationships between the metal concentrations and pH values for the precipitation of metals as hydroxides are shown in Figures 6.3 (a - c). These figures show that at greater concentration, the precipitation of metals as hydroxides occurs at lower pH. Table 6.3 depicts the pH values at which these metals will theoretically precipitate for metal concentration of 20 mg/L. Table 6.3 shows that theoretically zinc will precipitate as hydroxide at pH > 7.41 for zinc concentration of 20 mg/L. Taking this pH value into account and the pH value for $t < 80$ min that was decreasing from 8.23 to 7.40 (Figure 6.2 (c)), it is then assumed that precipitation might be the dominant process during this period ($0 \leq t < 80$ min).

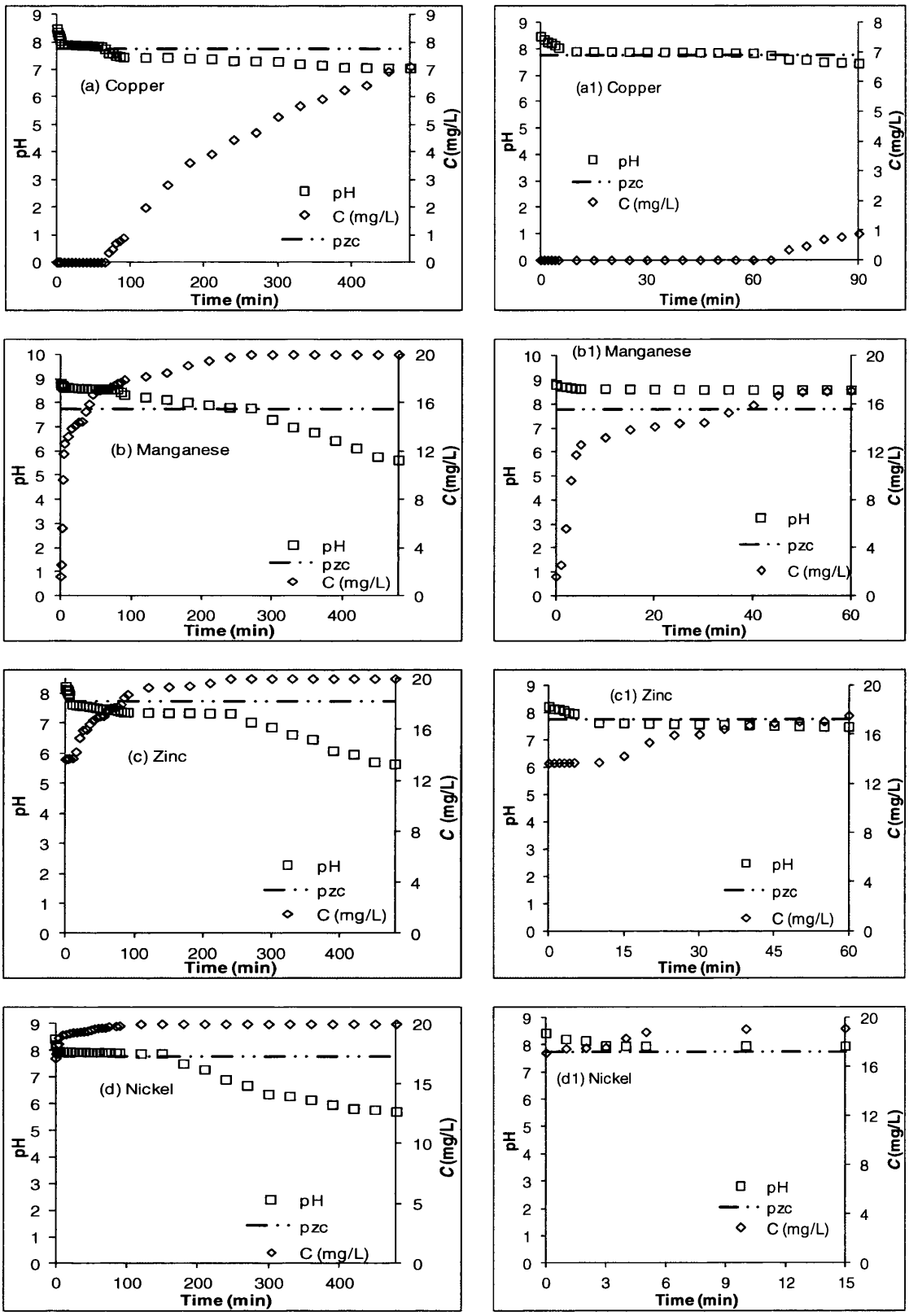

Figure 6.2 pH for individual metal solutions in AUSF (H = 450 mm, C_{in} = 20 mg/L, Q = 25.01 mL/min, m_{sand} = 869.77 g, d_{sand} = 0.400 mm, manganese to sand ratio = 0.0709 mg-manganese/g-sand) (a) Copper (b) Manganese (c) Zinc (d) Nickel (a1-d1) Enlargement

For nickel, as nickel will precipitate as hydroxide at pH > 8.23 for nickel concentration of 20 mg/L, and as the pH value for t < 1 min was decreasing from 8.44 to 8.22 (Figure 6.2 (d)), the precipitation process is thus assumed to be dominant at the first one minute ($0 \leq t < 1$ min) only. For manganese, however, as manganese will precipitate as hydroxide at pH > 9.32 for manganese concentration of 20 mg/L, and as the pH value was below 9.32 (decreasing from 8.81 to 5.64 (Figure 6.2 (b)) for 480 min period, manganese is then believed would not precipitate under these pH values.

The precipitation process of the metals may be written as follows:

$M^{2+}_{(aq)} + 2OH^-_{(aq)} \rightleftarrows M(OH)_{2(s)}$....(Equation 6.2) (Tchobanoglous et al., 2004)

or

$[M(H_2O)_6]^{2+}_{(aq)} + 2OH^-_{(aq)} \rightleftarrows [M(OH)_2(OH_2)_4]_{(s)} + 2H_2O_{(l)}$....(Equation 6.3) (Winter and Andrew, 2000). Where M = metal (copper, zinc or nickel).

The explanation of the release of hydroxide ions has been discussed previously in Section 5.4.

2. Electrostatic attraction

The point of zero charge (pzc) value of the coated sand has been found previously (Section 4.1.6) to be 7.75. As there was an increase in copper removal as the pH increased (pH = 8.48 – 7.75, $0 \leq t \leq 65$ min), the coated sand is then assumed to be negatively charged at pH > 7.75. This negative surface charge increased as the pH increased resulting in a greater electrostatic attraction between the surface and the copper ions.

For zinc, the period for electrostatic attraction is $0 \leq t < 10$ min in which the pH value decreased from 8.23 to 7.64. For nickel, electrostatic attraction is assumed to be occurred during the period of $0 \leq t \leq 150$ min in which the pH value decreased from 8.44 to 7.89. After 150 min, there was no removal of nickel as the pH values were decreasing from 7.51 to 5.71.

For manganese, electrostatic attraction is assumed to be occurred during the period of $0 \leq t \leq 270$ min in which the pH value was decreasing from 8.81 to 7.79. After 270 min, there was no removal of manganese as the pH values were decreasing from 7.32 to 5.64.

3. Adsorption/Ion exchange and surface complex formation

The pH values of the solutions were decreasing from the beginning to the end of the experiments (Figures 6.2 (a - d) and Table 6.3). This indicates that the mechanism by which copper was adsorbed onto the coated sand might involve an exchange reaction of metal cations (M^{2+}) with H^+ on the surface and surface complex formation.

As stated previously in Section 5.4, based on the principle of ion-exchange, the more metal adsorbed onto the coated sand, the more hydrogen ions are released resulting in the decrease in the pH value. The complex reactions of M^{2+} with manganese oxide may be written as follows (Stumm and Morgan, 1996):

$\equiv Mn{-}OH + M^{2+} \rightleftarrows \equiv Mn{-}O^{-}M^{2+} + H^+$ ....(Equation 6.4)

$\equiv Mn{-}O^{-} + M^{2+} \rightleftarrows \equiv Mn{-}O^{-}M^{2+}$ ....(Equation 6.5)

$2(\equiv Mn{-}OH) + M^{2+} \rightleftarrows (\equiv Mn{-}O^{-})_2M^{2+} + 2H^+$ ....(Equation 6.6)

$2(\equiv Mn{-}O^{-}) + M^{2+} \rightleftarrows (\equiv Mn{-}O^{-})_2M^{2+}$ ....(Equation 6.7)

$\equiv Mn{-}OH + M^{2+} + H_2O \rightleftarrows \equiv Mn{-}OMOH + 2\,H^+$ ....(Equation 6.8)

Equation 6.4, 6.6 and 6.8 show that the hydrogen ion concentration increased with an increasing amount of metal ions adsorbed onto the coated sand. This is in line with Figures 6.2 (a - d) that shows the adsorption of copper on the coated sand surface was highly dependent on pH. As the pH increased, the OH^- increased resulting in the increase in the surface activity of the coated sand. Copper, manganese, zinc and nickel would undergo adsorption/ion exchange and surface complexation processes at $0 \leq t \leq 480$ min, $0 \leq t \leq 270$ min, $0 \leq t \leq 240$ min, and $0 \leq t \leq 150$ min when the pH values were decreasing from 8.48 to 7.06, from 8.81 to 7.79, from 8.23 to 7.34, from 8.44 to 7.89 (Figures 6.2 (a - d)) respectively. For zinc, after 240 min, there was no removal and the pH value decreased from 7.34 to 5.66.

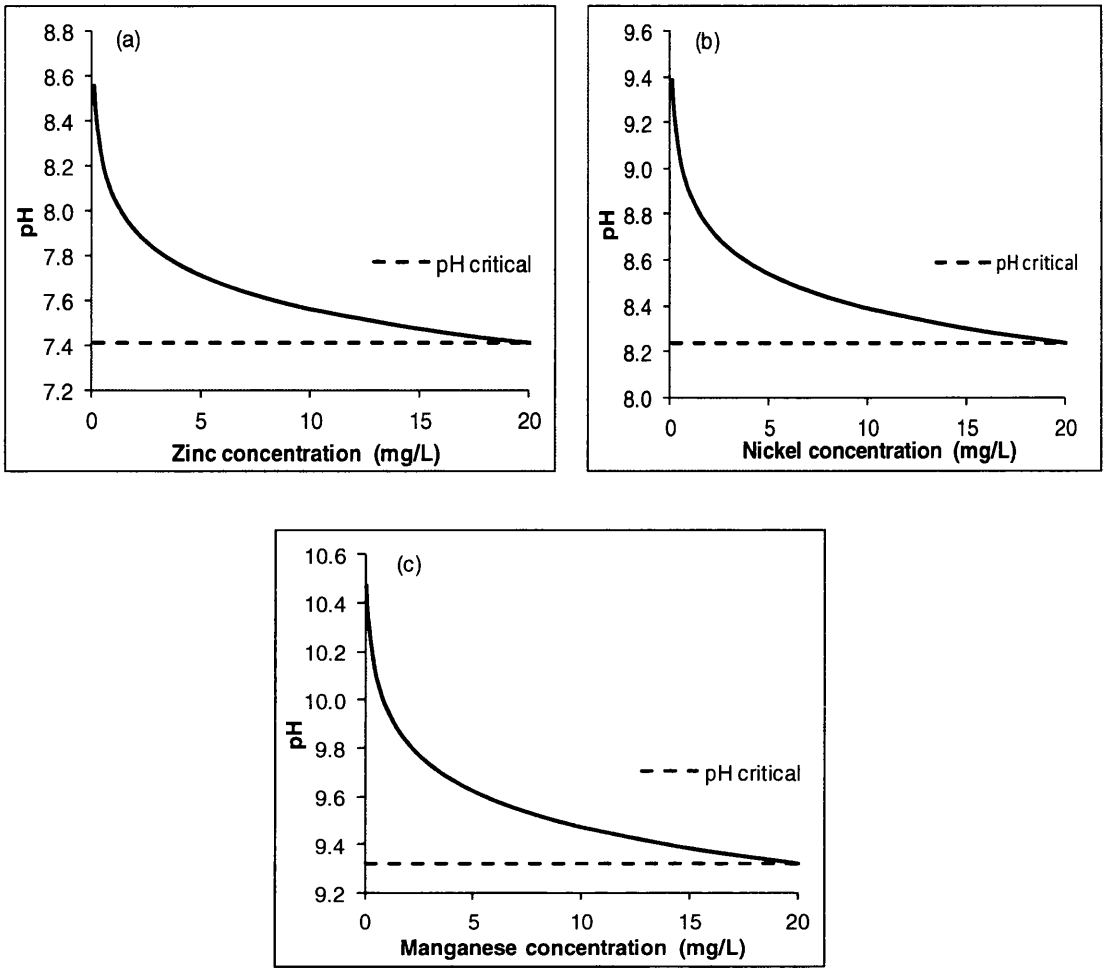

Figure 6.3 Metal concentrations as a function of pH for the precipitation of metals as hydroxides (at 25°C) (a) Zinc (p^cK_{s0} = 16.7 (Tchobanoglous et al., 2004)) **(b) Nickel (p^cK_{s0} = 15.0** (Tchobanoglous et al., 2004)) **(c) Manganese (p^cK_{s0} = 12.8** (Snoeyink and Jenkins, 1980))

Table 6.3 pH values for hydroxide precipitation of the studied metals*

Metal hydroxide	Theoretical pH	Solubility products (p^cK_{s0}) at 25°C	Experimental pH
$Cu(OH)_2$	> 5.92	19.66**	8.48 - 7.06
$Zn(OH)_2$	> 7.41	16.70**	8.23 – 5.66
$Ni(OH)_2$	> 8.23	15.00**	8.44 – 5.71
$Mn(OH)_2$	> 9.32	12.80***	8.81 – 5.64

Note:

* For metals concentration of 20 mg/L

** (Tchobanoglous et al., 2004)

*** (Snoeyink and Jenkins, 1980)

This theory of adsorption is supported by Eisler (2007) who stated that in solution, zinc is adsorbed by inorganic adsorbing agents such as hydrous oxides of manganese. He also described that the formation of zinc-ligands complexes raises the solubility of zinc and is likely to increase the adsorption of zinc, and the sorption of zinc to sediments was complete at pH>7.

Figures 6.2 (a - a1) shows that the removals curve of Cu^{2+} displayed two pH patterns. The removal amount increased rapidly with decreasing pH from 8.48 to 7.75 ($0 \leq t \leq 65$ min) and increased slowly with decreasing pH from 7.75 to 7.06 ($65 < t \leq 480$ min). Even though the removal of zinc was low, the curve has also displayed two pH patterns (Figures 6.2 (c - c1)). The removal amount increased rapidly with decreasing pH from 8.23 to 7.97 ($0 \leq t \leq 5$ min) and increased slowly with decreasing pH from 7.97 to 7.34 ($5 < t \leq 240$ min). The same case is applied to nickel (Figures 6.2 (d - d1)). The removal amount increased rapidly with decreasing pH from 8.44 to 8.22 ($0 \leq t < 1$ min) and increased slowly with decreasing pH from 8.22 to 7.89 ($1 \leq t \leq 150$ min). For manganese, even though its removal was higher than zinc and nickel, the curve only displayed one pH pattern (Figures 6.2 (b - b1)). The removal amount increased slowly with decreasing pH from 8.81 to 7.79 ($0 \leq t \leq 270$ min).

The assumed metals (zinc, manganese and nickel) speciation occurred in the water at certain pH are shown in Table 6.4 (a-c). Copper speciation has been shown previously in Table 5.40. The proposed reactions for the studied individual metals occurred in the AUSF are depicted in Figure 6.4. The order of the removal of the metals based on the reactions can then be concluded from Figure 6.4 as shown in Table 6.5.

Table 6.4 (a) Assumed zinc speciation at certain pH

Type of species		pH
Dominant	Other	
$Zn^{2+}_{(aq)}$ or $Zn(OH)^{2+}_{(aq)}$	$\equiv Mn-O^{-}Zn^{2+}$ or $(\equiv Mn-O^{-})_2Zn^{2+}$ or $\equiv Mn-OZnOH$	≤ 7.41
$Zn(OH)_{2\,(s)}$	$Zn^{2+}_{(aq)}$ or $Zn(OH)^{2+}_{(aq)}$ or $\equiv Mn-O^{-}Zn^{2+}$ or $(\equiv Mn-O^{-})_2Zn^{2+}$ or $\equiv Mn-OZnOH$	> 7.41

Table 6.4 (b) Assumed nickel speciation at certain pH

Type of species		pH
Dominant	Other	
$Ni^{2+}_{(aq)}$ or $Ni(OH)^{2+}_{(aq)}$	$\equiv Mn-O^{-}Ni^{2+}$ or $(\equiv Mn-O^{-})_2Ni^{2+}$ or $\equiv Mn-ONiOH$	≤ 8.23
$Ni(OH)_{2\,(s)}$	$Ni^{2+}_{(aq)}$ or $Ni(OH)^{2+}_{(aq)}$ or $\equiv Mn-O^{-}Ni^{2+}$ or $(\equiv Mn-O^{-})_2Ni^{2+}$ or $\equiv Mn-ONiOH$	> 8.23

Table 6.4 (c) Assumed manganese speciation at certain pH

Type of species		pH
Dominant	Other	
$Mn^{2+}_{(aq)}$ or $Mn(OH)^{2+}_{(aq)}$	$\equiv Mn-O^{-}Mn^{2+}$ or $(\equiv Mn-O^{-})_2Mn^{2+}$ or $\equiv Mn-OMnOH$	≤ 9.32
$Mn(OH)_{2\,(s)}$	$Mn^{2+}_{(aq)}$ or $Mn(OH)^{2+}_{(aq)}$ or $\equiv Mn-O^{-}Mn^{2+}$ or $(\equiv Mn-O^{-})_2Mn^{2+}$ or $\equiv Mn-OMnOH$	> 9.32

Note:
pH values of the experiment were below 9.32 thus $Mn(OH)_{2\,(s)}$ would unlikely to have been occurred in this experiment.

Figure 6.4 shows that copper, zinc and nickel would precipitate as hydroxides at $0 \leq t \leq 480$ min, $0 \leq t < 80$ min, and $0 \leq t < 1$ min respectively. Manganese, however, was unlikely to precipitate in the solution. Therefore the removal order for the studied metals based on the precipitation process is Cu > Zn > Ni > Mn. For electrostatic attraction process, the positively charged copper, manganese, zinc and nickel would be attracted to the negatively charged sand at $0 \leq t \leq 65$ min, $0 \leq t \leq 270$ min, $0 \leq t <$ 10 min, and $0 \leq t \leq 150$ min respectively. Therefore the order of the removal of the studied metals based on the electrostatic attraction process is Mn > Ni > Cu > Zn.

For adsorption/ion exchange and surface complexation processes, copper, manganese, zinc and nickel would undergo these processes at $0 \leq t \leq 480$ min, $0 \leq t \leq 270$ min, $0 \leq t \leq 240$ min, and $0 \leq t \leq 150$ min. Therefore the order of the removal of the studied metals based on the adsorption/ion exchange and surface complexation processes is Cu > Mn > Zn > Ni.

Section 6.1.1 reveals that the order of removal rate, saturation time, t_{95}, q_{Mmax}/q_{Mn}, the decrease in effluent concentration, mass retained, and removal capacity was copper > manganese > zinc > nickel. Taking these ranking of order altogether, the affinity of the adsorbent towards metal ions is then concluded to be in the order of copper > manganese > zinc > nickel. These observations are consistent with the results obtained in Section 6.1.1.

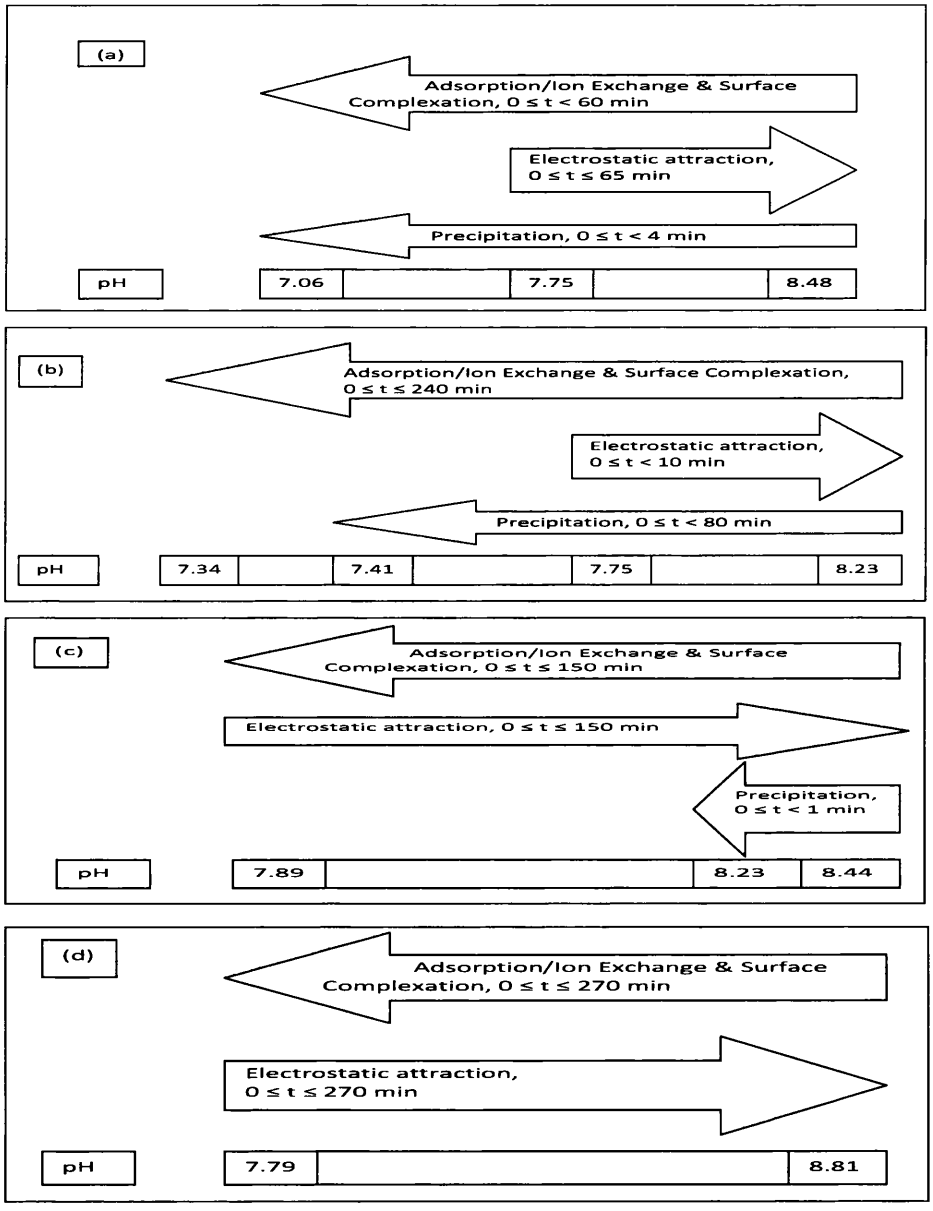

Figure 6.4 Proposed processes that occurred for individual metal removals in the AUSF (H = 450 mm, C_{in} = 20 mg/L, Q = 25.01 mL/min, m_{sand} = 869.77 g, d_{sand} = 0.400 mm, manganese to sand ratio = 0.0709 mg-manganese/g-sand) (a) copper (b) zinc (c) nickel (d) manganese

Table 6.5 The removal order of the studied metals for individual metal removal (H = 450 mm, C_{in} = 20 mg/L, Q = 25.01 mL/min, m_{sand} = 869.77 g, d_{sand} = 0.400 mm, manganese to sand ratio = 0.0709 mg-manganese/g-sand)

Parameter/Reaction	The removal order	The final order
Removal rate, R	Cu > Mn > Zn > Ni	Cu > Mn > Zn > Ni
Saturation time	Cu > Mn > Zn > Ni	
t_{95}	Cu > Mn > Zn > Ni	
q_{Mmax}/q_{Mn}	Cu > Mn > Zn > Ni	
The decrease in effluent concentration	Cu > Mn > Zn > Ni	
Mass retained	Cu > Mn > Zn > Ni	
Removal capacity	Cu > Mn > Zn > Ni	
Precipitation	Cu > Zn > Ni	
Electrostatic attraction	Mn > Ni > Cu > Zn	
Adsorption/Ion Exchange and Surface Complexation	Cu > Mn > Zn > Ni	

6.1.3 Removal of mixed metals (copper, manganese, nickel and zinc)

The removal of mixed copper, manganese, nickel and zinc in water was studied and the summaries are shown in Table 6.6 - 6.7 and Figures 6.5 (a – d). Q, H, m_{sand}, C_{in}, d_{sand}, and manganese to sand ratio were kept constants at 25.01 mL/min, 450 mm, 883.54 g, 20 mg/L, 0.400 mm, and 0.0709 mg-manganese/g-sand respectively.

Table 6.6 shows removal rates (R), saturation time, t_{95}, and q_{Mmax}/q_{Mn}. Similar to the removal of individual metals, the order of removal rate, saturation time, t_{95}, and q_{Mmax}/q_{Mn} was copper > manganese > zinc > nickel.

Copper was again best removed by AUSF; the removal rates in 30, 60, and 120 min were similar to that for individual metal. On the other hand, the removal rates of manganese, zinc and nickel were generally lower than that for the individual metal (0.2 – 1.0 times for manganese, 0.3 – 0.4 times for zinc, and 0.9 times for nickel). Nickel was still worst treated by AUSF. Although the removal rate in 120 min was recorded 26 times than that for individual metal, this is considered as an anomaly. Again no data available for copper for saturation time, as the experiment was only run in 480 min; thus, the saturation time for copper was assumed to be > 480 min. The saturation times for manganese and zinc were also lower than that for individual metal.

For nickel, the saturation time was the same as that for individual metal removal. Similar to individual metal removal, t_{95} for zinc and nickel were not recorded. q_{Mmax}/q_{Mn} for copper was not calculated as the data of saturation time was not available. However, as the saturation time of copper is predicted much longer than 480 min, thus its q_{Mmax}/q_{Mn} value would be greater than the other studied metals. q_{Mmax}/q_{Mn} was the greatest for manganese (19.68%) and the worst for nickel (2.16%). For zinc, q_{Mmax}/q_{Mn} was 4.76%.

Table 6.6 The removal rates (R), saturation time, t_{95}, and ratio of maximum metal adsorbed to the amounts of manganese (q_{Mmax}/q_{Mn}) for mixed copper, manganese, nickel and zinc (C_{in} = 20 mg/L, Q_{in} = 25.01 mL/min, d_{sand} = 0.400 mm, H = 450 mm, m_{sand} = 883.54 g, manganese to sand ratio = 0.0709 mg-manganese/g-sand)

Element	Removal Rate, R (%)			Saturation time (min)	t_{95} (min)	q_{Mmax}/q_{Mn} (%)
	30 min	60 min	120 min			
Copper	100.00	100.00	90.51	n/a	202.60	n/a
Manganese	28.27	9.21	1.52	240	5.42	19.68
Zinc	7.03	3.35	0.90	210	0.00	4.76
Nickel	3.2	1.54	0.52	150	0.00	2.16

Figure 6.5 (a) shows that effluent concentration decreased in the order of copper > manganese > zinc > nickel similar to that for individual metal. This may be due to the more mass metal retained within the bed as depicted in Figure 6.5 (b). Figure 6.5 (c) shows the removal capacity of AUSF for each element after saturation (except for copper where these removals were calculated at 480 min).

The order of these removals was the same as that for individual metal i.e. copper > manganese > zinc > nickel). The order shows that AUSF had a stronger affinity for Cu^{2+} than Ni^{2+} which is in good agreement with Boujelben et al (2009). Good agreement was also obtained by Reddad et al (2002a) while studying Ni(II) and Cu(II) binding properties of sugar beet pulp. The order also reflects that Cu^{2+} was better removed than Zn^{2+}. This is in line with Erdem et al (2004) and Pitcher et al (2004) who studied the metal removals by zeolites. In addition, the affinity order of copper > zinc > nickel is in good agreement with Reddad et al. (2002b) who studied the adsorption of these mixed metals onto sugar beet pulp.

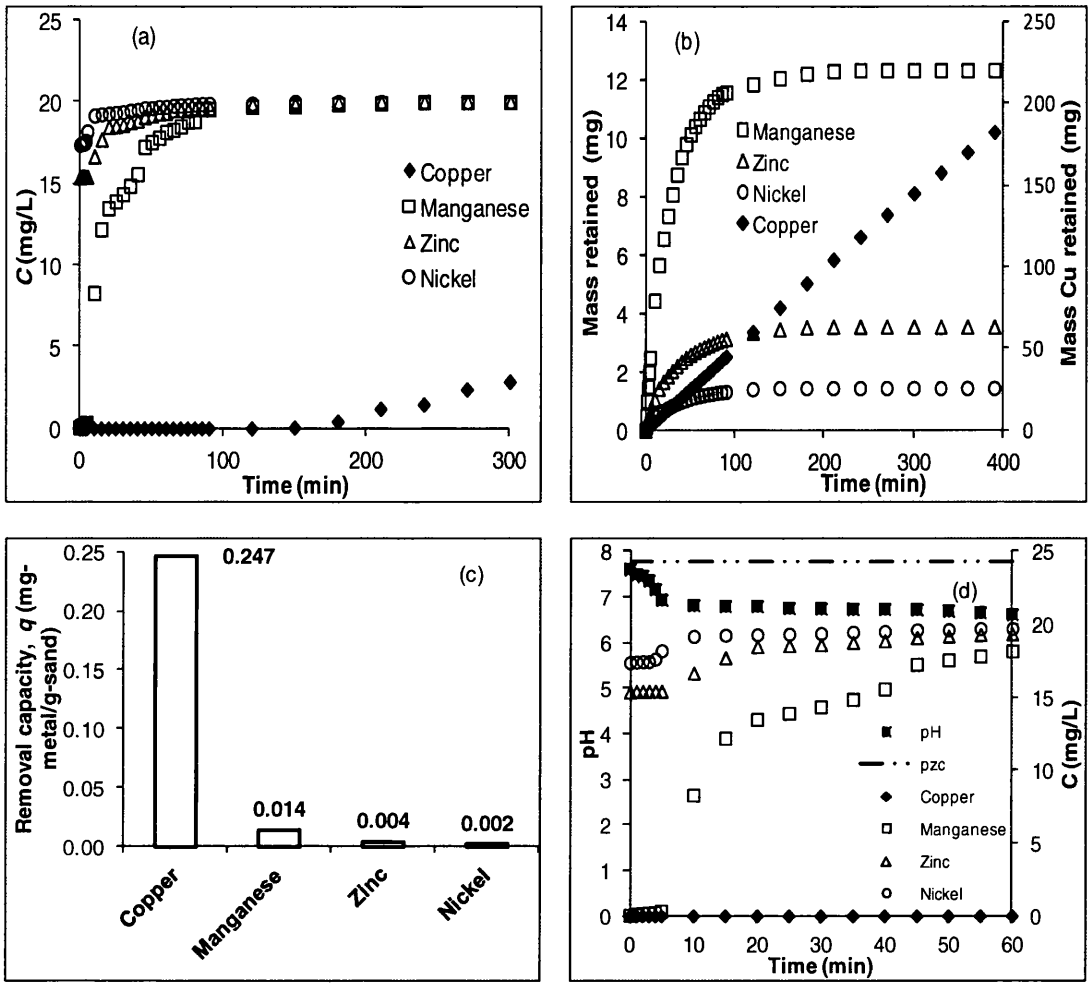

Figure 6.5 AUSF performances for mixed copper, manganese, nickel and zinc (C_{in} = 20 mg/L, Q_{in} = 25.01 mL/min, d_{sand} = 0.400 mm, H = 450 mm, m_{sand} = 883.54 g, manganese to sand ratio = 0.0709 mg-manganese/g-sand) (a) effluent metal concentration (b) mass metal retained vs time (c) removal capacity, q (d) pH

Nickel was shown worst removed by AUSF. This is also confirmed by Eisler (2007) who stated that copper, manganese and zinc reduced the binding of nickel to DNA. The poor removal of nickel was also confirmed by pH of mixed metal solutions (pH = 7.6 - 5.7) (Figure 6.5 (d)). At this pH range, indeed nickel was unlikely to precipitate (Section 6.1.2). The same case is applied to manganese that would not precipitate at that pH range. Only copper (for $0 \leq t < 270$ min) and zinc ($0 \leq t < 3$ min) would precipitate at that pH range. Therefore the order of the removal for the metals based on the precipitation process was Cu > Zn > Ni > Mn. This order is the same as that for the individual metal removal.

Because of the pzc of the sand was found to be 7.75 then at the pH range of 7.6 - 5.7 no electrostatic attraction would be occurred between the coated sand and the metal cations. This then left only adsorption/ion exchange and surface complexation to potentially be the other processes responsible for the observed metal removals. Indeed as the pH was decreasing from 7.6 to 5.7, adsorption/ion exchange and surface complexation are believed to be occurred in the AUSF (Section 6.1.2). The periods for these processes for copper, manganese, zinc and nickel ions were $0 \leq t \leq 480$ min, $0 \leq t < 240$ min, $0 \leq t < 210$ min and $0 \leq t < 150$ min respectively. Therefore, based on these processes, the order of the removal for the metals is Cu > Mn > Zn > Ni.

By taking into account those orders altogether and the period in which the removals occurred for each metal, the affinity order of the metals is then concluded to be that of Cu > Mn > Zn > Ni (Table 6.7).

Table 6.7 The removal order of the studied metals for mixed metals removal (C_{in} = 20 mg/L, Q_{in} = 25.01 mL/min, d_{sand} = 0.400 mm, H = 450 mm, m_{sand} = 883.54 g, manganese to sand ratio = 0.0709 mg-manganese/g-sand)

Reaction	The removal order	The final order
Precipitation	Cu > Zn > Ni > Mn	Cu > Mn > Zn > Ni
Removal rate	Cu > Mn > Zn > Ni	
Saturation time	Cu > Mn > Zn > Ni	
t_{95}	Cu > Mn > Zn > Ni	
q_{Mmax}/q_{Mn}	Cu > Mn > Zn > Ni	
The decrease in effluent concentration	Cu > Mn > Zn > Ni	
Mass retained	Cu > Mn > Zn > Ni	
Removal capacity	Cu > Mn > Zn > Ni	
Adsorption/Ion Exchange and Surface Complexation	Cu > Mn > Zn > Ni	

6.2 Removal of metals in artificial electroplating waste water

The removal of mixed copper, manganese, nickel and zinc in artificial electroplating water was studied and the summaries are shown in Table 6.8 - 6.10 and Figures 6.6 (a – d). Q, H, m_{sand}, d_{sand}, and manganese to sand ratio were kept constants at 25.01 mL/min, 450 mm, 876.05 g, 0.400 mm, and 0.0709 mg-manganese/g-sand respectively.

C_{in} for copper, manganese, zinc and nickel were 11.7800, 0.0610, 0.6135, and 0.8100 respectively. These metals were dissolved into the tap water. These concentrations mimicked those studied by Wang et al (2007b).

Table 6.8 shows removal rates (R), saturation time, t_{95}, and q_{Mmax}/q_{Mn} for the metals. The order of removal rate in 15 min was copper > manganese > zinc > nickel. As manganese was saturated in 25 min, this order became copper > zinc > nickel > manganese in 30, 60 and 120 min. Copper was again best removed by AUSF; copper was completely removed in 15 – 120 min. In fact, copper was 100% removed until 180 min. Manganese was also completely removed in 15 min, but saturated in 25 min. Zinc and nickel were removed by 77.08 – 25.55% and 66.31 – 21.97% in 15 – 120 min respectively. These removal rates were higher than those under optimal conditions both for individual or mixed metal (Section 6.1); that might be due to the metals concentrations were smaller in this artificial electroplating waste water, particularly for nickel, zinc and manganese.

Table 6.8 The removal rates (R), saturation time, t_{95}, and ratio of maximum metals adsorbed to the amounts of manganese (q_{Mmax}/q_{Mn}) for copper, manganese, nickel and zinc in artificial electroplating waste water (Q_{in} = 25.01 mL/min, d_{sand} = 0.400 mm, H = 450 mm, m_{sand} = 876.05 g, manganese to sand ratio = 0.0709 mg-manganese/g-sand, $C_{Cu\text{-}in}$ = 11.7800 mg/L, $C_{Mn\text{-}in}$ = 0.0610 mg/L, $C_{Zn\text{-}in}$ = 0.6135 mg/L, $C_{Ni\text{-}in}$ = 0.8100 mg/L)

Element	Removal Rate, R (%)				Saturation time (min)	t_{95} (min)	q_{Mmax}/q_{Mn} (%)
	15 min	30 min	60 min	120 min			
Cu	100.00	100.00	100.00	100.00	n/a	306.47	n/a
Mn	100.00	0.00	0.00	0.00	25.00	15.28	0.04
Zn	77.08	71.97	40.58	25.55	210.00	0.00	1.37
Ni	66.31	45.47	29.50	21.97	240.00	0.00	1.74

Again no data available for copper for saturation time, as the experiment only ran in 480 min; thus, the saturation time for copper was assumed to be > 480 min. The saturation times order was copper > nickel > zinc > manganese. The order for t_{95} was copper > manganese > zinc > nickel. The order for q_{Mmax}/q_{Mn} was, however, Cu > Ni > Zn > Mn.

Figure 6.6 (a) shows that effluent concentration decreased in the order of copper > manganese > zinc > nickel similar to that for mixed metal under optimal conditions. This might be due to the more mass metal retained within the bed as depicted in Figure 6.6 (b). Figures 6.6 (c) shows the removal capacity of AUSF for each element after saturation (except for copper where these removals were calculated at 480 min).

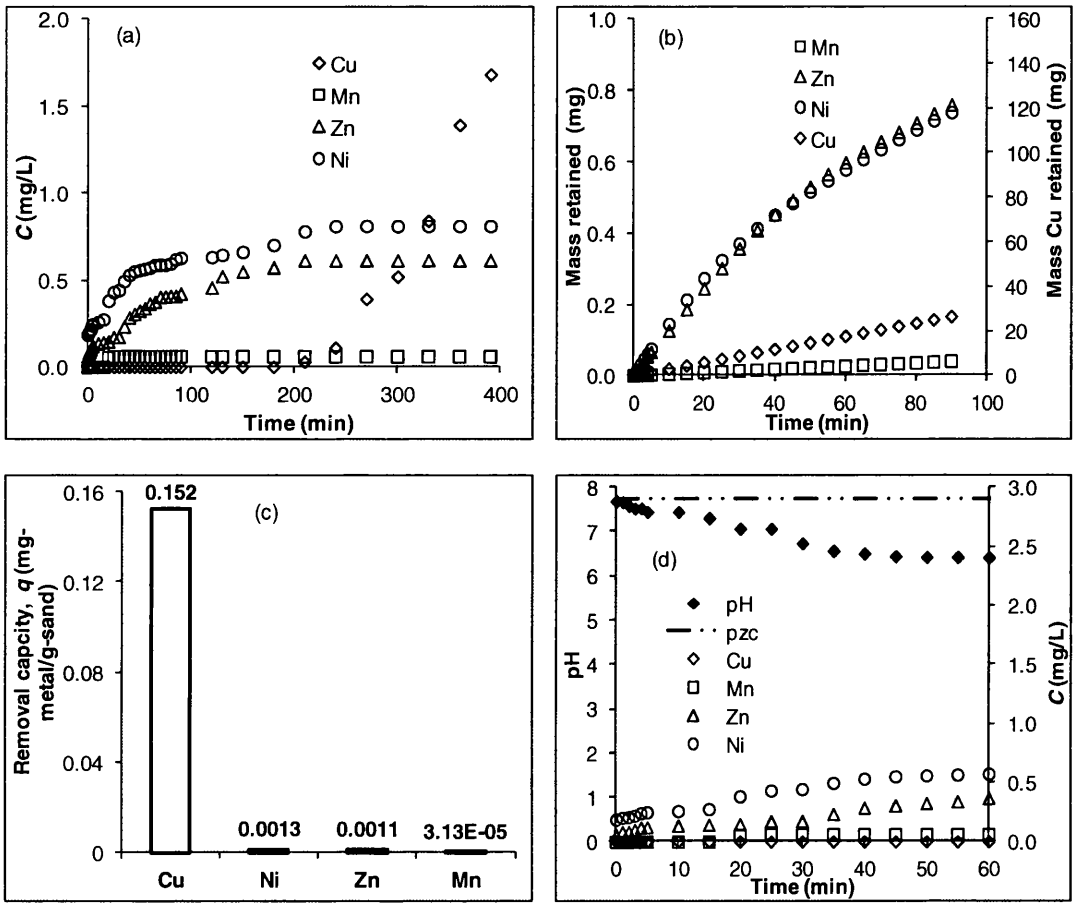

Figure 6.6 AUSF performances for mixed copper, manganese, nickel and zinc in artificial electroplating waste water (Q_{in} = 25.01 mL/min, d_{sand} = 0.400 mm, H = 450 mm, m_{sand} = 876.05 g, manganese to sand ratio = 0.0709 mg-manganese/g-sand, $C_{Cu\text{-}in}$ = 11.7800 mg/L, $C_{Mn\text{-}in}$ = 0.0610 mg/L, $C_{Zn\text{-}in}$ = 0.6135 mg/L, $C_{Ni\text{-}in}$ = 0.8100 mg/L) (a) effluent metal concentration (b) mass metal retained vs time (c) removal capacity, q (d) pH

The order of the removal capacity was copper > nickel > zinc > manganese (R^2 = 0.90). This might be due to the concentrations of manganese and zinc were smaller than nickel hence they were less adsorbed.

The pH values of effluent metal solution were 7.68 – 5.88 (Figure 6.6 (d)). Table 6.9 shows the pH value in which each metal will precipitate at its related concentration.

Table 6.9 pH values for hydroxide precipitation of the studied metals in waste water*

Metal hydroxide	Theoretical pH	Solubility products (p^cK_{s0}) at 25°C	Experimental pH
$Cu(OH)_2$	> 6.04	19.66**	7.68 – 5.88
$Zn(OH)_2$	> 8.16	16.70**	
$Ni(OH)_2$	> 8.93	15.00**	
$Mn(OH)_2$	> 10.58	12.80***	

Note:

* For metals concentration of: Cu = 11.780 mg/L, Mn = 0.061 mg/L, Zn = 0.6135 mg/L and Ni = 0.81 mg/L

** (Tchobanoglous et al., 2004)

*** (Snoeyink and Jenkins, 1980)

Table 6.9 reveals that in this range of pH only copper that might precipitate (at $0 \leq t < 330$ min). Thus the order of removal for the metals based on the precipitation process is Cu > Zn > Ni > Mn. This order was the same as that for the individual and mixed metal removal under optimal conditions.

Because the pzc was found to be 7.75 then there was no electrostatic attraction would occur in that pH range. However, as the pH was decreasing from 7.68 to 5.88, adsorption/ion exchange and surface complexation processes would likely to occur at $0 \leq t \leq 480$ min, $0 \leq t < 240$ min, $0 \leq t < 210$ min and $0 \leq t < 25$ min for copper, nickel, zinc and manganese respectively. Thus the order of removal for the metals based on these processes is Cu > Ni > Zn > Mn. By taking all the above observations together, the order of removal for the metals in waste water is then concluded to be that of Cu > Ni > Zn > Mn (Table 6.10).

Table 6.10 The removal order of the studied metals in waste water (Q_{in} = 25.01 mL/min, d_{sand} = 0.400 mm, H = 450 mm, m_{sand} = 876.05 g, manganese to sand ratio = 0.0709 mg-manganese/g-sand, $C_{Cu\text{-}in}$ = 11.7800 mg/L, $C_{Mn\text{-}in}$ = 0.0610 mg/L, $C_{Zn\text{-}in}$ = 0.6135 mg/L, $C_{Ni\text{-}in}$ = 0.8100 mg/L)

Parameter/Reaction	The removal order	The final order
R, 15 min	Cu > Mn > Zn > Ni	Cu > Ni > Zn > Mn
R, 30-120 min	Cu > Zn > Ni > Mn	
Saturation time	Cu > Ni > Zn > Mn	
t_{95}	Cu > Mn > Zn > Ni	
q_{Mmax}/q_{Mn}	Cu > Ni > Zn > Mn	
The decrease in effluent concentration	Cu > Mn > Zn > Ni	
Mass metal retained	Cu > Mn > Zn > Ni	
Removal capacity	Cu > Ni > Zn > Mn	
Precipitation	Cu > Zn > Ni > Mn	
Adsorption/Ion Exchange and Surface Complexation	Cu > Ni > Zn > Mn	

6.3 Conclusions

The pH theory was assumed to be best applied in the removal of individual and mixed metals either in artificial water or in artificial waste water. Similar to copper removal, precipitation, electrostatic attraction, adsorption/ion exchange and surface complexation processes were proposed to be occurred within the AUSF.

The order of removal for metals for individual metal and mixed metals under optimal conditions was Cu > Mn > Zn > Ni. For the metals in waste water this order became Cu > Ni > Zn > Mn. This may be due to the concentrations of manganese and zinc were smaller thus their removal capacity became lower. This order was based on the removals order with regard to the precipitation, electrostatic attraction, adsorption/ion exchange and surface complexation process and the removal rate, saturation time, t_{95}, q_{Mmax}/q_{Mn}, the decrease in effluent concentration, mass retained, and removal capacity.

The assumed metals (zinc, manganese and nickel) speciation occurred in the water at certain pH are as follows.

The dominant species for pH ≤ pH critical of metals, may be that of $M^{2+}_{(aq)}$ or $M(OH)^{2+}_{(aq)}$ whereas for pH > pH critical, may be that of $M(OH)_{2\,(s)}$. Other species for pH ≤ pH critical of metals, may be that of $\equiv Mn{-}O^{-}M^{2+}$ or $(\equiv Mn{-}O^{-})_2M^{2+}$ or $\equiv Mn{-}OMOH$ while for pH > pH critical, may be that of $M^{2+}_{(aq)}$ or $M(OH)^{2+}_{(aq)}$ or $\equiv Mn{-}O^{-}M^{2+}$ or $(\equiv Mn{-}O^{-})_2M^{2+}$ or $\equiv Mn{-}OMOH$.

CHAPTER 7

MODELLING

A suitable model is required in order to describe the behaviour of the metal removals in the column of AUSF as the results acquired from the batch studies for the metal adsorption studies may not be directly applied for practical applications in water treatment (Kumar and Bandyopadhyay, 2006). The Bohart-Adams equation (Bohart and Adams, 1920), a moderately simple fixed-bed model, was used in this work as the Bohart-Adams model is simple and practical, yet the model can estimate quantitatively the effects of the main system variables on the column dynamics (Chu and Hashim, 2007). The basic theory of the Bohart-Adams model has been discussed previously in Chapter 3. The use and application of this model in this work are initially described in this chapter. Next, the modelling of copper removals at various conditions such as different heights, diameters, concentrations, flow rates, manganese to sand ratios, and reusing times of sand media, using the Bohart-Adams equation are explained. The modellings of individual metal removals under optimal conditions using this equation are also illustrated in this chapter.

7.1 The use of Bohart-Adams model in AUSF

Bohart-Adams model (Equation 3.63) was used to describe the performance of AUSF in removing copper at different concentrations. The experimental conditions were the same as mentioned in Section 5.3.2. The results are shown in Figures 7.1 (a - b). Figures 7.1 (a - b) show time plotted versus $ln\ (C_{in}/C\text{-}1)/C_{in}$ according to Equation 3.63. Figure 7.1 (a) shows that relationship for C_{in} = 5, 10, 15 and 20 mg/L; while Figure 7.1 (b) for C_{in} = 3 and 4 mg/L. Generally, a linear relationship between t and $ln\ (C_{in}/C\text{-}1)/C_{in}$ was not valid in all cases, showing that the experimental results were not in line with the linearized Bohart-Adams model.

Therefore, the saturation capacity of the adsorbent per unit volume of the packed bed, a_{qs}, and the Bohart-Adams constant rate, r_{BA} cannot be calculated from these nonlinear curves. Chu and Hashim (2007) also obtained these nonlinear curves from their experimental data.

Another way to calculate a_{qs} and r_{BA} is to fit Equation 3.63 directly to the experimental data by Data Solver function in Microsoft Excel 2007. The following sections thus illustrate the fitting of Bohart-Adams equation to the experimental data in order to describe the performance of AUSF in removing copper in various conditions as well as removing individual metals under optimal conditions.

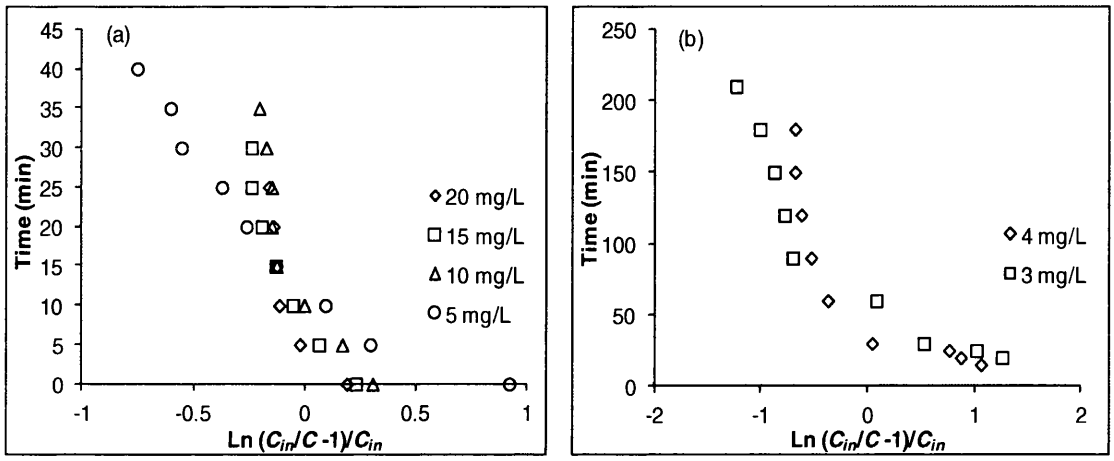

Figure 7.1 Bohart-Adams model for describing AUSF performance in removing copper at different concentrations (Q_{in} = 80.91 mL/min, H = 450mm, d_{sand} = 0.850 mm, manganese to sand ratio = 0.0709 mg-manganese/g-sand, m_{sand} = 891.13 g) (a) C_{in} = 5, 10, 15, 20 mg/L (b) C_{in} = 3, 4 mg/L

7.2 Model simulations for different concentrations

Copper removals for different input concentrations (C_{in} = 3, 4, 5, 10, 15 and 20 mg/L) were modelled based on the Bohart-Adams equation. The experimental conditions were the same as mentioned in Section 5.3.2. The results are shown in Table 7.1. Table 7.1 shows that a_{qs} increased as concentration decreased which is in good agreement with Chu and Hashim (2007). However, as Chu and Hashim (2007) used biomass as their adsorbent, they obtained much greater a_{qs} values than this AUSF.

The relationship between a_{qs} and concentration occurs as the less copper flows into the sand bed, the less void is occupied by the copper solution resulted in the more gas fraction in the void, hence copper saturation capacity increased. This correlation is shown in Figure 7.2 (R^2 = 0.69). Table 7.1 also illustrates that r_{BA} values were between 0.020 – 0.039 (L/mg.min).

Table 7.1 Bohart-Adams parameters for various concentrations (Q_{in} = 80.91 mL/min, H = 450mm, d_{sand} = 0.850 mm, manganese to sand ratio = 0.0709 mg-manganese/g-sand, m_{sand} = 891.13 g)

Concentration (mg/L)	Bohart-Adams parameters	
	a_{qs} (mg/L)	r_{BA} (L/(mg.min)
20	13.1783	0.0310
15	18.0311	0.0221
10	16.5876	0.0200
5	19.3427	0.0390
4	23.4271	0.0260
3	29.0765	0.0229

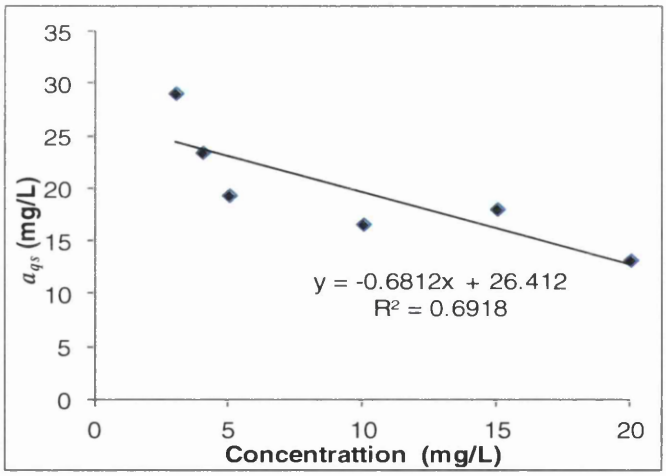

Figure 7.2 Correlation factor of Bohart-Adams parameter a_{qs} (mg/L) for various concentrations (Q_{in} = 80.91 mL/min, H = 450mm, d_{sand} = 0.850 mm, manganese to sand ratio = 0.0709 mg-manganese/g-sand, m_{sand} = 891.13 g)

Figure 7.3 shows the calculated C/C_{in} (C/C_{incalc}) versus time (t) curves, using the calculated values of a_{qs} and r_{BA} (shown in Table 7.1), along with C/C_{in} obtained from the experiment (C/C_{inexp}).

Generally, the conformity between the experimental and calculated C/C_{in} versus time curves was not perfectly accurate. The model especially over calculated the sharpness of the front and rear edges of the experimental curves. Other studies also found the similar tendency (Chu and Hashim, 2007; Han et al., 2009). The disagreement between the experimental and calculated curves can be attributed to the approximations intrinsic in employing the simple Bohart-Adams model, which is able to produce a symmetrical, sigmoidal curve (Chu and Hashim, 2007). The nonlinear curves in Figure 7.1 show that the experimental curves were non symmetrical. The wideness of the rear edge of the curves was likely the result of slow intra-particle diffusion within the pores of the manganese coated sand. Copper has to initially diffuse into the porous sand before interacting with hydroxide ion and manganese dioxide. The slow move of C/C_{in} towards 1 is usually noticed in liquid phase adsorption where intra-particle diffusion is the principal mass transfer process (Cooney, 1998). The disagreement between the experimental and calculated curves was due to the fact that the Bohart-Adams model does not clearly constitute in the phenomenon of intra-particle diffusion since the model employs a quasi chemical kinetic rate expression to illustrate mass transfer (Ruthven, 1984; Chu and Hashim, 2007).

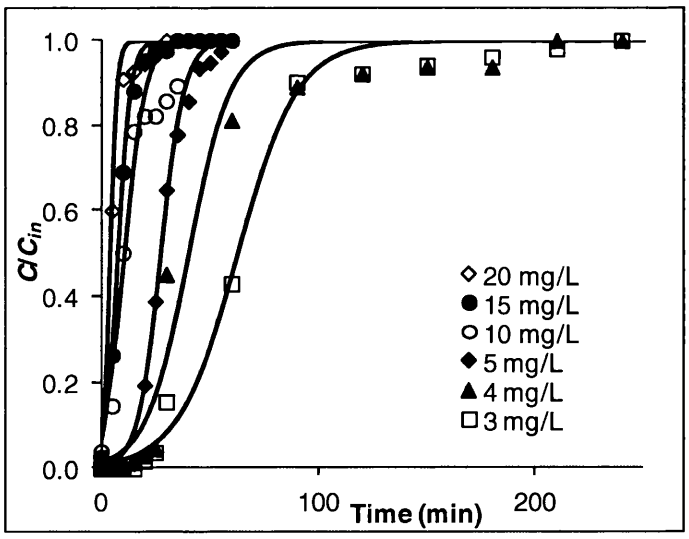

Figure 7.3 Best-fitting model simulations for various concentrations (Q_{in} = 80.91 mL/min, H = 450mm, d_{sand} = 0.850 mm, manganese to sand ratio = 0.0709 mg-manganese/g-sand, m_{sand} = 891.13 g) (markers are experimental data; curves are best-fitting model simulations derived from Equation 3.63)

Once mass transfer limitation occurs, the rate constant of r_{BA} is no longer the fundamental rate constant yet lumped rate constant consisting of the effects of the basic kinetics and mass transport (Chu, 2010). The role of intra-particle diffusion (physical adsorption) as the rate-limiting step in the process of copper removal by AUSF has been confirmed earlier in the batch studies (Section 5.2.2.1).

7.3 Model simulations for different heights

Model simulations were done to imitate the Bohart-Adams equation for copper removals for different heights of sand column (H = 150, 250, 350 and 450 mm). The experimental conditions were the same as mentioned in Section 5.3.3. The results are depicted in Table 7.2.

Table 7.2 and Figure 7.4 show that a_{qs} was likely to increase as height increased. This occurs as the higher the sand bed the more active part of the bed obtained resulted in more copper retained within the bed. This result is in good agreement with Han et al (2009). Table 7.2 also shows that the Bohart-Adams rate constant values were in the range of 0.008 – 0.028 (L/mg.min).

Table 7.2 Bohart-Adams parameters for various heights of sand column (C_{in} = 20 mg/L, Q_{in} = 80.91 mL/min, d_{sand} = 0.850 mm, manganese to sand ratio = 0.0709 mg-manganese/g-sand)

Height (mm)	Bohart-Adams parameters	
	a_{qs} (mg/L)	r_{BA} (L/(mg.min)
450	61.4156	0.0080
350	51.4567	0.0108
250	45.0951	0.0174
150	51.5494	0.0283

Figure 7.5 depicts the best fitting model simulations for various heights. Similarly to model simulations for different concentrations, the calculated curves apparently overestimated the sharpness of the leading and trailing edges of the experimental C/C_{in} versus t.

Han et al (2009) also found the similar tendency while studying copper removal through iron oxide-coated zeolite. Due to there was the slow movement of C/C_{in} towards 1, intra-particle diffusion is believed to play an important role in the mass transfer process (Cooney, 1998) as confirmed in Section 5.2.2.2.

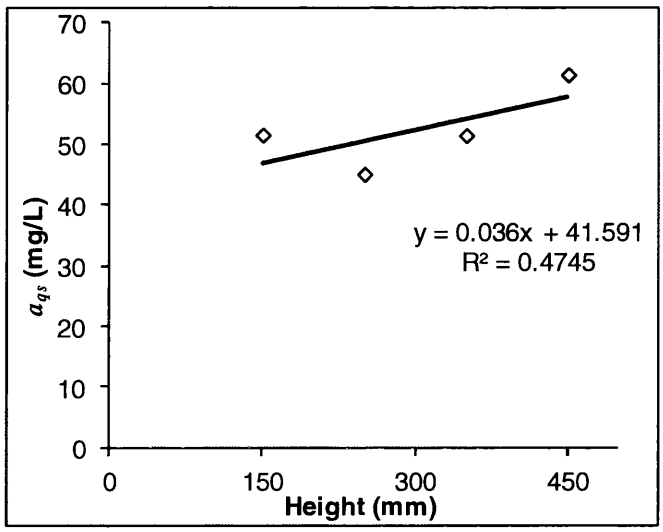

Figure 7.4 Correlation factor of Bohart-Adams parameter a_{qs} (mg/L) for various heights of sand column (C_{in} = 20 mg/L, Q_{in} = 80.91 mL/min, d_{sand} = 0.850 mm, manganese to sand ratio = 0.0709 mg-manganese/g-sand)

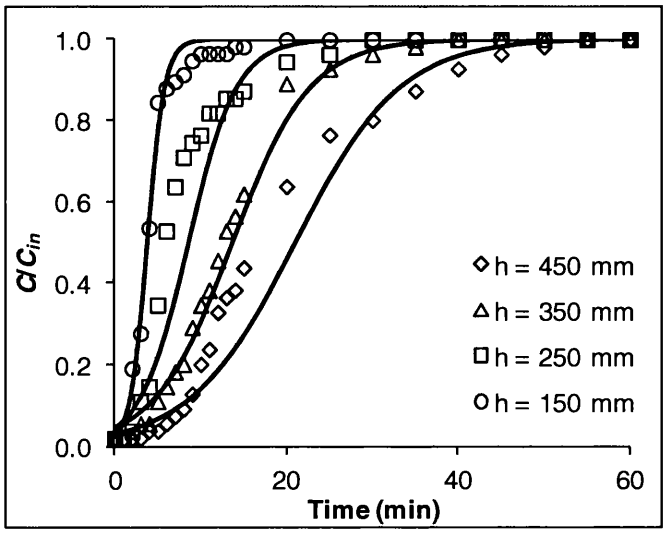

Figure 7.5 Best-fitting model simulations for various heights of sand column (C_{in} = 20 mg/L, Q_{in} = 80.91 mL/min, d_{sand} = 0.850 mm, manganese to sand ratio = 0.0709 mg-manganese/g-sand) (markers are experimental data; curves are best-fitting model simulations derived from Equation 3.63)

7.4 Model simulations for different flow rates

Copper removals for different flow rates (Q = 81.91 mL/min, 74.40 mL/min, 55.01 mL/min and 37.78 mL/min) were modelled based on the Bohart-Adams equation. The experimental conditions were the same as mentioned in Section 5.3.4. The results are depicted in Table 7.3.

Table 7.3 shows that a_{qs} generally increased as flow rate decreased which is confirmed by others (Chu and Hashim, 2007; Han et al., 2009). Nevertheless, they obtained much greater values of a_{qs} as they used biomass as their adsorbent. The relationship between a_{qs} and flow rate occurs as flow rate decreases the ratio of gas within the void increases resulted in the increase in copper saturation capacity. Table 7.3 also illustrates that r_{BA} values were between 0.039 – 0.151 (L/mg.min).

Figure 7.6 depicts the best fitting model simulations for various flow rates. The calculated curves apparently overestimated the sharpness of the leading and trailing edges of the experimental C/C_{in} versus t.

Other studies also showed the similar trends (Chu and Hashim, 2007; Han et al., 2009). A slow movement of C/C_{in} towards 1 was noticed and this is likely due to intra-particle diffusion involved in the mass transfer process (Cooney, 1998) as confirmed earlier in Section 5.2.

Table 7.3 Bohart-Adams parameters for various flow rates (C_{in} = 5 mg/L, H = 45 cm, m_{sand} = 920.59 g, d_{sand} = 0.850mm, manganese to sand ratio = 0.0709 mg-manganese/g-sand)

Flow rate (mL/min)	Bohart-Adams parameters	
	a_{qs} (mg/L)	r_{BA} (L/(mg.min)
81.91	19.3427	0.0390
74.40	21.3025	0.0515
55.01	21.4914	0.0455
37.78	21.1940	0.1510

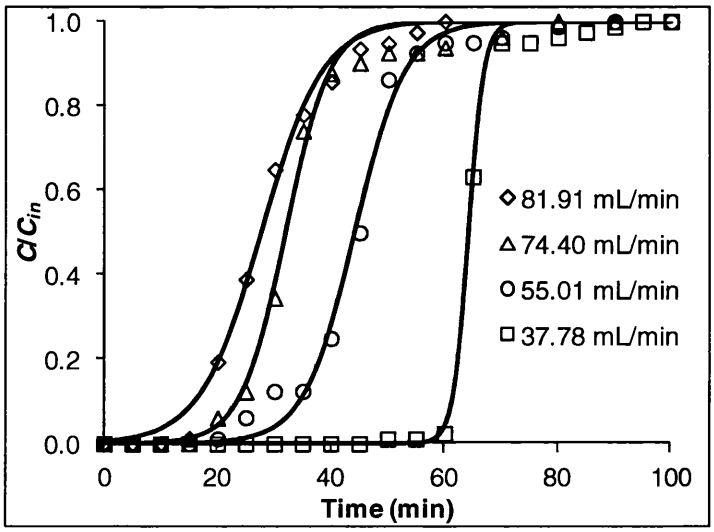

Figure 7.6 Best-fitting model simulations for various flow rates (C_{in} = 5 mg/L, H = 45 cm, m_{sand} = 920.59 g, d_{sand} = 0.850mm, manganese to sand ratio = 0.0709 mg-manganese/g-sand) (markers are experimental data; curves are best-fitting model simulations derived from Equation 3.63)

7.5 Model simulations for different diameters

Copper removals for different diameters (d_{sand} = 0.85, 0.71, 0.50 and 0.40 mm) were modelled based on the Bohart-Adams equation. The experimental conditions were the same as mentioned in Section 5.3.5. The results are shown in Table 7.4.

Table 7.4 shows that a_{qs} generally increased as diameter decreased. This relationship is clearly shown in Figure 7.7 (R^2 = 0.99). The increase of saturation capacity can be explained by the increased in surface area that resulted from a decrease in particle diameter. Table 7.4 also illustrates that r_{BA} values were between 0.004 – 0.039 (L/mg.min).

Figure 7.8 depicts the best fitting model simulations for various diameters. The calculated curves clearly overestimated the sharpness of the leading and trailing edges of the experimental C/C_{in} versus t. The reason of this has been stated previously in Section 7.2. A slow movement of C/C_{in} towards 1 was noticed and this is likely due to intra-particle diffusion involved in the mass transfer process (Cooney, 1998).

Table 7.4 Bohart-Adams parameters for various diameters of sand (C_{in} = 5 mg/L, H = 45 cm, m_{sand} = 875.51 g, manganese to sand ratio = 0.0709 mg-manganese/g-sand)

Diameter of sand (mm)	Bohart-Adams parameters	
	a_{qs} (mg/L)	r_{BA} (L/(mg.min)
0.85	19.3427	0.0390
0.71	22.0916	0.0144
0.50	29.9174	0.0213
0.40	33.8263	0.0041

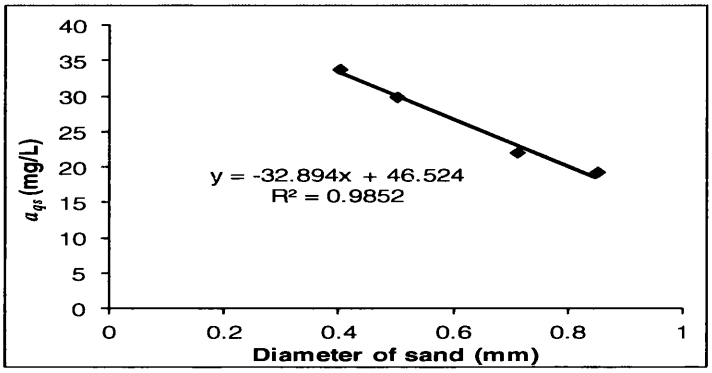

Figure 7.7 Correlation factor of Bohart-Adams parameter a_{qs} (mg/L) for various diameters of sand (C_{in} = 5 mg/L, H = 45 cm, m_{sand} = 875.51 g, manganese to sand ratio = 0.0709 mg-manganese/g-sand)

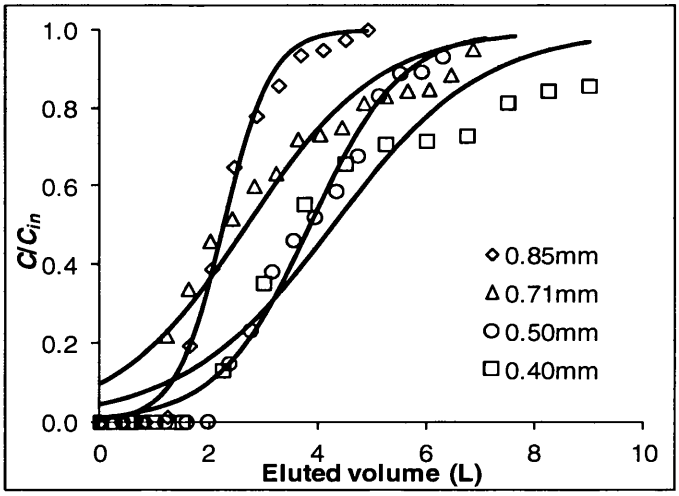

Figure 7.8 Best-fitting model simulations for various diameters of sand (C_{in} = 5 mg/L, H = 45 cm, m_{sand} = 875.51 g, manganese to sand ratio = 0.0709 mg-manganese/g-sand) (markers are experimental data; curves are best-fitting model simulations derived from Equation 3.63)

7.6 Model simulations for different manganese to sand ratios

Copper removals for different manganese to sand ratio (mg manganese/g sand = 0.00, 0.0709, 0.1261 and 0.1341) were modelled based on the Bohart-Adams equation. The experimental conditions were the same as mentioned in Section 5.3.6. The results are shown in Table 7.5.

Table 7.5 shows that a_{qs} increased as manganese to sand ratio increased. This relationship is clearly shown in Figure 7.9 (R^2 = 0.97). This occurs as the more manganese coated the sand particles, the higher the surface area produced resulting in the more active sites formed; hence the saturation capacity increased. Table 7.5 also illustrates that r_{BA} values were between 0.0004 – 0.0685 (L/mg.min).

Table 7.5 Bohart-Adams parameters for different manganese to sand ratios ratios (Q = 80.69 mL/min, C_{in} = 20 mg/L, H = 45 cm, m_{sand} = 884.49 g, d_{sand} = 0.71 mm)

Mn/sand ratio (mg-Mn/g-sand)	Bohart-Adams parameters	
	a_{qs} (mg/L)	r_{BA} (L/(mg.min)
0.00	8.9340	0.0685
0.0709	84.3821	0.0050
0.1261	221.4965	0.0006
0.1341	607.8459	0.0004

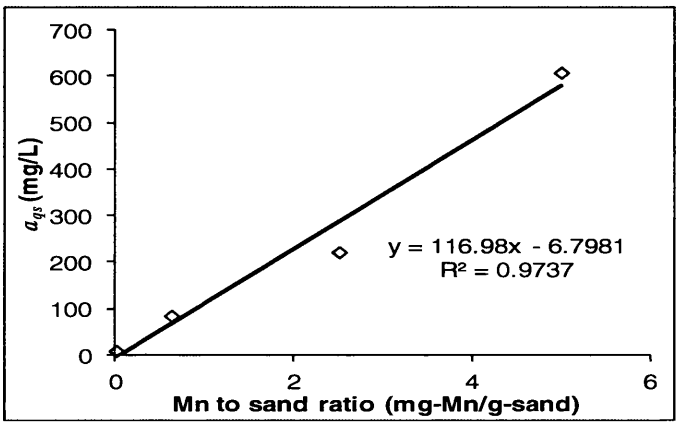

Figure 7.9 Correlation factor of Bohart-Adams parameter a_{qs} (mg/L) for various manganese to sand ratios (Q = 80.69 mL/min, C_{in} = 20 mg/L, H = 45 cm, m_{sand} = 884.49 g, d_{sand} = 0.71 mm)

Figures 7.10 (a – b) depicts the best fitting model simulations for different manganese to sand ratios. The calculated curves apparently overestimated the sharpness of the leading and trailing edges of the experimental C/C_{in} versus t. A slow movement of C/C_{in} towards 1 was occurred that might be due to intra-particle diffusion was involved in the mass transfer process (Cooney, 1998) as confirmed earlier in Section 5.2.2.5.

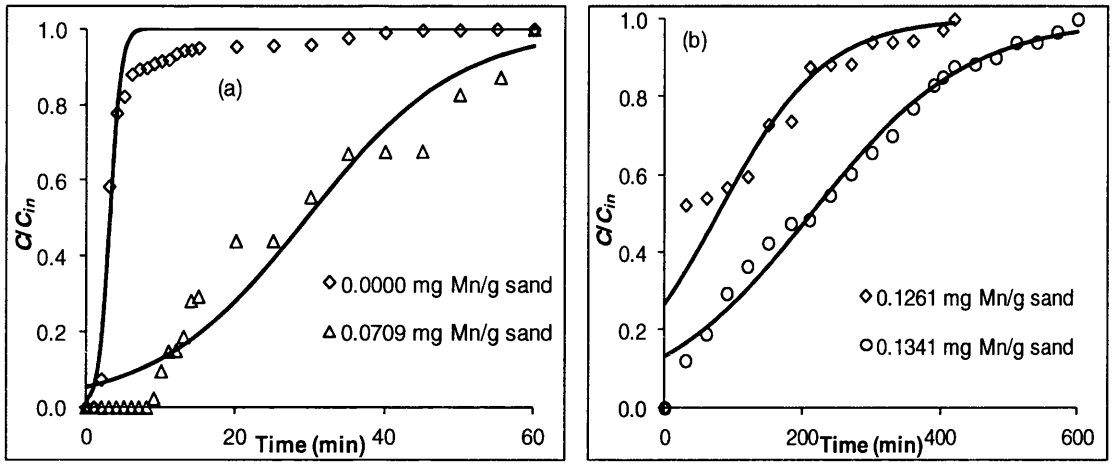

Figure 7.10 Best-fitting model simulations for various manganese to sand ratios sand (Q = 80.69 mL/min, C_{in} = 20 mg/L, H = 45 cm, m_{sand} = 884.49 g, d_{sand} = 0.71 mm) (markers are experimental data; curves are best-fitting model simulations derived from Equation 3.63): (a) 0 and 0.0709 mg Mn/g sand (b) 0.1261 and 0.1341 mg Mn/g sand

7.7 Model simulations for different times of reusing sand bed

Copper removals for different times of reusing sand bed (Reused-0, Reused-1, and Reused- 2) were modelled based on the Bohart-Adams equation. The experimental conditions were the same as mentioned in Section 5.3.7. The results are shown in Table 7.6. Table 7.6 shows that a_{qs} decreased as reusing times increased. This occurs as the more sand bed was reused the more manganese leached out (Section 5.3.7) resulted in a decrease in the saturation capacity. Table 7.6 also illustrates that r_{BA} values were between 0.0002 – 0.0003(L/mg.min). Figure 7.11 depicts the best fitting model simulations for various times of reusing sand bed. C/C_{in} for all cases $\neq$ 1 due to time constraints.

A slow movement of C/C_{in} towards 1 was clearly appeared resulting from intra-particle diffusion occurred in the mass transfer process (Cooney, 1998).

Table 7.6 Bohart-Adams parameters for different times of reusing sand bed bed (Q = 25.01 mL/min, C_{in} = 20 mg/L, H = 45 cm, m_{sand} = 906.19 g, d_{sand} = 0.71 mm, manganese to sand ratio = 0.0709 mg-manganese/g-sand)

Reusing time of sand bed material	Bohart-Adams parameters	
	a_{qs} (mg/L)	r_{BA} (L/(mg.min)
Reused-0	575.0708	0.0003
Reused-1	293.7356	0.0003
Reused-2	267.6457	0.0002

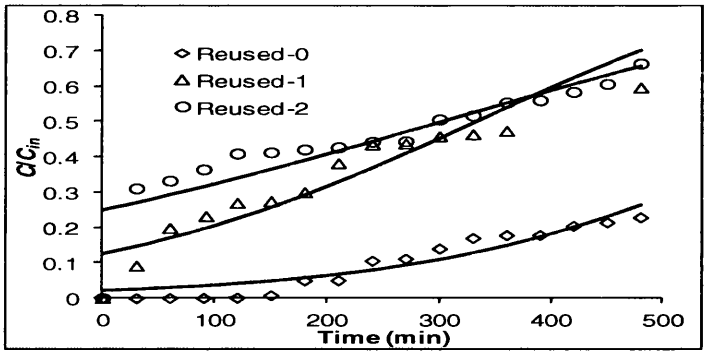

Figure 7.11 Best-fitting model simulations for various times of reusing sand bed (Q = 25.01 mL/min, C_{in} = 20 mg/L, H = 45 cm, m_{sand} = 906.19 g, d_{sand} = 0.71 mm, manganese to sand ratio = 0.0709 mg-manganese/g-sand) (markers are experimental data; curves are best-fitting model simulations derived from Equation 3.63)

7.8 Model simulations for individual element under optimal conditions

The removal of individual element under optimal conditions was modelled based on the Bohart-Adams equation. The experimental conditions were the same as mentioned in Section 6.1.1. Table 7.7 shows that the order of a_{qs} is Cu > Mn > Ni > Zn which is different from that occurred in Section 6.1.1. This may be due to the competition between Ni and Zn in binding onto the adsorbent in which the occurrence of Zn increased the binding of Ni onto the adsorbent (Eisler, 2007). r_{BA} values were between 0.0009 – 0.0115 (L/mg.min) (Table 7.7).

The best fitting model simulations were shown in Figure 7.12. The curve of copper is not formed as $C/C_{in} \leq 0.06$; this happens as the time period was only 180 min. A slow movement of C/C_{in} towards 1 was clearly appeared in the figure.

Table 7.7 Bohart-Adams parameters for individual element under optimal conditions (C_{in} = 20 mg/L, Q_{in} = 25.01 mL/min, d_{sand} = 0.400 mm, H = 450 mm, m_{sand} = 869.77 g, manganese to sand ratio = 0.0709 mg-manganese/g-sand)

Element	Bohart-Adams parameters	
	a_{qs} (mg/L)	r_{BA} (L/(mg.min)
Copper	283.5229	0.0115
Manganese	8.416722	0.0024
Zinc	-37.5845	0.0009
Nickel	-36.7995	0.0024

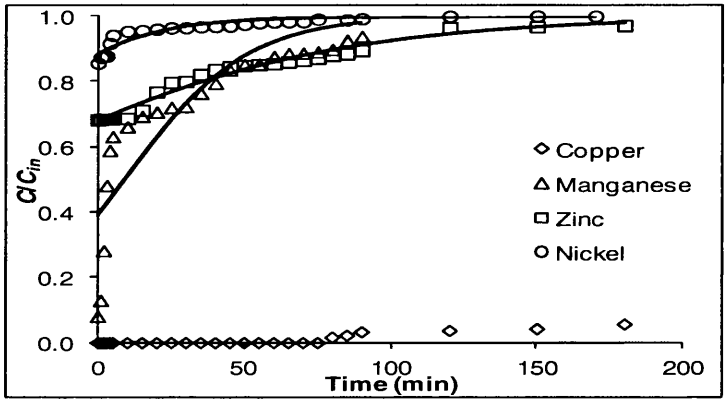

Figure 7.12 Best-fitting model simulations for individual metal under optimal conditions (C_{in} = 20 mg/L, Q_{in} = 25.01 mL/min, d_{sand} = 0.400 mm, H = 450 mm, m_{sand} = 869.77 g, manganese to sand ratio = 0.0709 mg-manganese/g-sand) markers are experimental data; curves are best-fitting model simulations derived from Equation 3.63)

7.9 Conclusions

Bohart-Adams model was used to describe the performance of AUSF in removing copper at different conditions and removing individual elements under optimal conditions.

To obtain the linear relationship between t and $ln\ (C_{in}/C\text{-}1)/C_{in}$, Equation 3.63 is fitted directly to the experimental data by Data Solver function in Microsoft Excel 2007 in order to calculate a_{qs} and r_{BA}.

The results showed that a_{qs} increased as input concentration (R^2 = 0.69), flow rate, diameter (R^2 = 0.99), reusing times decreased, and as height and manganese to sand ratio (R^2 = 0.97) increased. This is confirmed by the results obtained in Section 5.3.

In all cases, the Bohart-Adams model could not perfectly model the metal removals. This may be due to the fact that the Bohart-Adams model does not clearly constitute in the phenomenon of intra-particle diffusion since the model employs a quasi chemical kinetic rate expression to illustrate mass transfer (Ruthven, 1984; Chu and Hashim, 2007). The approximation of Bohart-Adams model produces a symmetrical, sigmoidal curve (Chu and Hashim, 2007); while the experimental data formed nonlinear curves resulted from a slow move of C/C_{in} towards 1 that is usually noticed in liquid phase adsorption where intra-particle diffusion is the principal mass transfer process (Cooney, 1998). The role of intra-particle diffusion as the rate-limiting step has been confirmed earlier in Section 5.2.2.

The modelling of the removal of individual element under optimal conditions (C_{in} = 20 mg/L) using Bohart-Adams equation showed that the order of a_{qs} is copper > manganese > nickel > zinc.

CHAPTER 8

CONCLUSIONS AND RECOMMENDATIONS

8.1 Conclusions

In this study an activated unsaturated sand filter (AUSF) was successfully developed. Activation of the sand was made by coating the sand with potassium permanganate. Activated sand particle characterisation was obtained through sieve analysis, BET surface area, SEM/EDX, acid/alkali resistance tests, point of zero charge, porosity and acid digestion analysis; while sand bed characterisation was done by tracer studies.

Sand was sieved to 0.850mm, 0.710 mm, 0.500mm and 0.400mm sand particle size. The porosity of sand is in the range of (36.92-38.04)%. The BET and SEM/EDX results support the assumed mechanisms of copper removal and also the results of the metal removals.

The acid and alkali resistance tests showed that a careful control of pH higher than 4.5 assures high resistance to manganese leaching as proven by acid digestion analysis and AUSF results. However, the results from batch studies showed that manganese coated sand was fragile under higher shaker speed ($r \geq 150$ rpm) and particularly at low pH (≤ 3) as more manganese leached compared to the acid alkali resistance test. Acid digestion analysis showed that the amount of manganese on the surface of the sand was 0.0709, 0.1261 and 0.1341 mg Mn/g sand respectively.

The point of zero charge (pzc) for the coated sand occurred at pH=7.75. Coating the sand apparently resulted in increasing pH (pH for uncoated sand = 7.3, for coated sand = 7.81).

Tracer studies showed that the flow approached plug flow but with low dispersion which validated the AUSF used to describe the observed experimental results.

Adsorption of copper onto the manganese coated sand may occur in one layer as Langmuir type 1 model was best fitted to model the copper removal in all cases of different initial concentrations. This favourable sorption of copper was also confirmed by the obtained value of R_L ($0 < R_L < 1$). In addition, chemisorptions were assumed to be involved in the removal of copper as shown by the well fitted of the pseudo second order type 1 model in all different conditions. Moreover, intra particle diffusion was assumed to be involved in the removal of copper as confirmed by the R^2 values of Weber and Morris. This thus suggests that the boundary layer (film) did not control the sorption process of copper as confirmed by the well fitted of the Bangham model, the results obtained from the column studies and the not perfectly fitted of Bohart-Adams equation to model the column behaviour. The results from the column studies showed that solid-phase mass transfer controlled the process and that adsorption was significant at low inlet concentrations; while precipitation was significant at greater inlet concentrations. The Bohart-Adams model could not perfectly model the metal removals as the experimental data formed nonlinear curves resulted from a slow move of C/C_{in} towards 1 that is usually noticed in liquid phase adsorption where intra-particle diffusion is the principal mass transfer process.

Aeration (i.e. unsaturated condition) played a significant role in enhancing activated sand filter performances in removing copper than the saturated condition. The AUSF also showed advantage as no pH adjustment was necessary. Moreover, the column studies also showed that operating at lower flow rates gave better removal percentages and proved that when the flow was introduced at the top of the column, the sand bed was not fully submerged in water, hence the system operated under unsaturated conditions.

The study also showed that the performance of AUSF increased as input concentration, flow rate, diameter of the sand particles, and reusing sand bed material decreased. Increasing the manganese to sand ratio and height of sand bed column, on the other hand, resulting in an increase in the performance of AUSF. The decrease in the performance as reusing sand bed material increased may be due to the more manganese was eluted resulting from the washing and drying processes of the coated sand after each used. The results obtained from column studies confirmed the results from batch studies.

Based on the pH values, precipitation, electrostatic attraction, adsorption/ion exchange/complex ion formation were proposed to contribute to the removal of metals by AUSF. The proposed reactions occurred in the AUSF are in line with the results obtained from the batch studies.

The pH theory was assumed to be best applied in the removal of individual, mixed metals, and mixed metals in waste water. The order of removal for metals for individual metal and mixed metals under optimal conditions was Cu > Mn > Zn > Ni. The order for individual metal removals was confirmed by Bohart-Adams equation that showed the similar order for its *a* values. For the metals in waste water this order became Cu > Ni > Zn > Mn. This may be due to the concentrations of manganese and zinc were smaller thus their removal capacity became lower. This order was based on the removals order with regard to the precipitation, electrostatic attraction, ion exchange and surface complexation process and the removal rate, saturation time, t_{95}, q_{Mmax}/q_{Mn}, the decrease in effluent concentration, mass retained, and removal capacity.

The assumed metals speciation occurred in the water at certain pH are as follows. The dominant species for pH ≤ pH critical of metals, may be that of $M^{2+}{}_{(aq)}$ or $M(OH)^{2+}{}_{(aq)}$ whereas for pH > pH critical, may be that of $M(OH)_{2\,(s)}$. Other species for pH ≤ pH critical of metals, may be that of $\equiv Mn{-}O^{-}M^{2+}$ or $(\equiv Mn{-}O^{-})_2M^{2+}$ or $\equiv Mn{-}OMOH$ while for pH > pH critical, may be that of $M^{2+}{}_{(aq)}$ or $M(OH)^{2+}{}_{(aq)}$ or $\equiv Mn{-}O^{-}M^{2+}$ or $(\equiv Mn{-}O^{-})_2M^{2+}$ or $\equiv Mn{-}OMOH$.

8.2 Recommendations

As the exact role of oxygen in the removal of metals in the AUSF has still not observed yet, thus future studies are required to find out the role of oxygen in the metal removal processes in the AUSF.

The DO contents during this experiment did not measured due to the difficulty in performing the DO measurements. Therefore, future investigations are needed to measure these DO contents.

As the peaks in the C-curves have been missed, future tracer studies are required to measure the peaks so as the results from the tracer studies would close to the plug flow model.

Future experiments regarding the surface area morphology by SEM are required to obtain the same magnification of the samples of the sand so as the comparison between samples could be made and validated. In addition, the different morphology in mixed metals both in artificial and real waste water obtained is challenging to be investigated in the future.

As the procedure of cleaning the used coated sand is assumed to affect the strength attachment of the permanganates, thus this procedure has to be studied so as the coated sand can be reused several times.

The Bohart-Adams model used in this study could not perfectly predict the column behaviour therefore future studies are required to find out the model that can accurately predict the AUSF column behaviour.

Future studies are needed to investigate the performance of AUSF in removing real waste water since this study merely observed the artificial waste water.

Characterisations of the coated sand using XRD analysis are required in order to find out the chemical composition of the sand since this study only investigated the element composition of the coated sand samples.

A larger AUSF is required to treat manganese, zinc and nickel in waters as the removal of these metals were lower compared to that of the copper removal.

The cost and benefit study is required to investigate the economic value of this AUSF in practical applications.

Comparative analysis with other technologies is required to observe the advantage and disadvantages of using this AUSF in practical applications.

BIBLIOGRAPHY

Ahammed M.M. and Meera V. (2010). Metal oxide/hydroxide-coated dual-media filter for simultaneous removal of bacteria and heavy metals from natural waters. *Journal of Hazardous Materials* **181**(1-3), 788-793.

Al-Layla M.A., S. A. and Middlebrooks E.J. (1978). Water Supply Engineering Design. Ann Arbor Science Publisher, Inc., Michigan, USA.

Ali N., Hameed A. and Ahmed S. (2009). Physicochemical characterization and Bioremediation perspective of textile effluent, dyes and metals by indigenous Bacteria. *Journal of Hazardous Materials* **164**(1), 322-328.

Alkan M., Kalay B., Dogan M. and Demirbas O. (2008). Removal of copper ions from aqueous solutions by kaolinite and batch design. *Journal of Hazardous Materials* **153**(1-2), 867-876.

Allen T. (1975). Particle Size Measurement. Chapman and Hall Ltd., London.

Alley E.R. (2007). Water Quality Control Handbook. McGraw-Hill Co., Inc., Alexandria, Virginia.

Alyuz B. and Veli S. (2009). Kinetics and equilibrium studies for the removal of nickel and zinc from aqueous solutions by ion exchange resins. *Journal of Hazardous Materials* **167**(1-3), 482-488.

American Planning Association (2006) Planning and urban design standards, John Wiley & Sons, Inc., Hoboken, New Jersey.

Atsushi T. (2003). Manganese action in brain function. *Brain Research Reviews* **41**(1), 79-87.

Balkaya N.and Cesur H. (2008). Adsorption of cadmium from aqueous solution by phosphogypsum. *Chemical Engineering Journal* **140**(1-3), 247-254.

Benaissa H. and Elouchdi M.A. (2007). Removal of copper ions from aqueous solutions by dried sunflower leaves. *Chemical Engineering and Processing* **46**(7), 614-622.

Bohart G.S. and Adams E.Q. (1920). Some aspects of the behavior of charcoal with respect to chlorine. *Journal of the Franklin Institute* **189**(5), 669.

Bojic A.L., Bojic D. and Andjelkovic T. (2009). Removal of Cu^{2+} and Zn^{2+} from model wastewaters by spontaneous reduction-coagulation process in flow conditions. *Journal of Hazardous Materials* **168**(2-3), 813-819.

Borah D., Satokawa S., Kato S. and Kojima T. (2009). Sorption of As(V) from aqueous solution using acid modified carbon black. *Journal of Hazardous Materials* **162**(2-3), 1269-1277.

Boujelben N., Bouzid J. and Elouear Z. (2009). Adsorption of nickel and copper onto natural iron oxide-coated sand from aqueous solutions: Study in single and binary systems. *Journal of Hazardous Materials* **163**(1), 376-382.

Bouzid J., Elouear Z., Ksibi M., Feki A. and Montiel A. (2008). A study on removal characteristics of copper from aqueous solution by sewage sludge and pomace ashes. *Journal of Hazardous Materials* **152**(2), 838-845.

Bowles J.E. (1979). Physical and Geotechnical Properties of Soils. McGraw-Hill Book Company, New York.

Broder M.V. and Byron J.C. (2005) Water treatment plant design, American Water Works Association, American Society of Civil Engineers. Baruth, E.E. (ed), p. 9.18, McGraw-Hill, New York.

Burger M.S., Mercer S.S., Shupe G.D. and Gagnon G.A. (2008). Manganese removal during bench-scale biofiltration. *Water Research* **42**(19), 4733-4742.

Calvo B., Canoira L., Morante F., Martinez-Bedia J.M., Vinagre C., Garcia-Gonzalez J.E., Elsen J. and Alcantara R. (2009). Continuous elimination of Pb^{2+}, Cu^{2+}, Zn^{2+}, H^{+} and NH^{4+} from acidic waters by ionic exchange on natural zeolites. *Journal of Hazardous Materials* **166**(2-3), 619-627.

Canterino M., Di Somma I., Marotta R. and Andreozzi R. (2008). Kinetic investigation of Cu(II) ions photoreduction in presence of titanium dioxide and formic acid. *Water Research* **42**(17), 4498-4506.

Carvalho W.A., Vignado C. and Fontana J. (2008). Ni(II) removal from aqueous effluents by silylated clays. *Journal of Hazardous Materials* **153**(3), 1240-1247.

Chen H., Zhao Y.G. and Wang A.Q. (2007a). Removal of Cu(II) from aqueous solution by adsorption onto acid-activated palygorskite. *Journal of Hazardous Materials* **149**, 346-354.

Chen Q., Luo Z., Hills C., Xue G. and Tyrer M. (2009). Precipitation of heavy metals from wastewater using simulated flue gas: Sequent additions of fly ash, lime and carbon dioxide. *Water Research* **43**(10), 2605-2614.

Chen S.S., Cheng C.Y., Li C.W., Chai P.H. and Chang Y.M. (2007b). Reduction of chromate from electroplating wastewater from pH 1 to 2 using fluidized zero valent iron process. *Journal of Hazardous Materials* **142**(1-2), 362-367.

Chen Z., Ma W. and Han M. (2008). Biosorption of nickel and copper onto treated alga (Undaria pinnatifida): Application of isotherm and kinetic models. *Journal of Hazardous Materials* **155**(1-2), 327-333.

Chinn T.D. (2003) Environmental Engineering (5th Edition). Salvato, J.A., Nemerow, N. L. Agardy, F. J. (ed), pp. 376, 388, 424-428, John Wiley & Sons, New Jersey.

Cho B.Y. (2005). Iron removal using an aerated granular filter. *Process Biochemistry* **40**(10), 3314-3320.

Choksi P.M. and Joshi V.Y. (2007). Adsorption kinetic study for the removal of nickel (II) and aluminum (III) from an aqueous solution by natural adsorbents. *Desalination* **208**(1-3), 216-231.

Choo K.H., Lee H. and Choi S.J. (2005). Iron and manganese removal and membrane fouling during UF in conjunction with prechlorination for drinking water treatment. *Journal of Membrane Science* **267**(1-2), 18-26.

Chu K.H. (2010). Fixed bed sorption: Setting the record straight on the Bohart-Adams and Thomas models. *Journal of Hazardous Materials* **177**(1-3), 1006-1012.

Chu K.H. and Hashim M.A. (2007). Copper biosorption on immobilized seaweed biomass: Column breakthrough characteristics. *Journal of Environmental Sciences* **19**(8), 928-932.

Chutia P., Kato S., Kojima T. and Satokawa S. (2009). Adsorption of As(V) on surfactant-modified natural zeolites. *Journal of Hazardous Materials* **162**(1), 204-211.

Cojocaru C. and Zakrzewska-Trznadel G. (2007). Response surface modeling and optimization of copper removal from aqua solutions using polymer assisted ultrafiltration. *Journal of Membrane Science* **298**(1-2), 56-70.

Company R.M. (1990) Handbook of ground water development, John Wiley & Sons, Inc., USA.

Cooney D.O. (1998). Adsorption design for waste water treatment. Lewis Publishers, Boca Raton.

Datta R. and Sarkar D. (2005) Water Encyclopedia Volumes 1-5. Water Quality and Resource Development. Keeley, J., Lehr, J. and Kingery III, T.B. (eds), pp. 5:369-365:370, John Wiley & Sons, Inc., New Jersey.

David Ball Specialist Sands (2009) Standard Reference Materials BS 1881-131: 1998.

Devi R., Alemayehu E., Singh V., Kumar A. and Mengistie E. (2008). Removal of fluoride, arsenic and coliform bacteria by modified homemade filter media from drinking water. *Bioresource Technology* **99**(7), 2269-2274.

Diels L., Spaans P.H., Van Roy S., Hooyberghs L., Ryngaert A., Wouters H., Walter E., Winters J., Macaskie L., Finlay J., Pernfuss B., Woebking H., Pumpel T. and Tsezos M. (2003). Heavy metals removal by sand filters inoculated with metal sorbing and precipitating bacteria. *Hydrometallurgy* **71**(1-2), 235-241.

Dimirkou A. (2007). Uptake of Zn^{2+} ions by a fully iron-exchanged clinoptilolite. Case study of heavily contaminated drinking water samples. *Water Research* **41**(12), 2763-2773.

Dizge N., Keskinler B. and Barlas H. (2009). Sorption of Ni(II) ions from aqueous solution by Lewatit cation-exchange resin. *Journal of Hazardous Materials* **167**(1-3), 915-926.

Doula M.K. (2006). Removal of Mn^{2+} ions from drinking water by using Clinoptilolite and a Clinoptilolite-Fe oxide system. *Water Research* **40**(17), 3167-3176.

Doula M.K. (2009). Simultaneous removal of Cu, Mn and Zn from drinking water with the use of clinoptilolite and its Fe-modified form. *Water Research* **43**(15), 3659-3672.

Eisler R. (2007). Eisler's Encyclopedia of Environmentally Hazardous Priority Chemicals. Elsevier, Amsterdam.

Erdem E., Karapinar N. and Donat R. (2004). The removal of heavy metal cations by natural zeolites. *Journal of Colloid and Interface Science* **280**(2), 309-314.

Eren E. (2008). Removal of copper ions by modified Unye clay, Turkey. *Journal of Hazardous Materials* **159**(2-3), 235-244.

Eren E. and Afsin B. (2008). An investigation of Cu(II) adsorption by raw and acid-activated bentonite: A combined potentiometric, thermodynamic, XRD, IR, DTA study. *Journal of Hazardous Materials* **151**(2-3), 682-691.

Fahim A. (2009) Level-3 Geometric Correction of FORMOSAT-2 Satellite Imagery and Efficient Image Resampling, National University of Sciences and Technology, Rawalpindi.

Farooq R., Wang Y., Lin F., Shaukat S.F., Donaldson J. and Chouhdary A.J. (2002). Effect of ultrasound on the removal of copper from the model solutions for copper electrolysis process. *Water Research* **36**(12), 3165-3169.

Foth H.D. (1990). Fundamentals of Soil Science. John Wiley & Sons, New York.

Fu F.L., Chen R.M. and Xiong Y. (2007). Comparative investigation of N,N '-bis-(dithiocarboxy)piperazine and diethyldithiocarbamate as precipitants for Ni(II) in simulated wastewater. *Journal of Hazardous Materials* **142**(1-2), 437-442.

Ghaedi M., Ahmadi F. and Soylak M. (2007). Preconcentration and separation of nickel, copper and cobalt using solid phase extraction and their determination in some real samples. *Journal of Hazardous Materials* **147**(1-2), 226-231.

Ghodbane I., Nouri L., Hamdaoui O. and Chiha M. (2008). Kinetic and equilibrium study for the sorption of cadmium(II) ions from aqueous phase by eucalyptus bark. *Journal of Hazardous Materials* **152**(1), 148-158.

Gibert O., de Pablo J., Cortina J.L. and Ayora C. (2005). Sorption studies of Zn(II) and Cu(II) onto vegetal compost used on reactive mixtures for in situ treatment of acid mine drainage. *Water Research* **39**(13), 2827-2838.

Goodhew P.J., Humphreys J. and Beanland R. (2001). Electron microscopy and analysis. Taylor & Francis, London.

Greenwood N.N. and Earnshaw A. (1997). Chemistry of the Elements. Butterworth Heinemann, Oxford.

Guan X., Ma J., Dong H. and Jiang L. (2009). Removal of arsenic from water: Effect of calcium ions on As(III) removal in the KMnO4-Fe(II) process. *Water Research* **43**(20), 5119-5128.

Guerra D.L., Airoldi C., Lemos V.P. and Angelica R.S. (2008). Adsorptive, thermodynamic and kinetic performances of Al/Ti and Al/Zr-pillared clays from the Brazilian Amazon region for zinc cation removal. *Journal of Hazardous Materials* **155**(1-2), 230-242.

Guven D.E. and Akinci G. (2011). Comparison of acid digestion techniques to determine heavy metals in sediment and soil samples. *Gazi University Journal of Science* **24**(1), 29-34.

Hach Company (2010) Copper USEPA Bicinchoninate Method, Hach Company, USA.

Halim M.A., Majumder R.K., Nessa S.A., Hiroshiro Y., Uddin M.J., Shimada J. and Jinno K. (2009). Hydrogeochemistry and arsenic contamination of groundwater in the Ganges Delta Plain, Bangladesh. *Journal of Hazardous Materials* **164**(2-3), 1335-1345.

Hamdaoui O. (2009). Removal of copper(II) from aqueous phase by Purolite C100-MB cation exchange resin in fixed bed columns: Modeling. *Journal of Hazardous Materials* **161**(2-3), 737-746.

Han R., Zou L., Zhao X., Xu Y., Xu F., Li Y. and Wang Y. (2009). Characterization and properties of iron oxide-coated zeolite as adsorbent for removal of copper(II) from solution in fixed bed column. *Chemical Engineering Journal* **149**(1-3), 123-131.

Han R., Zou W., Zhang Z., Shi J. and Yang J. (2006a). Removal of copper(II) and lead(II) from aqueous solution by manganese oxide coated sand: I. Characterization and kinetic study. *Journal of Hazardous Materials* **137**(1), 384-395.

Han R.P., Zou W.H., Li H.K., Li Y.H. and Shi J. (2006b). Copper(II) and lead(II) removal from aqueous solution in fixed-bed columns by manganese oxide coated zeolite. *Journal of Hazardous Materials* **137**(2), 934-942.

Heidmann I. and Calmano W. (2008). Removal of Zn(II), Cu(II), Ni(II), Ag(I) and Cr(VI) present in aqueous solutions by aluminium electrocoagulation. *Journal of Hazardous Materials* **152**(3), 934-941.

Hernandez-Bonilla D., Schilmann A., Montes S., Rodriguez-Agudelo Y., Rodriguez-Dozal S., Solis-Vivanco R., Rios C. and Riojas-Rodriguez H. (2011). Environmental exposure to manganese and motor function of children in Mexico. *NeuroToxicology* **32**(5), 615-621.

Hitachi (2002). Instruction Manual for Model S-4800 Field Emission Scanning Electron Microscope. Hitachi High-Technologies Corporation, Japan.

Hu P.Y., Hsieh Y.H., Chen J.C. and Chang C.Y. (2004). Characteristics of manganese-coated sand using SEM and EDAX analysis. *Journal of Colloid and Interface Science* **272**(2), 308-313.

Huisman P.d.i.L. (2004) Mechanical filtration, Delft University of Technology.

Indorama S.T. (2003) Environmental Management and Control Effort Document. Purwakarta, West Java, Indonesia. [Dokumen Upaya Pengelolaan Lingkungan (UKL) dan Upaya Pemantauan Lingkungan (UPL)]

Jha M.K., Van Nguyen N., Lee J.C., Jeong J. and Yoo J.M. (2009). Adsorption of copper from the sulphate solution of low copper contents using the cationic resin Amberlite IR 120. *Journal of Hazardous Materials* **164**(2-3), 948-953.

Jin Y., Chu Y. and Li Y. (2000). Virus removal and transport in saturated and unsaturated sand columns. *Journal of Contaminant Hydrology* **43**(2), 111-128.

Jones C.J. (2002). Basic Concepts in Chemistry II. d-and f-Block Chemistry. The Royal Society of Chemistry, Exeter.

Katsoyiannis I.A. and Zouboulis A.I. (2004). Biological treatment of Mn(II) and Fe(II) containing groundwater: kinetic considerations and product characterization. *Water Research* **38**(7), 1922-1932.

Kaw A. and Keteltas M. (2009) Trapezoidal Rule, University of South Florida, Florida.

Kawamura S. (2000) Integrated Design and Operation of Water Treatment Facilities, John Wiley & Sons, Canada.

Khosravi J. and Alamdari A. (2009). Copper removal from oil-field brine by coprecipitation. *Journal of Hazardous Materials* **166**(2-3), 695-700.

Kirby C.S. and Brady J.A.E. (1998). Field determination of Fe^{2+} oxidation rates in acid mine drainage using a continuously-stirred tank reactor. *Applied Geochemistry* **13**(4), 509-520.

Kotz J.C., Treichel, P. M. & Weaver, G. C. (2006). Chemistry & Chemical Reactivity. Thomson Learning, Inc., Australia.

Kuechler R. and Noack K. (2007). Comparison of the solution behaviour of a pyriteâ€"calcite mixture in batch and unsaturated sand column. *Journal of Contaminant Hydrology* **90**(3-4), 203-220.

Kumar U. and Bandyopadhyay M. (2006). Sorption of cadmium from aqueous solution using pretreated rice husk. *Bioresource Technology* **97**(1), 104-109.

Kundu S. and Gupta A.K. (2007). Adsorption characteristics of As(III) from aqueous solution on iron oxide coated cement (IOCC). *Journal of Hazardous Materials* **142**(1-2), 97-104.

Laus R., Geremias R., Vasconcelos H.L., Laranjeira M.C.M. and Favere V.T. (2007). Reduction of acidity and removal of metal ions from coal mining effluents using chitosan microspheres. *Journal of Hazardous Materials* **149**, 471-474.

Lazaridis N.K., Peleka E.N., Karapantsios T.D. and Matis K.A. (2004). Copper removal from effluents by various separation techniques. *Hydrometallurgy* **74**(1-2), 149-156.

Lee C.I., Yang W.F. and Chiou C.S. (2006). Utilization of water clarifier sludge for copper removal in a liquid fluidized-bed reactor. *Journal of Hazardous Materials* **129**(1-3), 58-63.

Lee C.I., Yang W.F. and Hsieh C.I. (2004). Removal of copper(II) by manganese-coated sand in a liquid fluidized-bed reactor. *Journal of Hazardous Materials* **114**(1-3), 45-52.

Lee L.Y., Ong S.L., Ng H.Y., Hu J.Y. and Koh Y.N. (2008). Simultaneous ammonium-nitrogen and copper removal, and copper recovery using nitrifying biofilm from the Ultra-Compact Biofilm Reactor. *Bioresource Technology* **99**(14), 6614-6620.

Lee M., Paik I.S., Kim I., Kang H. and Lee S. (2007). Remediation of heavy metal contaminated groundwater originated from abandoned mine using lime and calcium carbonate. *Journal of Hazardous Materials* **144**(1-2), 208-214.

Lenntech B.V. (2009). Water Treatment Solutions, Lenntech B.V., Delft, Netherlands.

Lesmana S.O., Febriana N., Soetaredjo F.E., Sunarso J. and Ismadji S. (2009). Studies on potential applications of biomass for the separation of heavy metals from water and wastewater. *Biochemical Engineering Journal* **44**(1), 19-41.

Levenspiel O. (1999). Chemical Reaction Engineering. John Wiley & Sons, New York.

Liu C., Bai R. and San Ly Q. (2008). Selective removal of copper and lead ions by diethylenetriamine-functionalized adsorbent: Behaviors and mechanisms. *Water Research* **42**(6-7), 1511-1522.

Liu C. and Evett J.B. (1997). Soil Properties Testing, Measurement and Evaluation. Prentice Hall, New Jersey.

Liu C.X. and Bai R.B. (2006). Adsorptive removal of copper ions with highly porous chitosan/cellulose acetate blend hollow fiber membranes. *Journal of Membrane Science* **284**(1-2), 313-322.

Logsdon G., Hess A. and Horsley M. (1999) Water Quality and Treatment - A Handbook of Community Water Supplies (5th Edition) American Water Works Association. Letterman, R.D. (ed), pp. 3.6-3.7, McGraw-Hill, New York.

Magalhaes M.C.F. (2002). Arsenic. An environmental problem limited by solubility. *Pure and Applied Chemistry* **74**(10), 1843-1850.

McGhee T.J. (1991). Water Supply and Sewerage. McGraw-Hill Book Co, New York.

Medircio S.N., Leao V.A. and Teixeira M.C. (2007). Specific growth rate of sulfate reducing bacteria in the presence of manganese and cadmium. *Journal of Hazardous Materials* **143**(1-2), 593-596.

Mohan S. and Sreelakshmi G. (2008). Fixed bed column study for heavy metal removal using phosphate treated rice husk. *Journal of Hazardous Materials* **153**(1-2), 75-82.

Mondal P., Balomajumder C. and Mohanty B. (2007). A laboratory study for the treatment of arsenic, iron, and manganese bearing ground water using Fe^{3+} impregnated activated carbon: Effects of shaking time, pH and temperature. *Journal of Hazardous Materials* **144**(1-2), 420-426.

Montgomery D.C., Runger G.C. and Hubele N.F. (2007). Engineering Statistics. John Wiley & Sons, Inc.

Murphy V., Hughes H. and McLoughlin P. (2007). Cu(II) binding by dried biomass of red, green and brown macroalgae. *Water Research* **41**(4), 731-740.

Nadaroglu H., Kalkan E. and Demir N. (2009). Removal of Cu from aqueous solution using red mud. *Desalination* **In Press, Corrected Proof**.

National Centre for BiotechnologyInformation (2011) Wilson's Disease, Hepatolenticular Degeneration, U.S. National Library of Medicine, Bethesda MD, USA.

Neal C. and Robson A.J. (2000). A summary of river water quality data collected within the Land-Ocean Interaction Study: core data for eastern UK rivers draining to the North Sea. *Science of the Total Environment* **251**, 585-665.

Nilchi A., Hadjmohammadi M.R., Garmarodi S.R. and Saberi R. (2009). Studies on the adsorption behavior of trace amounts of Sr-90(2+), La-140(3+), Co-60(2+), Ni^{2+} and Zr^{4+} cations on synthesized inorganic ion exchangers. *Journal of Hazardous Materials* **167**(1-3), 531-535.

Ning R.Y. (2005) Water Encyclopedia, Volumes 1-5. Lehr, J.K., J.; Lehr, Janet (ed), p. 414, John Wiley & Sons.

Noh J.S. and Schwarz J.A. (1989). Estimation of the point of zero charge of simple oxides by mass titration. *Journal of Colloid and Interface Science* **130**(1), 157-164.

Noyes R. (1994a) Unit Operations in Environmental Engineering, p. 117, William Andrew Publishing/Noyes, New Jersey.

Noyes R. (1994b) Unit Operations in Environmental Engineering. Noyes, R. (ed), p. 87, William Andrew Publishing/Noyes, New Jersey.

Noyes R. (1994c) Unit Operations in Environmental Engineering. Noyes, R. (ed), p. 299, William Andrew Publishing/Noyes, New Jersey.

Oxford Instruments (2009). INCAEnergy Applications training notes. Oxford Instruments Analytical Bucks, UK.

Pacini V.A., Ingallinella A.M. and Sanguinetti G. (2005). Removal of iron and manganese using biological roughing up flow filtration technology. *Water Research* **39**(18), 4463-4475.

Pan B.C., Meng F.W., Chen X.Q., Pan B.J., Li X.T., Zhang W.M., Zhang X., Chen J.L., Zhang Q.X. and Sun Y. (2005). Application of an effective method in predicting breakthrough curves of fixed-bed adsorption onto resin adsorbent. *Journal of Hazardous Materials* **124**(1-3), 74-80.

Panayotova M.I. (2001). Kinetics and thermodynamics of copper ions removal from wastewater by use of zeolite. *Waste Management* **21**(7), 671-676.

Papageorgiou S.K., Katsaros F.K., Kouvelos E.P. and Kanellopoulos N.K. (2009). Prediction of binary adsorption isotherms of Cu^{2+}, Cd^{2+} and Pb^{2+} on calcium alginate beads from single adsorption data. *Journal of Hazardous Materials* **162**(2-3), 1347-1354.

Papandreou A., Stournaras C.J. and Panias D. (2007). Copper and cadmium adsorption on pellets made from fired coal fly ash. *Journal of Hazardous Materials* **148**, 538-547.

Paramarta R.B., Wardhana J.N.I., Sodikin I., Gana M., Budianto D., Suryodipuro L.M. and Widayati T. (1988) Activated un-saturated sand filter as an alternative to reduce Fe and Mn in water treatment [Saringan pasir kering aktif sebagai alternative untuk menurunkan Fe and Mn dalam pengolahan air minum], Bogor, Indonesia.

Paulino A.T., Guilherme M.R., Reis A.V., Tambourgi E.B., Nozaki J. and Muniz E.C. (2007). Capacity of adsorption of Pb^{2+} and Ni^{2+} from aqueous solutions by chitosan produced from silkworm chrysalides in different degrees of deacetylation. *Journal of Hazardous Materials* **147**, 139-147.

Perez-Quintanilla D., Sanchez A., del Hierro I., Fajardo M. and Sierra I. (2009). Preconcentration of Zn(II) in water samples using a new hybrid SBA-15-based material. *Journal of Hazardous Materials* **166**(2-3), 1449-1458.

Petrov S. and Nenov V. (2004). Removal and recovery of copper from wastewater by a complexation-ultrafiltration process. *Desalination* **162**, 201-209.

Pitcher S.K., Slade R.C.T. and Ward N.I. (2004). Heavy metal removal from motorway stormwater using zeolites. *Science of the Total Environment* **334-335**(0), 161-166.

Pouchou J. and Pichoir F. (1991). Electron Probe Quantitation. Plenum Press, New York, USA.

Quantachrome Instruments (2011) NOVAe Series Quantachrome, Quantachrome Corporation, Florida, USA.

Rachmawati S.D., Indrayani S. and Sururi M.R. (2004). Unstratified activated dry sand filter to reduce Fe and Mn concentrations in the groundwater treatment [Saringan pasir kering aktif unstratified untuk menurunkan konsentrasi Fe and Mn dalam pengolahan air tanah]. *National Institute of Technology [Institut Teknologi Nasional (ITENAS)] Journal* **10** (3), 121-128.

Rachmawati S.D., Malasari D.N. and Sururi M.R. (2006a) A stratified activated dry sand filter as an alternative to remove Fe and Mn concentrations in ground water treatment technology [Saringan pasir kering aktif stratified untuk menurunkan konsentrasi Fe and Mn dalam pengolahan air tanah], Bandung Institute of Technology, Bandung, West Java, Indonesia.

Rachmawati S.D., Mariana R. and Sururi M.R. (2006b) Activated dry sand filter with zeolit as an alternative to remove Fe and Mn in groundwater treatment [Saringan pasir kering aktif dengan zeolit sebagai alternative penurunan konsentrasi unsure Fe dan Mn dalam pengolahan air tanah] National Institute of Technology. [Institut Teknologi Nasional (ITENAS)], Bandung, Indonesia.

Rachmawati S.D., Rohaeni A. and Subrata R. (2005) Water polllution control manager reference book [Buku referensi manajer pengelolaan pencemaran air], Indonesian West Java Environmental Protection Agency, Bandung, Indonesia.

Reddad Z., Gerente C., Andres Y., Ralet M.-C., Thibault J.F. and Cloirec P.L. (2002a). Ni(II) and Cu(II) binding properties of native and modified sugar beet pulp. *Carbohydrate Polymers* **49**(1), 23-31.

Reddad Z., Gerente C., Andres Y. and Cloirec P.L. (2002b). Adsorption of several metal ions onto a low-cost biosorbent:kinetic and equilibrium studies. *Environmental Science & Technology* **36**(9), 2067-2073.

Ricordel S., Taha S., Cisse I. and Dorange G. (2001). Heavy metals removal by adsorption onto peanut husks carbon: characterization, kinetic study and modeling. *Separation and Purification Technology* **24**(3), 389-401.

Ruthven D.M. (1984). Principles of adsorption and adsorption processes. John Wiley & Sons, Inc., New York.

Rutledge S.O. and Gagnon G.A. (2002). Comparing crushed recycled glass to silica sand for dual media filtration. *J. Environ. Eng. Sci.* **1**, 349-358.

Salim R. and Abu El-Halawa R. (2002). Efficiency of dry plant leaves (MULCH) for removal of lead, cadmium and copper from aqueous solutions. *Process Safety and Environmental Protection* **80**(B5), 270-276.

Sarikaya H.Z. (1990). Contact aeration for iron removal - a theoretical assessment. *Water Research* **24**(3), 329-331.

Sarioglu M., Atay U.A. and Cebeci Y. (2005). Removal of copper from aqueous solutions by phosphate rock. *Desalination* **181**(1-3), 303-311.

Sarkar M., Sarkar A.R. and Goswami J.L. (2007). Mathematical modeling for the evaluation of zinc removal efficiency on clay sorbent. *Journal of Hazardous Materials* **149**(3), 666-674.

Sayed S.A., Saleh S.M. and Hasan E.E. (2005). Removal of some polluting metals from industrial water using chicken feathers. *Desalination* **181**(1-3), 243-255.

Sekhar K.C., Subramanian S., Modak J.M. and Natarajan K.A. (1998). Removal of metal ions using an industrial biomass with reference to environmental control. *International Journal of Mineral Processing* **53**(1-2), 107-120.

Sen T.K. and Sarzali M.V. (2008). Removal of cadmium metal ion (Cd^{2+}) from its aqueous solution by aluminium oxide (Al2O3): A kinetic and equilibrium study. *Chemical Engineering Journal* **142**(3), 256-262.

Shamspur T. and Mostafavi A. (2009). Application of modified multiwalled carbon nanotubes as a sorbent for simultaneous separation and preconcentration trace amounts of Au(III) and Mn(II). *Journal of Hazardous Materials* **168**(2-3), 1548-1553.

Shimojima E. and Sharma M.L. (1995). The influence of pore water velocity on transport of sorptive and non-sorptive chemicals through an unsaturated sand. *Journal of Hydrology* **164**(1-4), 239-261.

Skoog D.A., Holler F.J. and Crouch S.R. (2007). Principles of Instrumental Analysis. Thomson Books/Cole, Belmont, California.

Snoeyink V.L. and Jenkins D. (1980). Water Chemistry. John Wiley & Sons New York.

Solisio C., Lodi A., Torre P., Converti A. and Del Borghi M. (2006). Copper removal by dry and re-hydrated biomass of Spirulina platensis. *Bioresource Technology* **97**(14), 1756-1760.

Sommerfield C. and Cooper M. (2009). Analytical Chemistry Coursebook. The University of Nottingham, Nottingham, UK.

Srivastava V.C., Swamy M.M., Mall I.D., Prasad B. and Mishra I.M. (2006). Adsorptive removal of phenol by bagasse fly ash and activated carbon: Equilibrium, kinetics and thermodynamics. *Colloids and Surfaces A: Physicochemical and Engineering Aspects* **272**(1-2), 89-104.

Stembal T., Markic M., Ribicic N., Briski F. and Sipos L. (2005). Removal of ammonia, iron and manganese from groundwaters of northern Croatia - pilot plant studies. *Process Biochemistry* **40**(1), 327-335.

Stumm W. and Morgan J.J. (1996). Aquatic Chemistry, Chemical Equilibria and Rates in Natural Waters. John Wiley & Sons, Inc., New York.

Styriakova I., Styriak I., Kraus I., Hradil D., Grygar T. and Bezdicka P. (2003). Biodestruction and deferritization of quartz sands by Bacillus species. *Minerals Engineering* **16**(8), 709-713.

Tang X.W., Li Z.Z. and Chen Y.M. (2009). Adsorption behavior of Zn(II) on calcinated Chinese loess. *Journal of Hazardous Materials* **161**(2-3), 824-834.

Tchobanoglous G., Burton F.L. and Stensel H.D. (2004). Wastewater Engineering Treatment and Reuse. McGraw-Hill, Boston.

Teefy S. (1996) Tracer studies in water treatment facilities: a protocol and case studies. Subject area: water treatment, AWWA (American Water Works Association) Research Foundations, USA.

Tekerlekopoulou A.G., Vasiliadou I.A. and Vayenas D.V. (2006). Physico-chemical and biological iron removal from potable water. *Biochemical Engineering Journal* **31**(1), 74-83.

Tekerlekopoulou A.G., Vasiliadou I.A. and Vayenas D.V. (2008). Biological manganese removal from potable water using trickling filters. *Biochemical Engineering Journal* **38**(3), 292-301.

Tekerlekopoulou A.G. and Vayenas D.V. (2007). Ammonia, iron and manganese removal from potable water using trickling filters. *Desalination* **210**(1-3), 225-235.

Teng Z., Huang J.Y., Fujita K. and Takizawa S. (2001). Manganese removal by hollow fiber micro-filter. Membrane separation for drinking water. *Desalination* **139**(1-3), 411-418.

Terashima Y., Ozaki H. and Sekine M. (1986). Removal of dissolved heavy-metals by chemical coagulation, magnetic seeding and high-gradient magnetic filtration *Water Research* **20**(5), 537-545.

The Perkin ElmerCorporation (1996). Atomic Absorption Spectroscopy - Analytical Methods. The Perkin Elmer Corporation, USA.

Thompson G.R. and Hower J. (1975). The Mineralogy of Glauconite. *Clays and Clay Mineral* **23**(4), 289-300.

Tiwari D., Laldanwngliana C., Choi C.-H. and Lee S.M. (2011). Manganese-modified natural sand in the remediation of aquatic environment contaminated with heavy metal toxic ions. *Chemical Engineering Journal* **171**(3), 958-966.

USATSDR (2009) Public Health Assessment, Rochester Property Traveler's Rest, Greenville County, South Carolina, Environmental Contamination and Other Hazards, United States Agency for Toxic Substances & Disease Registry, Atlanta, USA.

Vaaramaa K. and Lehto J. (2003). Removal of metals and anions from drinking water by ion exchange. *Desalination* **155**(2), 157-170.

Van Benschoten J.E., Lin W. and Knocke W.R. (1992). Kinetic modeling of manganese(II) oxidation by chlorine dioxide and potassium permanganate. *Environ. Sci. Technol.* **26**(7), 1327-1333.

Villaescusa I., Fiol N., Martinez M., Miralles N., Poch J. and Serarols J. (2004). Removal of copper and nickel ions from aqueous solutions by grape stalks wastes. *Water Research* **38**(4), 992-1002.

Wahab O.A. (2007). Kinetic and isotherm studies of copper (II) removal from wastewater using various adsorbents *Egyptian Journal of Aquatic Research* **33**(1), 125-143.

Wan M.W., Kan C.C., Rogel B.D. and Dalida M.L.P. (2010). Adsorption of copper (II) and lead (II) ions from aqueous solution on chitosan-coated sand. *Carbohydrate Polymers* **80**(3), 891-899.

Wang S.B., Li L. and Zhu Z.H. (2007a). Solid-state conversion of fly ash to effective adsorbents for Cu removal from wastewater. *Journal of Hazardous Materials* **139**(2), 254-259.

Wang Z., Liu G., Fan Z., Yang X., Wang J. and Wang S. (2007b). Experimental study on treatment of electroplating wastewater by nanofiltration. *Journal of Membrane Science* **305**(1-2), 185-195.

Weber W.J. and Moris J.C. (1963). Kinetics of adsorption on carbon from solution. *J. Sanit. Eng. Div. am. Soc. Civ. Eng.* **89**, 31-60.

Wentz D.A., Bonn B.A., Carpenter K.D., Hinkle S.R., Janet M.L., Rinella F.A., Uhrich M.A., Waite I.R., Laenen A. and Bencala K.E. (1998) Water Quality in Wilamette Basin, Oregon 1991-1995, Circular 1161.

Whiteley M. (-) Strategic Stone Study: A Building Stone Atlas of Bedfordshire, English Heritage.

WHO (2006) Guidelines for Drinking-water Quality. First addendum to third edition. Recommendations. Volume 1.

WHO and UNICEF (2010) Progress on sanitation and drinking water, 2010 update, France.

Winter M.J. (2009) Iron: Geological information. The University of Sheffield and Web Elements Ltd., UK.

Winter M.J. and Andrew J.E. (2000). Foundations of Inorganic Chemistry. Oxford Science Publications, New York.

Xue Y.J., Hou H.B. and Zhu S.J. (2009). Competitive adsorption of copper(II), cadmium(II), lead(II) and zinc(II) onto basic oxygen furnace slag. *Journal of Hazardous Materials* **162**(1), 391-401.

Yang S., Li J., Shao D., Hu J. and Wang X. (2009). Adsorption of Ni(II) on oxidized multi-walled carbon nanotubes: Effect of contact time, pH, foreign ions and PAA. *Journal of Hazardous Materials* **166**(1), 109-116.

Yang W.-C. (ed) (2005) Handbook of fluidization and fluid-particle system, Marcel Dekker, Inc., New York.

Zhou L.C., Li Y.F., Bai X. and Zhao G.H. (2009a). Use of microorganisms immobilized on composite polyurethane foam to remove Cu(II) from aqueous solution. *Journal of Hazardous Materials* **167**(1-3), 1106-1113.

Zhou L.M., Wang Y.P., Liu Z.R. and Huang Q.W. (2009b). Characteristics of equilibrium, kinetics studies for adsorption of Hg(II), Cu(II), and Ni(II) ions by thiourea-modified magnetic chitosan microspheres. *Journal of Hazardous Materials* **161**(2-3), 995-1002.

APPENDICES

Appendix 3.1

Sieving procedure

1. Turn on the exhaust fan.
2. Clean 0.850mm, 0.710mm, 0.500mm, 0.400mm, 0.300mm sieves by brushing each of them carefully on the under-side of the mesh. Extra attention has to be made on the finer ones (0.500mm, 0.400mm and 0.300mm) as they tend to be damaged easily.
3. Do the coarser sieve (0.850mm) initially.
4. Put a plastic shield around the sieve so as it would avoid shear stress between the sieve metal when the Russell Sieve is run. Put the sieve on the Russell Sieve. Put the cover on the sieve. Lock the Russell Sieve by pressing the four hands of it.
5. Place a plastic bin under the opening coarser material as well as under the output of finer material.
6. Put a plastic bag under the overflow side.
7. Turn on the electricity power. Turn on the Russell Sieve.
8. Open the output of finer material and close the output of coarser one.
9. Put sand on the sieve with the thickness of less than two times of sieve aperture. Sand is taken both from fraction B and C in turns in order to optimize the sieving.
10. To ensure the sieving, spread over the sand on the sieve by hand.
11. Close the output of finer material and open the output of coarser one when the sand flowing through the output of finer material seems to cease.
12. Repeat to do no. 11 to 14 subsequently until all the sand is sieved.
13. Notice that if the sieve is clogged, it has to be cleaned to guarantee the quality of sieving.
14. Turn off the Russell Sieve if the all the sand is filtered.
15. Unlock the Russell Sieve hands.
16. Open the cover of the Russell Sieve.
17. Take out the plastic shield surrounding the sieve.
18. Clean the sieve and put it back to the sieve lockers.
19. Do no. 4 to 22 respectively for finer sieve (0.710 mm to 0.300mm).

Appendix 3.2

Procedure to make active sand

Procedure of making active sand (Paramarta et al., 1988):

1. Dry sand at 105 °C in an oven for about 12 hours (Liu and Evett, 1997).
2. Cool it to room temperature.
3. Soak with KMnO4 0.01 N for about 24 hours, to make it active (Teng et al., 2001)
4. Dry at 105 °C in an oven for about 24 hours.
5. Wash with water (Teng et al., 2001) until the waste water is not coloured. Once it is discolour, wash it again by using Milli-Q water.
   Dry it again at 105 °C in an oven for about 24 hours (Teng et al., 2001).

References:

Liu C. and Evett J.B. (1997). Soil Properties Testing, Measurement and Evaluation. Prentice Hall, New Jersey.

Paramarta R.B., Wardhana J.N.I., Sodikin I., Gana M., Budianto D., Suryodipuro L.M. and Widayati T. (1988) Activated un-saturated sand filter as an alternative to reduce Fe and Mn in water treatment [Saringan pasir kering aktif sebagai alternative untuk menurunkan Fe and Mn dalam pengolahan air minum], Bogor, Indonesia.

Teng Z., Huang J.Y., Fujita K. and Takizawa S. (2001). Manganese removal by hollow fiber micro-filter. Membrane separation for drinking water. *Desalination* **139**(1-3), 411-418.

Appendix 3.3

Procedure to make $KMnO_4$ solution

Procedure of making 0.01 N $KMnO_4$ solution:

1. Weigh 1.58 gr $KMnO_4$.
2. Dilute that in 1L de-ionised water.
3. Homogenised the solution by mixing it.

1.58 gr $KMnO_4$ is obtained by the following calculation:

KMnO4 positive valence =1 → 0.01 N = 0.01 M

KMnO4 molecular weight = atomic weight of (K + Mn + 4O) ≈ 39+55+ 4 (16)≈ 158 gr

As $KMnO_4$ Molarity= moles : litre

And Moles = mass : molecular weight

Then Mass = molarity x molecular weight x litre

For 1 litre $KMnO_4$, the mass of $KMnO_4$ will be then = 0.01 x 158 = 1.58 gr.

Appendix 3.4

Photographs of AUSF along with the AUSF accessories

Picture 1. Activated Unsaturated Sand Filter

Picture 2. A glass column containing sand

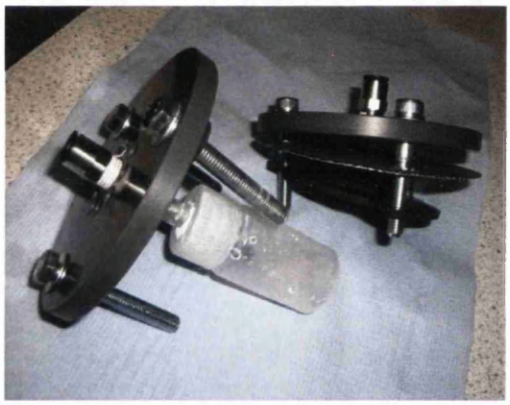

Picture 3. Left: Top perforated plate; right: bottom perforated plate

Picture 4. Top perforated plate along with its spray tube

Picture 5. Bottom perforated plate together with its accessories i.e. perforated screen (mesh), rubber plate, bolt and a plastic hose

Appendix 3.5

Procedure to measure flow rate of pump

1. Set the AUSF as shown in Figure 3.1.
2. Put 5L beaker close to the pump. This beaker will be served as an input tank.
3. Put 2L beaker next to the pump. This beaker will be served as an output tank.
4. Turn on the electricity power.
5. Set the pump up at 50% rotation.
6. Turn on the pump.
7. Time the water when it first discharges to 2L beaker until the volume is 0.5 L.
8. Turn off the pump.
9. Do no.5 to 8 for 60 – 100% rotation of the pump.
10. The flow rate is then calculated as: Volume (L) : time (min)... (Equation 3.1) (Tchobanoglous et al., 2004).

Reference:

Tchobanoglous G., Burton F.L. and Stensel H.D. (2004). Wastewater Engineering Treatment and Reuse. McGraw-Hill, Boston.

Appendix 3.6

Procedure to measure flow rate of AUSF

1. Set the AUSF as shown in Figure 3.1 or Picture 1 (Appendix 3.4).
2. Put 5L beaker close to the pump. This beaker will be served as an input tank.
3. Put 2L beaker next to the pump. This beaker will be served as an output tank.
4. Turn on the electricity power.
5. Set the pump up at 12% rotation.
6. Turn on the pump.
7. Time the water when it first discharges to 2L beaker until the volume is 0.5 L.
8. Turn off the pump.
9. Do no.5 to 8 for 11-5% rotation of the pump.
10. The flow rate is then calculated as: Volume (L) : time (min)... (Equation 3.1) (Tchobanoglous et al., 2004).

Reference:

Tchobanoglous G., Burton F.L. and Stensel H.D. (2004). Wastewater Engineering Treatment and Reuse. McGraw-Hill, Boston.

Appendix 3.7

Procedure to measure time of water passing through AUSF

1. Set the AUFS as shown in Figure 2.
2. Put 5L beaker close to the pump. This beaker will be served as an input tank.
3. Put 2L beaker next to the pump. This beaker will be served as an output tank.
4. Turn on the electricity power.
5. Set the pump up at 12% rotation.
6. Turn on the pump.
7. Time the water when it first discharges from the spray tube above the sand. This time is defined as t1.
8. Time the water when it first discharges from the filter. This time is defined as t2.
9. Turn off the pump.
10. Do no.4 to 9 for 11-5% rotation of the pump.
11. The amount of time of water passing through the AUSF is :

$$t\ (min) = t2\ (min) - t1\ (min) \ldots. \quad \text{(Equation 3.2)}$$

Appendix 3.8

Procedure to make copper (analyte) solution

Procedure to prepare 20 L of 20 ppm Cu^{2+} solution:

1. Dilute 400 mg of Cu^{2+} in 1L water.
2. Mix it with 19L water.

400 mg of Cu^{2+} is obtained by the following:

As concentration (ppm, mg/L) = mass: litre,

Then mass of Cu^{2+} = concentration x litre = 20 mg/L x 20 L = 400 mg.

To obtain 400 mg Cu^{2+} from reagent grade of $Cu(NO_3)_2$. $3H_2O$:

From the following reaction:

$Cu(NO_3)_2 \rightarrow Cu^{2+} + 2\ (NO3)^-$

As molecular weight of $Cu(NO_3)_2$. $3H_2O$ is 241.60 gr and from the above reaction:

1 mol $Cu^{2+} \approx$ 1 mol $Cu(NO_3)_2$. $3H_2O$

Then 1 mol $Cu^{2+} \approx$ 1 mol $Cu(NO_3)_2$. $3H_2O \approx$ 241.60 gr

As the atomic weight of Cu^{2+} is 63.546 then 400 mg Cu^{2+} = 400: 63.546 moles = 6.295 moles.

As 1 mol $Cu^{2+} \approx$ 1 mol $Cu(NO_3)_2$. $3H_2O$ then 6.295 moles $Cu^{2+} \approx$ 6.295 mol $Cu(NO_3)_2$. $3H_2O$

The mass of $Cu(NO_3)_2$. $3H_2O$ is then = 6.295 x molecular weight of $Cu(NO_3)_2$. $3H_2O$ = 6.295 x 241.60 = 1520.872 mg.

As 1520.872 mg/L of $Cu(NO_3)_2$. $3H_2O \approx$ 400 mg/L Cu^{2+} then to make 400 mg/L Cu^{2+} is simply done by taking 1520.872 mg of $Cu(NO_3)_2$. $3H_2O$ and dilute that in 1 L water.

Appendix 3.9

Procedure to measure surface area by NOVA 2000e Surface Area and Pore Analyzer

Procedure to measure surface area by using NOVA 2000e Surface Area and Pore Analyzer interfaced with Quantachrome Instruments version 11.0 software:

1. Weigh the sample cell.
2. Put the sand in the sample cell.
3. Put the sample sand in the heating mantles for degassing.
4. Turn on pump. Turn on instrument.
5. On the analysis selection keypad: Press Esc.
6. Press 3 (Control Panel).
7. Press 2 (Degas stations)
8. Press 1 (Yes)
9. Press 1 (Vacuum Degassing). Press Enter
10. On degas temperature control: Press 500 (^{0}C). Leave for about 3 hours.
11. After 3 hours, let it cool until the temperature is about 30-40(^{0}C).
12. Weigh the sample.
13. Press 2 (degas stations)
14. Press 1 (unload)
15. Press 2
16. Switch off T (temperature)
17. Prepare for liquid nitrogen to cool the sample.
18. Put the liquid nitrogen in the automated blanket elevator.
19. Turn on the Novawin software
20. Press Operation
21. Press Start analysis
22. Press Stations
23. Fill in weight (weight after degassing-weight of sample cell)
24. Type file name
25. Description
26. Press Start. Press Yes.

Appendix 3.10

Procedure of acid and alkali resistance test

1. Put some amount of coated sand in a glass beaker.
2. Add some amount of milipore water into that beaker so that the sand is soaked.
3. Place the beaker onto a magnetic stirrer. Turn on the magnetic stirrer (r scale ≈ 70).
4. Adjust pH until the required value, for example, pH = 2.
5. Take the sample from the beaker.
6. Analyse the sample with an AAS.

Appendix 3.11

Procedure to determine the pzc of sand particles

1. Put 100 gr of milipore water in a glass beaker.
2. Put the beaker onto a magnetic stirrer.
3. Stir the water and measure the pH after its stable.
4. Put 0.01 g coated sand into the beaker.
5. Stir the sample and sealed the beaker.
6. Measure the pH after 24 hours.Repeat no. 4-6 for 0.1, 1, 5, 10, 20, 30, 40, 50, and 60 g coated sand until there is no pH change is observed.

Appendix 3.12

Procedure of acid digestion analysis

1. Place 1 g of sample in 50 mL flask.
2. Heat the sample to 95^0C with 10 mL of 50% HNO_3 without boiling for 10 minutes.
3. Cool the sample.
4. Reflux the sample with 5 mL of 65% HNO_3 at 95°C for 30 minutes.
5. Cool the sample.
6. Reflux the sample with 10 mL of 36% HCl at 95°C for 15 minutes.
7. Cool the sample.
8. Filtrate the digestate.
9. Dilute the digestate to 100 mL for analysis.
10. Do triplicate for each sample.

Appendix 3.13

Procedure to perform a tracer study

1. Prepare 100 mg/L salt, i.e. sodium chloride (Na Cl).
2. Run AUSF.
3. Check output conductivity.
4. Inject 10 mL of salt from the top once the output conductivity is stable.
5. Take sample from the first output.
6. Note the time of water filling the sample tube.
7. Measure conductivity and temperature of the sample.
8. Take sample a lot as fast as it can until the output conductivity is stable.

Appendix 3.14

Procedure to use the Perkin – Elmer 272 AAS

1. Check the acetylene cylinder. This cylinder contains of acetylene gas dissolved in solvent (acetone).Make sure that the left pressure gauge is minimum 60 psi (2 bar). If it is below that it will break the gas pipe (in red colour). Tell the lab supervisor if this condition occurred.
2. Check the drain from the instrument. This drain tank should always full with water (until the marked is achieved) so as to certain the back pressure presents and avoid the 'boom' if the instrument is turned on.
3. Check the reservoir under the drain. This reservoir should not be fully filled with water as to avoid the overflow.
4. Switch on the extractor. If it sounds, it means it operates well. To make it sure, hold the tissue well below the extractor so as it will not suck by. If it flews, the extractor operates well. This extractor will extract the analysed metal ion.
5. Note that do not proceed with the analysis if one of the procedures of No. 1-4 is not met.
6. Check all the below conditions before switching on the instrument:
7. Lamp 1 should be in anti clock wise position.
8. Gain should be in anti clock wise position.
9. Recorder should be pointed to ABS (Absorbance).
10. Mode should be pointed to cont.
11. Signal should be pointed to Lamp 1.
12. Background corridor intensity should be in anti clock wise position.
13. Background corridor pointing is depended on the analysed element (wavelength). If the wavelength is below 350nm, it should be pointed to AA-BG. If it is beyond that, it should be pointed to AA.
14. Note: elements' wavelength list is in the Perkin Elmer handbook.
15. Check the lamp. Every element has its own lamp and every lamp has its own maximum current mA. For example: Cr maximum current = 12 mA, Na = 10.
16. Put the lamp in the instrument.
17. Switch on the power.

18. Set the needle in Lamp 1 to 8 by turning the switch clock wise. Note that do not touch this again after this has been set.
19. Set Signal to ABS, the needle in Lamp 1 then points to 0.
20. Turn the Gain. The Gain will amplify the detector to reach the peak absorbance.
21. Adjust wavelength until it reach the analyte wavelength. Do not press the button as this will be slipped and make the wavelength difficult to be found.
22. Note: set the wavelength some scales below the desired absorbance for the beginning to find out the peak absorbance. For instance: the desired wavelength is 216.5 nM, then set the wavelength first to about 210 nM then adjust the wavelength, gain and background corridor intensity until the paek is reached.
23. Adjust wavelength and gain so as the needle in Lamp 1 points to green. If the needle goes beyond the green area, adjust the wavelength and gain sequentially so as to reach the peak. If the peak is reached, turn the gain until it comes to the green area.
24. Note: Background corridor intensity can also be adjusted to reach the green area. Switch the background corridor to AA-BG. Turn the background corridor intensity until it reachs the green area. Switch the background corridor to AA. If the needle still in the green area, it means the peak has been reached. If not, adjust wavelength, gain and background corridor intensity again. Once the peak is reached, do not forget to switch the background corridor to AA.
25. Note: The peak absorbance can be reached also by adjusting the slit in the lamp area. Move the slit in or out to reach the peak.
26. Make sure the Fuel is off (points to down position) and the air is off.
27. Make sure the red valve of gas is in anti clock wise position.
28. Turn on the butterfly valve of the gas ¼ .
29. Adjust the red valve until the needle in the pressure gauge points to black mark.
30. Turn the valve in the compress air ¼ (turn to the right). Make sure that the source of compress air outside is in on position.

31. Make sure that there is enough deionised water in the beaker. Put the hose in the beaker.
32. Turn the fuel into on position (will be in 30 position).
33. Turn the air into air position (will be in 50 position).
34. Ignite the flame with the ignitor.
35. Press AZ to reach zero.
36. Press 5 then t to make 5 seconds interval reading. Then press AZ again to reach zero.
37. Put the hose in the beaker filled with the analyte.
38. If the reading displays 0-0.4, the analysis can be further done. If it is beyond that, dilution should be done first before analysing the element.
39. Wait until the display shows relatively the same readings because it does 2 solutions, one is deionised water, the other is element solution so there is some times before it displays the true reading.
40. Put the cable again to the water. Wait it till 23 seconds so as the burner is washed with water. If the analyte is copper or silver, the washing should be at least about 10 minutes so as there is no deposit in the burner that can be exploded. Note that Copper and silver will react with acetylene to produce acetylede that can be dried or deposited in the burner. Once the switch is on it can be exploded.
41. Please be sure to switch off the flame by turning off the fuel and the air if you are going to leave the instrument. Note that to switch it off, the fuel should be turned off first then the air. To switch on can be either one first.
42. Turn off the air valve.
43. Turn off the gas valve.
44. Turn the red button anti clockwise.
45. See the needle in the pressure gauge. If it above the marked line or doesn't come to zero after turning off, it means there is still air and gas in the pipes. To release them: Turn on the fuel. Turn on the air. Turn off the fuel. Turn off the air. Look at the needles until the needles go to zero.
46. Turn all the needle/button to the initial condition. Switch off the power. Switch off the extractor.

Appendix 3.15

Procedure to use Varian AA240FS AAS

1. Wear safety glasses to protect the eyes from ultraviolet radiation as this radiation emitted by flames, hollow cathode lamps, and deterium lamps, can seriously damage human eyes and skin.
2. Wear gloves to protect skin from hazardous sample.
3. Turn on the exhaust van. Heat, vapors and fumes produced by flame, furnace and vapour generation methods are hazardous to humans, therefore they have to be extracted from the instrument by an exhaust system.
4. Turn on the power.
5. Put standard solution and sample in the racks.
6. Open valve of air pressure. Set air delivery pressure to 50 psi (red area) (allowed range: 35-65 psi).
7. Open valve of acetylene cylinder.
8. Open valve of the acetylene regulator (by turning it left/anti clockwise).
9. Set acetylene delivery pressure to 11 psi (green area/bottom line) as a safe level (allowed range: 9.5-14.5 psi). At delivery pressure above 15 psi, acetylene can explode spontaneously. Note that acetylene cylinder must be replaced one the pressure in this cylinder is 100 psi as below 100 psi acetone may be carried over from the cylinder and into the spectrometer that may in turn damage seals, O-rings and hoses and degrade analytical performance and precipitate flashbacks.
10. Connect the little hose to the black plug for automatic reading then tighten it (to the right).
11. Turn on the computer.
12. Press SpectrAA.
13. Press Worksheet.
14. Press New.
15. Type name then press OK.
16. Press Develop.
17. Press Add methods (Method type: flame, type for example: Cu).
18. Press Edit methods.

19. Press Measurement.
20. Type Time measurement: 10 s.
21. Type Read delay: 45 s.
22. Press and Type Standards
23. Type Lower valid concentration.
24. Type Upper valid concentration. If the standards used are until 5 mg/L, for example, type upper valid concentration for 6 or 7 mg/L to give a better linear range.
25. Press Calibration. Choose Linear.
26. Press Analysis.
27. Press and Type Labels.
28. Type total rows.
29. Press Start.
30. Press Flame.
31. Press stop after the analysis is done.
32. Note: Always look at the result while doing the analysis so as if UNCAL occurs, the process can be stopped immediately. UNCAL often occurs due to improper calibration. Therefore, once it happened, it is advisable to change the standards solutions.
33. Close the regulator valve of acetylene gas.
34. Close the valve of acetylene.
35. Press Flame to release any remaining fuel.
36. Close the air valve.
37. Turn off the SpectrAA.
38. Turn off the instrument power.
39. Turn off the exhaust van.

Appendix 3.16

Procedure to make a standard solution of a metal ion

For example, to make 50 mg/L solution of Cu:

1. Pour 1000 mg/L Cu standard solution to the 50 mL centrifuge tube. (Note: never pipette the standard solution directly from its original container as it most likely to contaminate the original standard solution).
2. Pipette 5 mL Cu from 1000 mg/L Cu standard solution in the 50 mL centrifuge tube to the 100mL volumetric flask.
3. Dilute it with deionized water till the volume is 100mL. This step is based on equation: $V_1C_1=V_2C_2$, where:

   V_1= volume of standard solution to be taken (mL).

   C_1=concentration of standard solution (mg/L, i.e. Cu=1000mg/L)

   V_2=final volume of the desired concentration (mL).

   C_2= the desired concentration (mg/L).
4. Do similarly the above step to make the 2, 4, 6, 8, 10, 15, 10, 25, 30, 40, 50 mg/L Cu standard solution.
5. Do not forget to make the 0 mg/L standard solution (blank, 100 mL deionized water).
6. Do not forget also to homogenise the solution by mixing it thoroughly.

Appendix 3.17

Procedure to make a stabilized metal standard solution

For example: Copper

Preparing 20 mg/L Cu standard solution + 10% HNO_3:

1. Pour the 1000 mg/L Cu standard solution to the 50 mL centrifuge tube.
2. Pipette 20 mL of 1000 mg/L Cu standard solution from the 50 mL centrifuge tube to 1L volumetric flask.
3. Add deionized water.
4. Add 100 mL HNO_3 (10% HNO_3=100 mL HNO_3/1 L solution).
5. Dilute with deionized water till the volume is 1 L.
6. Homogenised it by mixing it thoroughly.

Appendix 3.18

Procedure to make a standard calibration graph to analyse copper using Perkin – Elmer 272 AAS

1. Make the stabilized (10% HNO_3) 0, 2, 4, 6, 8, 10, 15, 20, 25, 30, 40, and 50 mg/L standard solution of copper.
2. Measure the absorbance of each standard solution of copper for 216.5 nM - 0.2 slit, and 324.8 nM - 0.7 slit.
3. Plot absorbance value against concentration value for each standard solution of copper.
4. Calculate the equation line.
5. The graph produced will be used as a calibration standard graph for the next measurements.
6. Do not forget to calibrate the AAS instrument every time measurement is about to be taken.

Appendix 3.19

Sand Particles and Sand Bed Characterisation

1. Sand particles characterisation techniques

The comprehensive characterisation of particles requires the measurement and description of the particle characteristics of interest. There are various different ways and technology to characterise the particles due to they are generally irregular in shape and different in surface morphology (Yang, 2005).

1.1 Sand particles size

The size of a spherical homogenous particle is exclusively defined by its diameter. However, for irregular particles, such as those of sand particles, the particle size can be stated by using sieve diameter, *d*, that is defined as the width of the minimum square opening in the sieve screen through which the particle will pass (Yang, 2005). Sieve analysis, imaging technique, gravity and centrifugal sedimentation are some techniques used to measure the size of particle. Sieve analysis is illustrated below as it was used in this study.

Sieve analysis

The most frequently used technique for sorting sand is to sieve the particles to a various screen with standardised mesh sizes with shaking, but it is limited to particles coarser than 75μm (Allen, 1975). The sieve analysis offers a fairly accurate value for the mean particle size. Sieve analysis, however, does not distinguish the particle shape (Yang, 2005).

1.2 Sand particles surface area

Surface area of sand particle is theoretically defined as the area of the faces that bind the solid sand particle (Stout, 1994). However, due to surface irregularities i.e. roughness due to voids, pores or other defects, real or specific surface area is usually larger than the equivalent theoretical surface area (Lowell et al., 2004). Particle size, shape are factors affecting specific surface area.

The total surface area is more essential than the particle size in numerous applications involving chemical reactions. Two techniques are usually used to measure the particle surface area, i.e. the permeability technique and the gas adsorption technique (Yang, 2005). The permeability technique is a method for defining sand particle surface area by measuring the permeability of a sand bed.

The gas adsorption technique is a method usually employed to determine the specific surface of solids by the physical adsorption of a gas on the solid and the measurement of the monolayer capacity V_{m}. V_m is specified as the quantity of adsorbate needed to cover up the adsorbent with a monolayer. Experimental results of adsorption are usually plotted regarding the volume of gas adsorbed as a function of the equilibrium pressure. Isotherms are plots concerning the volume adsorbed and the pressure at which the adsorption occurs (Allen, 1975). Gas adsorption technique usually follows Langmuir's or Brunauer, Emmet and Teller (BET)'s theory as described below.

1.2.1 Langmuir's isotherm for ideal localised monolayers

Langmuir developed the first theoretical equation relating the amount of adsorbed gas to the equilibrium pressure of the gas. In Langmuir model, adsorption is only applied to a monolayer. Langmuir equation has also narrow application to physical adsorption but wider to chemical adsorption and the adsorption of solute from solution. Langmuir method is to associate the quantity of molecules evaporating from the surface with the quantity condensing on the surface.

Langmuir's equation is shown as below (Allen, 1975):

$\frac{P}{V} = \frac{1}{bV_m} + \frac{P}{V_m}$.....(Equation A19-1).

where: $b = \frac{\propto_0}{\sqrt{2mkTn_0}} \exp(-\frac{Q}{RT})$, P = pressure at which adsorption occurs, V = volume of gas adsorbed.

A plot of P/V against P leads to the monolayer capacity V_m. Surface area from the monolayer capacity is defined by Equation 3.9.

1.2.2 BET isotherm for multilayer adsorption

Brunauer, Emmet and Teller proposed the multilayer adsorption of gases theory, known as BET theory, on solid surfaces. With the assumption that the forces that create condensation are mainly responsible for the binding energy of multimolecular adsorption, they progressed to derive the isotherm equation for multimolecular adsorption using a method that was actually a generalisation of Langmuir's method of the unimolecular layer. The generalisation of the ideal localised monolayer method is executed on the assumption that each first layer adsorbed molecule offers a site for the adsorption of a molecule into the second layer and so forth. Therefore, the concept of localisation exists at all layers and the forces of common interaction are disregarded. Equation 3.8 shows the BET equation.

Factors affecting adsorption

The first important step in measuring the adsorption isotherm is removing any gases or vapours forming a physically adsorbed film that usually covers solid surfaces. This step is usually called degassing. Pressure, temperature and time are factors affecting the level of degassing achieved (Allen, 1975).

1.2.3 Gas adsorption measurement methods

Three methods are commonly used to measure the surface area of particle i.e volumetric methods, gravimetric methods, and continuous-flow gas methods. The continuous-flow gas method is explained below as it was used in this study.

Continuous-flow gas-chromatographic methods

Nelsen and Eggertsen proposed the continuous-flow method, a modification of gas-adsorption chromatography in which the sample acts as the column packing and the mobile gas phase is a mix between an adsorbate and an inert gas. Nitrogen as the adsorbate and helium as the carrier gas are used as follows. Nitrogen and helium are mixed in certain amount then passed through the sample and then through a thermal conductivity cell linked to a recording potentiometer. Once the sample is cooled in liquid nitrogen, the sample then adsorbs the nitrogen from the mobile phase; this is shown by a peak on the recorder chart, and after equilibrium is obtained, the recorder pen recommences its initial position. Removing the coolant leads to a desorption peak similar in area and in the reverse route to the adsorption peak and each peak can be used to calculate the nitrogen adsorbed. The major advantages of this method compared to the conservative BET method are as follows: no delicate and complex glassware, and a high vacuum system are employed; no dead-space correction are required; automatically permanent records; speed and simplicity (Allen, 1975).

Helium, an extremely expensive gas, may be changed by other gases which are not adsorbed under the experimental conditions, e.g. hydrogen. There are commercially available continuous-flow-type apparatus such as those of from Perkin-Elmer Ltd or Quantachrome (Allen, 1975).

1.3 Sand particles surface area morphology

Characterisation of particles surface area morphology can be done by optical and electron microscopy (Skoog et al., 2007).

A microscope is a system which converts an object into an image. Optical microscopy is a classical method to obtain information regarding the physical nature of surfaces. The two most important methods of electron microscopy are scanning electron microscopy (SEM) and transmission electron microscopy (TEM). The optical microscope has severe limitations, i.e. its small depth of focus. Thus, this result in diffraction effects, that makes the boundaries of the images seen in a microscope are blurred. For electron microscopy, on the other hand, the depth of focus is almost 300 times than that of optical microscope; therefore the images produced, particularly at higher magnification, are better than the images from the optical microscope (Allen, 1975). Although SEM and TEM are quite similar in terms of the electron beams used and thus their certain components (i.e. electron gun, condenser lenses and vacuum system), SEM, however, gives information about the surface, or near surface of bulk specimens; whereas TEM is mainly employed to study the internal structure of thin specimens (Goodhew et al., 2001).

1.3.1 Scanning electron microscope (SEM)

The SEM has the capability to significantly broaden the limited magnification range of the optical microscope, which usually extends to merely 1500x, to beyond 50,000x. The depth of field of the SEM that almost 300x greater than that of the optical microscope makes the SEM also particularly useful to obtain images that have lots of surface relief such as those found on fracture surfaces. The depth of field is defined as the variety of positions for the object in which no change in the sharpness of the image is noticed by eyes. However, the SEM's image is usually poorer to that of the optical microscope at low magnifications (below 300 to 400x) (Goodhew et al., 2001).

The SEM is thus performed better at higher magnifications and with surfaces having strong relief; whereas the optical microscope is performed better at low magnifications with relatively flat surfaces (Abbaschian et al., 2009).

1.3.2 Basic concept of SEM

The tungsten filament thermionic emission type is generally used as the electron source (gun), although for higher resolution, field emission gun sources are progressively being employed more. Resolution is defined as the adjoining spacing of two points which can clearly be seen through the microscope to be separate units. The basic concept of SEM is described in Section 3.2.1.1.c. The magnification of the image requires not any lenses. The electron beam scans the raster on the specimen smaller than the raster shown on the CRT. The side length of the CRT divided by the side length of the raster on the specimen defines the linear magnification (Goodhew et al., 2001).

1.3.3 Electron beam interactions

The usefulness of the SEM and electron microprobe for the study of solids derives from the various signals produced once the electron beam interacts with the solid. The signals that can be generated in an SEM are shown in Figure 3.3. The contacts of a solid with an electron beam can be classified into two groups: (1) elastic contacts, that influence the paths of the electrons in the beam without changing their energies drastically, and (2) inelastic contacts, that transfer part or all of the energy of the electrons to the solid (Skoog et al., 2007). Nearly all of the kinetic energy which was held by the electron beam will turn out to become heat in the sample. A little amount of the energy may escape as X-rays, light, secondary or backscattered electrons (Goodhew et al., 2001).

There are generally three types of signals produced once the electron beam hits the sample that are used in an SEM and electron microprobe. First are *backscattered electrons*. When electrons go through the surface sample, some of the electrons finally lose energy by inelastic collisions and stay in the solid; yet most of them, experience many collisions, resulting in a final departure from the surface as backscattered electrons. It should be noted that the diameter of the beam of backscattered electrons are much larger than the incident beam, that is, for a 5nm incident beam, the diameter of backscattered beam may come to several micrometers.

This large diameter of the backscattered beam is one of the factors restraining the resolution of an electron microscope. Backscattered electrons have a wide energy spread, from 50eV up to the energy of the incident beam (Skoog et al., 2007).

The second type of signals is *secondary electrons*. Once the surface of a sample is hit with an electron beam having energy of several keV, electrons having energies of ≤ 50eV are released from the surface together with the backscattered electrons. Secondary electrons are formed resulting from the interactions between the energetic beam electrons and weakly bound conduction electrons in the solid, which results in the ejection of conduction band electrons with a few electron volts of energy. Secondary electrons are generated from a depth of only 50 to 500^0A ($1A^0 = 10^{-16}$ micrometer) and emit in a beam that has a little larger diameter than the incident beam (Skoog et al., 2007).

The third type of signals is *X-ray photons*. Photon is a particle like electron, etc that has energy, momentum, and spin, and can be made and destroyed. However, it has no mass thus it always moves fast at the speed of light (Ford, 2011). This X-ray radiation serves as the basis for the electron microprobe for X-ray analysis of SEM images (Skoog et al., 2007).

Due to the unobstructed flow of electrons to ground minimises objects with regard to the build up of charge, samples that conduct electricity are simplest to study. Conductive samples (of electricity and heat) also minimise the likelihood of their thermal degradation. Many techniques have been thus created to capture SEM images of non conducting samples; the most common techniques are to coat the surface of the sample with a thin (about 10nm) metallic film formed by sputtering or by vacuum evaporation. However, this coating has to be done carefully as an excessive coating may disrupt surface details and may impede with other detection modes (e.g. X-ray emission) (Skoog et al., 2007).

1.3 **Sand particles elemental substances**

Sand particles may contain elements depending on their condition i.e. whether they are virgin/raw sand or sand bearing elements resulting from their exposure to any treatment.

SEM is now equipped with x-ray analytical instruments so as not only topographic and crystallographic but also compositional information that can be achieved well, fast, and concurrently from the same exposure sample. Today, the energy-dispersive spectrometer (EDS) is usually used in conjunction with SEM. EDS provides fast analysis of elemental composition of the sample (in 10s for major elements and 100s for minor elements) qualitatively and quantitatively. EDS, however, has drawbacks such as its fairly poor energy resolution which resulted in regular unsettled spectral interferences, poor peak-to-background values, and the resultant poor detection limit (Goldstein et al., 1981).

Whenever electrons with some kilo electron volts of energy hit a solid sample, X-rays characteristic of the atoms within the sample are formed. Two micro analysis basically can be defined from the X-ray spectrum emitted by any sample. First is qualitative analysis. The type of elements within the sample can be defined by measuring the wavelength (or energy) of each emitted characteristic X-ray. Second is quantitative analysis. The amount of elements within the sample can be defined by measuring the amount of any type of emitted X-rays (Goodhew et al., 2001)

Three types of electron microscopes, generally employed for microanalysis, are those of SEM with X-ray detectors, Electron probe microanalyser (EPMA) and TEM, and scanning TEM (STEM) with X-ray detectors. An SEM with X-ray detectors is actually an EPMA (Goodhew et al, 2001). Due to the SEM is used to characterise the surface of the specimen, and as it is the objective of this work, the SEM with X-ray detectors (SEM-EDX) is thus described below. Before proceeding with the explanation of the SEM-EDX, basic theory of electron shells and the relaxation of excited atoms are explained first as follows.

1.4.1 Electron shells

The structure of a typical isolated atom can be illustrated in two ways as shown in Figure A19-1. A positive charge is carried by the nucleus. Electrons which carry negative charge surround the nucleus. The negative charge of electrons neutralises the positive charge of the nucleus. Most electrons are localised, or remain associated with a particular atom, once each atom is close to another in a solid. However, some outer electrons may be shared depend on the bonding type with adjacent atoms. The first three electron shells surrounding an atom are K, L and M shell. The potential energy of a free electron in a distant from any atom is usually defined as a zero of the energy scale. Therefore, the energies of localised electrons are negative (Figure A19-1). Figure A19-1 shows the first three electron shells surrounding a molybdenum atom. The K shell electrons (the innermost electrons) are the most firmly bound and as the figure shown, they have to be knocked out by about 20 keV. On the other hand, outer electrons are relatively easy to be isolated from their atom as only a little amount of energy is required to knock them out (Goodhew et al., 2001).

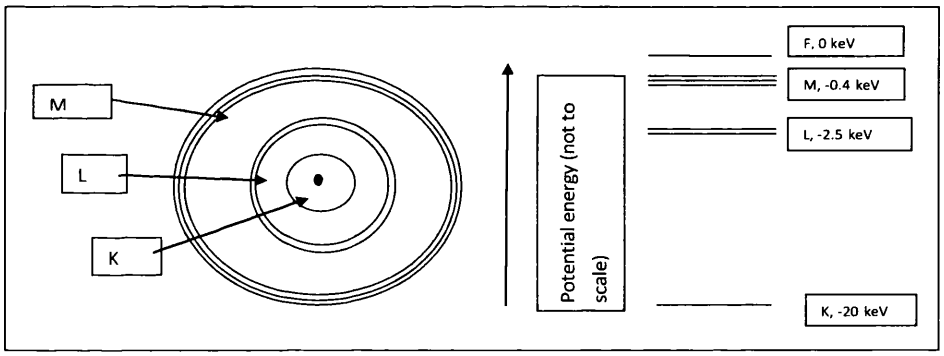

Figure A19-1 The structure of a typical isolated atom (Goodhew et al., 2001)

Relaxation of excited atoms

If a localized electron has been ejected from an atom, the atom is in an excited or high energy state. Once the vacant electron state is filled, the atom will relax, releasing the excess energy as a secondary effect.

A secondary effect is an effect brought by the primary beam which can be identified outside the sample. This relaxation can occur in three ways as follows.

First, the energy to be released will be small and is usually emitted as photon which perhaps in the visible range if the empty electron state is an outer state. This effect is termed as *cathodoluminescence* (Goodhew et al., 2001).

Second, the quantity of energy to be released is larger and may be emitted as *a characteristic X-ray* if the empty state is an inner state, or third, as *a characteristic (Auger) electron* (Goodhew et al., 2001). These two processes are depicted in Figure A19-2.

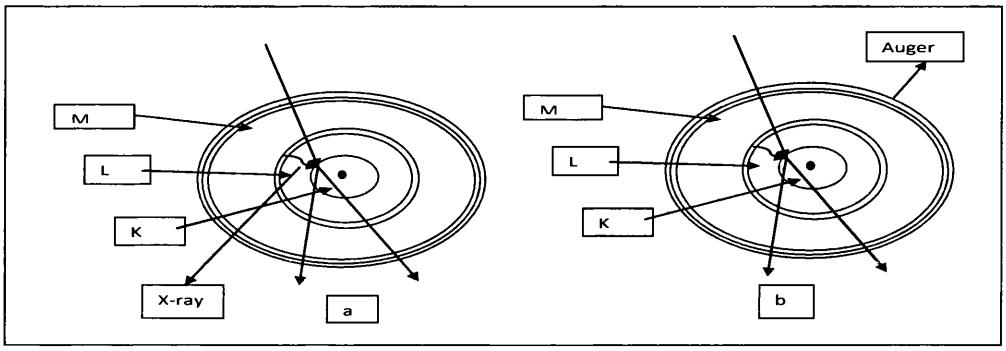

Figure A19-2 Relaxation of excited atoms (a) Emission of a characteristic X-ray (b) Ejection of an Auger electron (Goodhew et al., 2001)

A primary electron may also excite an X-ray without knocking out an inner shell electron. The electron can lose any quantity of energy (up to its total kinetic energy) and the X-ray is no longer characteristic of a specific atom. This process is known as *Bremsstrahlung* ("braking radiation") and results in *a background of X-rays* in any electron-generated X-ray spectrum (Goodhew et al., 2001).

Figure A19-2 (b) shows Auger emission in which an electron is ejected carrying the surplus energy as kinetic energy. Auger electron and characteristic X-ray emission are alternative processes by which energy can be released once an excited atom relaxes. Nevertheless, these processes do not happen with equal probability. In addition, the portion of atoms which emits an X-ray, known as the fluorescence yield, varies significantly with atomic number. Auger electrons will be emitted significantly greater than X-rays from a light element (small atomic number (Z)); whereas for heavy elements the situation is in the contrary (Goodhew et al., 2001).

1.4.2 The production of X-rays within a sample

Once high energy electrons hit a sample, 'characteristics' X-rays, whose wavelengths are specific for the atoms in the specimen, and white radiation (or Bremssthrahlung) of all wavelengths will be emitted. Before using the X-rays for analytical purposes, the most intense X-ray lines have to be defined first, so as the best line to be used as an index of how much of each element is present in the sample can be chosen (Goodhew et al., 2001).

The line of $K_{\alpha 1}$ and $K_{\alpha 2}$ (or the K 'doublet' which are so close together that they cannot be segregated) is most often used for analysis as they are seven to eight times more intense than $K_{\beta 1}$ and $K_{\beta 2}$. Nevertheless, as the atomic number of the emitting element raises, the energy needed to knock out a K-shell electron also increases, thus it is sometimes impossible to excite the K series of lines in an electron beam instrument. For instance, elements heavier than tin (Z = 50) require electrons of > 25keV to excite any K lines at all, and are inefficient generators of K X-rays until the incident electron energy is close to 75keV (Goodhew et al., 2001).

As in an SEM only 30keV electron energies are perhaps available, other characteristic X-rays which are more easily excited in order to identify heavy elements have to be found. Luckily, it turns out that the L series of lines or yet the M series for heavy elements have these properties. It is also appears that from the enormous quantity of possible lines, $L_{\alpha 1}$ and $L_{\alpha 2}$ as well as $M_{\alpha 1}$ and $M_{\alpha 2}$ are much stronger than the remainder.

There is another process, known as *fluorescence*, by which X-ray can be produced. X-rays, which are possibly initially produced by electron excitation and passed through a sample, can themselves excite atoms which then release characteristic X-rays of a slightly lower energy. For instance, in a brass sample the zinc K_{α} X-rays (which has energy of 8.64 keV) can excite additional copper K_{α} X-rays whose energy is less (8.05 keV) (Table 3.1) (Goodhew et al., 2001).

The interaction volume and the sampling volume are important factors in microanalysis using SEM. The sampling volume is the volume of the sample from which the detected X-rays originate.

The sampling volume for X-rays is nearly similar to the interaction volume as X-rays produced deep in the specimen can escape from the specimen and be identified. For low energy electrons and heavy elements, the interaction volume is the smallest. 1 $(\mu m)^3$ is the smallest practicable volume to be analysed in a scanning microscope (Goodhew et al., 2001).

The energy of the X-rays and the average atomic weight of the sample affect the fraction of the generated X-rays that reach the specimen surface and are emitted. For instance, soft X-rays (low energy, long wavelength) such as carbon (light element) K_α are readily absorbed by solids and thus quite a little escape from the surface. In contrast, hard X-rays (high energy, short wavelength) such as molybdenum (heavy element) K_α can go deep (many micrometers) in most solids, and are only absorbed a few by solids and thus most escape from the surface (Goodhew et al., 2001).

It is thus appeared that the volume which is being studied as well as the fraction of the X-rays which are emitted from the sample are greatly affected by (a) the energy of the electron beam, (b) the energy (wavelength) of the X-ray being analysed and (c) the local atomic weight of the sample. This complication thus results in severe difficulty in analysis (Goodhew et al., 2001).

1.4.3 Energy dispersive analysis

There are two methods to obtain X-rays data (a) Wavelength dispersive analysis (WDS), and (b) Energy dispersive analysis (EDS). Many SEMs and TEMs are provided with an EDS detection system which has less precision and resolution than WDS although can detect and display most of the X-ray spectrum (Goodhew et al., 2001). The EDS system is explained in Section 3.2.1.1.d.

There are some disadvantages of the EDS system. One of them is that the energy resolution of the detector is inferior; as such each X-ray line is not identified as a sharp line, but as abroad peak, usually 100-200eV. This, results in the impossibility in resolving closely spaced lines and the reduction in the peak height as any X-ray line now dwells in several channels of the multichannel analyser (MCA).

This factor, along with the fairly large number of electronic noise in the system, results in rather low peak to background ratios in comparison with WDS. A low peak to background ratio affects the limit of detectability of the analyser and its use for quantitative analysis (Goodhew et al., 2001).

There are, however, the advantages of energy-dispersive analysis. The X-rays can be collected extremely successfully as a detector can be located extremely close to the specimen. In addition, an entire spectrum (and thus a qualitative analysis) can be obtained within a few minutes as X-rays of all energies are collected simultaneously (Goodhew et al., 2001).

1.4.4 Sample analysis displays

The distribution of a single element in a sample can be displayed in two ways. First, is by using a linescan method. The linescan method is a one dimensional scanning. A line scan is performed along the area of interest. Secondly, is by using an X-ray mapping. This is basically an extension of the linescan method to two-dimensional scanning. The display is provided bright each time an X-ray photon is assessed. The image then comprises of bright dots; the brightness or the dot density is a qualitative measure of the concentration of the analysed element. Nevertheless, the quality of an X-ray map is inferior to that of an electron image due to the poor counting statistics for X-rays as compared with electrons (Goodhew et al., 2001).

1.4.5 Practical problems encountered in qualitative analysis

Two of various problems practically encountered in qualitative analysis are described as follows. Firstly, X-rays cannot be detected from sections of the sample which are not in the line sight of the detector, as X-rays, contrast to secondary electrons, move in straight lines from the sample to the detector. Consequently, on rough specimen, this should be interpreted carefully as a topographical effect rather than one resulted from a variation of chemical composition across the sample.

Secondly, as X-rays come deep from the sample, thus X-rays may be detected from regions which are not visible in the electron image (Goodhew et al., 2001).

1.4.6 Detection limit

The minimum detection limit (MDC) for any element in a sample is important once low concentrations are involved. X-ray counts, as well as other signals in the SEM, come at random, and the peak in the spectrum can only be detected if it is noticeable from the background.

The MDC for all except the lighter elements is about 0.1% by using an EDS system. However, the exact figure will be affected by the atomic weight of the trace element compared to that of the sample as the soft X-rays from a light element will be greatly absorbed by a matrix of high element (Goodhew et al., 2001).

1.5 Sand particles resistance towards acid and alkali

The characteristic of sand particle may change resulting from its exposure towards acid and/or alkali condition. At some points (usually measured by its pH), the sand may retain its virgin/previous properties, yet by adding acid and/or alkali solutions, it may lose its previous characteristics (usually its intrinsic elements or any elements under studied) (Hu et al., 2004).

Acid and alkali resistance test can be done by soaking the solid sample in HCl and NaOH solution (pH 2-11 ± 0.1) at different temperatures for 4 hours subsequently (Hu et al., 2004).

1.5.1 Technique for measuring pH

pH is a measure of the amounts of hydrogen ion in waters and is defined as follows. Water experiences auto-ionization due to its amphoteric properties (can both function as an acid and a base) (Snoeyink and Jenkins, 1980):

$H_2O \rightleftarrows H^+ + OH^-$ .... (Equation A19-2)

With the equilibrium constant:

$K = \frac{\{H^+\}\{OH^-}{\{H_2O\}}$.....(Equation A19-3)

By neglecting ionic strength effect and because $\{H_2O\} = 1$ in dilute solution (Section 3.2.4), K can be written as:

$K = [H^+][OH^-] = K_w$ .....(Equation A19-4)

$K_w = 1.0 \times 10^{-14}$ at 25°C

By using the notation pX to signify $-\log X$ thus

$pH + pOH = pK_w = 14$ .....(Equation A19-6)

Where:

$$pH = -\log \{H^+\}$$
$$pOH = -\log \{OH^-\}$$
$$pK_w = -\log K_w$$

When ionic effects are negligible:

$pH = -\log [H^+]$ .....(Equation A19-7)

$pOH = -\log [OH^-]$.....(Equation A19-8)

pH can be measured by pH meter, pH papers or indicator solutions that change colour at certain pH values.

1.5.2 The Brønsted concept

According to Brønsted concept, an acid is a term used for any substance that can donate proton to any other substance. On the other hand, a base is any substance that accepts a proton from another substance (Stumm and Morgan, 1996).

1.5.3 The Lewis concept

According to Lewis concept, an acid is a term used for any substance that can accept and share a lone pair of electrons donated by a Lewis base. Lewis bases are also Brønsted bases as protons readily attach themselves to lone electron pairs.

Nevertheless, Lewis acids include many other substances in addition to proton donors, for instance, metal ions (Stumm and Morgan, 1996).

1.6 Sand particle point of zero charge

A point of zero charge is another characteristic of particle that defines the level of the pH needed to provide zero net surface charge. The H^+ and OH^- are the potential determining ions responsible for electric surface potential. When the negative charge density equals the positive charge density, the net surface charge will become zero. The pH value of this zero net surface charge (pH_o) is defined as iso-electric point (IEP) or the point of zero charge (pzc) of solids (Tan, 2011).

Kosmulski (2011) stated that the techniques for determining pzc/IEP basically can be categorised as follows:

a) cip (common intersection point of potentiometric titration curves gained at three or more ionic strengths or equivalent methods),
b) intersection (intersection point of potentiometric titration curves gained at two ionic strengths),
c) pH (pH drift, e.g., mass titration and potentiometric titration at one electrolyte concentration),
d) IEP (isoelectric point gained through electrophoresis, electroosmosis, streaming potential, or electroacoustic method).

1.7 Sand particle effect on pH

Sand particle in a solution may change the pH of the solution depending on the sand conditions i.e. whether the sand is raw or is previously treated by chemicals.

1.8 Sand particle porosity

Porosity is a determination of the void spaces in a substance, and is defined as a fraction, between 0 - 1; or a percentage between 0 - 100%. In soil science, the porosity of a porous medium, i.e. soil or sand, defines the proportion of void space in the substance, where the void may consist of air and/or water. Pores or voids are the open spaces between soil or sand particles (Bowles, 1979).

The porosity is determined by the ratio (Bowles, 1979; Aysen, 2005):

$\emptyset = V_v/V_t$ ....(Equation A19-9)

Where V_v is the volume of void space, and V_t is the total volume of substance, consisting of the solid and void components (air and water).

There are many methods available to determine porosity as stated by Bourbié et al (1987) such as: buoyancy in mercury, setting of wetting fluid by total saturation, calculation of the solid density, etc. The most simple method is that of water evaporation/saturation method (pore volume in cubic centimetres = weight of saturated sample in grams – weight of dried sample in grams). In water evaporation method, oven dry sample (sand or soil) is placed in a container, after it is first weighed, then saturated with water and reweighed. Once the sand or soil is saturated, the pore space within it is filled with the water, excluding for a little amount of trapped air. The volume of water in a saturated sample roughly equal to the amount of pore space, and is utilized to calculate the sample's roughly porosity (Foth, 1990). Porosity is measured as in Equation 3.2. It should be noted that good sorting results in higher porosity because less small grains take place between the larger grains (Pettijohn et al., 1987).

1.9 Manganese content on the sand

In order to determine the amount of manganese on the sand, the solid form has to be transformed to liquid phase. This process is called digestion (Guven and Akinci, 2011).

The principle of the digestion process is to release the metal from the solid matrix to the acid solution during extraction process. There are generally two methods that are used in the acid extraction process, i.e. conventional and microwave assisted acid digestion system. The conventional acid extraction method is an open system in which the solid metal is extracted on a heating source in the occurrence of acid and/or acid mixtures. Different heating systems may be employed i.e. sand-bath, heating plate and aluminium blocks. The microwave acid digestion method is a closed system that provides higher temperature in a closed vessel. The important parameters in these methods are the digestion temperature, time and the reactivity of the chemicals used.

HNO_3 and HCl are the most commonly reactive used. HCl (boiling point 110°C) is of use for wet digestion of salts of carbonates, phospates, some oxides and some sulfides. HNO_3 (boiling point 122°C) does an oxidizing attack on several samples that are not dissolved by HCl.

2 Sand bed characterisation

2.1 Flow hydrodynamic characterisation

Flow hydrodynamic characterisation of reactors used in water/wastewater treatment is required so as to provide the performance of the reactors particularly in relation to chemical reactions occurring within the reactors.

Before proceeding with the technique for characterising flow hydrodynamic, the types of reactors used in the water or wastewater treatment plant are briefly discussed below.

The two most generally used ideal reactors models describe reverse extreme regarding the extent of mixing, from infinite to none (Teefy, 1996). These models are a continuous flow stirred tank reactor (CSTR) and a plug flow reactor (PFR). Ideally, the degree of back-mixing inside a CSTR is infinite, thus ideally, parts of the flow inflowing to the reactor directly discharge from the outlet and thus have no residence time inside the unit. This model can thus be defined as a completely mixed rapid mix chamber.

In contrast, a PFR is a reactor without back-mixing, thus all flow fractions stay inside the reactor for some time equal to the theoretical hydraulic detention time (= volume/flow rate). This model can thus be pictured as an idealized pipe without frictions along the walls. Full-scale of reactors are likely to behave more like one of these models, depending upon their configurations.

As all fractions reside in the reactor for the maximum amount of time, chemical reaction efficiencies obtained in a PFR are always higher than those obtained in a CSTR of equal volume. As a result, the more likely an environmental reactor comes close to a PFR, the more effective will be the chemical reactions for the given quantity of a chemical substance (Teefy, 1996).

In the majority real reactors, the hydrodynamic conditions can be approximated mathematically by an arrangement of CSTRs and PFRs joined in series or parallel. For example, the CSTR cascade model contains some CSTRs linked in series. As the quantity of CSTR in the cascade increases, reaction efficiencies are likely to come close to those equivalents to a PFR (Teefy, 1996).

2.2 Technique for characterising flow hydrodynamic

A tracer study is used to measure the hydraulic performance of reactors (Tchobanoglous et al., 2004).

The test is executed by putting a non reactive (conservative) tracer into a reactor and examined the alteration of concentration of this tracer over time in the reactor effluent until a steady state is obtained (Teefy, 1996).

The profile of the concentration versus time curve gives information about short circuiting within the reactor and the actual residence time of the water in the reactor.

Generally, tracer test that mainly employed are pulse and step inputs. The results of these tests can be graphed regarding the concentration of the tracer versus time. The shape of the resulting curve can specify which reactor models most likely to be close to the reactor being studied.

Thus, the expected chemical reactions efficiencies can be estimated (Teefy, 1996). Pulse input test is described below as it is used in this study.

2.2.1 Pulse input test

A pulse input tracer test is done by adding a certain amount of tracer instantaneously upstream from a reactor inlet. The tracer is added all at once, as soon as possible theoretically. As the tracer is added into the upstream inlet, the measurement of the tracer concentration at the outlet is performed. The corresponding data of tracer concentrations and times then are plotted and known as a tracer curve (Teefy, 1996). The normalised pulse input tracer data are usually known as C curves, whereas the normalised step input data are known as F curves.

In the case of a pulse input test done within an ideal CSTR, the resulting tracer curve would show an initial peak concentration, followed by a steady decrease in tracer concentration, as shown in Figure A19-3. In contrast, a pulse input test performed within a PFR, would indicate no tracer flowing from the reactor until the whole theoretical residence time had passed, in which the monitored tracer concentration would be the same as the whole quantity of feed tracer (Teefy, 1996).

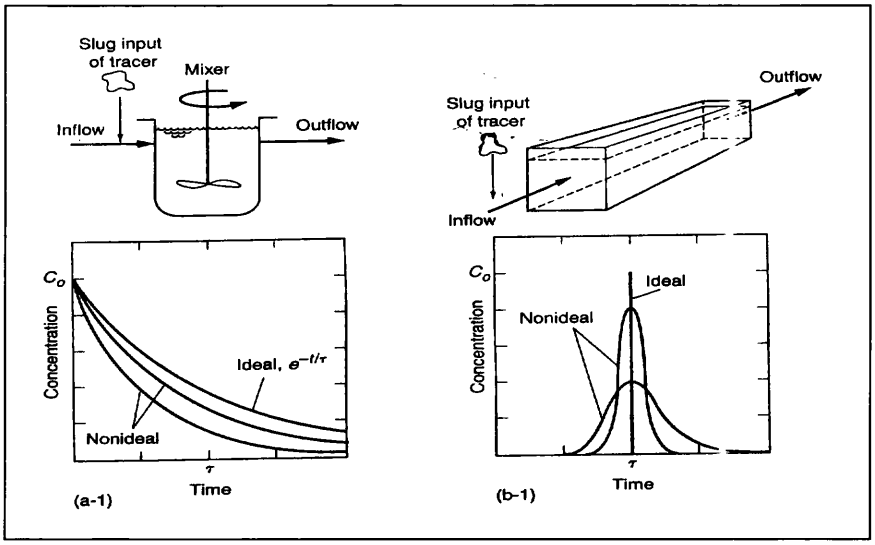

Figure A19-3 Normalised pulse input tracer curves for CSTR and PFR

(Tchobanoglous et al., 2004)

2.2.2 Tracer test parameters

Tracer test parameters required for analysing tracer data are those of mean residence time, variance, tracer mass (recovery rate) and T_x. T_x, residence time, is measured as the time for x percent of the tracer mass to come to the effluent for a pulse input tracer test.

The major advantages of this test are the mean residence time and the recovery rate can be calculated readily so as the validity of the results can be assured (Teefy, 1996).

2.2.3 Plug flow reactor with axial dispersion

The hydraulic performances of non ideal reactors can be modelled by taking dispersion into account. For instance, the PFR with axial dispersion is equal to a CSTR if dispersion becomes infinite.

For a closed system, where there is no dispersion upstream or downstream of the boundaries of the reactor, the performance of a reactor can be approximated by using a normalised effluent concentration versus time curve (which is a symmetrical output tracer response curve) obtained from a unit pulse input (Levenspiel, 1999):

$$C_0 = \frac{1}{2\sqrt{\pi\left(\frac{D}{uL}\right)}} \exp\left[-\frac{(1-\theta)^2}{4\left(\frac{D}{uL}\right)}\right] \text{ .... (Equation A19-10)}$$

Equation A19-10, nevertheless, for a very low dispersion, can be employed to estimate the performance of a closed or an open reactor, in spite of the boundary situations. As Equation A19-10 has the same form as for the normal probability distribution, thus the corresponding mean and variance are (Tchobanoglous et al., 2004):

$$\bar{\theta} = \frac{\bar{t}_c}{\tau} = 1 \text{ .....(Equation A19-11)}$$

$$\sigma_\theta^2 = \frac{\sigma_c^2}{\tau^2} = 2\,\frac{D}{uL} \text{ .....(Equation A19-12)}$$

where: $\bar{\theta}$ = normalised mean detention time (unitless), $\bar{t}_c$ = mean detention time obtained from C curve (s), τ = theoretical detention time (s), σ_θ^2 = variance of normalised tracer response C curve (s^2), σ_c^2 = variance obtained from C curve (s^2).

The unit-less dispersion number is used to estimate the dispersion as shown in Equation 3.21. Calculations for an open system are described in Section 3.3.1.

References:

Abbaschian R., Abbaschian L. and Reed-Hill R.E. (2009) Physical Metallurgy Principles. Gowans, H. (ed), Cengange Learning, Stamford, USA.

Allen T. (1975). Particle Size Measurement. Chapman and Hall Ltd., London.

Aysen A. (2005). *Soil Mechanics: Basic Concepts and Engineering Applications.* Taylor & Francis Group plc, London.

Bourbié T., Coussy O. and Zinszner B. (1987) Acoustics of porous media, Editions Technip, Paris.

Bowles J.E. (1979). Physical and Geotechnical Properties of Soils. McGraw-Hill Book Company, New York.

Ford K.W. (2011) 101 Quantum Questions, what you need to know about the worlds you can't see, The President and Fellows of Harvard College, USA.

Foth H.D. (1990). Fundamentals of Soil Science. John Wiley & Sons, New York.

Goldstein J.I., Newbury D.E., Echlin P., Joy D.C., Fiori C. and Lifshin E. (1981). Scanning Electron Microscopy and X-Ray Microanalysis, A Text for Biologists, Material Scientists, and Geologists. Plenum Press, New York.

Goodhew P.J., Humphreys J. and Beanland R. (2001). Electron microscopy and analysis. Taylor & Francis, London.

Guven D.E. and Akinci G. (2011). Comparison of acid digestion techniques to determine heavy metals in sediment and soil samples. *Gazi University Journal of Science* **24**(1), 29-34.

Hu P.Y., Hsieh Y.H., Chen J.C. and Chang C.Y. (2004). Characteristics of manganese-coated sand using SEM and EDAX analysis. *Journal of Colloid and Interface Science* **272**(2), 308-313.

Kosmulski M. (2011). The pH-dependent surface charging and points of zero charge: V. Update. *Journal of Colloid and Interface Science* **353**(1), 1-15.

Levenspiel O. (1999). Chemical Reaction Engineering. John Wiley & Sons, New York.

Lowell S., Shileds J.E., Thomas M.A. and Thommes M. (2004) Particle technology series: Characterization of porous solids and powders: surface area, pore size and density, Luwer Academic Publisher, Dordrecht.

Pettijohn F.J., Potter P.E. and Siever R. (1987) Sand and Sandstone, Springer Verlag New York Inc., New York.

Skoog D.A., Holler F.J. and Crouch S.R. (2007). Principles of Instrumental Analysis. Thomson Books/Cole, Belmont, California.

Snoeyink V.L. and Jenkins D. (1980). Water Chemistry. John Wiley & Sons New York.

Stout K. (1994) Maximum Math, Design-A-Study, Wilmington, DE.

Stumm W. and Morgan J.J. (1996). Aquatic Chemistry, Chemical Equilibria and Rates in Natural Waters. John Wiley & Sons, Inc., New York.

Tan K.H. (2011) Principle of soil chemistry, CRC Press, Taylor & Francis Group, Boca Raton, Florida.

Tchobanoglous G., Burton F.L. and Stensel H.D. (2004). Wastewater Engineering Treatment and Reuse. McGraw-Hill, Boston.

Teefy S. (1996) Tracer studies in water treatment facilities: a protocol and case studies. Subject area: water treatment, AWWA (American Water Works Association) Research Foundations, USA.

Yang W.C. (ed) (2005) Handbook of fluidization and fluid-particle system, Marcel Dekker, Inc., New York.

Appendix 3.20

Atomic Absorption Spectrometry (AAS)

There are many analytical methods to measure elements (heavy metals) concentration in waters. Thus, it is important to choose the most suited method to the work carried out. The important thing to select the method is the accuracy of that method. Therefore, it is essential to record the performance characteristics along with the chosen analytical method. WHO ranked the analytical methods for inorganic chemicals (WHO, 2006) as follows: (1) Volumetric and colorimetric methods, (2) Electrode method, (3) Ion chromatography, (4) High-performance liquid chromatography (HPLC), (5) Flame atomic absorption spectrometry (FAAS), (6) Electrothermal atomic absorption spectrometry (EAAS), (7) Inductively coupled plasma (ICP)/atomic emission spectrometry (AES), (8) Inductively coupled plasma (ICP)/mass spectrometry (MS). The more complex the process regarding equipment and/or operation, and the more expensive the total cost, the higher is the rank. AAS is described below as it was used in this study.

Basic concepts of atomic absorption spectrometry (AAS)

Atomic emission as well as atomic absorption is the properties of an atom that are employed in analytical chemistry. An atom is constructed from a nucleus encircled with electrons. Each element has a particular number of electrons related to the atomic nucleus in an orbital structure which is distinctive to every element. The electrons inhabit orbital positions in a systematic way. The ground state, the normal position of an atom, is the lowest energy and most stable electronic position. Once energy in the right amount is given to an atom, this energy will be absorbed by the atom, and an electron will be moved to a less stable position known as excited state. This process is known as excitation process.

The atom will then quickly return to its normal and stable position (ground state position) as the excited state is unstable, and radiant energy equal to the amount of energy absorbed in the excitation process will be emitted. This process is known as emission. These processes shown in Figure A20-1 are utilised in atomic spectroscopy (Skoog et al., 2007).

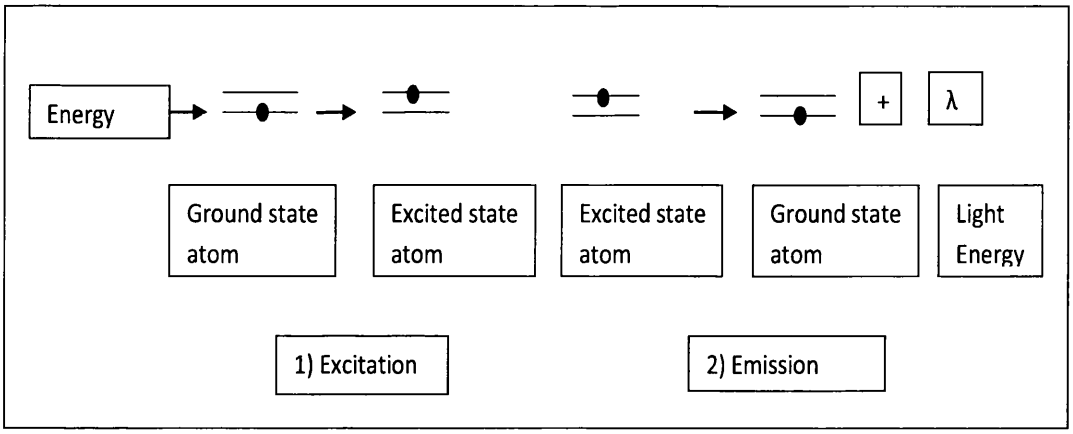

Figure A20-1 Excitation and emission processes (Skoog et al., 2007)

References:

Skoog D.A., Holler F.J. and Crouch S.R. (2007). Principles of Instrumental Analysis. Thomson Books/Cole, Belmont, California.

WHO (2006) Guidelines for Drinking-water Quality. First addendum to third edition. Recommendations. Volume 1.

Appendix 3.21

Reactions

1. Precipitation

A precipitation reaction forms a water-insoluble product, recognized as a precipitate. The reactants are usually water-soluble ionic compounds. They dissociate to produce the relevant cations and anions, once these substances dissolve in water. Precipitation happened if the cation from one compound can produce an insoluble compound with the anion from the other compound in the solution (Kotz, 2006).

The removability of substances from water by precipitation depends primarily on the solubility of the various complexes formed in water. For example, heavy metals are found as cations in water and many will form both hydroxide and carbonate (and sulfides in the case of sulphide addition) solid forms. These solids have low solubility limits in water. Thus, as a result of the formation of insoluble hydroxides, carbonates or sulfides, the metals will be precipitated out of solution. Precipitation of the metal hydroxide is the most common method of removing toxic heavy metals from water. Generally caustic soda or lime is added to the water to adjust the solution pH to the point of maximum insolubility (Benefield and Morgan, 1999).

The solubility product

Solubility product is the term used for the equilibrium constant that describes the reaction in which a precipitate dissolves in water to form its constituent ions as follows (Snoeyink and Jenkins, 1980):

$A_zB_{y\,(s)} \rightleftarrows zA^{y+} + yB^{z-}$.....(Equation A21-1)

The equilibrium constant, K_{so}, is:

$K_{so} = \frac{\{A^{y+}\}^z \{B^{z-}\}^y}{\{A_zB_{y\,(s)}\}}$ .....(Equation A21-2)

$\{A_zB_{y(s)}\}$ or the activity of the solid phase is taken as unity (=1) (The activity of solids or liquids in equilibrium with a solution, {i} = 1).

The form of the concentration product, ${}^cK_{so}$, is the same as that for the equilibrium constant except that the concentrations are used instead of their activities. Thus:

$${}^cK_{so} = [A^{y+}]^z[B^{z-}]^y = \frac{K_{so}}{(\gamma A^{y+})^z(\gamma B^{z-})^y} \quad \text{.....(Equation A21-3)}$$

By assuming that the solution components have activity coefficients = 1 and that the solid has an activity of one, then ${}^cK_{so} = K_{so}$. If the activity coefficients ≠ 1, then ${}^cK_{so} \neq K_{so}$,and ${}^cK_{so}$ is a function of ionic strength.

2. Filtration

Filtration is a process in which the water to be treated is passed through the screen media removing the suspended particles that are larger than the opening of the screen (Huisman, 2004). Filtration retained the particles that are previously precipitated. An accumulation of retained particles occurred with time by which the effective opening of the filter media is reduced and eventually clogged, hence little particles and finally none are retained. Filtration is seldom used alone in water treatment; it often requires pre-treatment before such as precipitation, coagulation and flocculation. It also needs post-treatment after, especially if the final water product is aimed to be used as potable water. In this case, disinfection has to be employed after filtration.

3. Adsorption

Adsorption is a mass transfer process in which the accumulation of a substance at the interface between two phases occurs (Alley, 2007). The adsorbate is the constituent that is adsorbed or being transferred from the liquid phase at the boundary; while the adsorbent is the solid, liquid or gas onto which the adsorbate retained.

The primary types of adsorbents are those of activated carbon, synthetic polymeric and silica-based adsorbents.

The main force responsible for the interaction between the adsorbate and the adsorbent is the electrostatic attraction and repulsion between molecules of the adsorbate and the adsorbent. These driving forces can be occurred physically or chemically (Alley, 2007).

Adsorption process is generally occurred in four or less steps, i.e. (1) bulk solution transport, (2) film diffusion transport, (3) pore transport, and (4) adsorption (or sorption). Bulk solution transport is the transport of the constituent to be adsorbed through the bulk liquid to the interface of fixed film of liquid adjoining the adsorbent, usually by advection and dispersion. Film diffusion transport is the movement of the substance through the stagnant liquid film to the opening of the pores of the adsorbent by diffusion. Pore transport or intraparticle diffusion is the movement of the constituent to be adsorbed through the pores by a mixture of molecular diffusion through the pore liquid (pore diffusion) and/or by diffusion along the surface of the adsorbent (surface diffusion). Adsorption is the process in which the constituent to be adsorbed is attached onto the adsorbent at an available adsorption site. The term "sorption" is used due to it is not easy to distinguish chemical and physical adsorption (Tchobanoglous et al., 2004).

3.1 Physical adsorption

Physical adsorption is resulted from intermolecular forces that occurred between the adsorbate and the adsorbent. These physical electrostatic forces consist of the van der Waals force, including weak attraction and repulsion through dipole-dipole interactions and dispersing interactions, and hydrogen bonding. Dipole-dipole interactions are resulted from polar compounds orienting themselves so as a lower joint free energy is resulted from their charges. Dispersing interactions are resulted from the attractive forces between electrons and nuclei of molecular systems. Repulsive forces can push the molecules away from each other if the molecules are close to each other.

Hydrogen bonding, a particular type of dipole-dipole interaction, is the bonding of the hydrogen atom in a molecule that has a partial positive charge with another atom or molecule that has a partial negative charge. The van der Waals force is the major physical force driving adsorption for liquid phase system.

Physical adsorption usually has low adsorption energy and is not site specific as it does not involve the sharing of electrons. It is a readily reversible reaction and involves mono as well as multilayer coverage. The substance is adsorbed onto the adsorbent surface once the intermolecular forces between the substance molecule in a liquid stream and the adsorbent are higher than the forces between the molecules of the liquid stream (Alley, 2007).

3.2 Chemisorption

Similar to physical adsorption, chemical adsorption (chemisorption) also depends on electrostatic forces. The mechanisms of chemisorption are the same as those for physical adsorption, but they are even stronger (almost as strong as the adsorption energies of chemical bonds). Chemisorption is resulted from the transfer of electrons and the formation of chemical bonds between the adsorbate and the adsorbent. The adsorbate may change chemically due to the reaction. Chemisorption may be an irreversible reaction and involves high adsorption energies. It includes only monolayer coverage and is a site specific reaction occurred at particular functional groups locations (Alley, 2007).

3.3 Factors affecting adsorptive capacity

The adsorptive capacity of an adsorbent material is generally proportional to the surface area available. Nevertheless, several factors affect adsorption such as charge, molecular weight, temperature, surface area, pore size distribution, the adsorbent bed depth, waste stream velocity and desired removal efficiency (Alley, 2007).

4. Complexation

4.1 Aqua complexes of metal

In aqeous solution, all d-block metal ions are hydrated. d-block metals are those metals located in the 10 colomns (3 -12) in the periodic table. A lone pair of electrons from each of the water molecules is attracted to the central metal ion fairly; the bonding between them may be described as between uncomplicated electrostatic attraction and coordinate covalent. A coordinate covalent bond is a specific type of covalent bond in which the shared electron derives from one of the atoms only but it equally shared by both in a molecular type bonding orbital (Mobile Reference, 2007). A covalent bond occurs once the atoms share their electrons (Evans, 1976).

Complexation is a term used for a molecule that contains a central cation surrounded by electron pair donors. The number of coordinate bonds formed is called the coordination number and the electron pair donors are ligands. Hexa-aqua complexes are produced once all metals in the first row of the d-block with an oxidation state of +2 or +3 are dissolved in aqueous solution. The solids that may be cristallised from aqueous solution maintain the hydrated metal ion in several cases. The common formula of hexa-aqua complexes of metal is $[M(H_2O)_6]^+$, where M is the metal ion (Winter and Andrew, 2000).

5. Interaction of metal ions with hydrous oxide surfaces

Oxides, particularly those of Si, Al and Fe, are ubiquitous in the earth's crust. Thus majorly the solid phase in natural waters, sediments and soils contain such oxides or hydroxides. The surfaces of these oxides are usually covered with surface hydroxyl groups (S–OH). These functional surface groups have the ability to act as coordinating sites of the surface. The functional groups at the surface experience acid-base and other coordinative reactions.

Adsorption of metal ions is known as competitive complex formation which involves either one or two surface hydroxyl groups as follows (Stumm and Morgan, 1996):

$S{-}OH + M^{z+} \rightleftarrows S{-}OM^{(z-1)+} + H^{+}$ .... (Equation A21-4)

$2\ S{-}OH + M^{z+} \rightleftarrows (S{-}O)_2M^{(z-2)+} + 2\ H^{+}$ .... (Equation A21-5)

$S{-}OH + M^{z+} + H_2O \rightleftarrows S{-}OMOH^{(z-2)+} + 2\ H^{+}$ .... (Equation A21-6)

6. Speciation

Speciation refers to the specific chemical form in which an element exists in water (Stumm and Morgan, 1996). For instance, an element can occur as a simple hydrated ion, as a molecule or as a complex with another ion or molecule. Information on the types of species found under different chemical conditions is important to know the distribution and behaviour of elements in waters.

References:

Alley E.R. (2007). Water Quality Control Handbook. McGraw-Hill Co., Inc., Alexandria, Virginia.

Benefield L.D. and Morgan J.M. (1999) Water Quality and Treatment - A Handbook of Community Water Supplies - American Water Works Association (5th Edition). Letterman, R.D. (ed), pp. 10.51-10.53., McGraw-Hill, Inc., New York.

Evans R.C. (1976) An introduction to crystal chemistry, Cambridge University Press, Cambridge, UK.

Huisman P.d.i.L. (2004) Mechanical filtration, Delft University of Technology.

Kotz J.C., Treichel, P. M. & Weaver, G. C. (2006). Chemistry & Chemical Reactivity. Thomson Learning, Inc., Australia.

Mobile Reference (2007) Chemistry quick study guide.

Snoeyink V.L. and Jenkins D. (1980). Water Chemistry. John Wiley & Sons New York.

Stumm W. and Morgan J.J. (1996). Aquatic Chemistry, Chemical Equilibria and Rates in Natural Waters. John Wiley & Sons, Inc., New York.

Tchobanoglous G., Burton F.L. and Stensel H.D. (2004). Wastewater Engineering Treatment and Reuse. McGraw-Hill, Boston.

Winter M.J. and Andrew J.E. (2000). Foundations of Inorganic Chemistry. Oxford Science Publications, New York.

LIST OF FIGURES

LIST OF TABLES